

**TIME-DEPENDENT LOSS OF POST-TENSIONED
DIAPHRAGM AND FIN MASONRY WALLS**

by

Siti Hamisah Tapsir

(B.Sc., M.Sc.)

Thesis Submitted in Accordance with the Requirement
of the Degree of Doctor of Philosophy

Department of Civil Engineering

The University of Leeds

February 1994

The candidate confirms that the work submitted is her own and that appropriate credit
has been given where reference has been made to the work of others.

ABSTRACT

This thesis reports an investigation on time-dependent loss of post-tensioned masonry box and tee sections representing diaphragm and fin walls, respectively. The prestress loss due to creep and shrinkage of masonry, and relaxation of steel bars were quantified separately and the main influencing factors considered were geometry and masonry type. For each type of masonry three diaphragm and three fin walls were built to determine prestress loss (decreasing load), creep (constant load) and shrinkage (zero load). The walls were constructed from undocked clay, calcium silicate and concrete block units with grade (ii) mortar with cement:lime:sand in the proportions of $1:\frac{1}{2}:4\frac{1}{2}$ and water/cement ratio of 1.27. Creep and shrinkage were also measured on unbonded masonry units and mortar prisms for predicting the deformations in the masonry walls by using a previously developed composite model. The masonry units and mortar prisms were partly sealed to simulate the corresponding volume/surface ratio of the bonded masonry units and mortar joints in the masonry walls.

The calcium silicate walls exhibited the highest prestress loss, creep and shrinkage compared with the clay and concrete block diaphragm and fin walls. The current methods of prediction of prestress loss for masonry are only suitable for specific types of masonry for which they were developed. On the other hand, the methods developed for prestressed concrete gave reasonable predictions for all the masonry types investigated, with one particular method being very accurate. For all test results it was confirmed that long-term deformations were influenced by geometry, fin walls exhibiting greater deformations than diaphragm walls. The composite model did not predict shrinkage very well in calcium silicate and concrete block walls because some moisture in the mortar was absorbed by the masonry units. As a result the partly sealed unbonded mortar prisms had higher water content than the mortar bed joint in the walls, and thus a higher shrinkage in the partly sealed mortar prisms occurred. Consequently, when the creep and shrinkage of the partly sealed mortar prisms was applied to the model, the masonry deformation was overestimated.

A modified water absorption test was carried out which confirmed that for units laid dry the mortar bed joint had a reduced shrinkage compared to the unbonded mortar prisms. From the results, creep and shrinkage adjustment factors were correlated with unit water absorption, and when adjusted creep and shrinkage were incorporated with the composite model, satisfactory predictions of masonry deformations were achieved.

**Dedicated
to**

My husband
Ahmad Fikri

and our daughter
Siti Umyra

ACKNOWLEDGEMENTS

I would like to express my sincere gratitude to Dr. J.J. Brooks for the constant encouragement, advice, discussions and supervision throughout the research and during the preparation of this thesis. His patience, understanding and readiness to help, particularly at times of difficulty are highly appreciated. I would also like to thank Mr. M.D. Parker for the supervision during the early stage of the research and his careful review and constructive comments of the thesis.

Thanks are due to Professor A.D. May, Head of the Department of Civil Engineering, for providing the research facilities.

Thanks are also extended to the technical staff of George Earle Laboratory and in particular to Mr. V.W. Lawton for the discussions, suggestions and assistance during the experimental work.

I would also like to thank my sponsors, the University of Technology Malaysia and the Public Service Department of Malaysia for having offered the opportunity to carry out the research programme.

Thanks are further extended to Marshalls Clay Products, Mansfield Brick, Plasmor Ltd. and McCalls Special Products for generously supplying the materials.

I am grateful to my husband, Ahmad Fikri who was also doing PhD, for his enduring support especially during the first few months of the research when our daughter, Siti Umyra, was only 3 months old. Their presence have undoubtedly eased the pressure of doing this research.

CONTENTS

	Pages
ABSTRACT	i
ACKNOWLEDGEMENTS	ii
CONTENTS	iii
LIST OF TABLES	xi
LIST OF FIGURES	xiv
LIST OF PLATES	xxi
NOTATIONS	xxii

CHAPTER 1: INTRODUCTION

1.1	General.....	1
1.2	Prestress loss in post-tensioned masonry members.....	2
1.3	Outline of problem.....	3
1.4	Purpose and scope of research.....	5
1.5	Definition of terms.....	6

CHAPTER 2: REVIEW ON TIME-DEPENDENT LOSS OF POST-TENSIONED DIAPHRAGM AND FIN MASONRY WALLS

2.1	Introduction.....	14
2.2	Previous research on prestress loss of masonry.....	14
2.3	Factors affecting prestress loss of post-tensioned masonry.....	18
	2.3.1 Creep of masonry.....	19
	2.3.1 (a) Mechanism of creep.....	20
	2.3.1 (b) Factors affecting creep.....	20
	2.3.2 Moisture movement of masonry.....	24
	2.3.2 (a) Mechanism of moisture movement in masonry.....	25

2.3.2 (b)	Factors affecting moisture movement strain.....	27
2.3.3	Relaxation of prestressing steel.....	31
2.4	Effect of shape and size on creep and shrinkage of concrete.....	32

CHAPTER 3: REVIEW OF METHODS FOR PREDICTING PRESTRESS LOSS OF POST-TENSIONED MASONRY

3.1	Introduction.....	43
3.2	Prediction of time-dependent prestress loss in masonry.....	43
3.2.1	Prediction of time-dependent prestress loss in masonry by Codes of Practice.....	43
3.2.1 (a)	BS 5628: Part 2 (1985).....	44
3.2.2	Prediction of time-dependent prestress loss in masonry by previous researchers.....	44
3.2.2 (a)	Lenczner.....	45
3.2.2 (b)	Tatsa.....	46
3.3	Methods of predicting elastic modulus.....	47
3.3.1	Elastic modulus of masonry by Codes of Practice.....	47
3.3.1 (a)	BS 5628: Part2 (1985).....	47
3.3.1 (b)	ACI 530-88/ASCE 5-88 (1990).....	48
3.3.1 (c)	Eurocode No 6 (1988).....	48
3.3.2	Prediction of elastic modulus by previous researchers.....	48
3.3.2 (a)	Lenczner.....	48
3.3.2 (b)	Brooks.....	49
3.4	Methods of predicting creep.....	50
3.4.1	Creep of masonry by Codes of Practice.....	50
3.4.1 (a)	BS 5628: Part2 (1985).....	50
3.4.1 (b)	ACI 530-88/ASCE 5-88 (1990).....	51
3.4.1 (c)	Eurocode No 6 (1988).....	51
3.4.2	Prediction of creep by previous researchers.....	51
3.4.2 (a)	Lenczner.....	52
3.4.2 (b)	Brooks.....	52
3.5	Methods of predicting shrinkage.....	53
3.5.1	Moisture movement of masonry by Codes of Practice.....	53

3.5.1 (a)	BS 5628: Part2 (1985).....	53
3.5.1 (b)	ACI 530-88/ASCE 5-88 (1990).....	54
3.5.1 (c)	Eurocode No 6 (1988).....	54
3.5.2	Prediction of shrinkage by previous researchers.....	54
3.5.2 (a)	Brooks method.....	54
3.6	Methods of predicting relaxation of steel.....	55
3.6.1	Prediction of relaxation of steel by Codes of Practice.....	55
3.6.1 (a)	BS 5628: Part2 (1985).....	55
3.6.2	Prediction of relaxation of steel by previous researchers.....	55
3.6.2 (a)	Magura et. al	55
3.6.2 (b)	Glowdowski et. al	56
3.7	Prediction of time-dependent prestress loss in prestressed concrete.....	57
3.7.1 (a)	Dilger method	57
3.7.1 (b)	Abeles method.....	58

CHAPTER 4: EXPERIMENTAL DETAILS

4.1	Introduction.....	63
4.2	Outline of the test programme.....	63
4.3	Materials.....	65
4.3.1	Masonry units.....	65
4.3.1 (a)	Clay brick.....	65
4.3.1 (b)	Calcium silicate brick.....	65
4.3.1 (c)	Concrete block.....	65
4.3.2	Mortar.....	66
4.3.3	Base and capping beams.....	66
4.3.4	Prestressing steel.....	67
4.4	Test Procedure.....	67
4.4.1	Test set-up.....	67
4.4.1 (a)	Prestressing procedure for bar anchored to concrete bases for creep and prestress loss walls.....	67
4.4.1 (b)	Building the masonry walls.....	68
4.4.1 (c)	Prestressing procedure.....	69
4.5	Creep tests of masonry units and mortar prisms.....	70
4.6	Strain measurements.....	71
4.6.1	Reinforced concrete bases and capping beams.....	71

4.6.2	Masonry.....	71
4.6.3	Prestressing steel bar.....	72
4.6.4	Creep and shrinkage of masonry units and mortar prisms.....	73
4.6.5	Strain measurement on creep dynamometer.....	73
4.7	Environmental conditions.....	73
4.8	Testing.....	74
4.8.1	Deformation of masonry walls.....	74
4.8.1 (a)	Elastic modulus.....	74
4.8.1 (b)	Shrinkage.....	74
4.8.1 (c)	Creep.....	74
4.8.1 (d)	Prestress loss of masonry walls.....	75
4.8.2	Deformations of masonry units and mortar prisms.....	75
4.8.2 (a)	Elastic modulus.....	75
4.8.2 (b)	Moisture movement strain.....	75
4.8.2 (c)	Creep.....	76
4.8.3	Stress Relaxation test.....	76
4.9	Control tests.....	76
4.9 (a)	Compressive strength	76
4.9 (b)	Standard dropping ball test for mortar.....	78
4.9 (c)	Macalloy prestressing steel tensile test.....	78

CHAPTER 5: ANALYSIS AND DISCUSSION OF TEST RESULTS

5.1	Introduction.....	109
5.2	Brickwork.....	109
5.2.1	Elasticity	109
5.2.1 (a)	Measured elasticity	109
5.2.1 (b)	Elasticity by finite elements.....	110
5.2.2	Creep of masonry walls.....	111
5.2.2 (a)	Influence of geometry	112
5.2.2 (b)	Influence of masonry units.....	112
5.2.2 (c)	Ultimate creep.....	113
5.2.2 (d)	Creep coefficient.....	114
5.2.3	Shrinkage masonry walls.....	115

5.2.3 (a)	Influence of geometry	115
5.2.3 (b)	Influence of masonry units	115
5.2.3 (c)	Ultimate shrinkage.....	116
5.2.4	Prestress loss of masonry walls.....	116
5.2.4 (a)	Influence of geometry	117
5.2.4 (b)	Influence of masonry units	117
5.2.4 (c)	Measured strain on prestress loss walls.....	118
5.3	Mortar prisms.....	118
5.3.1	Elasticity.....	118
5.3.2	Creep.....	119
5.3.2 (a)	Ultimate creep.....	120
5.3.3	Shrinkage.....	120
5.3.3 (a)	Ultimate shrinkage.....	120
5.4	Masonry units.....	120
5.4.1	Elasticity.....	120
5.4.2	Creep.....	121
5.4.2 (a)	Ultimate creep.....	121
5.4.3	Shrinkage/moisture expansion.....	122
5.4.3 (a)	Ultimate shrinkage.....	122
5.5	Relaxation loss.....	122
5.6	Individual prestress loss.....	123
5.7	Temperature and humidity.....	124

CHAPTER 6: PREDICTION OF SHRINKAGE, CREEP AND PRESTRESS LOSS USING COMPOSITE MODEL

6.1	Introduction.....	152
6.2	Elastic deformation.....	152
6.2.1	Prediction of elastic modulus by Codes of Practice.....	152
6.2.1 (a)	BS 5628: Part2 (1985):	152
6.2.1 (b)	ACI 530-88/ASCE 5-88 (1990).....	153
6.2.1 (c)	Eurocode No 6 (1988).....	154
6.2.2	Prediction of elastic modulus by previous researchers.....	154
6.2.2 (a)	Lenczner method.....	155

	6.2.2 (b)	Brooks method.....	155
6.3	Creep.....		156
	6.3.1	Prediction of creep by Codes of Practice.....	156
		6.3.1 (a) BS 5628: Part2 (1985).....	156
		6.3.1 (b) ACI 530-88/ASCE 5-88 (1990).....	157
		6.3.1 (c) Eurocode No 6 (1988).....	157
	6.3.2	Prediction of creep by previous researchers.....	158
		6.3.2 (a) Lenczner method.....	158
		6.3.2 (b) Brooks method.....	158
6.4	Shrinkage.....		159
	6.4.1	Prediction of shrinkage by Codes of Practice.....	159
		6.4.1 (a) BS 5628: Part2 (1985).....	159
		6.4.1 (b) ACI 530-88/ASCE 5-88 (1990).....	159
		6.4.1 (c) Eurocode No 6 (1988).....	160
	6.4.2	Prediction of shrinkage by previous researchers.....	160
6.5	Prestress loss.....		161
	6.5.1	Prediction of prestress loss by Codes of Practice.....	161
		6.5.1 (a) BS 5628: Part2 (1985).....	162
		6.5.1 (b) ACI 530-88/ASCE 5-88 (1990).....	163
		6.5.1 (c) Eurocode No 6 (1988).....	164
	6.5.2	Prediction of prestress loss by previous researchers.....	164
		6.5.2 (a) Lenczner method.....	164
		6.5.2 (b) Tatsa method.....	165
6.6	Methods of predicting of prestress loss in prestressed concrete		165
	6.6.1	Dilger method.....	166
	6.6.2	Abeles method.....	168
6.7	Comparison of proposed method of predicting prestress loss of brickwork with the experimental results and previous researchers.....		168
6.8	Conclusion.....		169

**CHAPTER 7: IMPLICATIONS OF UNIT WATER ABSORPTION
ON PREDICTION OF DEFORMATION AND
PRESTRESS LOSS OF MASONRY**

7.1	Introduction.....	186
7.2	Experimental details	187

7.2.1	Control tests.....	187
7.2.1 (a)	Initial rate of suction test.....	187
7.2.1 (b)	Standard water absorption test.....	187
7.2.2 (c)	Modified water absorption test.....	188
7.2.2	Long-term test.....	189
7.2.2 (a)	Modified water absorption test.....	189
7.2.2 (b)	Shrinkage test.....	189
7.2.2 (c)	Reduced water/cement ratio of mortar prisms.....	190
7.3	Measurements.....	191
7.3.1	Modified units water absorption	191
7.3.2	Shrinkage.....	191
7.3.3	Reduced water/cement ratio of mortar prisms.....	192
7.4	Test results.....	192
7.4.1	Short-term water absorption.....	192
7.4.1 (a)	Initial suction rate.....	192
7.4.1 (b)	Standard water absorption	192
7.4.1 (c)	Modified water absorption test.....	193
7.4.2	Long-term water absorption tests.....	193
7.4.2 (a)	Modified water absorption	193
7.4.2 (b)	Shrinkage	194
7.4.2 (c)	Reduced water/cement ratio of mortar prisms.....	201
7.5	Summary on the effects of unit water absorption on prediction on deformation of masonry.....	203

CHAPTER 8: CONCLUSIONS AND RECOMMENDATIONS FOR FUTURE RESEARCH

8.1	Introduction.....	234
8.2	Prestress loss.....	234
8.3	Creep and shrinkage	236
8.4	Composite modelling.....	237
8.5	Comparison between the ultimate values obtained by extrapolation of the experimental results and prediction methods.....	238
8.6	Suggestions for future research.....	241

REFERENCES**APPENDIX**

- APPENDIX A WORKING STRESS**
- APPENDIX B TEST RESULTS (WALLS)**
- APPENDIX C TEST RESULTS (MORTAR AND UNIT)**
- APPENDIX D PREDICTION OF SHRINKAGE, CREEP AND
PRESTRESS LOSS**
- APPENDIX E RE-PREDICTION OF SHRINKAGE, CREEP AND
PRESTRESS LOSS**
- APPENDIX F TEST RESULTS (MORTAR WITH REDUCED
WATER/CEMENT RATIO)**

LIST OF TABLES

CHAPTER 2	Pages
Table 2.1	Experimental Work on Prestress Loss of Post-tensioned Masonry by Previous Researcher..... 34-35
Table 2.2	Effect of Geometry on Creep of Plain Masonry 36
Table 2.3	Effect of Unit Type on Creep of Plain Masonry..... 37
Table 2.4	Effect of Geometry on Shrinkage of Plain Masonry..... 38-39
Table 2.5	Effect of Unit Type on Shrinkage of Plain Masonry..... 40
Table 2.6	Creep and Shrinkage Correction Factors for Average Thickness of Concrete Members ≥ 5.1 mm..... 41
Table 2.7	Creep and Shrinkage Correction Factors for $(V/S) \geq 38$ mm..... 42
CHAPTER 3	
Table 3.1	Characteristic Compressive Strength of Masonry (BS5628 1985)... 59
Table 3.2	Elastic Modulus of Clay Masonry by ACI - 530 (1990)..... 60
Table 3.3	Elastic Modulus of Concrete Masonry by ACI - 530 (1990)..... 61
Table 3.4	Relaxation Loss at 1000 hour in Accordance with BS 5896 (1980) and BS 4480 (1980)..... 61
CHAPTER 4	
Table 4.1	Work Test Certificate for McCall Special Products Bars..... 79
Table 4.2	Details of Prestressing Force Applied on the Masonry Walls..... 79
Table 4.3	Volume/exposed Surface Ratios of the Walls, Masonry Units and Mortar Prisms..... 80
Table 4.4	Mean Compressive strength of Concrete Cubes..... 80
Table 4.5	Mean Compressive strength of Mortar Cubes..... 81
Table 4.6	Mean Compressive strength of Masonry Units..... 81

CHAPTER 5

Table 5.1	Modulus of Elasticity of Clay, Calcium Silicate Brickwork and Concrete Blockwork (GPa).....	125
Table 5.2	Ultimate Creep of Clay, Calcium Silicate Brickwork and Concrete Blockwork	125
Table 5.3	Creep Coefficient of Clay, Calcium Silicate Brickwork and Concrete Blockwork	126
Table 5.4	Ultimate Shrinkage of Clay, Calcium Silicate Brickwork and Concrete Blockwork	126
Table 5.5	Deformation of Mortar as Sampled during Construction of the Masonry Walls	127
Table 5.6	Modulus of Elasticity of Masonry Unit Between Header and Bed Face.....	128
Table 5.7	Deformation of Masonry Units.....	129-130
Table 5.8	Ultimate Individual Prestress Loss of Masonry Walls.....	131

CHAPTER 6

Table 6.1	Modulus of Elasticity of Clay, Calcium Silicate Brickwork and Concrete Blockwork Predicted by Codes of Practice.....	171
Table 6.2	Modulus of Elasticity of Clay, Calcium Silicate Brickwork and Concrete Blockwork Predicted by Previous Researchers.....	171
Table 6.3	Ultimate Specific Creep of Clay, Calcium Silicate Brickwork and Concrete Blockwork Predicted by Codes of Practice.....	172
Table 6.4	Ultimate Specific Creep of Clay, Calcium Silicate Brickwork and Concrete Blockwork Predicted by Previous Researchers.....	173
Table 6.5	Predicted Shrinkage of Clay, Calcium Silicate Brickwork and Concrete Blockwork	174

Table 6.6	Predicted Prestress Loss of Clay, Calcium Silicate Brickwork and Concrete Blockwork by Codes of Practice.....	175
Table 6.7	Predicted Prestress Loss of Clay, Calcium Silicate Brickwork and Concrete Blockwork by Codes of Practice (Measured Strain).....	176
Table 6.8	Predicted Prestress Loss of Clay, Calcium Silicate Brickwork and Concrete Blockwork by Previous Researchers	177
Table 6.9	Estimated Individual Prestress Loss of the Masonry Walls by Composite Model.....	178

CHAPTER 7

Table 7.1	Compressive Strength of Mortar for Water Absorption and Shrinkage Test.....	205
Table 7.2	Volume/exposed Surface Ratios of the Masonry, Masonry Units and Mortar Prisms.....	205
Table 7.3	Initial Suction Rate and Water Absorption Test.....	206
Table 7.4	Average Shrinkage Factors of Masonry Units and Mortar Prisms.....	206

LIST OF FIGURES

CHAPTER 1	Pages
Fig. 1.1 Typical Plan of Clay and Calcium Silicate Diaphragm Wall.....	8
Fig. 1.2 Typical Plan of Concrete Block Diaphragm Wall.....	8
Fig. 1.3 Typical Isometric View of Diaphragm Wall.....	9
Fig. 1.4 Typical Plan of Clay and Calcium Silicate Fin Wall.....	9
Fig. 1.5 Typical Plan of Concrete Block Fin Wall.....	10
Fig. 1.6 Typical Isometric View of Fin Wall.....	11
Fig. 1.7 Schematic Creep Strain-time Curve of Masonry.....	12
Fig. 1.8 Schematic Shrinkage strain-time Curve of Calcium Silicate and Concrete Block Masonry.....	12
Fig. 1.9 Schematic Moisture Movement Strains of Clay Masonry.....	13
CHAPTER 3	
Fig. 3.1 Reduction of Relaxation Coefficient.(Dilger et al 1983).....	62
CHAPTER 4	
Fig. 4.1 Sieve Analysis of Sand in Accordance with BS1200.....	82
Fig. 4.2 Plan and Section of the Concrete Base for Diaphragm and Fin Walls.....	83
Fig. 4.3 Plan and Section of the Concrete Capping Beams for Diaphragm Walls.....	84
Fig. 4.4 Reinforcement Details and Sections of the Concrete Capping Beams for Fin Walls.....	85
Fig. 4.5 Prestressed Bar Anchorage System to the Concrete Base.....	85
Fig. 4.6 Prestressing Details of Bar Anchored to Concrete Base.....	86
Fig. 4.7 Section Details of Diaphragm Walls.....	87
Fig. 4.8 Section Details of Fin Walls.....	88

Fig. 4.9	Prestressing Details for Bar at the top of Concrete Capping Beams.....	89
Fig. 4.10	Anchorage System at the Top of Capping Beams of Diaphragm and Fin Walls.....	89 - 91
Fig. 4.11	Creep Frame for Masonry Units and Mortar Prisms.....	91
Fig. 4.12	Location of Strain Measurement on Clay and Calcium Silicate Diaphragm Walls.....	92
Fig. 4.13	Location of Strain Measurement on Clay and Calcium Silicate Fin Walls.....	93
Fig. 4.14	Location of Strain Measurement on Concrete Block Diaphragm Walls	94
Fig. 4.15	Location of Strain Measurement on Concrete Block Fin Walls...	95
Fig. 4.16	Full Bridge Configuration of Electrical Strain Gauges Connection.....	96
Fig. 4.17	Variation of Laboratory Temperature with Time.....	97
Fig. 4.18	Variation of Laboratory Humidity with Time.....	98
Fig. 4.19	Partial Sealing of Masonry Units and Mortar Prisms	99
Fig. 4.20	Intrinsic Relaxation Test	100
Fig. 4.21	Stress-strain Curve of the Prestressing Bars.....	101

CHAPTER 5

Fig. 5.1	Typical Displacement of Clay, Calcium Silicate and Concrete Block Walls by Pafec	132
Fig. 5.2	Creep-time Curve of Clay Walls under 3 MPa Stress.....	132
Fig. 5.3	Creep-time Curve of Calcium Silicate Walls under 1.57 MPa Stress.....	133
Fig. 5.4	Creep-time Curve of Concrete Block Walls under 2.0 MPa Stress.....	133
Fig. 5.5	Specific Creep-time Curve of Diaphragm Walls	134
Fig. 5.6	Specific Creep-time Curve of Fin Walls	134
Fig. 5.7	Shrinkage-time Curve of Clay Walls	135
Fig. 5.8	Shrinkage-time of Calcium Silicate Walls	135
Fig. 5.9	Shrinkage-time of Concrete Block Walls	136
Fig. 5.10	Shrinkage-time of Curve of Diaphragm Walls	136

Fig. 5.11	Shrinkage-time of Curve of Fin Walls	137
Fig. 5.12	Prestress Loss-time of Curve of Clay Walls	137
Fig. 5.13	Prestress Loss-time of Curve of Calcium Silicate Walls.....	138
Fig. 5.14	Prestress Loss-time of Curve of Concrete Block Walls	138
Fig. 5.15	Prestress Loss-time of Curve of Diaphragm Walls	139
Fig. 5.16	Prestress Loss-time of Curve of Fin Walls	139
Fig. 5.17	Strain-time Curve of Prestress Loss Clay Walls	140
Fig. 5.18	Strain-time Curve of Prestress Loss Calcium Silicate Walls	140
Fig. 5.19	Strain-time Curve of Prestress Loss Concrete Block Walls	141
Fig. 5.20	Creep-time Curve of Mortar Prisms for Clay Walls	141
Fig. 5.21	Creep-time Curve of Mortar Prisms for Calcium Silicate Walls ..	142
Fig. 5.22	Creep-time Curve of Mortar Prisms for Concrete Block Walls ..	142
Fig. 5.23	Specific Creep-time Curve of Mortar Prisms for Diaphragm Walls.....	143
Fig. 5.24	Specific Creep-time Curve of Mortar Prisms for Fin Walls	143
Fig. 5.25	Shrinkage-time Curve of Mortar Prisms for Clay Walls	144
Fig. 5.26	Shrinkage-time Curve of Mortar Prisms for Calcium Silicate Walls.....	144
Fig. 5.27	Shrinkage-time Curve of Mortar Prisms for Concrete Block Walls.....	145
Fig. 5.28	Shrinkage-time Curve of Mortar Prisms for Diaphragm Walls...	145
Fig. 5.29	Shrinkage-time Curve of Mortar Prisms for Fin Wall.	146
Fig. 5.30	Creep-time Curve of Clay Units.....	146
Fig. 5.31	Creep-time Curve of Calcium Silicate Units.....	147
Fig. 5.32	Creep-time Curve of Concrete Block Units.....	147
Fig. 5.33	Specific Creep-time Curve of Masonry Units for Diaphragm Walls.....	148
Fig. 5.34	Specific Creep-time Curve of Masonry Units for Fin Walls.....	148
Fig. 5.35	Moisture Movement-time Curve of Clay Units.....	149
Fig. 5.36	Shrinkage-time Curve of Calcium Silicate Units	149
Fig. 5.37	Shrinkage-time Curve of Concrete Block Units	150
Fig. 5.38	Moisture Movement/Shrinkage-time Curve of Masonry Units for Diaphragm Walls.....	150
Fig. 5.39	Moisture Movement/Shrinkage-time Curve of Masonry Units for Fin Walls.....	151
Fig. 5.40	Relaxation-time Curve of Prestressing Bars.....	151

CHAPTER 6

Fig. 6.1	Measured and Predicted Creep in Clay Walls.....	179
Fig. 6.2	Measured and Predicted Creep in Calcium Silicate Walls.....	179
Fig. 6.3	Measured and Predicted Creep in Concrete Block Walls.....	180
Fig. 6.4	Measured and Predicted Shrinkage in Clay Walls.....	180
Fig. 6.5	Measured and Predicted Shrinkage in Calcium Silicate Walls....	181
Fig. 6.6	Measured and Predicted Shrinkage in Concrete Block Walls.....	181
Fig. 6.7	Measured and Predicted Prestress Loss in Clay Diaphragm Walls.....	182
Fig. 6.8	Measured and Predicted Prestress Loss in Clay Fin Walls.....	182
Fig. 6.9	Measured and Predicted Prestress Loss in Calcium Silicate Diaphragm Walls.....	183
Fig. 6.10	Measured and Predicted Prestress Loss in Calcium Silicate Fin Walls.....	183
Fig. 6.11	Measured and Predicted Prestress Loss in Concrete Block Diaphragm Walls.....	184
Fig. 6.12	Measured and Predicted Prestress Loss in Concrete Block Fin Walls.....	184

CHAPTER 7

Fig. 7.1	Positions of Demec Studs and Vibrating Wire Gauge on Clay, Calcium Silicate and Concrete Block Masonry.....	207
Fig. 7.2	Water Absorption of Bonded Units Masonry Over 24-hour Period.....	208
Fig. 7.3	Modified Water Absorption in Relation to the Standard Water Absorption	208
Fig. 7.4	Water Absorption of Bonded Clay Units in 2-course Masonry Over 70-day Period.....	209
Fig. 7.5	Water Absorption of Bonded Calcium Silicate Units in 2-course Masonry Over 70-day Period.....	209

Fig. 7.6	Water Absorption of Bonded Concrete Block Unit Over 70-day Period.....	210
Fig. 7.7	Shrinkage-time Curve of Mortar Prisms in Modified Water Absorption Tests	210
Fig. 7.8	Moisture Movement-time Curve of Bonded and Unbonded Clay Units	211
Fig. 7.9	Moisture Movement-time Curve of Bonded and Unbonded Calcium Silicate Units	211
Fig. 7.10	Moisture Movement-time Curve of Bonded and Unbonded Concrete Block Units	212
Fig. 7.11	Shrinkage-time Curve of 3-Course Clay Masonry.....	212
Fig. 7.12	Shrinkage-time Curve of 3-Course Calcium Silicate Masonry....	213
Fig. 7.13	Shrinkage-time Curve of 2-Course Concrete Block Masonry....	213
Fig. 7.14	Shrinkage-time Curve of Mortar in 3-Course Clay Masonry.....	214
Fig. 7.15	Shrinkage-time Curve of Mortar in 3-Course Calcium Silicate Masonry.....	214
Fig. 7.16	Shrinkage-time Curve of Mortar in 2-Course Concrete Block Masonry.....	215
Fig. 7.17	Shrinkage of Bonded/unbonded Ratio-time Curve of Masonry Units.....	215
Fig. 7.18	Shrinkage of Mortar/Mortar Prism-time Curve	216
Fig. 7.19	Shrinkage Reduction Factor of Mortar-Water Absorption for Masonry Made from Dry Units.....	216
Fig. 7.20	Shrinkage Enlargement Factor of Masonry Units-Water Absorption for Masonry Made from Dry Units.....	217
Fig. 7.21	Shrinkage-Specific Creep of Mortar Prisms for Diaphragm Walls.....	217
Fig. 7.22	Shrinkage-Specific Creep of Mortar Prisms for Fin Walls.....	218
Fig. 7.23	Expansion-Specific Creep of Clay Units for Diaphragm and Fin Walls.....	218
Fig. 7.24	Shrinkage-Specific Creep of Masonry Units for Diaphragm Walls.....	219
Fig. 7.25	Shrinkage-Specific Creep of Masonry Units for Fin Walls.....	219
Fig. 7.26	Measured and Predicted Creep-time Curve of Diaphragm Clay Wall.....	220

Fig. 7.27	Measured and Predicted Creep-time Curve of Fin Clay Wall.....	220
Fig. 7.28	Measured and Predicted Creep-time Curve of Diaphragm Calcium Silicate Wall.....	221
Fig. 7.29	Measured and Predicted Creep-time Curve of Fin Calcium Silicate Wall.....	221
Fig. 7.30	Measured and Predicted Creep-time Curve of Diaphragm Concrete Block Wall.....	222
Fig. 7.31	Measured and Predicted Creep-time Curve of Fin Concrete Block Wall.....	222
Fig. 7.32	Measured and Predicted Shrinkage-time Curve of Diaphragm Clay Wall.....	223
Fig. 7.33	Measured and Predicted Shrinkage-time Curve of Fin Clay Wall.....	223
Fig. 7.34	Measured and Predicted Shrinkage-time Curve of Diaphragm Calcium Silicate Wall.....	224
Fig. 7.35	Measured and Predicted Shrinkage-time Curve of Fin Calcium Silicate Wall.....	224
Fig. 7.36	Measured and Predicted Shrinkage-time Curve of Diaphragm Concrete Block Wall.....	225
Fig. 7.37	Measured and Predicted Shrinkage-time Curve of Fin Concrete Block Wall.....	225
Fig. 7.38	Measured and Predicted Prestress Loss-time Curve of Diaphragm Clay Wall.....	226
Fig. 7.39	Measured and Predicted Prestress Loss-time Curve of Fin Clay Wall.....	226
Fig. 7.40	Measured and Predicted Prestress Loss-time Curve of Diaphragm Calcium Silicate Wall.....	227
Fig. 7.41	Measured and Predicted Prestress Loss-time Curve of Fin Calcium Silicate Wall.....	227
Fig. 7.42	Measured and Predicted Prestress Loss-time Curve of Diaphragm Concrete Block Wall.....	228
Fig. 7.43	Measured and Predicted Prestress Loss-time Curve of Fin Concrete Block Wall.....	228
Fig. 7.44	Creep-time Curve of Mortar with Original and Reduced Water/cement Ratio.....	229

Fig. 7.45	Shrinkage-time Curve of Mortar with Original and Reduced Water/cement Ratio.....	229
Fig. 7.46	Creep-water/cement Ratio of Mortar Curve for Calcium Silicate Diaphragm Wall	230
Fig. 7.47	Creep-water/cement Ratio of Mortar Curve for Calcium Silicate Fin Wall	230
Fig. 7.48	Shrinkage-water/cement Ratio of Mortar Curve for Calcium Silicate Diaphragm Wall	231
Fig. 7.49	Creep-water/cement Ratio of Mortar Curve for Calcium Silicate Fin Wall	231

LIST OF PLATES

CHAPTER 4

Plate 4.1	Prestressing Details Of Bar Anchored to the Concrete Base.....	102
Plate 4.2	During Construction of Diaphragm Wall.....	103
Plate 4.3	During Construction of Fin Wall.....	103
Plate 4.4	Prestressing Details Of Bar ^{at} the top of Concrete Capping Beam....	104
Plate 4.5	Clay Brickwork under Test.....	105
Plate 4.6	Calcium Silicate Brickwork under Test.....	106
Plate 4.7	Concrete Blockwork under Test.....	107
Plate 4.8	Masonry Units and Mortar Prisms under Test.....	108

CHAPTER 6

Plate 6.1	Migration of Water to Calcium Silicate Units During Laying.....	185
-----------	---	-----

CHAPTER 7

Plate 7.1	Two-Course Clay and Calcium Silicate Masonry for Modified Water Absorption Test.....	232
Plate 7.2	Concrete Block Unit for Modified Water Absorption Test.....	232
Plate 7.3	Three-Course Clay and Calcium Silicate Masonry for Shrinkage Test.....	233
Plate 7.4	Two-Course Concrete Block Masonry for Shrinkage Test.....	233

NOTATIONS

A_{bw}	area of prestressed brickwork member
A_c	cross-sectional area of concrete
A_b	cross-sectional area of bricks
A_m	cross-sectional area of vertical mortar joints
A_s	area of prestressing bars
A_t	transformed section area
A_w	cross sectional area of masonry
b_y	depth of unit
B	the compressive brick strength
C	number of courses
$C + 1$	number of mortar courses
C_c	creep ratio
C_{cc}	weight of cement
C_{oc}	coefficient of creep
C_s	specific creep of masonry
DL_{mas}	length of Demec gauge used to measure overall strain on masonry (mm)
E_{bw}	elastic modulus of brickwork
E_{by}	modulus elasticity of brick or block
E'_{by}	effective modulus of brick unit
E_m	modulus of elasticity of horizontal mortar joint
E'_m	effective modulus of mortar
E_{mw}, E_{wy}	elastic modulus of masonry
E_s	Young's modulus of steel
E'_{wy}	effective modulus of brickwork
f_{ave}	average prestress on masonry at transfer

$f_{ci,p}$	initial concrete stresses at the position of prestressing tendon
f_k	characteristic compressive strength of masonry
f_o	initial stress
f'_r	reduced relaxation
f_t	total stress at time t under varying stress
f_s	the remaining stress at any time t after prestressing
f_{si}	initial stress
f_{sr}	reduced stress due to relaxation of (steel stress after relaxation)
f_{su}	characteristic ultimate strength of bar
f_{sy}	stress at 1% elongation;
F_R	residual force in the prestressing bars
h, H	height of masonry
K_{ct}	joint to block creep ratio at time t
K_n	creep and shrinkage reduction factor for non-tensioned steel in prestressed concrete
K_{st}	joint to block shrinkage ratio at time t
L	overall length of prestressing bar
m_y	height of mortar joint
n_o	modular ratio at first application of load
P_i	initial load in the member
PL	stress loss
PL_e	tension loss in prestressed concrete
PL_{cr}	creep tension loss
PL_r	relaxation loss of the prestressing wire (Magura's method)
PL_{sh}	shrinkage tension loss
R_w	strain ratio for walls
R_{st}	relaxation of prestressing bar

s	suction rate
S_{by}	axial shrinkage of brick or block
S_m	shrinkage of mortar
S_{wy}	axial shrinkage of masonry
% SR	% relaxation
T	period of frequency
y_1	distance from the neutral axis to the prestressing bar;
w	water absorption
W/C_R	reduced water/cement ratio
W_O	mass of water in the mortar joint
WA	water absorbed by the units from the modified water absorption test
W/C_O	original water/cement ratio
ϕ	creep coefficient
ϵ_c	creep strain
ϵ_{ct}	creep of block per unit stress at time t
ϵ_i	initial elastic strain
ϵ_m	moisture strain (positive for shrinkage)
ϵ_{ov}	overall strain of masonry
ϵ_{sh}	shrinkage strain
ϵ_{st}	shrinkage at time t
ϵ_{sunits}	average shrinkage strain of the units
ϵ_{smas}	average measured shrinkage strain on the masonry
$\epsilon_{smortar}$	shrinkage strain of the mortar
σ_{bw}	stress in brickwork at transfer
σ_{ct}	initial prestress in the block (Tatsa's method)
σ_w	stress in brickwork
$\delta\sigma_{st,r}$	relaxation loss in steel

$\delta\sigma_{st,1}$	local loss in steel (Tatsa's method)
α	ratio of block depth to wall height
α_r	reduction coefficient from Fig. 3.1
χ	aging coefficient
δf_s	change of stress
$\delta\varepsilon$	change of strain

CHAPTER 1

INTRODUCTION

1.1 General

Prestressed masonry is not a new technology as records (Roberts et al 1986 and Shrive 1988a, 1988b) show that it was used some 150 years ago in the construction of Thames Tunnel Project by Marc Brunel. Development of prestressed masonry has been quite slow due to the lack of experience and design guides, and consequently the exploitation of prestressed masonry has also been slow. It was not until the early seventies that the importance of post-tensioned brickwork was fully realized. Since then several tests have been carried out on lateral resistance of post-tensioned diaphragm walls which have proved to be cost effective, in being faster and easier to construct than prestressed concrete, especially in retaining walls and tall single storey buildings that require open spaces (Curtin 1987 and Curtin et.al. 1982a, 1982b).

Like concrete, masonry is capable of resisting high compressive stresses but not tensile stresses. Its ability to resist tensile stresses could be improved by either reinforcing or precompressing the structural element. Precompression has an advantage over normal reinforcement because the whole members is active in resisting the load whereas in normal reinforced only the uncracked section is active. Therefore prestressed members are not only designed to eliminate tensile stresses but also utilise the material effectively and prevent any permanent cracks. Such cracks

may lead to penetration of moisture and thus to corrosion of the reinforcement.

Compared to prestressed concrete, generally it is more common to post-tension masonry rather than pretension. However when pretensioning (Curtin et. al. 1982b and Wass 1969), the bars are stressed first to the required tension and anchored to moulds before the masonry is built around it. When the mortar has reached the required strength, the bars are released and thus the prestressing force is transmitted to the masonry. Pretensioning of masonry is normally carried out in the construction of lintels and beams. In post-tensioned masonry members, the bars are jacked to the required tension and anchored at the ends of the member after the mortar has acquired sufficient strength. Due to time constraint in construction, sometimes post-tensioning is carried out at 14 days instead of 28 days.

Since prestressed masonry is still in its infancy, most of the research being carried out is on the lateral strength of these structures. Other important research aspects such as **prestress loss** in steel bars are still lagging behind that of prestressed concrete.

1.2 Prestress loss in post-tensioned masonry members

It is well established that steel stresses in prestressed concrete structures reduce with time. This reduction of stresses is known as the **prestress loss**. **Prestress loss** is normally expressed in terms of percentage of the initial stress of the prestressing steel. Major **prestress loss** in masonry is primarily due to the deformation of its constituents, only a small amounts due to relaxation of the steel and the prestressing system. Elastic and time-dependent deformation of masonry cause instantaneous and long-term **prestress loss**, respectively. Most loss takes place due to the time-dependent deformation, creep and shrinkage, of the masonry.

Instantaneous loss in prestressed masonry is due to partial effect of elastic

shortening, the effect of anchorage set and frictional loss in the ducts. This type of prestress loss takes place at the transfer of prestressing force from the jack to the member to be stressed and depends mainly on the system used in stressing the prestressing steel. No short-term loss occurs due to elastic shortening if the brickwork is post-tensioned and the bars are stressed simultaneously. This is because the bars are stretched against the masonry member and then locked to the required stress. In cases where more than one prestressing bar is used, loss can be avoided by stressing the bars simultaneously. If the bars are stressed in sequence, the loss in the bars can be avoided by restressing the rod which was stressed initially. Loss due to friction is non-existent in most prestressed masonry members. Slip in anchorage is negligible if the prestressing system uses threaded bar with nuts as the locking device instead of strands with wedges.

Unlike loss at transfer, long-term loss caused by time-dependent deformations is very complicated. This is because of the interdependent factors such as relaxation of the prestressing bar, creep and shrinkage of masonry. Knowledge of **prestress loss** is essential to engineers especially at the design stage where the magnitude of applied stress has to be determined.

1.3 Outline of problem

In spite of the increasing popularity of post-tensioned masonry, only limited information is available on the subject. This is because for the most part, when compared to prestressed concrete, post-tensioned masonry is still at the initial stage even though it started a century ago. Another reason is because loss on site is usually minimised by restressing the bar either on the same day or a few days later and thus there is no real demand for the **actual prestress loss** as far as the engineers are concerned. However, despite the latter reason, **actual prestress loss** which

reflects the substantial behaviour of masonry is necessary for the purpose of long-term behaviour. The fact that brickwork is composed of bricks and mortar complicates the prediction of **prestress loss** because both materials behave differently when subjected to stress.

Although masonry walls of different geometrical cross-sections are increasingly popular, to date research on prestress loss of masonry has been limited to certain masonry members built from a few types of masonry units only. No research has been carried out on calcium silicate brickwork with different geometries in relation to deformation of masonry. The influence of geometry can be quantified by the volume/exposed surface ratio of the masonry, which can indirectly determine prestress loss since creep and shrinkage of masonry depend on drying surface. Creep and shrinkage decrease with an increase in volume/exposed surface ratio. The volume/exposed surface ratio of diaphragm or cavity walls is much lower than of fin walls.

Several researchers have agreed that a detailed study on **prestress loss** in masonry should be carried out in order to gain confidence from practicing engineers, that masonry is as good as other structural materials. *Phipps* (1991) states that whatever practical means are carried out to reduce loss, there is no substitute for an accurate knowledge of the relevant properties of the materials in a wall. *Phipps* (1991) also suggests that measurements should be carried out to make sure that the wall will behave satisfactorily throughout its life span.

Furthermore none of the previous research determines the component loss of prestress. *Shrive* (1988b) states that more research is required before loss of prestress due to creep of the masonry and relaxation of the steel can be calculated to the same level of accuracy and with the same confidence as is currently enjoyed in the design of prestressed concrete members. Further reviews and developments on **prestress loss** are discussed in Chapter 2.

1.4 Purpose and scope of research

The main objective of this research was to quantify prestress loss in post-tensioned masonry members built from clay, calcium silicate and concrete block units with grade (ii) mortar. For each type of masonry three diaphragm and three fin walls were built to determine prestress loss (decreasing load), creep (constant load) and shrinkage (zero load). Other primary aims of this research were:

1. To measure **prestress loss** in the prestressing steel bars due to relaxation of prestressing steel and deformation of masonry. Losses due to relaxation of the prestressing steel and time-dependent deformation of masonry (creep and shrinkage) were quantified separately. Even though creep data are available for unreinforced masonry, creep in prestressed masonry is different because the members are subjected to a higher stress than normal loadbearing members.
2. To investigate the influence of geometry and masonry type on time-dependent deformation and prestress loss in masonry. The masonry strength considered for the test programmes varied from 27 to 100 MPa.
3. To use a composite model theory for predicting long-term deformations in prestressed brickwork, and for predicting prestress loss in masonry.
4. To compare the current methods of prediction of time-dependent **prestress loss** of post-tensioned masonry.
5. To use similar methods developed for prestressed concrete in predicting prestress loss in masonry.

Figures 1.1 to 1.6 represent the box and tee shape sections chosen to meet the above research objectives.

1.5 Definition of variables

Diaphragm wall

A diaphragm wall is formed when two skins of brickwork are joined by cross-ribs at regular interval to form 'box' or I sections. When subjected to bending stresses and shear forces, the skins and the ribs act as flanges and webs, respectively.

Fin wall

Fin walls are formed when deep piers are required to support conventional cavity walls.

Diaphragm and fin walls are suitable for tall single storeys buildings such as sports and assembly halls.

Prestress loss

Prestress loss is defined as the difference between the stresses in the bar at transfer and stresses after all loss has taken place.

Creep

Creep is defined as the gradual increase in strain over long periods of time at constant stress. Creep consists of two components:

1. Basic or true creep which occurs under hygral equilibrium where there is no moisture movement involved.
2. Drying creep that is a result of moisture movement between the member and the surrounding air.

Figure 1.7 shows a typical creep curve for masonry which consists of primary, secondary and tertiary creep. Tertiary creep only occurs at high static stresses i.e 0.6-0.7 of static strength. However primary and secondary creep take

place at normal working loads, i.e 0.2-0.3 of static strength.

Creep is sometimes expressed in terms of creep coefficient (ratio of creep to elastic strain) and specific creep (creep per unit stress).

Moisture movement

Moisture movements (strain/strain) in masonry are a result of the change in volume caused by composite action of moisture movement and carbonation with the surrounding air. Clay brickwork often undergoes a moisture expansion instead of shrinkage which occurs in calcium silicate or concrete block masonry. Figures 1.8 and 1.9 show the moisture movement strain of masonry with time. Moisture movement strains are measured as linear movements.

Relaxation of steel

Relaxation of steel is a loss of tensile stress in a prestressed steel maintained at constant length and temperature.

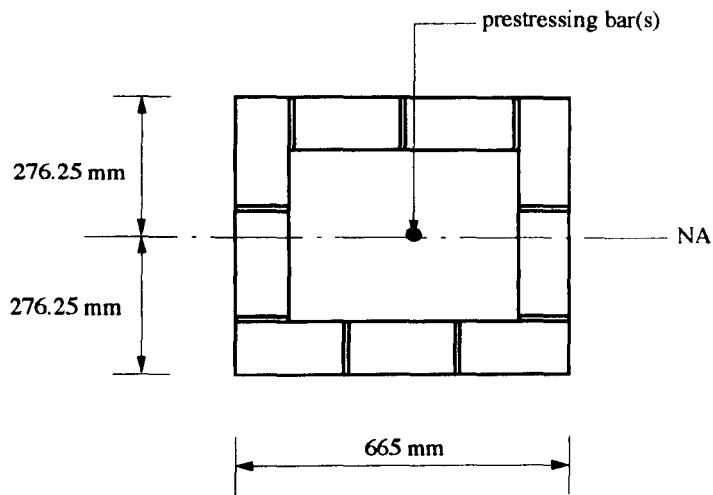


Fig. 1.1 Typical Plan of Clay and Calcium Silicate Diaphragm Wall

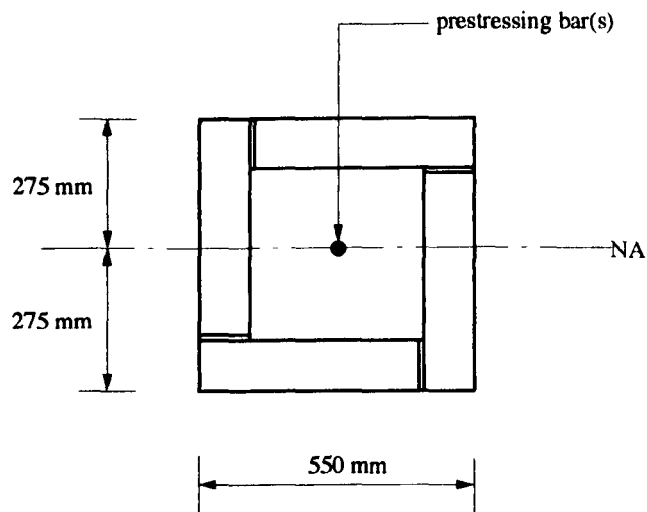


Fig. 1.2 Typical Plan of Concrete Block Section of a Diaphragm Wall

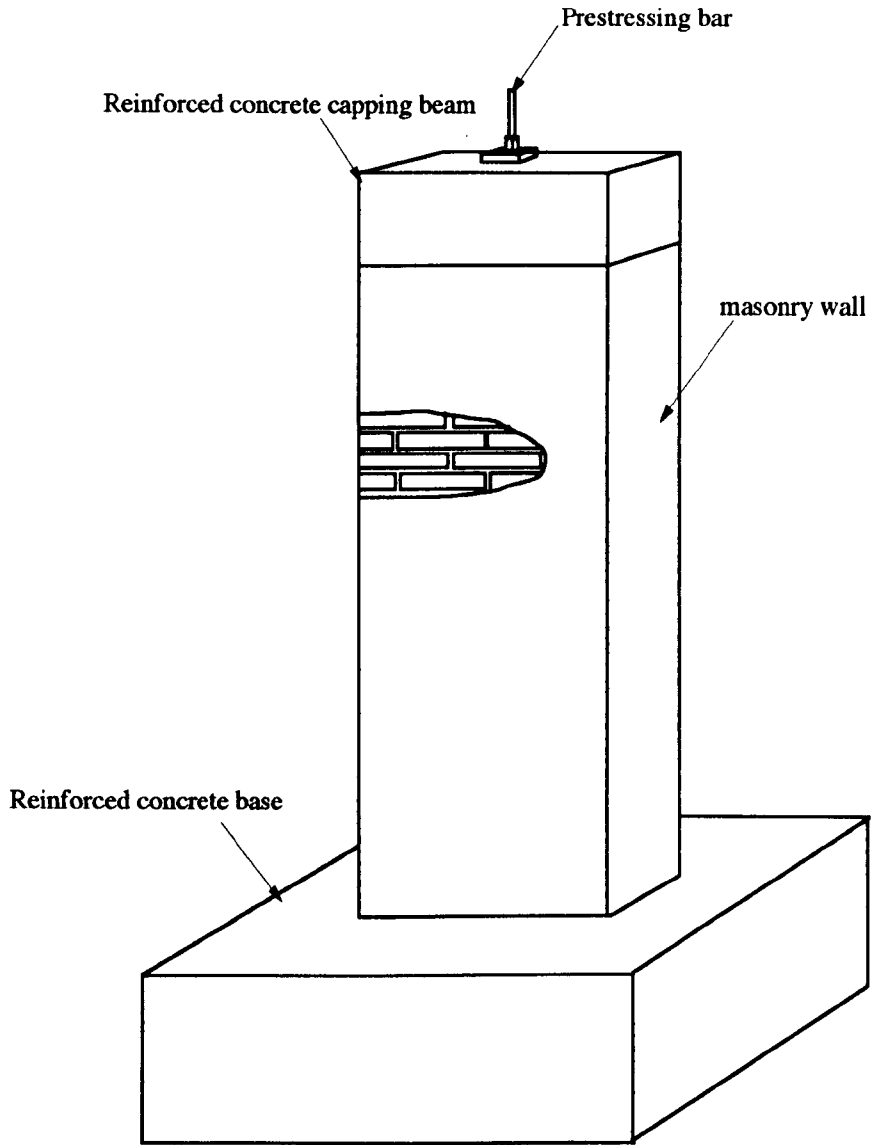


Fig. 1.3 Typical Isometric View of Diaphragm Wall

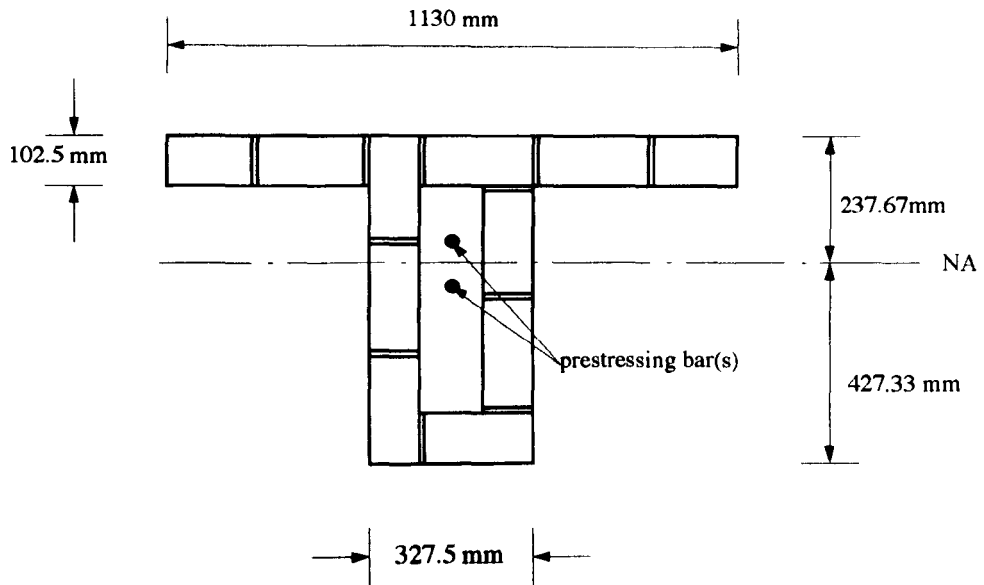


Fig. 1.4 Typical Plan of Clay and Calcium Silicate Fin Wall

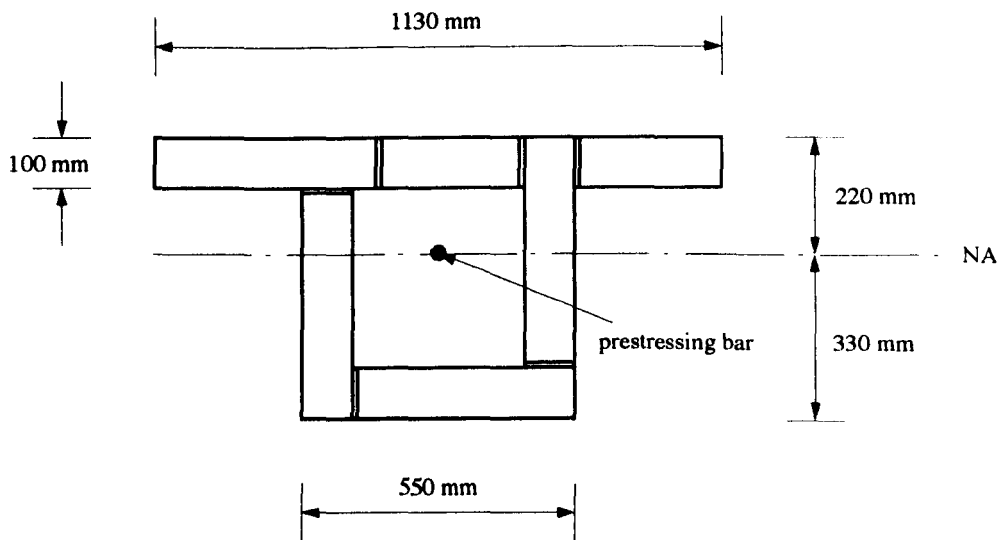


Fig. 1.5 Typical Plan of Concrete Block Section of a Fin Wall

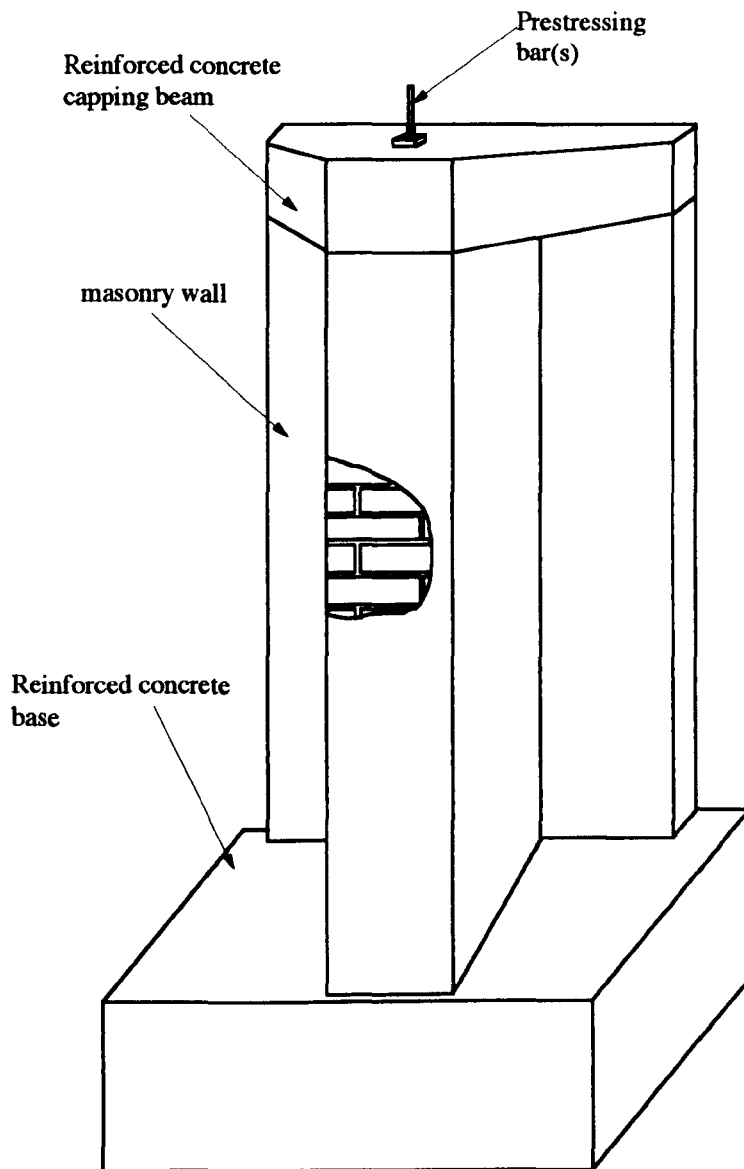


Fig. 1.6 Typical Isometric View of Fin Wall

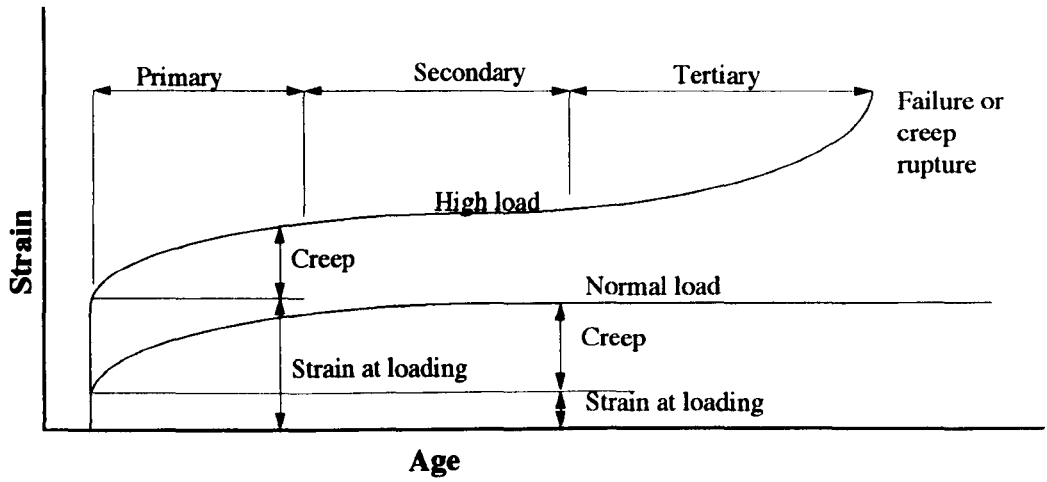


Fig. 1.7 Schematic Creep Curve of Masonry

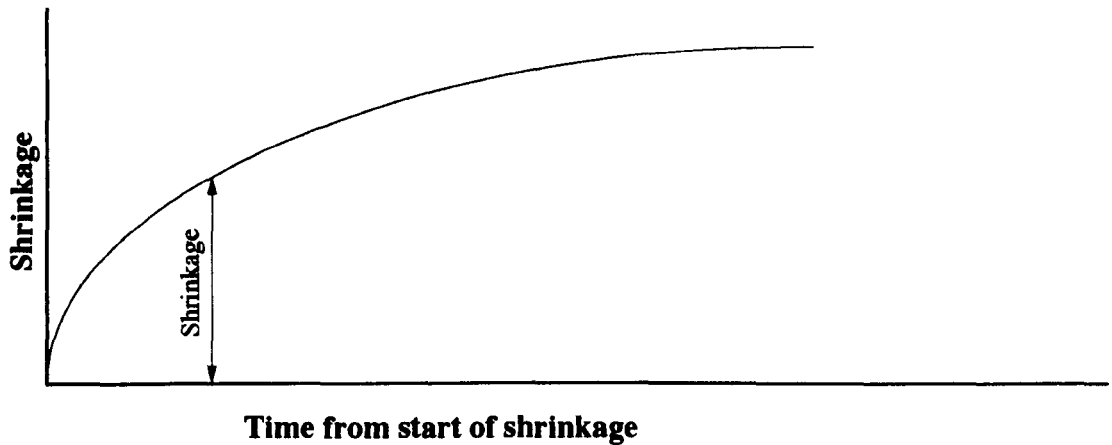
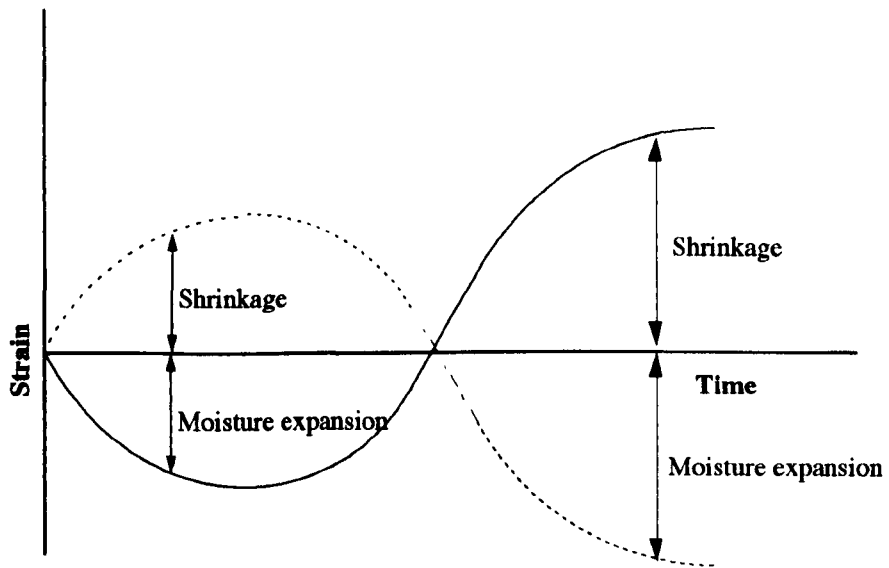


Fig. 1.8 Schematic Shrinkage-time Curve of Calcium Silicate and Concrete Block Masonry



**Fig. 1.9 Schematic Moisture Movement-time Curve of Clay
Masonry**

CHAPTER 2

REVIEW ON TIME-DEPENDENT LOSS OF POST-TENSIONED DIAPHRAGM AND FIN MASONRY WALLS

2.1 Introduction

The prestressing force in steel does not stay constant throughout the life span of the structure. It is necessary to estimate the magnitude of the total stress reduction during the life span of the structure in order to determine all prestress loss at the design stage and evaluate the effective prestressing force. Thus elastic and long-term behaviour of masonry need to be known before any attempt in predicting prestress loss can be made.

2.2 Previous research on prestress loss of masonry

Hendry et al (1987) recommend that loss suggested by BS 5628: Part 2 (1985) should only be used in the absence of specific data. This is because the recommended values are based on limited experience and knowledge of the properties of masonry.

Based on experience with prestressed concrete, Curtin et al (1982a 1982b) recommend a value of 10-15% and 25-30% for losses in fired clay brickwork and concrete blockwork, respectively. Curtin explained that the difference is because

creep of fired-clay brickwork only occurs in the mortar joints. During his early work on post-tensioned masonry pier, Curtin (1987) assumed that the prestress loss was less than in prestressed concrete. However it was assumed that prestress loss due to creep was twice as much. The assumption was made because there is lack of information on prestress loss of masonry.

Recently, however, the value of post-tensioned masonry loss is assumed to be of the order of 20 % (Curtin et al 1989). During a lateral load test on a diaphragm wall, Curtin (1986) loaded the wall using air bags between the diaphragm and a larger reaction wall. On completion of the tests and removal of the lateral load, the reaction wall was destressed to 0.344 MPa and overnight the stress increased to 0.55 MPa. The stress was again reduced to 0.276 MPa and within 24 hours the wall was found to have a stress of 0.3 MPa. The units used were Fletton bricks having a characteristic compressive strength of 25 MPa. The increase of stress was due to creep recovery of the wall. In another test Curtin et al (1991) measured prestress loss in the range of 3.6 to 12.4 % over of a period of 70 weeks i.e the mean loss was 8.8 %. The clay brickwork was made with units having a mean compressive strength of 70 MPa and mortar grade (ii). The loss was assumed to be due to creep only, because the walls were several months old. Curtin (1982 - 1991) used Macalloy bars throughout the tests.

A study on the prestress loss of several months old previously prestressed concrete block walls, where initially the walls were used for lateral load tests, was carried out by Phipps et. al (1976) over a period of 70 weeks. The measured loss was assumed to be due to creep alone. The blockwork, 3 to 4 m high, was built from 10 MPa solid dense aggregate blocks with 1:1:6 mortar. The 4 m high walls were stressed to 1 and 1.5 MPa whereas the 3 m high walls were stressed to 3 and 3.5 MPa. The percentage of prestress loss was in the order of 22%, 20 %, 15% and 13%

for the initial stress levels of 1.0 MPa, 1.5 MPa, 3.0 MPa and 3.5 MPa, respectively. Macalloy bars were used throughout the test.

Tatsa et al (1973) post-tensioned eight cavity walls constructed from hollow and aerated concrete blocks with and without mortar joints in order to study the effect of joints on prestress loss of the block course. The concrete blocks, with compressive strength greater than 2.45 MPa, were used throughout the test and subjected to approximately 45% of their ultimate strength. The prestressing steel had relaxation loss of 4.5% after 2 weeks, 6.3 % after two months and 6.5 % after 6 months. The elastic modulus of the prestressing steel was in the range of 200 GPa. The walls, ranging from 0.9 to 3 m high, were subjected to 0.98 - 1.47 MPa stress with a 1:2:9 (cement:lime:sand) mortar. Tatsa compared the measured loss of up to 20% with theoretical expressions which gave about 12.5 %. The theoretical expression developed by Tatsa will be discussed in Chapter 3.

Taneja (1986) carried out 3-D finite element analysis involving a time-step procedure in estimating long-term prestress loss in post-tensioned brick and concrete block walls. The time-step procedure is to allow time interaction of dependent loss due to creep and shrinkage of the masonry and steel relaxation. The maximum loss in blockwork and brickwork were predicted to be in the order of 30% and 20%, respectively. It should be noted however that the aging coefficients used for the finite element models are of those for concrete. Shrive (1988b) predicted the loss in the same bricks and blocks using an equation developed by Ghali et al (1986) in predicting loss for partially prestressed concrete. The maximum difference between the two methods was about 4% which was attributed to the finite element method allowing for stress concentration near the anchorages. An aging coefficient of 0.8 was used for creep, shrinkage and relaxation. The equation claimed to give good predictions by Taneja but no experimental verifications were carried out.

A series of tests designed to study the effect of brick, stress level of

brickwork at transfer and geometry on the loss of prestress in post-tensioned clay brickwork walls, columns and beams were carried out by Lenczner (1986a). The walls were constructed from Fletton and Ibstock units with compressive strength of 34 and 119 MPa, respectively. The walls were post-tensioned after 28 days of laying and the stress loss ceased after 150 days in Fletton walls, 175 days in Ibstock walls and after one year for both Fletton and Ibstock columns. Lenczner concluded that the loss of prestress varies from 11 to 15 % in prestressed walls, 8 to 10 % in prestressed columns and 12 % in prestressed beams. When compared to his theoretical method the calculated loss gave a good agreement with the measured loss especially in Fletton walls and columns. The recommended method proposed by Lenczner will be also discussed in Chapter 3.

In another study Lenczner et al (1988) measured stress loss in walls that had been prestressed earlier for a period of one year. The walls were later destressed and prestressed again to about 20 % higher than the previous stress level. The walls were 20 courses high with a $1:\frac{1}{4}:3$ of mortar mix. The units were Butterley bricks with a mean compressive strength of 68 MPa. It was observed that the walls experienced a lower loss in the second stage of prestressing even though they were subjected to a higher level of stress. This is because most of the creep has taken place at early age. When his method was used to predict the second loss the theoretical values gave higher estimates than the measured ones. After 100 days from the second post-tensioning the increase in creep was negligible. Lenczner concluded that only about one eighth of the prestress loss occurs in post-tensioned walls having a stress history.

Using a similar equation, Lenczner (1986a, 1985) reported that prediction of prestress loss on various types of brick walls and columns are closer to the loss measured experimentally than those given by BS 5628: Part 2 (1985). The predicted loss was overestimated by a factor of 1.46 in walls and columns by a factor of 1.65 according to BS 5628: Part 2 (1985).

Harvey and Lenczner (1993) measured prestress loss in concrete block masonry walls and columns built from grade (i), (ii) and (iii) mortar over 1 year period. The concrete masonry was post-tensioned using Macalloy bars. The prestress loss ranged from 7% to 37%, where the columns exhibited lower prestress loss than the walls. Details of the prestress loss is shown in Table 2.1.

Based on volume changes of masonry, VSL International (1991) predicted loss of prestress for clay and concrete masonry at 7 % and 18 %, respectively. The prediction was based on the use of high strength steel strands instead of high strength bars. It is normal to use bars compared to strands in prestressed masonry because of difficulty in construction when using the latter.

It is interesting to note that Foster (1970) used low tensile steel in prestressed masonry cylindrical water tank. He estimated the loss of stress due to friction in the ducts to be about 37 % of the allowable working stress but only about 0.4 % due to creep (due to the low stress). Foster however allowed more than 10% loss due to relaxation of steel. The water tank was constructed of class A engineering clay bricks with a $1:\frac{1}{4}:3$ ordinary Portland cement:hydrated lime: sand mortar. The tank was stressed vertically and circumferentially by stressing steel of 7 mm diameter wires.

Table 2.1 shows the summary of previous research on prestress loss of masonry.

2.3 Factors affecting prestress loss of post-tensioned masonry

Basically, long-term prestress loss of post-tensioned masonry depends on the magnitude of deformations of its components with time, i.e masonry units, mortar and prestressing steel. Different masonry units undergo different deformations because of their compositions and manufacturing process. For example, moisture expansion in clay units can cause the brickwork to expand instead of contract as in

calcium silicate and concrete blocks units. The three main components of time-dependent prestress loss in masonry are creep, shrinkage/moisture expansions and relaxation. Creep and shrinkage of calcium silicate and concrete block masonry cause a reduction in the stress of the prestressing bars (Roberts et al 1986).

Another factor, which is not considered in this study, is diurnal effect (daily temperature and humidity variations) on prestress loss in masonry. The effect is similar to that of shrinkage in term of volumetric changes. An increase in temperature induces additional stress in post-tensioned masonry. However, the effect of temperature is not critical in cases of normal prestress levels. Diurnal effect is generally reversible and depends not only on the range of exposed temperature but also on the initial temperature and moisture content of the units at laying. BS 5628: Part 3 (1985) recommends thermal coefficients varying from 5×10^{-6} to 15×10^{-6} per °C in masonry to be used in determining diurnal effect. Jessop (1980) suggested that thermal expansions are typically 5×10^{-6} to 7×10^{-6} per °C for clay bricks and 6×10^{-6} to 13×10^{-6} per °C for concrete blocks. In extreme cases the range of temperature of clay masonry could get up to 105 °C (British Development Association 1988). Thus the expected expansion in the clay masonry can be as high as 525×10^{-6} and this could result in an 18% increase in the stress of the prestressing bars (see Appendix A.1).

2.3.1 Creep of masonry

Although there has been an increase in the usage of the vast range of type of units used for prestressed masonry, limited knowledge is available on creep of masonry, and most research has been on clay brickwork. Most researchers (Lenczner 1981, Shrive et al 1981 and Jessop 1980) assumed that masonry undergoes creep in a similar manner to concrete. Neville et al (1983) defines creep in concrete as the additional strain with time due to constant stress, and creep consists of

two components: basic (true) and drying creep. Basic or true creep occurs under hygral equilibrium when no moisture movement is involved. Drying creep is due to moisture movement between the member and the surrounding air. In structural concrete, basic and drying creep take place simultaneously, whereas in mass concrete only basic creep occurs. Consequently, basic and drying creep (or expansion creep in the case of clay brickwork) are likely to occur in brickwork with the exception of covered foundations etc. where basic creep would occur.

2.3.1 (a) Mechanisms of creep

Jessop (1980) believed that the mechanism of creep in masonry is basically the same as in concrete which is due to a combination of moisture transfer (within the gel structure) and collapse of gel structure in cement paste. Lenczner (1986a) states that creep in brickwork is due to the internal seepage of absorbed layers of water in the mortar and to a much lesser extent, a crystalline rearrangement of the brick matrix under pressure of the externally applied load.

2.3.1 (b) Factors affecting creep

Creep is influenced by the material properties such as composition of the units, type and proportion of mortar, suction rate, water absorption, magnitude of stress, relative humidity and temperature (before and after loading), and other time-dependent factors such as age of member when loaded, duration of loading and geometry. The method of curing affects creep, e.g autoclaved blocks creep less than low pressure steam-cured blocks.

This section is primarily concerned with the influencing factors which were experimentally investigated in this research programme such as masonry unit strength, shape and size, suction rate and water absorption. The effect of masonry

shape and size, and type is studied in Chapter 4, whereas investigations on the effect of suction rate and water absorption are being carried out in Chapter 7.

Effect of Shape and Size

Lenczner (1978-1990) has made a major contribution in quantifying creep of masonry. Lenczner (1970,1978,1981,1990) observed that plain masonry wall creep more than piers. Based on a series of tests, Lenczner (1978b) reported that creep coefficients for brickwork and blockwork piers and cavity walls were in the range of 2 -2.4. For single-leaf walls the creep coefficients varied from 3-4. The brick and block units had compressive strengths of 56 and 3.3 MPa, respectively. In another report Lenczner (1981) suggested an empirical method ^{for} predicting creep in masonry hollow piers, single leaf and cavity walls .

Brooks (1988, 1990a, 1990b) quantified shape and size of masonry in term of its volume/exposed surface ratio (V/S). The V/S ratio simulates the average drying path length of moisture. Thus larger sections dry more slowly and exhibit a lower shrinkage and creep. In a series of tests, Brooks et al (1990a, 1990b) observed that the creep of masonry is similar to concrete in that it decreases with an increase of V/S ratio. Brooks et al (1988) measured the relative creep of clay brickwork which ranged from 1.64 (single leaf wall):1.44 (cavity wall):1.07 (hollow pier):1 (solid pier) for V/S ratios of 44, 51,78 and 112 mm, respectively. For the same range of V/S ratio as in clay brickwork (Brooks et al 1990a, 1990b), the relative creep in calcium silicate and concrete blockwork were in the range of 1.63 (single leaf wall):1.50 (cavity wall):1.13 (hollow pier):1 (solid pier), and 1.55 (single leaf wall):1.40 (cavity wall):1.35 (hollow pier):1 (solid pier), respectively.

The different creep values for different V/S ratios demonstrates the influence of geometry and recommendations for single values of creep coefficient are not sufficient. Table 2.2 shows creep of plain masonry with different V/S ratios.

Since limited work has been carried out to study the effect of shape and size on creep of brickwork, it is appropriate to review its effect for concrete (see Section 2.4).

Effect of masonry unit

As stated earlier, Lenczner (1978b) observed that creep coefficients in clay brickwork and concrete blockwork were of the order of 2 - 4, the higher value being concrete blockwork. Lenczner (1978a) also developed an empirical method based on units strength for predicting creep. The method does not allow for different mortar types.

Brooks et al (1992a) reported creep of various strengths of clay walls. The walls were built from 30-120 MPa clay units and subjected to a stress of 1.5 MPa. The estimated ultimate creep coefficients for these single-leaf brick walls varied from 0.9 - 6.7. Abdullah (1989) monitored creep of walls subjected to 1.5 MPa stress, built from three different types of masonry i.e clay, calcium silicate and concrete blocks. The clay and calcium silicate brick and concrete block units had a compressive strength of 93.7, 25.4 and 13.0 MPa, respectively. He observed that concrete blockwork exhibited more creep than clay and calcium silicates brickwork. The estimated ultimate creep coefficients in clay and calcium silicate brickwork and concrete blockwork varied from 4.2 - 4.9, 2.7 - 3.5 and 3.0 - 3.9, respectively. Table 2.3 shows the effect of unit strength on creep (in terms of creep coefficient).

Effect of suction rate and water absorption

Warren and Lenczner (1981) carried out creep tests for single-leaf walls built from seven different types of clay units and a 1: $\frac{1}{4}$:3 mortar, where the walls for two of the brick types were soaked before laying. It was found that walls built with soaked units exhibited a lower strain ratio $\left(\frac{\text{elastic strain} + \text{creep}}{\text{elastic strain}}\right)$ than

those laid dry. In one case (Fletton) that was laid dry, Warren and Lenczner (1981) found that the wall exhibited a higher strain ratio (5.32) than that of the same wall laid wet (2.68). However, the tests were not carried out at the same time and the experimental details for one of the tests (for example unit strength) are not available.

Based on tests of six different types of clay brickwork, Johnson (1984) recommended a hyperbolic equation that expressed overall strain (creep and shrinkage) of seven course masonry in terms of suction rate and water absorption of the bricks. The overall strain (ϵ_{ov}) was in the following form:

$$\epsilon_{ov} = \frac{(b \sigma + a) t}{(-b \sigma' + a') + t}$$

where $a = 941.05 (w/s)^{-0.493}$

$$b = 107.98 \left[\frac{5(7.55 + w)}{54} - \left(\frac{2(7.55 + w)}{54} \right)^2 \right]$$

$$a' = 213.365 \left[\frac{4(w/s)}{74} - \left(\frac{2(w/s)}{74} \right)^2 \right]$$

$$b' = 30.957 \left[\frac{4(w/s)}{75} - \left(\frac{2(w/s)}{75} \right)^2 \right]$$

w = water absorption

and s = suction rates

According to Johnson (1984), the effect of suction rate and water absorption is quite complex: one would expect a porous brick to cause a higher creep in masonry than a dense brick. However, this is not always true as demonstrated below that both bricks might exhibit similar (low) creep despite the difference in

properties. Since suction rate and water absorption are correlated, Johnson (1984) gave the following general recommendations in determining creep:

Water Absorption (%)	Specific Creep
less than 7.0	75×10^{-6}
7.0 - 25.0	150×10^{-6}
Over 25.0	75×10^{-6}

2.3.2 Moisture movement of masonry

A clay brick fresh from the kiln, after firing within the range of 950°C and 1220°C, is bone dry, and when it comes into contact with moist air it will absorb moisture until moisture equilibrium is reached (Lenczner 1972). The absorption of moisture is accompanied by volume expansion in the clay bricks which is termed irreversible moisture expansion. On the other hand, calcium silicate or concrete blocks units slowly lose moisture after manufacture and exhibit shrinkage. Moisture movement strain in clay masonry may be moisture expansion or shrinkage depending on the types of clay unit and the shrinkage of mortar. However, concrete and calcium silicate masonry always undergo shrinkage.

There are three types of shrinkage in masonry namely carbonation, drying and plastic shrinkage. Reaction of carbon dioxide in atmosphere with calcium silicate hydrate in cement paste is accompanied by a shrinkage known as carbonation. Drying shrinkage occurs when moisture is lost from hardened mortar or concrete and calcium silicate units. However carbonation and drying shrinkage cannot be separated. Plastic shrinkage takes place when mortar is 'plastic' due to losses of free water before setting. This research is only concerned with drying and carbonation shrinkage.

Masonry units undergo reversible moisture movements when subjected to wetting and drying. Wetting and drying generally cause an expansion and contraction of the masonry units.

2.3.2 (a) Mechanism of moisture movement in masonry

Moisture movement strain is mainly due to moisture movements which cause the volume of the units to vary. Moisture absorbed or dissipated by the specimens results in expansion or contraction respectively. Jessop (1980) explained that the dimensional changes were due to interaction of water molecules and internal surfaces of the material. These movements are affected by the concentration of water molecules and the exposed surface area of the material. The amount of water absorbed increases with concentration of water molecules in the atmosphere (relative humidity) and the internal surface area of the material. Permanent moisture expansion in clay brickwork is due to the physical adsorption of water and possibly due to chemical reactions between water and certain constituents of ceramic bodies. Moisture movement in clay masonry is treated separately in the following section due to the different nature of moisture movement in fired-clay masonry as compared to calcium silicate and concrete block masonry.

Moisture expansion of clay bricks

A change in volume of clay bricks is often neglected in design. Clay brick units experience irreversible moisture expansion, that continues even years after manufacture, and reversible expansion and contraction that is caused by wetting and drying. Newly fired clay bricks absorb moisture and thus expand on exposure to air. Most of the moisture expansion take place within a few hours of the brick leaving kiln and slows down as time progresses. Most of the long term moisture expansion of

clay units takes place within the first 6 months.

Foster (1991) reviewed several research publications from 1938 to 1980 on the importance of moisture expansion for design of clay brickwork. They stated that moisture expansion in the design of modern loadbearing brickwork structures needs to be considered. Previously, walls were thicker than the contemporary brickwork, which resulted in negligible effects from moisture expansion. Foster et al (1982) suggested ranges of time-dependent irreversible moisture expansion as follows:

High	600×10^{-6} to 1080×10^{-6}
Medium	360×10^{-6} to 600×10^{-6}
Low	360×10^{-6}

It has been reported that for walls of 6 and 7 years old, the expansion could be as high as 2000×10^{-6} (Lenczner 1986b). Such magnitude of expansion should definitely be considered in the design so as to avoid any structural failure.

Based on several tests from other researchers on different types of clay unit and methods of tests, Jessop (1980) concluded that reversible moisture strain in clay masonry, between completely dry and saturated states, lies in the range of 70×10^{-6} to 200×10^{-6} .

Shrinkage of calcium silicate bricks and concrete blocks

Unlike clay, calcium silicate bricks shrink on exposure to air. However limited work has been done on the shrinkage behaviour of calcium silicate bricks. A shrinkage strain of 210×10^{-6} was observed by Brooks (1986b) over a period of 300 days. Using an equation that expresses shrinkage as a hyperbolic function of time, the ultimate strain (based on measured shrinkage) was estimated as 232×10^{-6} . When the estimated ultimate strain is compared to the predicted values using composite modelling (see Section 3.5), there was a reasonable accuracy.

Based on work by other researchers, Baker et al (1982) concluded that concrete masonry exhibits considerably higher irreversible moisture strains than clay masonry. The permanent shrinkage in concrete masonry is in the order of 350×10^{-6} to 600×10^{-6} . It is thought that this shrinkage is mainly due to carbonation. Brooks et al (1990a) reported similar values of shrinkage to that of concrete, for concrete blockwork walls and piers constructed from a dense aggregate block.

2.3.2 (b) Factors affecting moisture movement strain

Moisture movement strain of masonry is partially reversible. Jessop (1980) explained that in clay brick units other factors such as manufacturing process in particular temperature of firing, time of exposure, time of laying, mortar, humidity, temperature, cyclic wetting and drying, and clay components all contribute to volume changes. To avoid problems with moisture expansion, bricks are normally laid at least 2 weeks after leaving the kiln. Moisture expansion increases as the relative humidity increases.

Jessop (1980) also stated that for concrete blocks, time of exposure or laying, the method of curing, moisture content, relative humidity, types of aggregate and mortar joints affect shrinkage. Saturated autoclaved block units tend to have less moisture movement strain than saturated blocks cured in low pressure steam. The main reason for autoclaving in concrete blocks is to minimise shrinkage. The longer blocks are left to stand before laying the lower the shrinkage in the walls. Blocks made from sand and gravel aggregate show the least shrinkage, because as in concrete, shrinkage mostly takes place in the cement paste and aggregate tends to restrain shrinkage because of its stiffness. Jessop also explained that walls built with weak mortar tend to exhibit twice as much shrinkage as walls built with strong mortar.

Brooks et al (1990a, 1990b) verified experimentally that shrinkage of calcium silicate and concrete blocks units are influenced by the geometry of the masonry which can be expressed as the V/S ratio of the members as discussed in the following section. As in creep, suction rate and water absorption also affect shrinkage of masonry and these parameters are investigated in Chapter 7.

Effects of shape and size

Bingel (1984) reported that an increase in the V/S ratio generally resulted in a lower shrinkage in both calcium silicate and concrete masonry. Based on tests of Fletton clay, calcium silicate and lightweight concrete masonry, Bingel concluded that axial shrinkage of calcium silicate brickwork and lightweight concrete blockwork was linearly related to V/S ratio but Fletton clay brickwork did not follow this trend. Table 2.4 shows the influence of geometry on shrinkage of several concrete blockwork members.

Brooks et al (1985) observed that axial shrinkage of calcium silicate and light-weight concrete block masonry (S_{wy}) depended on size and was related to the V/S ratio. For calcium silicate brickwork:

$$S_{wy} = x - y \left[\frac{V}{S} \right] \quad (2.1)$$

where x and y are expressed as hyperbolic function of time t (days):

$$x = \frac{100t}{(81 + 0.81t)}$$

$$\text{and } y = \frac{t}{(9.5 + 0.51t)}$$

The axial shrinkage of lightweight concrete blockwork was given by:

$$S_{wy} = x' - y' \left[\frac{V}{S} \right] \quad (2.2)$$

where x and y are expressed as hyperbolic function of time t (days):

$$x' = \frac{100t}{(8 + 0.15t)}$$

and
$$y' = \frac{t}{(9.3 + 0.3t)}$$

Shrinkage decreases with an increase in the V/S ratio because it takes longer time for moisture to diffuse from a larger section (Brooks et. al 1988, 1990a and 1992b). The rate of shrinkage decreases as the relative humidity increases.

Brooks (1986b) suggested that the V/S rates effect could be predicted using composite modelling which considers the separate behaviour and properties of mortar and bricks. The model was verified experimentally on a single-leaf Fletton wall and the experimental data results were modified by a factor to allow for the effect of the V/S ratio. Following this experiment, Brooks et al (1990a, 1990b) further verified the composite model by measuring the unbonded properties of moisture movement of both the units and the mortar when these were partly sealed according to the V/S ratio of the single-leaf Fletton wall.

Lenczner (1978b) observed that the vertical moisture strain for a single-leaf clay brickwork wall and a pier were about approximately the same. However the vertical moisture strain in a blockwork pier was much higher than in the blockwork walls. Since limited work had been carried out to study the effect of shape and size on shrinkage of brickwork, it is appropriate to review its affect in concrete (see Section 2.4)

Effect of masonry unit

Lenczner (1978b) reported that the vertical moisture strains in blockwork were about 5-6 times higher than in brickwork. In certain cases, blockwork shrinkage can exceed the combined elastic and creep strain.

Brooks et al (1992a) reported that generally weaker clay unit walls tend to exhibit long-term expansion, while the stronger unit walls tended to show long-term shrinkage. Initially low unit strength brickwork undergoes shrinkage, followed by moisture expansion. It was observed that moisture expansion was higher in Fletton brickwork than in the unbonded units, which suggested an interactive effect between mortar and unit.

In a series of tests with various strengths of masonry unit, Abdullah (1989) observed that concrete blockwork undergoes greater vertical moisture movement as compared to clay or calcium silicate brickwork. The clay, calcium silicate and concrete block units had compressive strengths of 93.0, 25.4 and 13.0 MPa, respectively.

Effect of suction rate and water absorption

Based on tests of different types masonry, Johnson (1984) concluded that shrinkage in masonry increases with suction rate and water absorption. Johnson (1984) explained that moisture from the mortar joint is lost to the external atmosphere via diffusion through the brick. Initially the moisture (in liquid water) is transferred to the brick during laying through the liquid water absorption from the wet mix. When the mortar has set, the liquid water is by now in the form of vapour, the water vapour in the mortar joint will diffuse through the brick from the mortar and continues to do so during drying process.

The following are general guidelines relating (Johnson 1984) shrinkage and water absorption:

Water Absorption (%)	Shrinkage
less than 7.0	150×10^{-6}
7.0 - 25.0	300×10^{-6}
Over 25.0	300×10^{-6}

2.3.3 Relaxation of prestressing steel

Prestressing steel loses stress with time when subjected to constant strain. Such loss in steel is referred^{to} as relaxation loss which is affected by the ratio of initial stress to the yield strength of the steel. Under constant strain, the term intrinsic relaxation is used, but actual relaxation in prestressed structures is very complicated because the stress is continuously changing due to the deformation of the prestressed materials. Several investigations on relaxation of prestressing wire strands have been carried out but data on relaxation of bars is limited.

Most of the research on relaxation of steel wires was carried out by Magura et. al (1964). Based on 501 individual tests investigating stress relaxation of hot rolled and cold drawn wires, Magura concluded that relaxation is not short lived but may continue indefinitely at a diminishing rate. It was observed that relaxation may be neglected if the steel is stressed to less than 50% of its tensile strength. Glodowski and Lorenzetti (1972) observed that the method suggested by Magura et al does not predict-short term relaxation as accurately as long-term relaxation. As a result they proposed a method for predicting long-term relaxation loss based on short-term stress relaxation.

Part II

BS 5628^{Part II}(1985) recommends that loss of prestress due to relaxation may be assumed as the maximum relaxation of the tendon after 1000 hours duration obtained from the manufacturer's certificate of approval. However, clause 4.8.2.1 of BS 8110 (1985) suggests that prestress loss in concrete due to steel relaxation be obtained by multiplying relaxation factors with the 1000 hour relaxation test values.

Al-Khaja (1986) found that relaxation loss predicted by BS 8110 (1985) tends to overestimate the measured prestress loss and suggested the use of the previous British Code CP110 in allowing the 1000 hour relaxation loss to be the

maximum long-term relaxation.

Besides being influenced by the initial stress/strength ratio, Magura et al (1964) also concluded that relaxation is influenced by pre-stretching, temperature, types of steel and duration of sustained prestress force. It was observed that as the initial stress increases, the relaxation loss increases at an increasing rate. Pre-stretching influences relaxation loss only if the steel is stretched for a period of time. The temperature effect is negligible if the bars are stressed at normal temperature. Section 3.6 presents two major methods, both consider the effect of initial stress/strength ratio in predicting loss due to relaxation of prestressing bars.

2.4 Effect of shape and size on creep and shrinkage of concrete

Extensive work has been carried out on the effect of shape and size on creep and shrinkage of concrete. A full review of previous work is given by Branson (1977), Neville (1983) and Abdullah (1989).

There are two approaches available in taking into account the effect of shape and size in predicting creep and shrinkage in concrete, i.e average thickness and volume/exposed surface area (V/S) method. The average thickness method is suitable for members with average thickness up to 300 to 380 mm. Branson (1977) summarised previous work on the creep and shrinkage correction factors as in Table 2.6. Branson also expresses the creep and shrinkage correction factors (C.F.)_T for short and long-term period as follows:

$$\text{Creep (C.F.)}_T = 1.14 - 0.023T \quad \text{for } \leq 1 \text{ year loading}$$

$$\text{Creep (C.F.)}_T = 1.10 - 0.017T \quad \text{for ultimate values}$$

$$\text{Shrinkage (C.F.)}_T = 1.23 - 0.038T \quad \text{for } \leq 1 \text{ year drying}$$

$$\text{Shrinkage (C.F.)}_T = 1.17 - 0.029T \quad \text{for ultimate values}$$

where T = average thickness (mm)

The V/S method is recommended for larger members, i.e average thickness greater than about 30 to 38 mm. Table 2.7 shows the creep and shrinkage correction factors by using the V/S method (Branson 1977). Hansen et al (1966) and Committee of Prestress Losses (1975) recommend the use of the following creep and shrinkage correction factors:

$$\text{Creep (C.F.)}_T = 1.12 - 0.08 \left[\frac{V}{S} \right] \quad \text{for } V/S \geq 38 \text{ mm}$$

$$\text{Shrinkage (C.F.)}_T = 1.14 - 0.09 \left[\frac{V}{S} \right] \quad \text{for } V/S \geq 3.8 \text{ mm}$$

**Table 2.1 Experimental Work on Prestress Loss of Post-tensioned
Masonry by Previous Researchers**

Researchers (Year)	Masonry type and Strength (MPa)	Geometry	Mortar Mix (cement:li- me:sand)	Applied Stress (MPa)	Loss due to creep	Loss due to shrink- age	Loss due to relaxat- ion	Total Loss
Harvey and Lenczner (1993)	Concrete Block (12.36)	Walls	1:1:6	0.43	-	-	-	36.76%
		Columns		0.44			18.11%	
	(12.48)	Walls	$1:0\frac{1}{2}:4\frac{1}{2}$	2.19				18.37%
		Columns		2.24			7.15%	
	(11.54)	Walls	$1:\frac{1}{4}:3$	3.29				30.50%
		Columns		2.54			11.86%	
Curtin (1991)	Clay (70)	Diaphragm	$1:0\frac{1}{4}:3$	3.31	7.8 %	-	1 %	8.8 %
Lenczner (1986)	Fletton (34)	Walls	$1:\frac{1}{4}:3$	4.42-5.87	-	-	-	11-17%
		Columns						9-10%

Table 2.1 Continued

Researchers (Year)	Masonry type and Strength (MPa)	Geometry	Mortar Mix (cement:lime:sand)	Applied Stress (MPa)	Loss due to creep	Loss due to shrinkage	Loss due to relaxation	Total Loss
Lenczner (1986)	Ibstock (119)	Walls	$1:\frac{1}{4}:3$	3.41-7.76	-	-	-	9-11%
		Columns						8%
	Butterley (68)	Walls		5-6.18				13-14%
		Columns		10%				
Phipps (1976)	Concrete Blockwork (10)	Diaphragm	1:1:6	1-1.5 3-3.5	-	-	-	22-20 % 15-13 %
Tatsa (1973)	Concrete Blockwork (2.48)	Walls	1:2:9	0.98-1.47	-	-	-	20 %

Table 2.2 Effect of Geometry on Creep of Plain Masonry

Researcher	Masonry Type	V/S (mm)	Unit Type and strength (MPa)	Mortar cement:lime:sand	Ultimate Creep Coefficient
Lenczner (1978,1990)	pier	-	Rustic Brown (56)	1: $\frac{1}{4}$:3	2.23
			Aglite Block (3.3)		3.46
	wall	-	Fletton (23)		1.91
			Fletton (23)		3.94
			Aglite Block (3.3)		2.14
			Rustic Brown (56)		2.41
Brooks et al (1990a 1990b)	single leaf wall	44	Clay (93.7)	1: $\frac{1}{4}$:3	3.20
	cavity wall	51			3.91
	hollow pier	78			3.48
	solid pier	112			3.21
	single leaf wall	44	Calcium Silicate (25.4)	1: $\frac{1}{4}$:3	2.51
	cavity wall	51			2.22
	hollow pier	78			1.96
	solid pier	112			1.69
	single leaf wall	44	Concrete Block (13)	1: $\frac{1}{4}$:3	2.88
	cavity wall	51			2.29
	hollow pier	78			2.05
	solid pier	112			1.96

Table 2.3. Effect of Unit Type on Creep of Plain Masonry

Researcher	Unit Type and strength (MPa)	Mortar cement:lime:sand	Estimated Ultimate Creep Coefficient
Lenczner (1978)	Rustic Brown (56)	1: $\frac{1}{4}$:3	2.23-2.41
	Aglite Block (3.3)		2.14-3.46
	Fletton (23)		1.91-3.94
Abdullah (1989)	Clay (93.7)	1: $\frac{1}{4}$:3	3.20-3.91
	Calcium Silicate (25.4)		1.69-2.51
	Concrete Block (13)		2.05-2.88
Brooks et. al.(1992a)	Fletton (28.20)	1: $\frac{1}{4}$: $\frac{1}{4}$	1.4
	Birtley Old English (31)		0.9
	Dorket Honeygold (54)		3.0
	Smooth Red (92.2)		3.0
	Nori (108)		4.6
	Waingrove Smooth Red (123.7)		6.7

Table 2.4 Effect of Geometry on Shrinkage of Plain Masonry

Researcher	Member	V/S (mm)	Unit Type and strength (MPa)	Mortar cement:lime:sand	Estimated Ultimate Shrinkage (10 ⁻⁶)
Lenczner (1990)	pier		Fletton (28.69)	1:¼:3	-125
	wall		Fletton (28.69)		-146
Lenczner (1978)	pier		Butterley (56)		99
			Aglite Block (3.3)		637
	wall		Butterley (56)		81
			Aglite Block (3.3)		426
Abdullah (1989)	single-leaf wall	44	Clay (93.7)	1:¼:3	149
	cavity wall	51			151
	hollow pier	78			156
	solid pier	112			158
	single-leaf wall	44	Calcium Silicate (25.4)	1:¼:3	341
	cavity wall	51			330
	hollow pier	78			306
	solid pier	112			293
	single-leaf wall	44	Concrete Block (13.0)	1:¼:3	409
	cavity wall	51			394
	hollow pier	78			377
	solid pier	112			350

Table 2.4 Continued

Researcher	Member	V/S (mm)	Unit Type and strength (MPa)	Mortar cement:lime:sand	Estimated Ultimate Shrinkage (10 ⁻⁶)
Bingel (1984)	single-leaf wall	44	Calcium Silicate (30)	1: $\frac{1}{4}$: $4\frac{1}{4}$	300
	cavity wall	51			400
	hollow pier	79			400
	solid pier	112			275
	single-leaf wall	44	Concrete Block (8.6)	1: $\frac{1}{4}$: $4\frac{1}{4}$	450
	cavity wall	51			-
	hollow pier	79			300
	solid pier	112			120
	single-leaf wall	44	Clay (Fletton) (23)	1: $\frac{1}{4}$: $4\frac{1}{4}$	-800
	cavity wall	51			-640
	hollow pier	79			-780
	solid pier	112			-190

Table 2.5 Effect of Unit Type on Shrinkage of Plain Masonry

Researcher	Unit type and strength (MPa)	Mortar cement:lime:sand	Estimated Ultimate Shrinkage (10^{-6})
Lenczner (1978)	Fletton (28.69)	1: $\frac{1}{4}$:3	-125 to -146
	Butterley (56.0)	1: $\frac{1}{4}$:3	81 - 99
	Aglite Block (3.3)	1: $\frac{1}{4}$:3	426-637
Abdullah (1989)	Clay (93.7)	1: $\frac{1}{4}$:3	149-158
	Calcium Silicate (25.4)	1: $\frac{1}{4}$:3	293-341
	Concrete Block (13)	1: $\frac{1}{4}$:3	350-409

Table 2.6 Creep and Shrinkage Correction Factors for Average Thickness of Members ≥ 51 mm (Branson 1977)

Average thickness of member		Creep (C.F.) _T		Shrinkage (C.F.) _T	
in.	mm	≤ 1 year	ultimate value	≤ 1 year	ultimate value
2	51	1.3	1.3	1.35	1.35
3	76	1.3	1.3	1.25	1.25
4	102	1.11	1.11	1.17	1.17
5	127	1.04	1.04	1.08	1.08
6	152	1.00	1.00	1.00	1.00
8	203	0.96	0.96	0.93	0.94
10	254	0.91	0.93	0.85	0.88
12	305	0.86	0.90	0.77	0.82
15	381	0.80	0.85	0.66	0.74
20	508	0.68	0.76	0.47	0.59

**Table 2.7 Creep and Shrinkage Correction Factors for V/S
 ≥ 38 mm (Branson 1977)**

Volume/exposed surface ratio		Creep (C.F.) _T	Shrinkage (C.F.) _T
in	mm		
1.5	38	1.0	1.0
2	51	0.96	0.96
3	76	0.88	0.87
4	102	0.80	0.78
5	127	0.72	0.69
6	152	0.64	0.60
8	203	0.48	0.42

CHAPTER 3

REVIEW OF METHODS FOR PREDICTING PRESTRESS LOSS OF POST-TENSIONED MASONRY

3.1 Introduction

For prestressed concrete, design engineers have the option of choosing several methods to predict prestress loss. However limited methods are available in predicting prestress loss of post-tensioned masonry, and those methods are only applicable to certain types of masonry. In the following sections the author presents current methods in predicting prestress loss in post-tensioned masonry. Since methods for predicting prestress loss in masonry are limited, a review on methods developed for prestressed concrete are also presented.

3.2. Prediction of time-dependent prestress loss in masonry

In this section, methods recommended by Codes of Practice and previous researchers are given.

3.2.1 Prediction of time-dependent prestress loss in masonry by

Codes of Practice

The only national standard that gives provisions on prestress loss of post-tensioned masonry is the BS 5628 (1985). Sutherland (1982) stated that BS 5628

(1985), then in draft form, is the first masonry code to give provisions on prestressed masonry members. No provisions are made for prestressed masonry in ACI 530 (1990) and Eurocode No 6 (1988). However these codes provide coefficients for determining the effect of creep and shrinkage in masonry. These effects are presented in sections 3.4.1 and 3.5.1. At present, an update of Eurocode No 6 (1988) is being drafted by European countries and will include a design guide for prestressed masonry.

3.2.1.(a) BS 5628 (1985)

Clause 30.2 in the BS 5628: Part 2 (1985) recommends that allowances should be made for loss due to relaxation of the tendons, elastic deformation and time-dependent (creep and shrinkage) deformations of masonry, draw-in of the tendons during anchoring, friction and thermal effects in prestressed masonry. Only the loss due to relaxation of the tendon and time-dependent deformations of masonry will be presented in this chapter. The Code suggests single values of creep coefficients for clay or calcium silicate brick masonry and dense aggregate concrete block in predicting creep. The reduction of stress due to creep and shrinkage is predicted by multiplying the appropriate strain due to creep and shrinkage by the elastic modulus of the prestressing bar. This method does not consider the effect^{of} varying stress.

3.2.2 Prediction of time-dependent prestress loss in masonry by previous researchers

The following methods are based^a on experimental results of prestress loss in^a variety of clay brickwork (Lenczner 1986a) and limited types of concrete

blockwork (Tatsa 1973). None of these methods has been verified on calcium silicate brickwork.

3.2.2.(a) Lenczner method

Based on a study of post-tensioned clay brickwork walls, columns and beams Lenczner (1986a) suggested that the residual force in the prestressing bars (F_R) can be calculated in term of percentage of initial load at transfer as follows:

$$F_R = 100 \left(\sigma_{bw} A_{bw} - (\epsilon_m + C_c \frac{\sigma_{bw}}{E_{bw}}) \frac{h}{L} E_s A_s \right) \quad (3.1)$$

$$\text{or } F_R = 100 (1-R)$$

$$\text{where } R = (\epsilon_m + C_c \frac{\sigma_{bw}}{E_{bw}}) \frac{h}{L} \frac{E_s A_s}{C_c A_{bw}}$$

$$C_c = \text{creep ratio} = \left(\frac{\epsilon_c}{\epsilon_i} \right);$$

ϵ_c = creep strain;

ϵ_i = initial (elastic strain);

ϵ_m = moisture strain (positive for shrinkage);

σ_{bw} = stress in brickwork at transfer;

E_{bw} = elastic modulus of brickwork in MPa;

$$= 3750 (fb)^{0.5} - 10000;$$

E_s = elastic modulus of steel;

A_s = area of prestressing bars;

A_{bw} = area of prestressed brickwork member;

h = height of member;

and L = length of prestressing bar.

The residual force predicted is an overall magnitude of loss after all the deformations of the material have taken place. Application of the above formula requires knowledge of the deformations of the masonry, i.e creep coefficient and shrinkage strain. The above equation has been verified on clay units only, and does not take into account the effect of varying stress on prestress loss.

3.2.2.(b) Tatsa method

Based on a study of aerated post-tensioned blockwork, Tatsa (1973) suggested that the overall prestress loss at any time is given by:

$$\delta\sigma_{st} = E_s \{ \sigma_{ct} \epsilon_{ct} [\alpha + (1-\alpha) K_{ct}] + \epsilon_{st} [\alpha + (1-\alpha) K_{st}] \} + \delta\sigma_{st,r} + \delta\sigma_{st,1} \quad (3.2)$$

where $\alpha = a/L$ length ratio of block and wall;

σ_{ct} = initial prestress in the block;

ϵ_{ct} = creep of block per unit stress at time t ;

ϵ_{st} = shrinkage at time t ;

E_s = Young's modulus of steel;

K_{ct} = joint to block creep ratio at time t ;

K_{st} = joint to block shrinkage ratio at time t ;

$\delta\sigma_{st,r}$ = relaxation loss in steel at time t ;

and $\delta\sigma_{st,1}$ = local loss in steel (estimated as 1% for a length of 1m, and then decreasing with increasing length).

The above equation predicts the increment of loss of prestress at any time, instead of ultimate loss. A factor expressing a ratio of mortar joint to the block

for creep (K_{ct}) and shrinkage (K_{st}) is incorporated into the equation so as to consider the deformations of concrete units and the mortar joint. The effect of short panels is also introduced into the equation where it is expressed in terms of the ratio of block to panel. Thus the application of the above equation requires the knowledge of deformations of masonry units and mortar. The above equation has been verified on aerated concrete blocks only, and does not consider the effect of varying stress on prestress loss.

3.3 Methods of predicting elastic modulus

Methods of predicting elastic modulus of brickwork are considered because some of the methods in predicting creep of masonry require the knowledge of elastic modulus of brickwork.

3.3.1 Elastic modulus of masonry by Codes of Practice

3.3.1 (a) BS 5628 (1985)

Clause 19.1.7 of BS 5628:Part 2 (1985) suggests that elastic moduli of clay, calcium silicate and concrete masonry (including reinforced masonry) be taken as:

$$E_{mw} = 0.9 f_k \text{ GPa} \quad (3.3)$$

where E_{mw} = elastic modulus of masonry;

and f_k = characteristic compressive strength of masonry.

The characteristic compressive strength of masonry is determined from Table 3.1 where it is expressed in terms of the compressive strength of structural units and mortar designation.

3.3.1 (b) ACI 530-88/ASCE 5-88 (1990)

Clause 5.5.1 of the ACI 530 code (1990) suggests that the elastic moduli of clay and concrete masonry can be determined from Tables 3.2 and 3.3, respectively. The Code defines the modulus of elasticity in terms of compressive strength of units and mortar types.

3.3.1 (c) Eurocode No 6 (1988)

Clause 3.2.6.1 of the Eurocode No 6 (1988) suggests that elastic modulus of masonry be determined as follows:

$$E_{mw} = 1000 f_k \text{ MPa} \quad (3.4)$$

where E_{mw} = elastic modulus of masonry;

and f_k = characteristic compressive strength of masonry (Table 3.1).

3.3.2 Prediction of elastic modulus by previous researchers

Elastic modulus of masonry can be predicted empirically (Lenczner 1986a) and theoretically (composite modelling by Brooks 1986a and Ameny 1983 and 1984). Composite modelling presented by Ameny (1983 and 1984)) is limited for vertically stacked, bedded units and face shell bedded hollow units in stack bonds. Brooks (1986a, 1986b, 1987a,b and 1990) developed a model that is applicable to all types of bricks and mortar provided that the properties of bricks and mortar are known. This method is discussed later.

3.3.2 (a) Lenczner method

Most of the work by Lenczner has been based on clay units and thus the applications are limited to such brickwork. Based on tests of wide selection of

single-leaf cavity walls and piers, Lenczner (1986a) proposed that elasticity be predicted using the following expressions in terms of square root of brick strength regardless of mortar grade:

For bricks with compressive strength (B) of 20-70 MPa

$$E_{bw} = 300B - 2000 \quad (3.5)$$

For bricks with compressive strength greater than 70 MPa

$$E_{bw} = 12750 + 100B \quad (3.6)$$

For an approximate estimate of elasticity, the following equation should be used:

$$E_{bw} = 3750(B)^{0.5} - 10000 \quad (3.7)$$

For bricks units with compressive strength less than 20 MPa, elasticity should be taken as 5000 MPa. Equation (3.7) is recommended for brickwork with mortar designation (i) but gives reasonably good results when mortar grade (ii) is used, but not with weaker mortars than grade (iii).

3.3.2 (b) Brooks method

Brooks (1986a) expressed the modulus of elasticity of masonry in terms of moduli of brick units and mortar. Brooks (1986a) suggests that elastic modulus of masonry be determined as follows:

$$\frac{1}{E_{wy}} = \frac{b_y C}{H} \left[\frac{A_w}{E_{by} A_b + E_m A_m} \right] + \frac{m_y (C + 1)}{H} \frac{1}{E_m} \quad (3.8)$$

where E_{wy} = modulus of masonry perpendicular to the bed joint;

E_{by} = modulus of elasticity of brick/mortar component;

E_m = modulus of elasticity of horizontal mortar joint;

H = height of masonry;

C = number of courses;

$C + 1$ = number of mortar courses;

b_y = depth of unit,

m_y = height of mortar joint;

A_w = cross sectional area of masonry ;

A_b = cross-sectional area of bricks;

and A_m = cross-sectional area of vertical mortar joints = $A_w - A_b$.

The modelling was verified experimentally on clay and calcium silicate single-leaf brick walls and clay brick piers with one type of mortar. Generally the predicted elasticity was within 13 % of that measured, and is independent of the geometry of the masonry. The model is applicable to any type of masonry unit and mortar provided that properties of masonry unit and mortar are known, and an equivalent expression is available for predicting the elastic modulus parallel to the bed joints.

3.4 Methods of predicting creep

Several standards have started to recognize the significance of creep in the design of load bearing masonry members. Methods suggested by Codes of Practice and previous researchers are presented in this section.

3.4.1 Creep of masonry by Codes of Practice

3.4.1 (a) BS 5628 (1985)

BS 5628 : Part 2 (1985) suggests that creep is numerically equal to 1.5 and 3.0 times the elastic deformation of the masonry in fired clay or calcium

silicate brick masonry and dense aggregate concrete block, respectively. No distinctions are made for different ages of loading, temperature, relative humidity, size of units, mortar types and geometry of masonry.

3.4.1 (b) ACI 530-88/ASCE 5-88 (1990)

Clause 5.5.5 of ACI 530-88/ASCE 5-88 code (1990) suggests the use of coefficients of creep in predicting creep. The suggested coefficients of creep of masonry are 101.5×10^{-6} per MPa and 360×10^{-6} per MPa for clay and concrete masonry, respectively. The suggested coefficients of creep values given are regardless of the strength of the units and mortar types used. As in BS 5628: Part 2 (1985), no distinctions are made for different age of loading, temperature, relative humidity, size of units, mortar types and geometry of masonry. The Code does not give any provisions for creep of calcium silicate brickwork.

3.4.1 (c) Eurocode No 6 (1988)

Eurocode No 6 (1988) suggests creep coefficients of 0.7 and 1.5 for clay and calcium silicate/concrete masonry, respectively. As in BS 5628 (1985) and ACI 530 (1990), the suggested creep coefficients are single values for different type of masonry units and mortar. As before no distinctions are made for other factors.

3.4.2 Prediction of creep by previous researchers

As for the prediction of elastic modulus, prediction of creep by previous researchers is divided into empirical and theoretical methods.

3.4.2 (a) Lenczner method

Based on several years of observations on the behaviour of brickwork subjected to axial load, Lenczner (1985) proposed that strain ratio (R) should be used in predicting creep in brickwork, where $R = \text{maximum strain} / \text{initial elastic strain}$.

From experimental studies on piers, cavity walls and single-leaf walls on wide selection of bricks, Lenczner (1985) concluded that there are linear relationships between the strain ratio for walls, and for columns, and the square root of brick strength. The strain ratio for walls and piers, respectively, are:

$$\text{For walls:} \quad R_w = 5.46 - 0.33(B)^{0.5} \quad (3.9)$$

$$\text{For piers:} \quad R_w = 2.73 - 0.14(B)^{0.5} \quad (3.10)$$

where B is the compressive strength of bricks (MPa).

The above equations apply to brickwork with 1: $\frac{1}{4}$:3 and 1:1:6 mortar mixes of Portland cement, dry hydrated lime and sand. The linear regression analysis of the data for Equations (3.9) and (3.10) were 0.82 and 0.88, respectively.

3.4.2 (b) Brooks method

Brooks (1986a) proposed ^{that} the specific creep of masonry can be expressed in terms of the effective and elastic moduli of brickwork. The specific creep of masonry (C_s) is given by:

$$C_s = \frac{1}{E'_{wy}} - \frac{1}{E_{wy}} \quad (3.11)$$

where E_{wy} = elastic modulus of brickwork as in Eq.(3.8);

E'_{wy} = effective modulus of brickwork;

$$\text{and } \frac{1}{E'_{wy}} = \frac{b_v C}{H} \left[\frac{A_w}{E'_{by} A_b + E'_m A_m} \right] + \frac{m_v (C + 1)}{H} \frac{1}{E'_m} \quad (3.12)$$

where E'_{by} = effective modulus of brick unit;

and E'_m = effective modulus mortar.

Equation.(3.11) was verified experimentally (Brooks et al 1986b, 1988, 1990a, 1990b) for clay, calcium silicate and concrete masonry.

3.5 Methods of predicting shrinkage

Methods suggested by Codes of Practice and previous researchers are presented in this section. To date, only one theoretical method is available in predicting shrinkage of masonry (Brooks 1987b). Codes of Practice suggest either a single value for ultimate shrinkage or coefficients of shrinkage for different types masonry units and mortar grades.

3.5.1 Moisture movement of masonry by Codes of Practice

3.5.1 (a) BS 5628 (1985)

Clause 30.2.4 of BS 5628: Part 2 (1985) suggests a maximum shrinkage (ϵ_{sh}) of 500×10^{-6} for both calcium silicate and concrete block masonry regardless of the mortar type. Since these values are based on limited research, there is no distinction between shrinkage of calcium silicate and concrete masonry. Any movement in clay and masonry is assumed to be negligible. As for the moisture movement of clay, calcium silicate and concrete units, and mortar, Clause A.5 of BS 5628: Part 3 (1985) gives a range of typical reversible and irreversible movements.

3.5.1 (b) ACI 530-88/ASCE 5-88 (1990)

The Code suggests that the irreversible moisture expansion of clay masonry be taken as 3×10^{-4} . For concrete masonry, the coefficient of shrinkage is taken as 0.15-0.5 multiplied by the total linear drying shrinkage of concrete units. As in BS 5628 (1985), these values fail to consider the type of mortar used.

3.5.1 (c) Eurocode No 6 (1988)

Clause 3.2.6.4 of Eurocode No 6 (1988) recommends moisture movement of -100 to 200×10^{-6} for clay masonry. A value of 200×10^{-6} of shrinkage is suggested for calcium silicate and concrete masonry. As in other codes these values are single ultimate values which do not account for the type of mortar.

3.5.2 Prediction of shrinkage by previous researchers

3.5.2 (a) Brooks method

Using a similar composite model to that for creep of masonry, Brooks (1987b) expressed the vertical shrinkage of masonry in term of vertical shrinkage of mortar and units as follows:

$$S_{wy} = \frac{b_y C}{H} S_{by} + \frac{m_y (C+1)}{H} S_m + \frac{b_y C}{H} \frac{(S_m - S_{by})}{\left[1 + \frac{A_b}{A_m} \frac{E'_{by}}{E'_m} \right]} \quad (3.13)$$

where S_{by} = axial shrinkage of brick or block;

E'_{by} = effective modulus of brick or block;

E'_m = effective modulus of mortar;

and S_m = shrinkage of mortar.

It should be noted that effective modulus of units (E'_{by}) and mortar (E'_m) allow for creep of the unit and mortar because shrinkage reduces stresses. Equation (3.13) has been verified experimentally on three types of masonry units (clay, calcium silicate and concrete block units) made with grade ii mortar.

3.6 Methods for predicting relaxation of steel

3.6.1 Prediction of relaxation of steel by Codes of Practice

3.6.1 (a) BS 5628: Part 2 (1985)

The Code suggests that loss of prestress due to relaxation should be taken to be the maximum relaxation of the tendon after 1000 hours duration given in the manufacturer's UK Certificate of Approval. In the absence of the manufacturer's Certificate of Approval, loss of prestress should be obtained from BS 5896 (1980) or BS 4486 (1980). The Standards suggests the 1000 hour relaxation value may be assumed to decrease from the value given for 60% to zero at 30% of the breaking load. Table 3.4 shows the 1000 hour relaxation loss (%) in accordance to BS 5896 (1980) and BS 4486 (1980).

3.6.2 Prediction of relaxation of steel by previous researchers

3.6.2 (a) Magura method (1964)

Magura (1964) suggests that the reduction of stress due to relaxation be predicted by the following equation:

$$f_s(t) = -f_{si} \log_{10} 24t \frac{\left(\frac{f_{si}}{f_{sy}} - 0.55\right)}{10} \quad (3.14)$$

where f_s = the remaining stress at any time t after prestressing;

f_{si} = the initial stress;

and f_{sy} = stress at 1% elongation;

Equation (3.14) is valid only for $(\frac{f_{si}}{f_{sy}} \geq 0.55)$.

3.6.2 (b) Glowdowski et al method (1972)

Glowdowski et al (1972) suggests a quadratic equation in predicting prestress loss due to relaxation of prestressing steel:

$$SR = A + B \ln t + C (\ln t)^2 \quad (3.15)$$

where SR = % relaxation;

t = test time in hours;

and A, B, C = function of the stress level ratio (initial stress/measured strength).

Glowdowski et al (1972) claimed that Equation (3.15) is quite accurate for short term as well as reasonably consistent with other methods of predicting long-term stress relaxation loss.

3.7 Prediction of time-dependent prestress loss in prestressed concrete

Two of the established methods for predicting prestress loss in prestressed concrete are considered. One of the methods (Dilger 1983) takes into account the effect of varying stress in the concrete.

3.7.1 Dilger method

Dilger (1983) presented an analytical method for calculating prestress loss by taking into account the effect of creep under varying stress. This effect is expressed in terms of an aging coefficient, which is less than 1.

The following equation expresses stress loss in one layer of steel:

$$\delta f_s(t) = \frac{n_o f_o \phi(t, t_o) + \epsilon_{sh}(t, t_o) E_s + f'_r(t)}{1 + \rho n_o (1 + y_1^2/r^2)(1 + \chi \phi(t, t_o))} \quad (3.16)$$

where $\delta f_s(t)$ = change of stress;

$n_o = \frac{E_s}{E(t_o)}$ = modular ratio at the time at first application of load, t_o ;

f_o = initial stress;

$\phi(t, t_o)$ = creep coefficient at time t for concrete loaded at age t_o ;

$\epsilon_{sh}(t, t_o)$ = free shrinkage developed between times t_o and t ;

E_s = elastic modulus of prestressing steel;

$\rho = \frac{A_s}{A_c}$

y_1 = distance from the neutral axis to the prestressing bar;

$r^2 = \frac{I_c}{A_c}$

$\chi(t, t_o)$ = aging coefficient = $\frac{f_o}{f_o - f_t} - \frac{1}{\phi(t, t_o)}$

f_o = initial stress on the concrete

f_t = total stress at time t under varying stress

$f'_r(t) = \alpha_r f_s(t)$ = reduced relaxation;

α_r = reduction coefficient from Fig. 3.1;

$f_s(t) = -f_{si} \log_{10} 24t \frac{(\frac{f_{si}}{f_{sy}} - 0.55)}{10}$ for stress relieved steel;

$f_s(t) = -f_{si} \log_{10} 24t \frac{(\frac{f_{si}}{f_{sy}} - 0.55)}{45}$ for stress low-relaxation

steel;

$f_s(t)$ = the remaining stress at any time t after prestressing;

f_{si} = the initial stress;

and f_{sy} = stress at 1% elongation.

3.7.1 Abeles method

Abeles (1966) recommends an analytical method that does not consider the effect of varying stress in the concrete members. The stress loss (PL) is given by:

$$PL = [PL_e + K_n (PL_{cr} + PL_{sh}) + PL_r] \quad (3.17)$$

where PL_e = tension loss (applied to the pre-tensioned member only);

K_n = creep and shrinkage reduction factor for non-tensioned steel;

$$= [A_c + (n-1) A_{ps}] / A_t$$

A_c, A_t = concrete area and transformed section area, respectively;

PL_{sh} = shrinkage tension loss = $\epsilon_{sh} E_s$;

PL_{cr} = creep tension loss = $n f_{ci,p} C_t$;

C_t = creep coefficient

$f_{ci,p}$ = initial concrete stresses at the level of prestress;

and PL_r = relaxation loss of the prestressing wire (Magura's).

Table 3.1 Characteristic Compressive Strength of Masonry
(BS5628: Part 2 1985)

(A) Constructed with bricks or other units having a ratio of height to least horizontal dimension of 0.6									
Mortar designation	Characteristic compressive strength of masonry, f_k (MPa)								
	Compressive strength of unit (MPa)								
	7	10	15	20	27.5	35	50	70	100
(i)	3.4	4.4	6.0	7.4	9.2	11.4	15.0	19.2	24.0
(ii)	3.2	4.2	5.3	6.4	7.9	9.4	12.2	15.1	18.2
(B) Constructed with solid concrete having a ratio of height to least horizontal dimension of 1.0									
	Compressive strength of unit (MPa)								
	7	10	15	20	35	50	70 or greater		
(i)	4.4	5.7	7.7	9.5	14.7	19.3	24.7		
(ii)	4.1	5.4	6.8	8.2	12.1	15.7	19.4		
(C) Constructed with solid concrete having a ratio of height to least horizontal dimension between 2.0 and 4.0									
	Compressive strength of unit (MPa)								
	7	10	15	20	35	50	70 or greater		
(i)	6.8	8.8	12.0	14.8	22.8	30.0	38.4		
(ii)	6.4	8.4	10.6	12.8	18.8	24.4	30.2		
(D) Constructed with structural units other than solid concrete blocks having a ratio of height to least horizontal dimension between 2.0 and 4.0									
	Compressive strength of unit (MPa)								
	7	10	15	20	35	50	70 or greater		
(i)	5.7	6.1	6.8	7.5	11.4	15.0	19.2		
(ii)	5.5	5.7	6.1	6.5	9.4	12.2	15.1		

Table 3.2 Elastic Modulus of Clay Masonry by ACI 530-88/ASCE 5-88 (1990)

Net area compressive strength of units psi (MPa)	Modulus of elasticity (Linear interpolation permitted)		
	Type N mortar $E_m, \text{psi} \times 10^6$ (GPa)	Type S mortar $E_m, \text{psi} \times 10^6$ (GPa)	Type M mortar $E_m, \text{psi} \times 10^6$ (GPa)
> 12,000 (> 82.74)	2.8 (19.31)	3 (20.68)	3 (20.68)
10,000 (68.94)	2.4 (16.55)	2.9 (19.99)	3 (20.68)
8,000 (55.15)	2.0 (13.79)	2.4 (16.55)	2.8 (19.45)
6,000 (41.26)	1.6 (11.03)	1.9 (13.10)	2.2 (15.29)
4,000 (27.58)	1.2 (8.27)	1.4 (9.65)	1.6 (11.12)
2,000 (13.79)	0.8 (5.52)	0.9 (6.21)	1.0 (6.89)

**Table 3.3 Elastic Modulus of Concrete Masonry by
ACI 530-88/ASCE 5-88 (1990)**

Net area compressive strength of units psi (MPa)	Modulus of elasticity (Linear interpolation permitted)	
	Type N mortar E_m , psi x 10^6 (GPa)	Type M or S mortar E_m , psi x 10^6 (GPa)
> 6,000 (> 41.26)	-	3.5 (24.13)
5,000 (34.47)	2.8 (19.31)	3.2 (22.06)
4,000 (27.58)	2.6 (17.93)	2.9 (20.15)
3,000 (20.68)	2.3 (15.86)	2.5 (17.24)
2,500 (17.24)	2.2 (15.17)	2.4 (16.55)
2,000 (13.79)	1.8 (12.41)	2.2 (15.17)
1,500 (10.34)	1.5 (10.34)	1.6 (11.03)

**Table 3.4 Relaxation Loss (%) at 1000 hour in Accordance
with BS 5896 (1980) and BS 4486 (1980)**

Material	Cold drawn wire or strand to BS 5896 (1980)		Cold drawn in mill coil to BS 5896 (1980)	Bar to BS 4486 (1980)
	Relaxation			
Initial load (% of breaking load)	Class 1	Class 2		
60	4.5	1.0	8.0	1.5
70	8.0	2.5	10.0	3.5

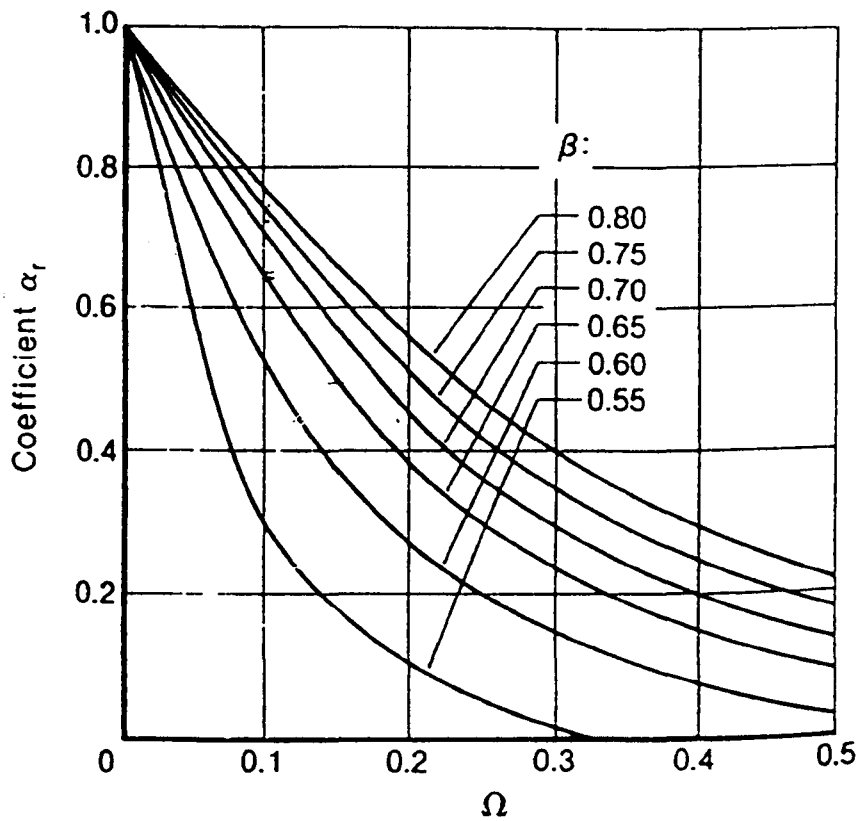


Fig. 3.1 Relation between Relaxation Reduction Coefficient (α_r)

and Ω^* for Different values of β^{} (Dilger et al 1983)**

* $\Omega = \frac{\text{loss due to creep and shrinkage}}{\text{initial prestress}}$

** $\beta = \frac{\text{initial prestress}}{\text{ultimate strength of prestressing steel}}$

CHAPTER 4

EXPERIMENTAL DETAILS

4.1 Introduction

The geometries investigated for this research were post-tensioned diaphragm and fin walls that were represented by a box and a single-tee section. The geometric walls were specifically chosen so as to study the influence of volume/exposed surface area on the behaviour of the post-tensioned walls. The post-tensioning system adopted in this research was high strength Macalloy bars that complied with BS 4486 (1980). The walls represent typical retaining walls which have been constructed on various sites.

4.2 Outline of the test programme

The research programme consisted of measuring prestress loss and time-dependent deformations on the two types of geometric members constructed from three types of masonry units. The research was divided into three separate tests as described below;

Test 1 Clay brickwork

In Test 1, diaphragm and fin walls were built from clay units with a grade (ii) mortar. Three walls were constructed for each geometry to measure the prestress

loss, creep and shrinkage/moisture movement separately. Only two of these walls were post-tensioned for 120 days. The three walls for the measurements of prestress loss, creep and shrinkage/moisture strains are described as follows:

(i) Moisture strain wall

The wall was unloaded and the strain measured was due to shrinkage/moisture movement only; there may have been some movement due to temperature variations as all the walls were located in the laboratory where the humidity and temperature were not controlled. However, the variation in the atmospheric temperature and humidity is insignificant compared to the variations of temperature and humidity on sites (Fig. 4.17 and 4.18).

(ii) Creep wall

The wall was loaded under constant stress so as to measure creep of the brickwork. The wall had to be restressed during the research to maintain the initial post-tensioned force throughout the duration of the test.

(iii) Prestress loss wall

The wall was loaded to the same level of stress as in the creep wall; although the wall was not restressed during the test so as to allow for loss of the initial prestress force in the bars to take place.

Test 2 Calcium silicate brickwork

Similar tests were carried out as in Test 1 using calcium silicate units.

Test 3 Concrete block units

Similar tests were carried out as in Test 1 using concrete block units.

4.3 Materials

4.3.1 Masonry units

Generally, in practice it is more common to prestress brickwork and reinforce blockwork because brickwork has a higher compressive strength and can be easily formed into different sections for prestressing. Furthermore, concrete blockwork tends to undergo creep and shrinkage more than clay brickwork. However, for this particular research, it was considered important to investigate prestress loss of masonry constructed from clay, calcium silicate and concrete block. Since bricks with ^a strength greater than 27 MPa ^{are} normally used in reinforced and prestressed masonry, the tests programme used units with a compressive strength of atleast 27 MPa.

4.3.1 (a) Clay brick

The clay brick units used were of solid red smooth class B Engineering bricks manufactured and supplied by Marshalls Clay Products, Robinhood, Wakefield, West Yorkshire. The brick units, with compressive strength of 103 MPa, were of standard size (215 mm x 102.5 mm x 65 mm) with three 25-30 mm diameter perforations. The units were approximately 12 months old when laid.

4.3.1 (b) Calcium Silicate brick

The Grade 4 solid calcium silicate brick units used in Test 2 were manufactured and supplied by Mansfield Brick, Mansfield, Nottinghamshire. The calcium silicate units had similar dimensions to the clay units. The brick units, with compressive strength of 27 MPa, were approximately 9 months old when laid.

4.3.1 (c) Concrete block

The dense aggregate solid concrete blocks manufactured and supplied by Plasmor Ltd., Knottingley, West Yorkshire were used in Test 3. The blocks had dimensions of 440 mm x 100 mm x 220 mm. Dense aggregate concrete block with compressive strength of 14 MPa was chosen for the research to represent medium strength masonry units. The units were approximately 9 months old when laid.

4.3.2 Mortar

The test walls were built with grade (ii) mortar, i.e. cement:lime:sand ratio (by mass) of $1:\frac{1}{2}:4\frac{1}{2}$, using ordinary Portland cement, hydrated building lime and building sand, respectively. A sieve analysis in accordance with BS 1200 (1976) was carried out on the sand. Fig. 4.1 shows the results which complied with BS 1200 (1976). Preliminary dropping ball tests were performed to determine the water cement ratio as required by BS 4551 (1980). From the dropping ball test, a 10.0 mm penetration of mortar was achieved with a water cement ratio of 1.27. The grade (ii) mortar was chosen because BS 5628 (1985) recommends that grade (ii), or better, should be used for reinforced masonry.

4.3.3 Base and capping beams

For this study, six 1.3 m by 1.3 m heavily reinforced concrete bases and capping beams were cast about 6 months before building the masonry walls (Fig. 4.2 to Fig. 4.4). An ordinary Portland cement (OPC) concrete mix of 1:2:4 with 0.52 water/cement ratio was used throughout the construction of these concrete members. The bases and the beams were cast earlier to minimise any effects of creep and shrinkage of the concrete members on the stress reduction in the prestressing

steel. High strength concrete was used to minimise deformations in the base and capping beams; resulting in negligible prestress losses. The bases and capping beams were of 450 mm and 250 mm thick, respectively. The reason for having thick bases and capping beams was mainly to produce uniform stress distributions in the masonry.

4.3.4 Prestressing steel

Macalloy cold rolled high tensile alloy steel bars to BS 4486 (1980) were used throughout the experiments. Table 4.1 shows the work test certificate for the bars provided by the manufacturer: McCalls Special Products. A total of nine 25 mm and nine 26.5 mm diameter of high tensile alloy steel bars were used. The 26.5 mm diameter bars were partially threaded at both ends, i.e 1 m plain rolled in the centre, but this resulted in slightly curvature of the bars. The 25 mm diameter bars were supplied fully threaded so as to avoid excessive curvature of the bars.

4.4 Test procedure

4.4.1 Test set-up

The following sections describe the test set-up before measurements commenced on the masonry walls, masonry units and mortar prisms.

4.4.1 (a) Prestressing procedure for bar anchored to concrete bases for creep and prestress loss walls

Initially, one end of the prestressing bars was locked to a 200 x 200 x 40 mm thick end plate with a washer and nut, through a 40 mm diameter hole at the bottom of the base as shown in Fig. 4.5. Another end plate was then placed over the bar on top of the base and followed by a washer and nut. After placing two bottle

jacks on each side of end plate, spacers were positioned on top of the bottle jack. With three 400 x 400 mm slotted plates placed on the spacers, washer and nut were screwed on top of the plates. Pressure was applied to the bottle jack through a calibrated 700 kN capacity Budenberg hydraulic pump (see Fig. 4.6 and Plate 4.1). When the required force was reached (about 4 % higher than the intended force for the brickwork), the nut on the base was run up to the end plate and tightened against it. The reason for locking the bars at the top of the base was to avoid any movement of the end plate located below the base. It was undesirable to weld the nuts to the end plate in the pocket of the base because the anchorage accessories were required to be re-used throughout the experiments.

4.4.1 (b) Building the masonry walls

The walls were constructed on the reinforced concrete bases with the prestressed bar locked in position. Three masonry walls were built at the same time for each geometry using the same batch of mortar; 4 courses at a time and all the three walls had the same height at the end of the day. Plates 4.2 and 4.3 show the diaphragm and fin walls during construction. Fin walls were built a week after the diaphragm walls. For all the tests, a total of eighteen walls were constructed. The height of the 26-course clay and calcium silicate walls was 1960 mm, while the 9-course blockwork walls had a height of 2080 mm. The walls were cured under polythene sheet for 7 days and on the 7th day, the top of the brickwork was bedded and levelled with mortar before positioning the capping beam. The walls were re-covered with polythene until 2 days before stressing the bars. The control (moisture movement strain) diaphragm and fin walls were constructed in the same manner but without the prestressing steel.

Two days before stressing the bar at the top of the capping beam, the polythene sheets covering the wall were removed so that gauge points could be fixed

to the concrete bases, capping beams and each face of the wall. The gauge points were stainless steel Demec studs for 750 mm and 200 mm demountable mechanical extensometers. Brackets for an invar bar for measuring the total movement of the walls were later screwed to the base and the capping beams. Demec readings were taken the next day.

Figures 4.7 and 4.8 show section details of the prestressed masonry walls.

4.4.1 (c) Prestressing procedure

A day before stressing the bars, a purpose made loadcell was placed over the bar against a 200 x 200 x 40 mm thick spreader plate on top of the capping beam. A similar spreader plate and washer and nut were screwed onto the load cell (see Fig. 4.9 and Plate 4.4). After locating bevel housing together with jack over the nut, a spacer and a nut were screwed onto the jack. Twenty-one days after construction, the bars were jacked to the required working stress and locked using a nut system against a spreader plate at the top of the capping beams.

Just before prestressing, initial readings of the loadcells and strains at the bases, the capping beams and the masonry walls were taken. The stress was then applied to the bar by applying pressure to the jack through the hydraulic pump. The load was checked on a digital Peekel instrument and also by the calibrated pressure gauge on the hydraulic pump. The bars were stressed between 54 to 64 % of the breaking load as recommended by the steel manufacturers and Codes of Practice. Table 4.2 shows the prestressing force applied to the bars, the number of bars per wall and the corresponding percentage of breaking load used in the test programme. The load was applied at 50 kN increments for the calcium silicate brickwork and concrete blockwork, and 155 kN increments for the clay brickwork. Where 2 bars were used in each wall, the bars were stressed in sequence. For each increment of

load, Demec and invar bar readings were taken on the walls and also Peekel readings for the bars were taken. Fig. 4.10 shows the anchorage system at the top of the capping beams on prestress loss and creep walls. The walls were subjected to a load up to 46% of its working stress (Appendix A). Plate 4.5 to 4.7 show the post-tensioned masonry walls under test.

4.5 Creep tests of masonry units and mortar prisms

Description of creep loading frame

The loading apparatus and method of measuring creep for masonry units and mortar were developed at the Department of Civil Engineering, the University of Leeds, for cylindrical concrete specimens. The creep frames for concrete cylinders was modified to suit masonry units and mortar prisms as shown in Fig. 4.11 and Plate 4.8. Two masonry units or mortar prisms and a calibrated cylindrical steel-tube load dynamometer held by four tie bars comprise a creep frame. The constant load was applied by stressing the tie bars manually by tightening the four nuts. The steel dynamometer was used to check the load and any loss of load was compensated by retightening the tie bars to the required load, i.e until the required value of strain on the dynamometer was within ± 2 divisions (equivalent to ± 0.22 MPa). The cylindrical dynamometers were calibrated using Avery Dennison Universal testing machine with maximum capacity of 500 kN.

Sampling of creep and moisture movements specimens

For the creep and shrinkage tests, a total of twelve 75x75x200 mm mortar prisms were prepared. The mortar prisms were sampled as follows: four prisms from first mortar mix, four from middle mortar batch and another four from the final mortar batch. Six of the prisms were positioned in the creep frames and subjected to

the same axial load as in the creep wall. The other six mortar prisms were left beside the walls so as to represent the free shrinkage of the mortar.

Only two units were used to represent each geometry for the creep test, and they were loaded between the header faces.

4.6 Strain measurements

Load cells and electrical strain gauges were used to measure prestress force and strain changes on the bars. Strain measurements on the concrete bases, capping beams and brickwork were made using the following three different sizes of Demec gauges;

- (i) 750 mm gauge ---- 2.1×10^{-6} per division
- (i) 200 mm gauge ---- 8.0×10^{-6} per division
- (i) 150 mm gauge ---- 10.8×10^{-6} per division

4.6.1 Reinforced concrete bases and capping beam

The strains on the concrete bases and capping beams were measured using 200 mm Demec gauges. Fig. 4.12 to Fig. 4.15 show the locations of Demec points on the concrete bases and the capping beams.

4.6.2 Masonry

Four strain measurements were taken on each face of the masonry walls using 750 mm and 200 mm Demec gauges. The locations of these demec points are as shown in Figure 4.12 to 4.15. Total strains on each side of the walls was measured using a dial gauge fixed to Invar bars.

4.6.3 Prestressing steel bar

Force and strain in the bars were measured by loadcells and electrical strain gauges as described below :

Electrical strain gauge

The strain on the prestressing bars was measured using two sets of full bridges for high sensitivity and for compensation of temperature changes. The full bridge consisted of two FCA-6 rosettes. Before mounting the gauges, the 26.5 mm diameter bars were filed and smoothed by fine sand paper. As for the fully threaded 25 mm diameter bars, the threads in the mid length of the bars were taken off by lathe machines to a 23.5 mm diameter. The grease on the bars was removed in three stages of washing using acetone, conditioner and neutralizer, respectively. The gauges were protected by applying two layers of M-coat D. Finally, the gauges were protected against mortar droppings during bricklaying by sealing them in PVC tube filled with expanding foam. Prior to applying the insulation, the gauges were tested for insulation and resistance. Figure 4.16 shows the configuration of the rosette.

Load cell

The tension force in the steel bar was measured by purpose-made tubular shape loadcells located at the anchorage point of the capping beam. The loadcells, positioned between the end plates and the locking nuts, were mounted with full bridge electrical strain gauges on its steel collar by semi-filled curing epoxy resin. The full bridge consisted of four PL-6 gauges manufactured by Micromeritics. Standard hot bonding procedures were carried out in two cycles: by heating at 100°C in the oven for two hours in each cycle. The strain gauge for full bridge connection to the distribution box is as shown in Fig. 4.16. The loadcells were calibrated each time before use and had an accuracy of ± 0.45 kN.

Hydraulic jack

The bars were stressed using hydraulic operated jack, Mark 13, provided by McCalls Special Products. The jack was supplied with a pump and a calibrated gauge for direct reading of the load, and could stress bars up to 400 kN.

4.6.4. Creep and shrinkage of masonry units and mortar prisms

The creep and shrinkage/moisture movements of all the masonry units and mortar prisms were measured using two Demec gauge lengths of 150 mm. The Demec points were positioned along the unsealed stretcher face on the brick units and along the unsealed (200 mm) face of the mortar prisms. The Demec points were fixed on the specimens two days before the prestressing of the walls.

4.6.5. Strain measurement on creep dynamometer

Four 200 mm length Demec gauge were positioned longitudinally on the cylindrical dynamometers to monitor the applied load on the creep specimens. The dynamometer was placed in the creep frame in such a way that the Demec points were located half way between the tie rods of the creep frame as shown in Fig. 4.11.

4.7 Environmental conditions

Due to the size of the wall, all the test specimens were kept in a non-controlled environment in the laboratory. Temperature and humidity changes were recorded using a temperature and humidity monitor. The variations in temperature and humidity during the experiment are shown in Fig.4.17 and 4.18 respectively.

4.8 Testing

The following describes tests and measurements carried out on the masonry walls, masonry units and mortar prisms in this study.

4.8.1 Deformations of masonry walls

4.8.1 (a) Elastic modulus

The elastic modulus was measured by taking strain measurements using Demec gauges and Invar bar deflections on each face of the creep and prestress loss walls at every load increment during the prestressing process. The locations of the Demec gauges are given in Section 4.6.2 and Figs. 4.12 to 4.15.

4.8.1 (b) Shrinkage

The zero readings on each face of the masonry control walls were taken within 2 hours after prestressing the bars in the creep and prestress loss walls. Subsequent readings were taken every day during the first week after loading, twice a week up to 80 days and once a week thereafter. The locations of the strain measurements were identical to those of the creep and prestress loss walls.

4.8.1 (c) Creep

The zero readings of the creep walls were taken when the bars were jacked to the full load following the elastic modulus measurement. Subsequently, readings were taken at the same time as the control walls. The sustained load on the bars was monitored using the Peekel instrument and the load was maintained at ± 10 kN (2.5% of the initial load). The bars were required to be stressed almost everyday during the first five days after the prestressing process, twice a week up to 80 days and once a week thereafter.

4.8.1 (d) Prestress loss of the masonry walls

Similar intervals of time as for the creep masonry walls were chosen for the readings of prestress loss. The prestress loss (strain gauge) changes of load (loadcell), were monitored immediately after transfer.

4.8.2 Deformations of masonry units and mortar prisms

The deformations of the masonry units and mortar prisms were for the verification of composite model that was developed by Brooks (1986a and 1987b) as discussed in Chapters 2 and 3. The models required information on elastic and time-dependent deformation, i.e creep and moisture movement strain of the masonry units and mortar prisms.

4.8.2 (a) Elastic modulus

Since no standard method of measuring modulus of elasticity of masonry units exists, the elastic modulus was obtained from strains measured during the loading of the creep specimens (secant modulus of elasticity).

For the clay and calcium silicate units, single units were also loaded between bed faces and between header faces so as to measure the elastic degree of anisotropy. An Avery Denison Universal testing machine with maximum capacity of 500 kN was used for this purpose, the units being tested between 3 mm plywood platens. Deformations^{of} the units were measured using electrical strain gauges.

4.8.2 (b) Moisture movement strain

The specimens for this test were the control specimens for the creep tests, and measurements were taken at the same time as for creep.

4.8.2 (c) Creep

The mortar specimens sampled during bricklaying were stored together with the walls under polythene sheet for 7 days. On the 7th day, the prisms were partly sealed with bituminous paint and polythene sheet to the same volume/exposed surface ratios (V/S) of the mortar in the walls. The volume/surface ratios for the units and mortar are shown in Table 4.3. Figure 4.19 shows details of the partial sealing of the masonry units and mortar prisms. Creep was measured between header faces in individual creep frames within 24 hours of stressing the bars in the walls. For the concrete block units, the specimens were cut to the brick size normal to the bed face of block units. Plate 4.8 shows the masonry units and mortar prisms under test.

4.8.3 Stress relaxation test

Fig. 4.20 shows the intrinsic relaxation test set-up. The bars were fixed at a constant length, i.e constant strain by stressing them between 2 steel plates rigidly fixed to a steel channel and a spacer. The bars were subjected to loads of 354.9 and 397.7 kN corresponding to 64% of the ultimate tensile strength of the 25 and 26.5 mm bars, respectively.

4.9 Control tests

4.9 (a) Compressive strength

Concrete bases and capping beams.

The 28-day compressive strength test of concrete was carried out using a Dartec Tonipact test machine of 3000 kN capacity in accordance with BS 1881: Part 116 (1970). 100 x 100 x 100 mm concrete cubes placed between platens were subjected to a constant load of 0.4 MPa per sec (0.4 N/s or 0.4 MPa/s) until

failure. The ultimate load (kN) was read from the instrument digital display. The compressive strength of the concrete members was measured by tests on concrete cubes at 28 days and the results are shown in Table 4.4.

Mortar

For the compressive strength three cubes (100 x 100 x 100 mm) and prisms were made from each batch of mortar used in the walls. The cubes and the prisms were tested at 21 days in accordance with BS 4551 (1980). Table 4.5 shows the average compressive strength of mortar cubes.

Clay bricks

Compressive strength test on ten bricks, as specified in BS 3921 (1985), was carried out on the Dartec testing machine at a constant loading rate of 5.5 kN/sec (15 MPa.min) until failure. The specimens, which were previously immersed in water, were loaded on bed faces tested between 4 mm plywood sheet as specified in BS 3921 (1985). The results are given in Table 4.6.

Calcium Silicate

The compressive strength of calcium silicate bricks was determined as required by BS 187 (1978). Ten bricks, previously immersed in water at a temperature of 20 ± 5 C for 18 ± 2 hour, were tested between 4 mm thick plywood. A constant load of 6.6 kN/sec (18 MPa.min) was applied perpendicular to the bed faces until failure. Table 4.6 lists the results.

Concrete blocks

The compressive strength of blocks was determined in accordance with BS 6073 (1981) where the blocks were immersed in water for 16 hours prior to capping with mortar. The mortar has a 1:1 mix of high alumina cement complying

with the requirements of BS 915: Part 2 (1972), and sand complying with the requirements of grading zones 2 or 3 of BS 882; 1201:Part 2 (1992). When the mortar had reached at least 28 MPa, in accordance with the procedures given in BS 4551 (1980), the mortar capped specimens were subjected to a constant rate of 10 ± 1 MPa until failure. Table 4.6 shows the compressive strength results.

4.9 (b) Standard dropping ball test for mortar

The standard consistency test for mortar is to measure the penetration of a methyl methacrylate ball when it is allowed to fall on to brass mould filled with mortar. The penetration of the ball was measured to the nearest 0.1 mm as specified by BS 4551 (1980). In these tests, the mortar penetration was 10 ± 0.5 mm.

4.9 (c) Macalloy prestressing steel tensile test

The test was performed on the 25 and 26.5 mm bars in an Avery Universal tension/compression test machine with 1000 kN capacity. Since the machine was only able to measure the load, electrical strain gauges were used for measuring strains changes. Fig. 4.21 shows a typical stress-strain curve of the bars when tested accordance with BS 4486 (1980).

Table 4.1. Work Test Certificate for the McCalls Special Products Bars

Nominal size (mm)	0.1 % Proof Load (kN)	Proof Stress (GPa)	Ultimate Load (kN)	Ultimate Stress (MPa)	Elongation at Fracture (%)	Modulus of Elasticity (GPa)
25	467	947	560	1135	13	188
26.5	480	838	625	1083	13	176

Table 4.2. The Prestressing Force Applied on the Bars, Number of Bars per Wall and the Corresponding Percentage of Breaking Load used in the Experiments.

Units	Diaphragm wall			Fin Wall		
	Prestress force (kN)	No of bars	% breaking load	Prestress force (kN)	No of bars	% breaking load
Clay	309	2 No 25	55%	363.1	2 No 26.5	58%
Calcium Silicate	323.4	1 No 25	58%	379.94	1 No 26.5	61%
Concrete Blocks	302.4	1 No 25	54%	399.84	1 No 26.5	64%

Table 4.3. Volume/exposed Surface Ratios of the Walls, Masonry Units and Mortar Prisms.

Wall	Volume (10^7 mm^3)			Exposed surface area (10^5 mm^2)			V/S (mm)			Total Sealed length (mm)**	
	Mas.*	Brick	Mortar	Mas.*	Brick	Mortar	Mas.*	Brick	Mortar	Brick	Mortar
Diaph. (Clay)	38	31	7.35	47.7	39.5	8.3	80	79	89	12.5	21.8
Fin. (Clay)	44.9	36.5	8.4	72.5	56.1	12.2	62	65	69.3	8.5	17.2
Diaph. (Calcium Silicate)	40.7	33	7.35	47.7	39.5	8.3	85	84.26	89	12.8	21.8
Fin. (Calcium Silicate)	47.4	39	8.4	72.5	56.1	12.2	65.47	69.5	69.3	8.6	17.2
Diaph. (Concrete Block)	37.4	34.1	2.57	45.8	41.8	2.97	81.82	81.48	86.55	12.5	21.25
Fin. (Concrete Block)	49.5	45.9	3.54	69.89	65.1	4.7	70.83	70.5	75.11	9.45	18.78

* masonry

** see Fig. 4.19

Table 4.4. Compressive Strength of Concrete Cubes at 28 day

Base and Capping Beam no.	Mean Concrete Strength (MPa)
1	57.3
2	55.2
3	64.24
4	62.38
5	62.67
6	67.95

Table 4.5 Mean Compressive Strength and Standard Deviation of Mortar Cubes (MPa)

Age	Clay Brickwork		Calcium Silicate Brickwork		Concrete Blockwork	
	Diaphragm	Fin	Diaphragm	Fin	Diaphragm	Fin
21 days	10.13 (0.72)	11.52 (1.28)	10.42 (0.84)	9.66 (0.94)	12.27 (1.36)	13.04 (1.72)

() - standard deviation

Table 4.6 Mean Compressive Strength and Standard Deviation of Masonry Units (MPa)

Unit Type	Header Face	Bed Face
Clay Brick	15.75 (1.06)	103 (9.7)
Calcium Silicate Brick	18.5 (6.9)	27.08 (1.41)
Concrete Block	-	14.87 (1.14)

() - standard deviation

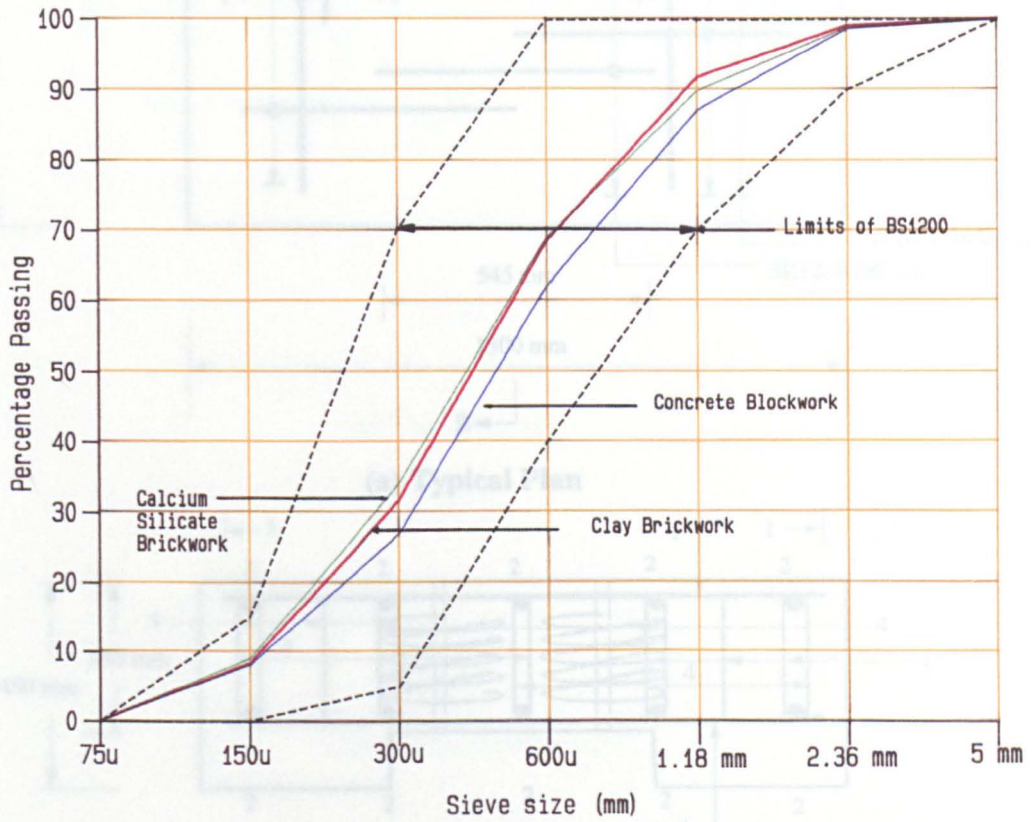
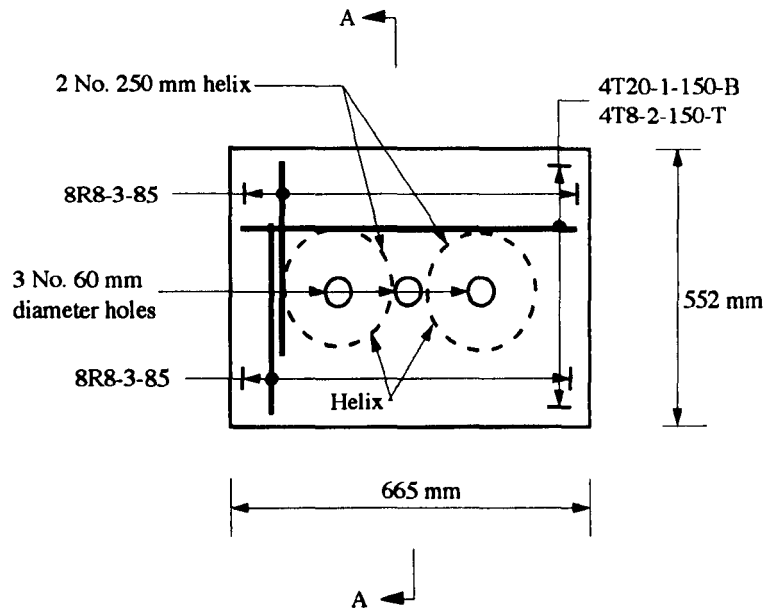


Fig. 4.1 Sieve Analysis of Sand

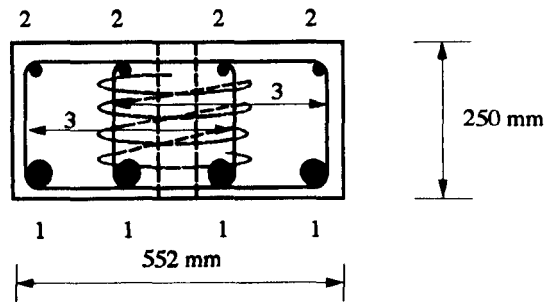


(c) Section B-B

Fig. 4.2 Plan and Section of the Concrete Base for Diaphragm and Fin Walls

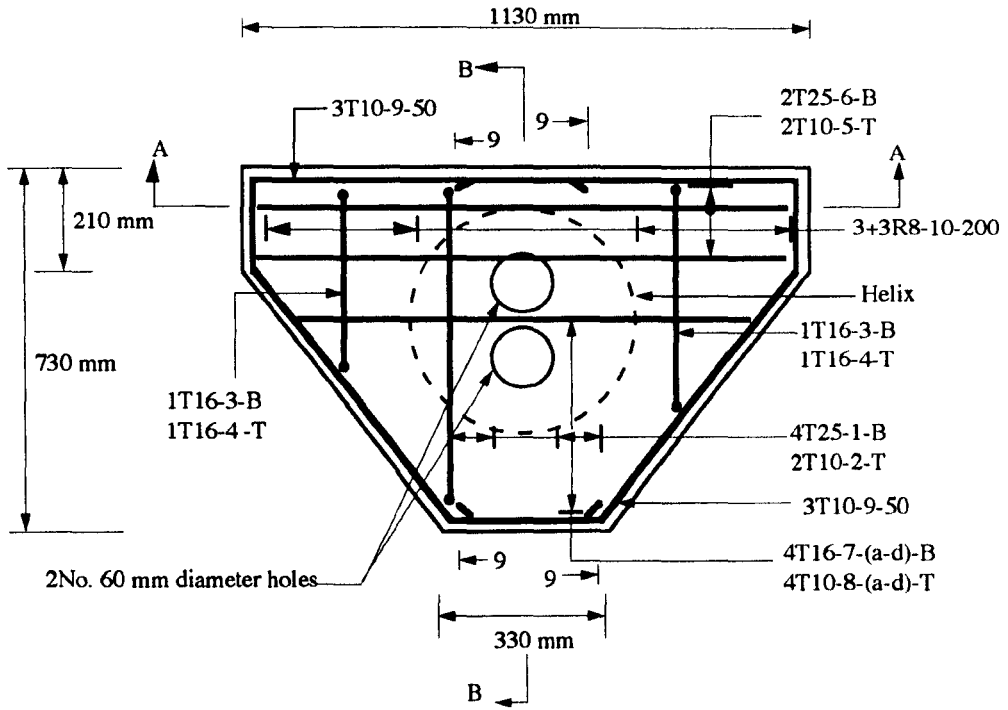


(a) Typical Plan

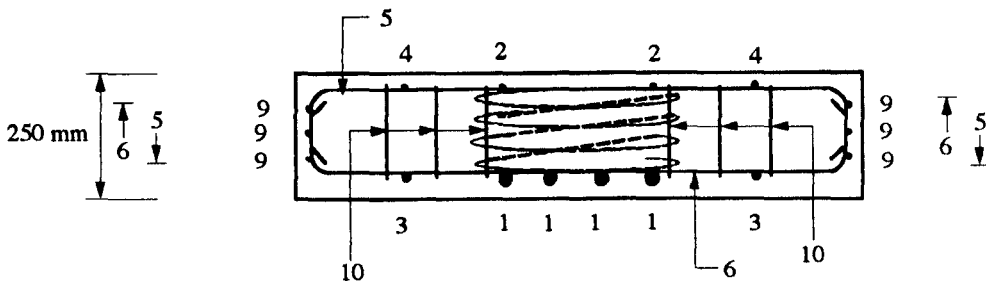


(b) Section A-A

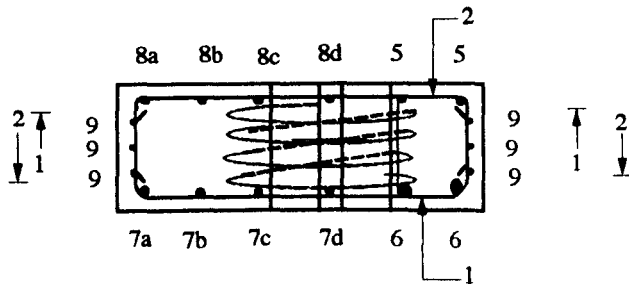
Fig. 4.3 Plan and Section of the Concrete Capping Beams for Diaphragm Walls



(a) Typical Reinforcement Details



(b) Section A-A



(c) Section B-B

Fig. 4.4 Reinforcement Details and Sections of the Concrete Capping Beams for Fin Walls

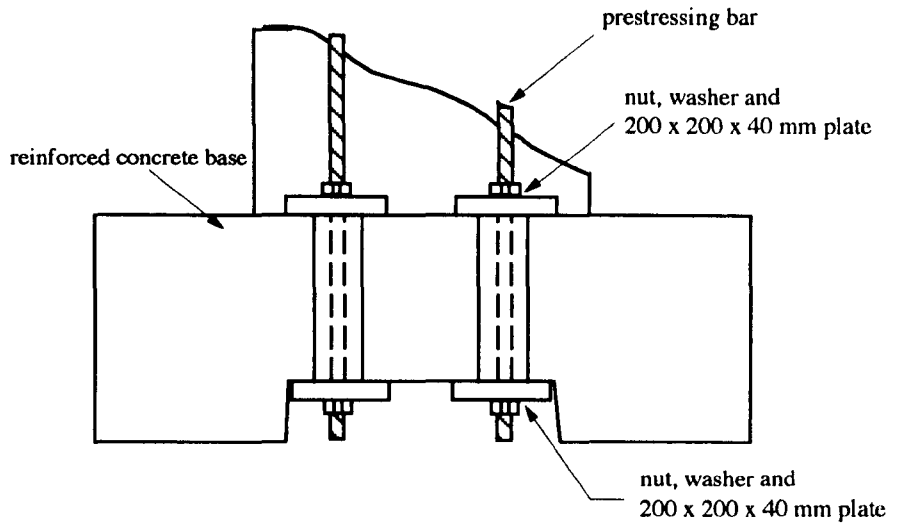


Fig. 4.5 Prestressed Bar Anchorage System to the Concrete Base

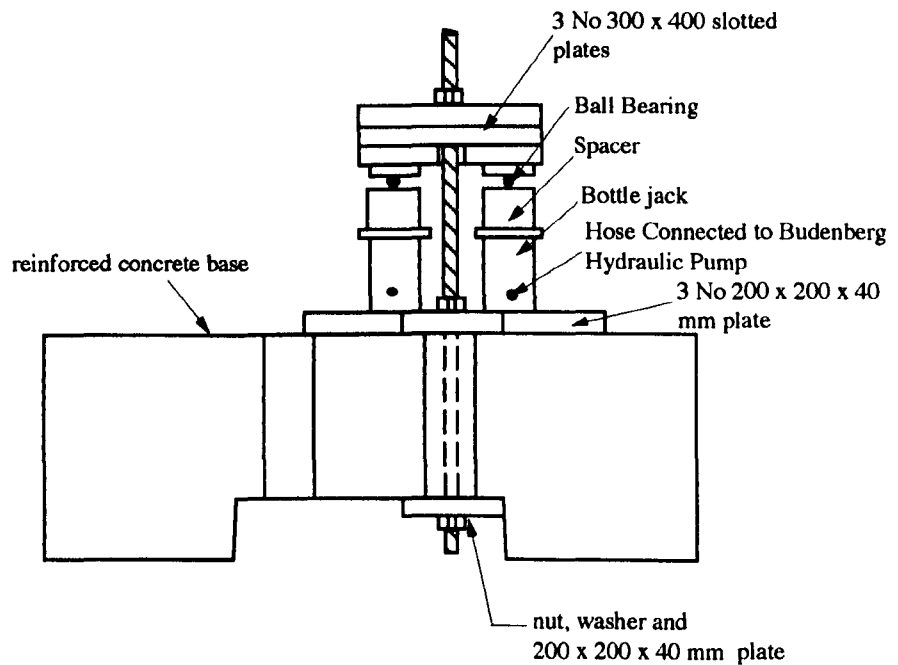
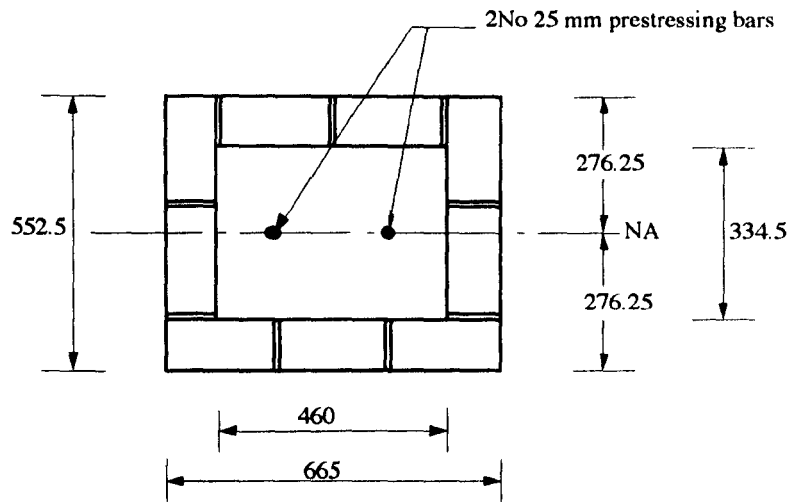
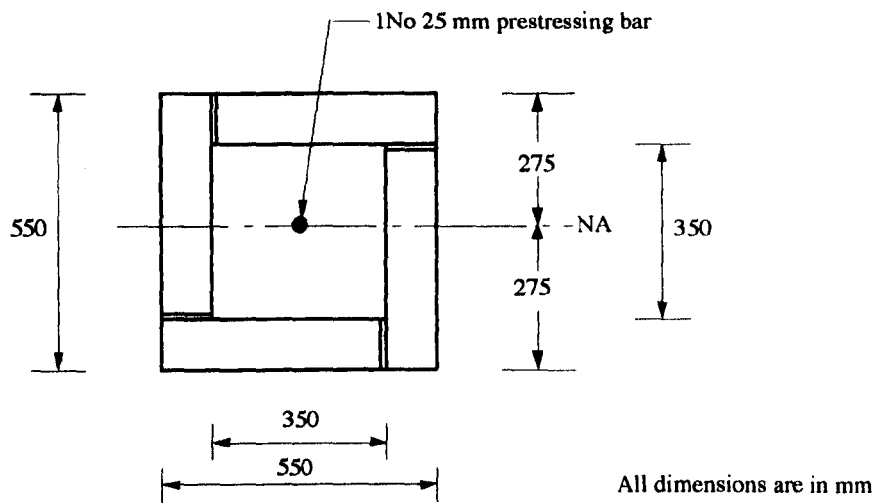


Fig. 4.6 Prestressing Details of Bar Anchored to Concrete Base

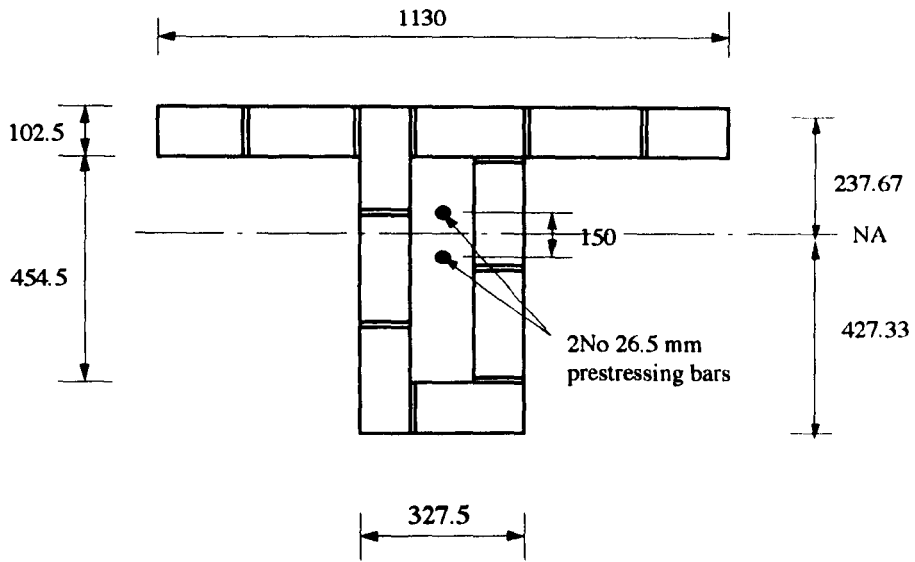


(a) Clay and Calcium Silicate

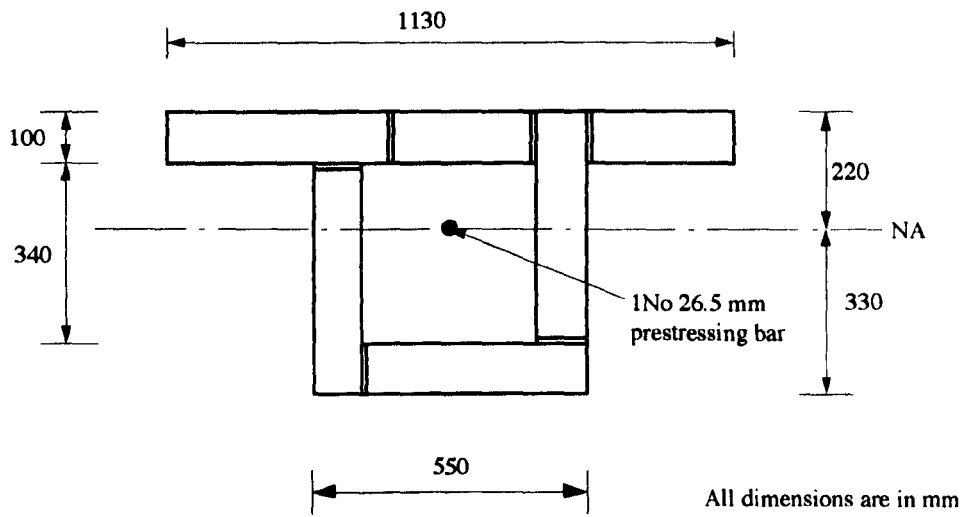


(b) Concrete Block

Fig. 4.7 Section Details of Diaphragm Walls



(a) Clay and Calcium Silicate



(b) Concrete Block

Fig. 4.8. Section Details of Fin Walls

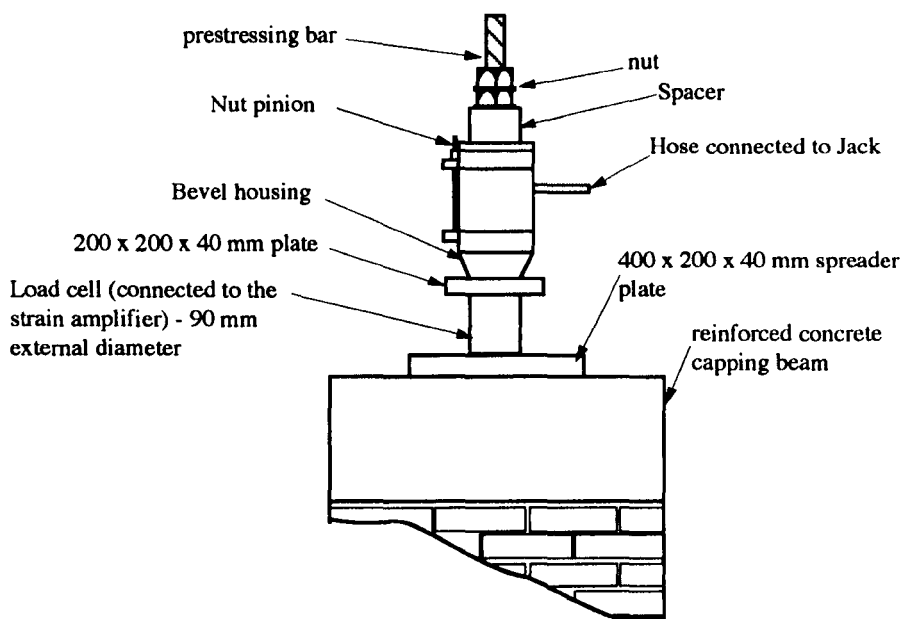
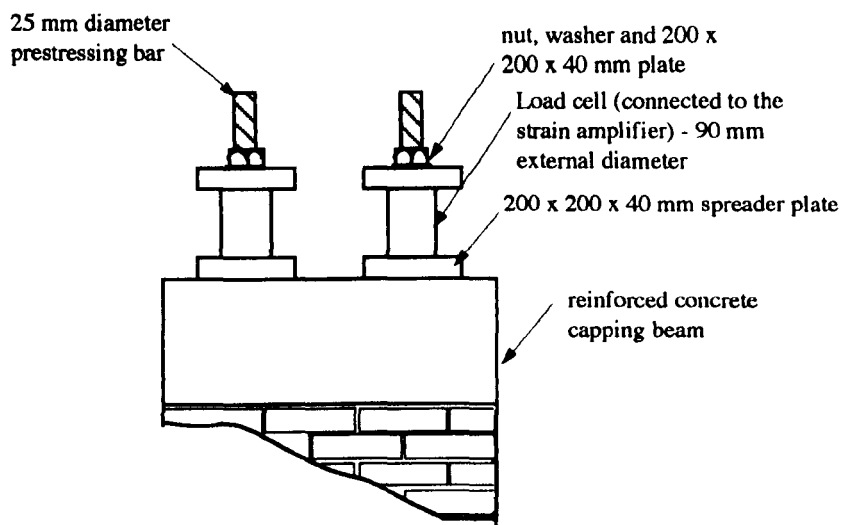
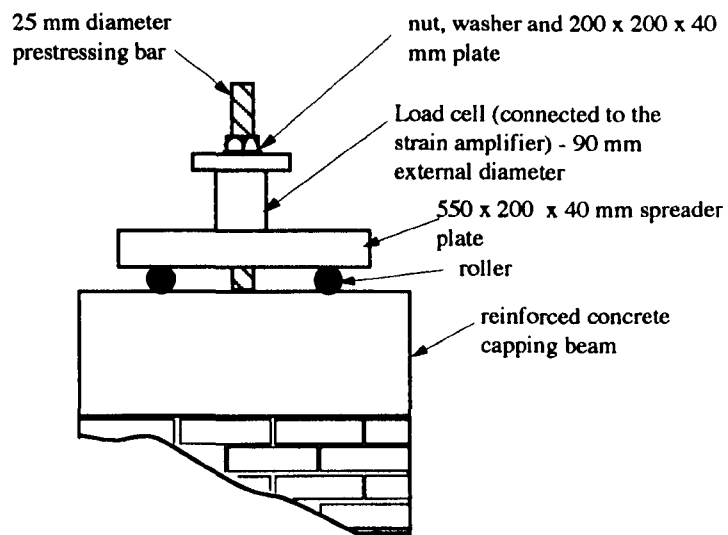


Fig. 4.9 Prestressing Details for the Bar at the top of Concrete Capping Beams

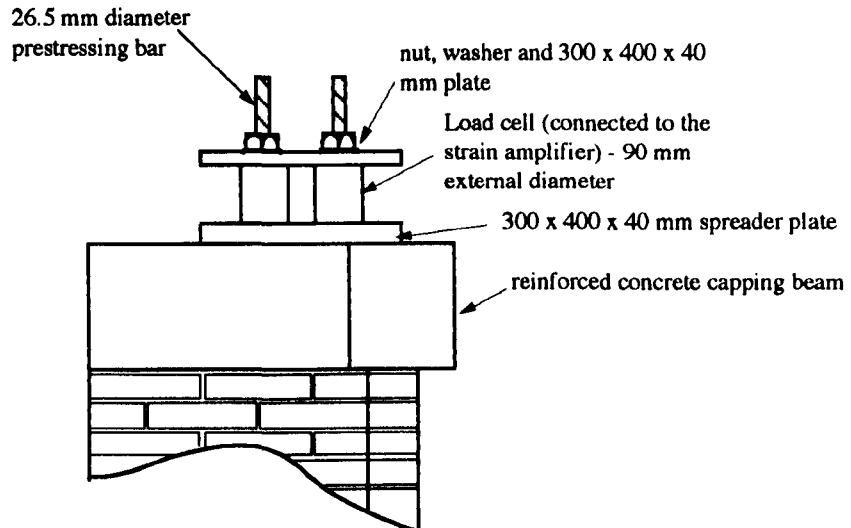


(a) Anchorage System at the Top of Clay Diaphragm Walls

Fig. 4.10 Anchorage System at the Top of Capping Beams for Diaphragm and Fin Walls

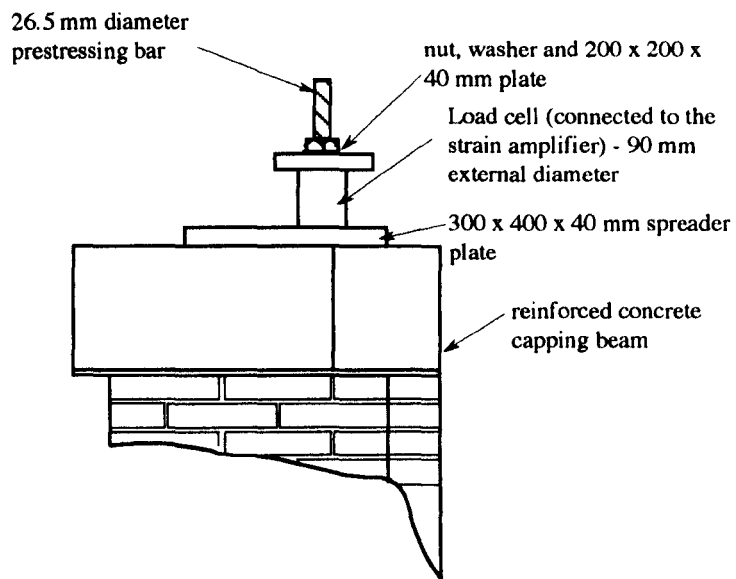


(b) Anchorage System at the Top of Calcium Silicate and Concrete Block Diaphragm Walls.



(c) Anchorage System at the Top of Clay Fin Walls

Fig. 4.10 continued



(d) Anchorage System at the Top of Calcium Silicate and Concrete Block Fin Walls

Fig. 4.10 continued

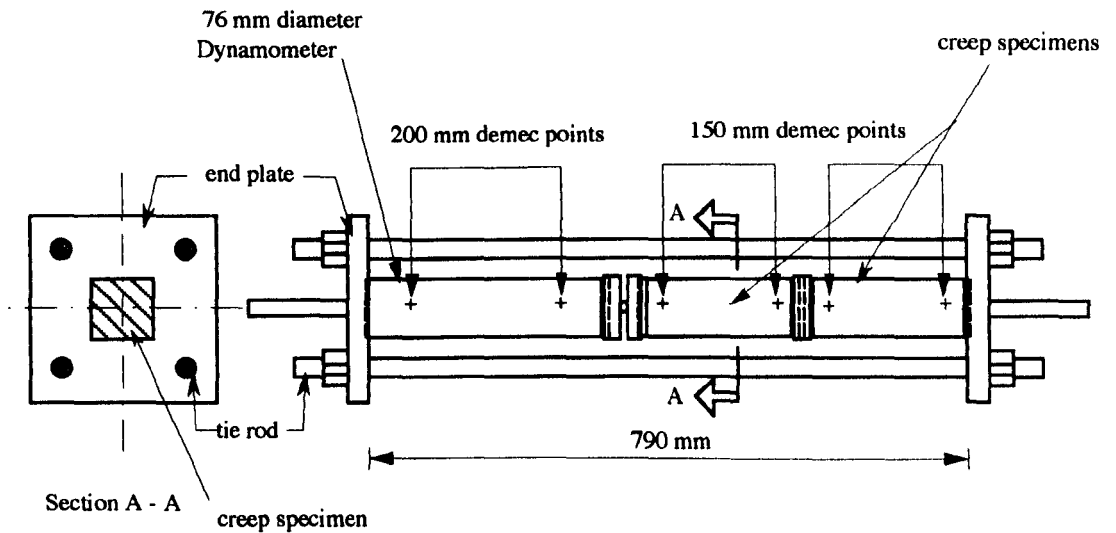


Fig. 4.11 Creep Frame for Masonry Units and Mortar Prisms

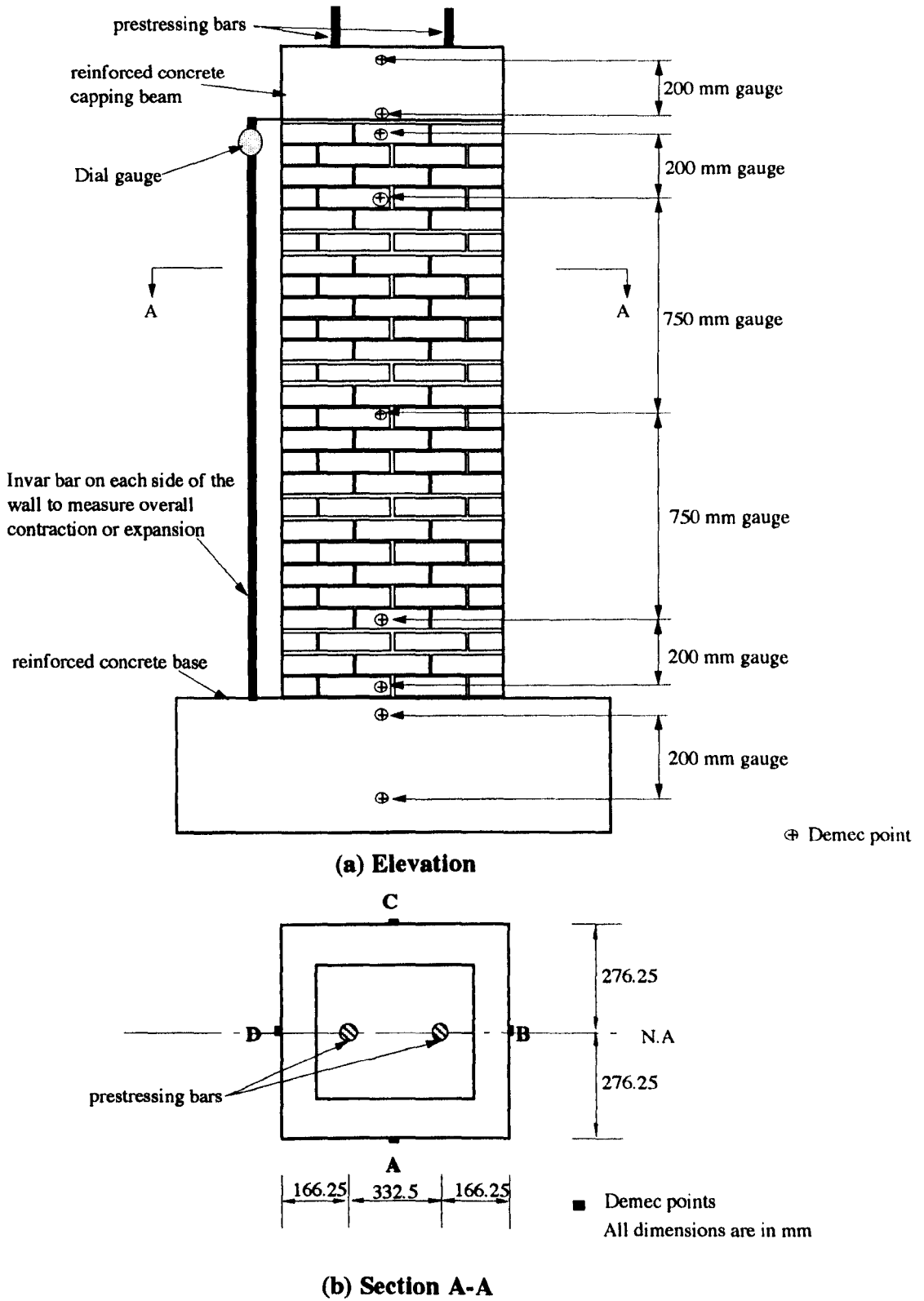


Fig. 4.12 Location of Strain Measurement Points on Clay and Calcium Silicate Diaphragm Walls

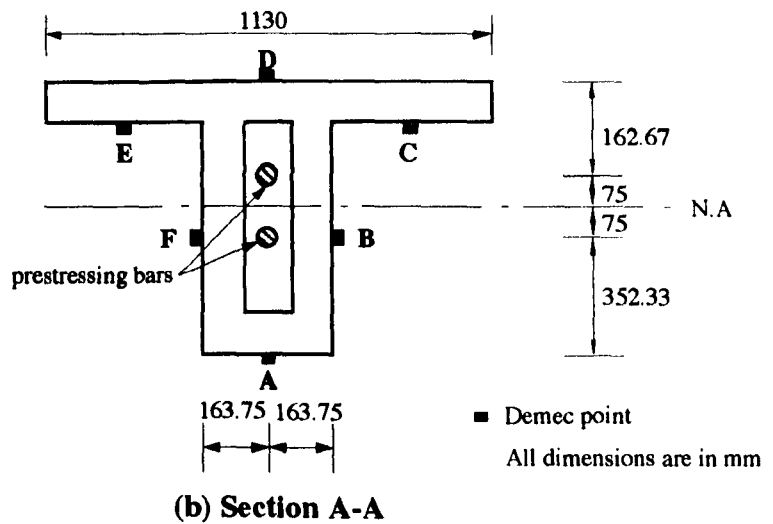
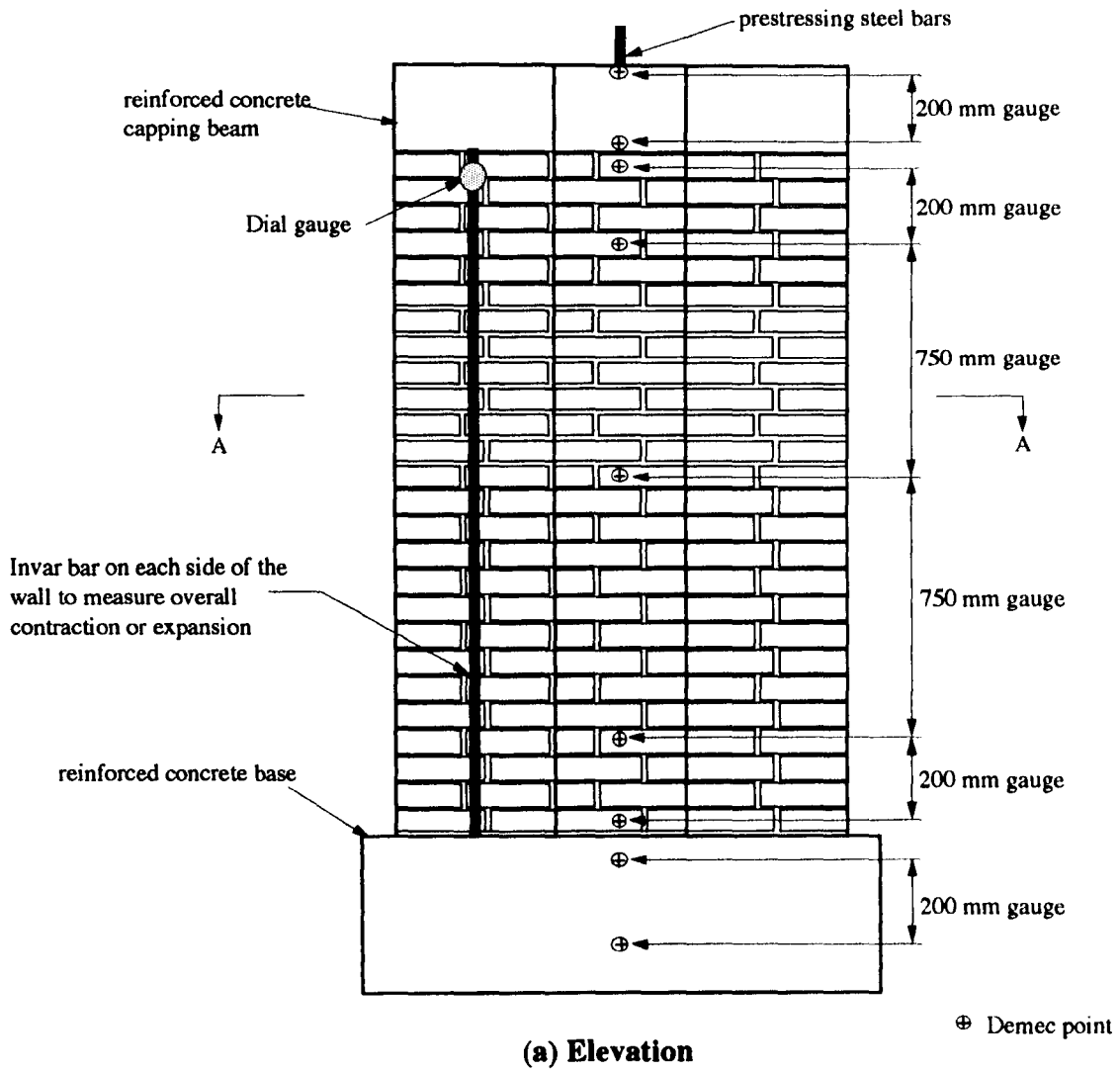
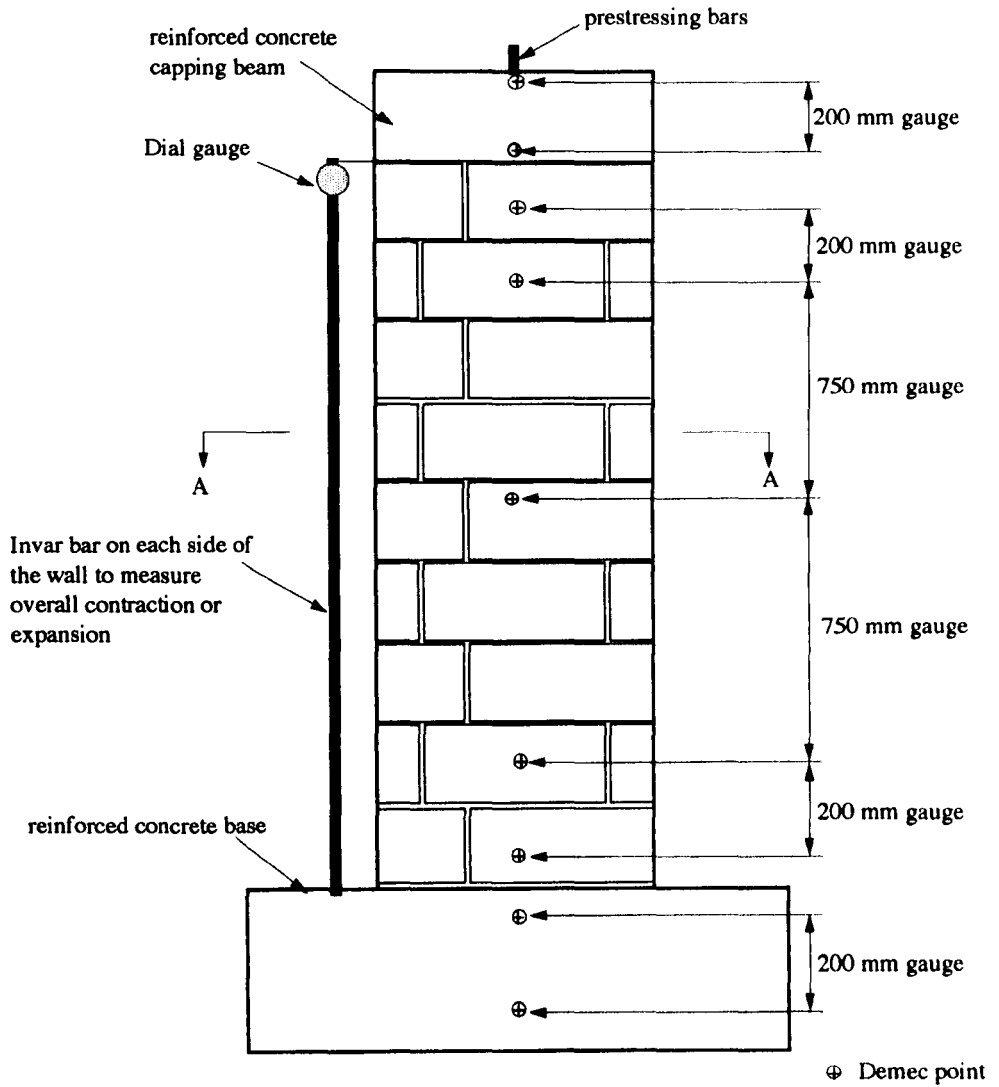
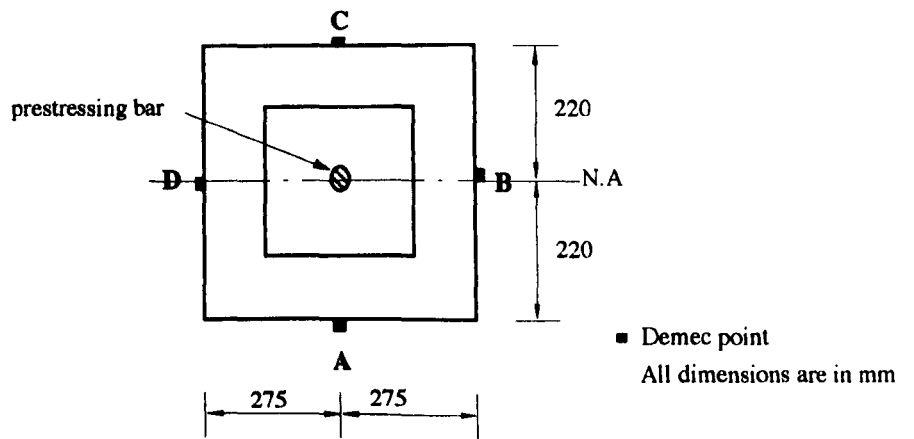


Fig. 4.13 Location of Strain Measurement Points on Clay and Calcium Silicate Fin Walls

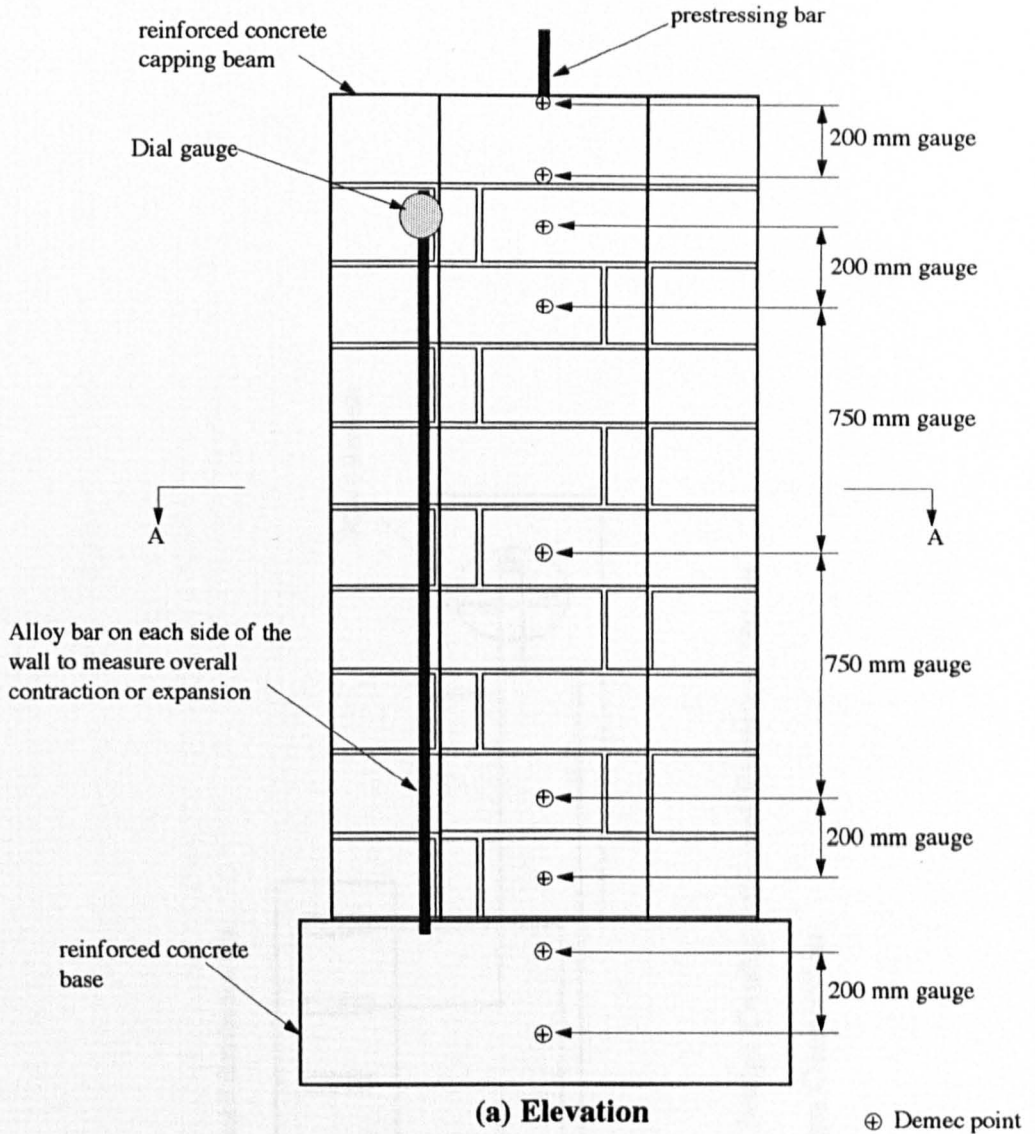


(a) Elevation



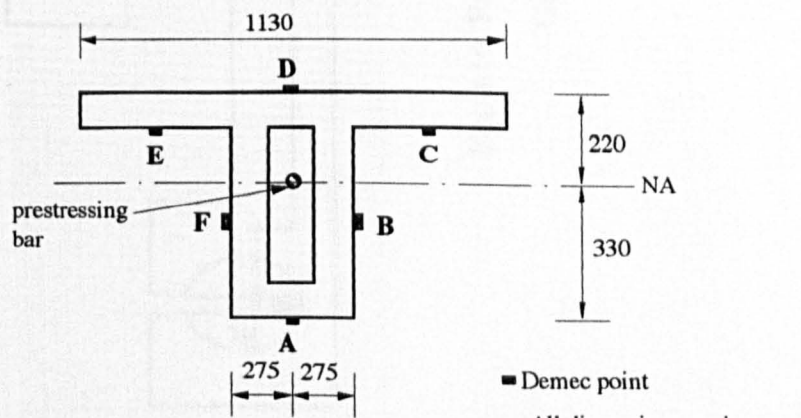
(b) Section A-A

Fig. 4.14 Location of Strain Measurement Points on Concrete Block Diaphragm Walls



(a) Elevation

⊕ Demec point



(b) Section A-A

■ Demec point

All dimensions are in mm

Fig. 4.15 Location of Strain Measurement Points on Concrete Block Fin Walls

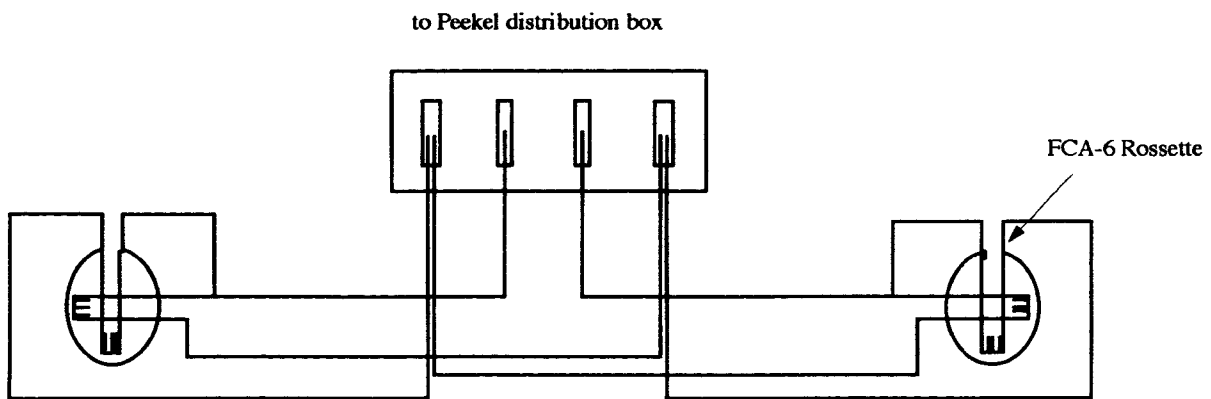


Fig. 4.16 Full Bridge Configuration of Electrical Strain Gauges Connection

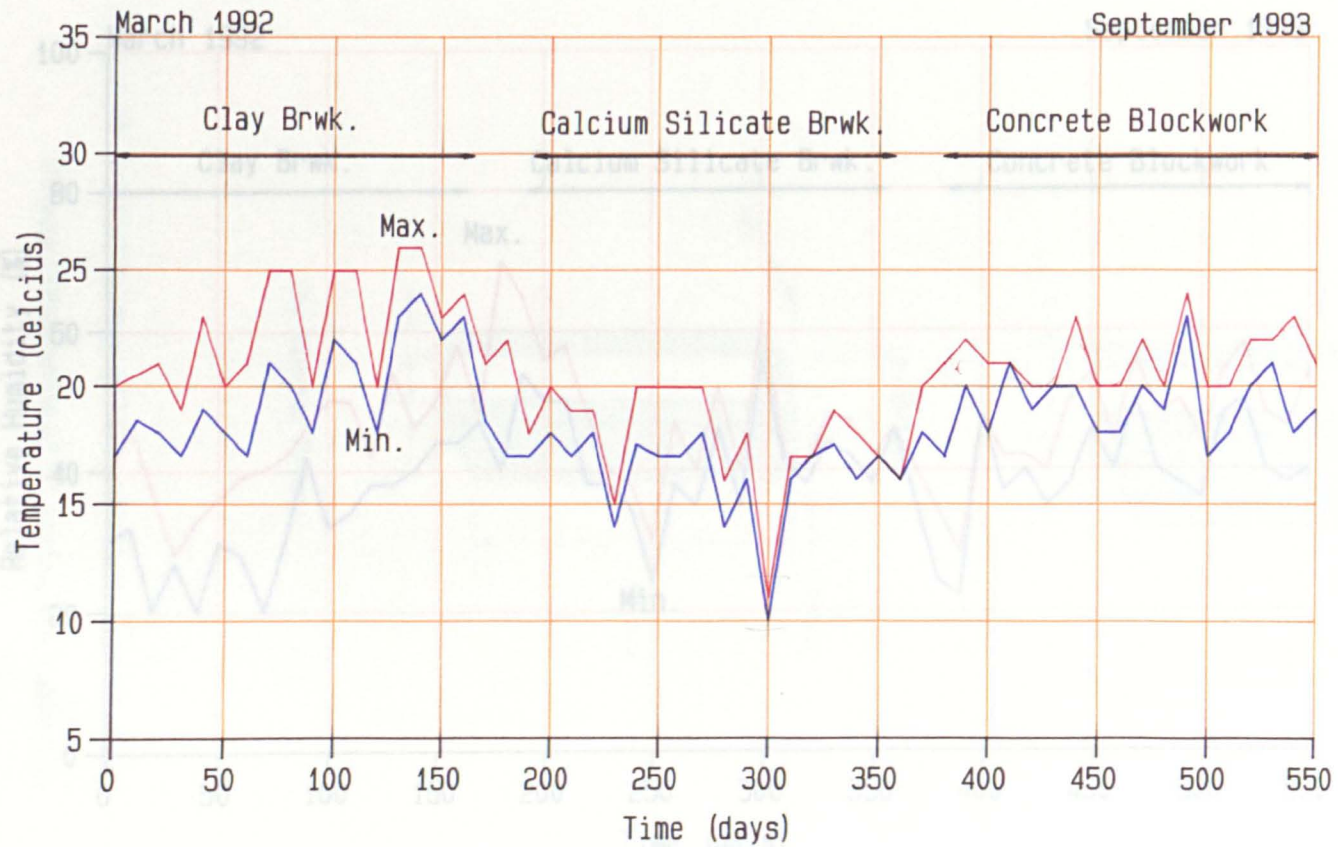


Fig. 4.17 Variation of Laboratory Temperature with time

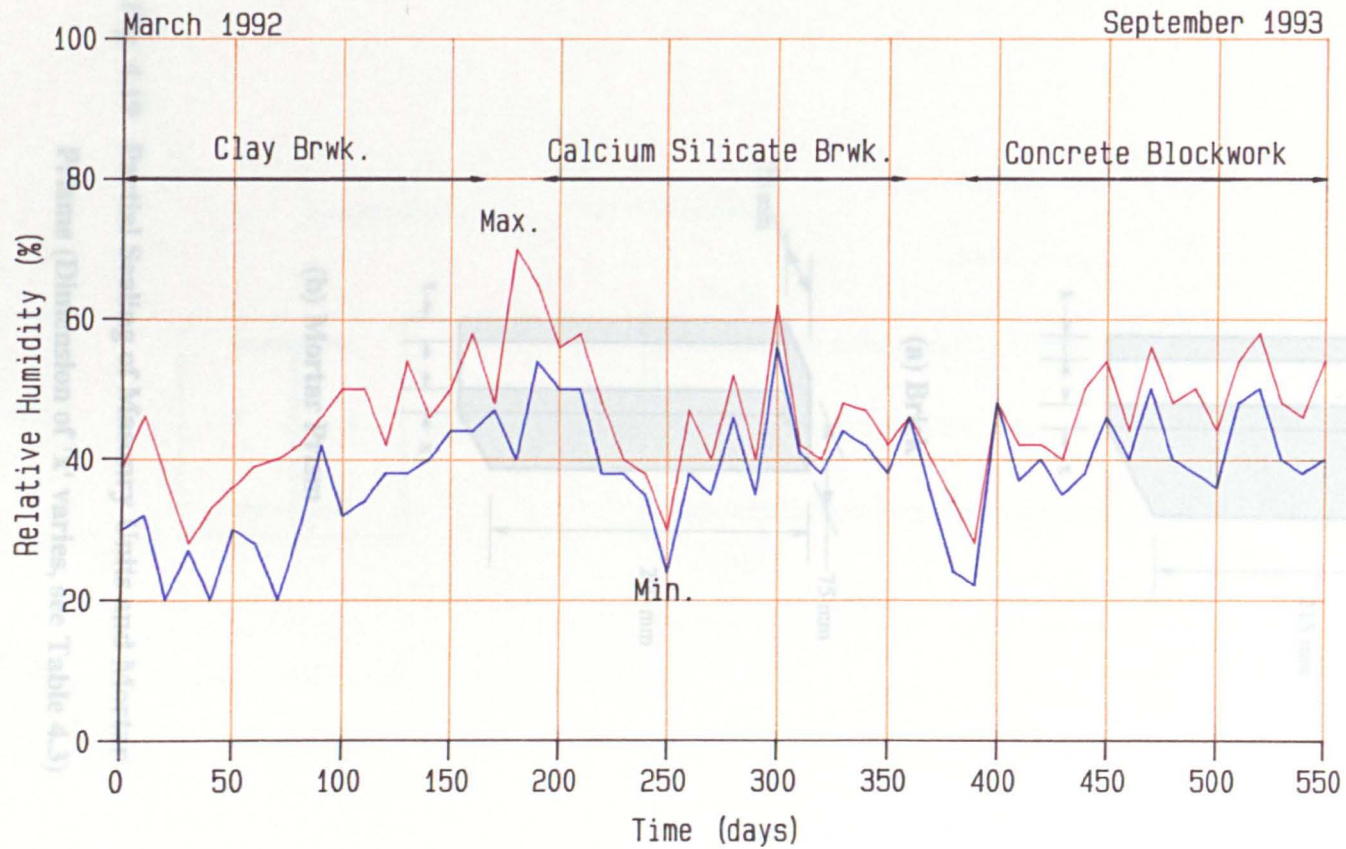
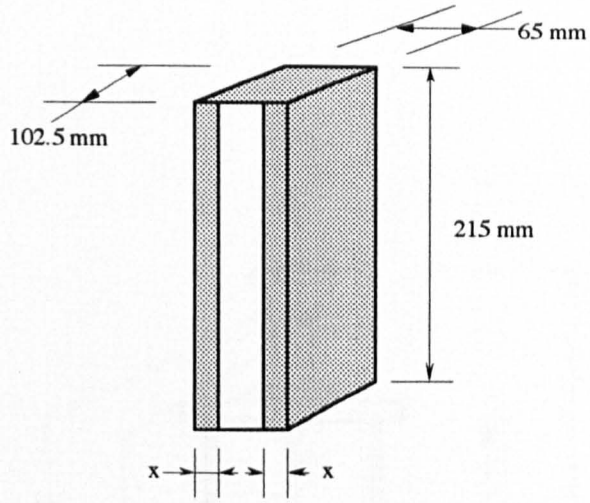
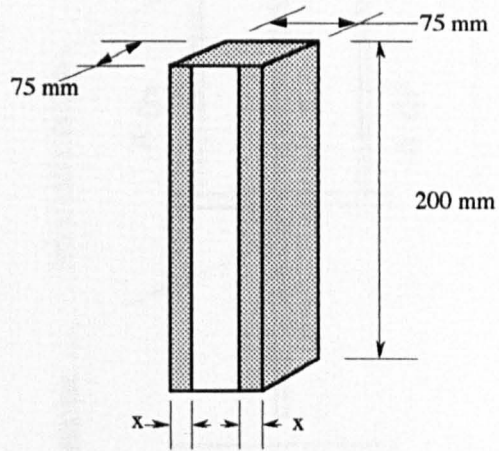


Fig. 4.18 Variation of Laboratory Humidity with Time

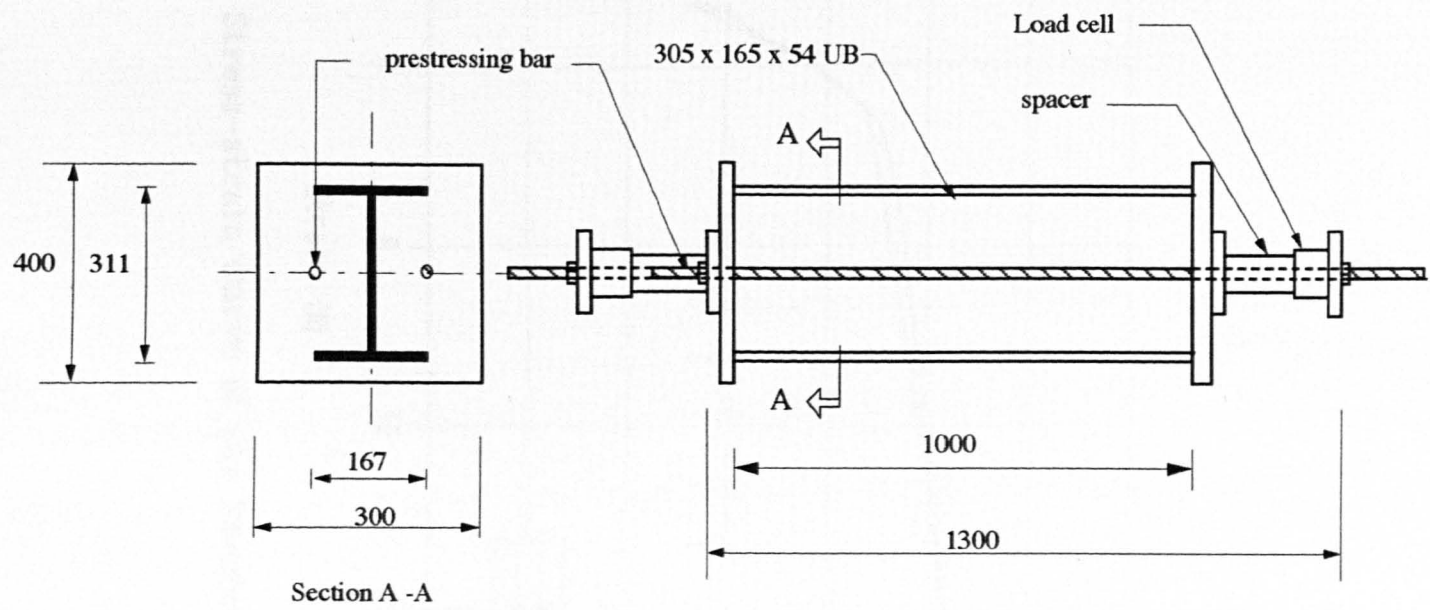


(a) Brick



(b) Mortar Prism

Fig. 4.19 Partial Sealing of Masonry Units and Mortar Prisms (Dimension of 'x' varies, see Table 4.3)



All dimensions are in mm

Fig. 4.20 Intrinsic Relaxation Test

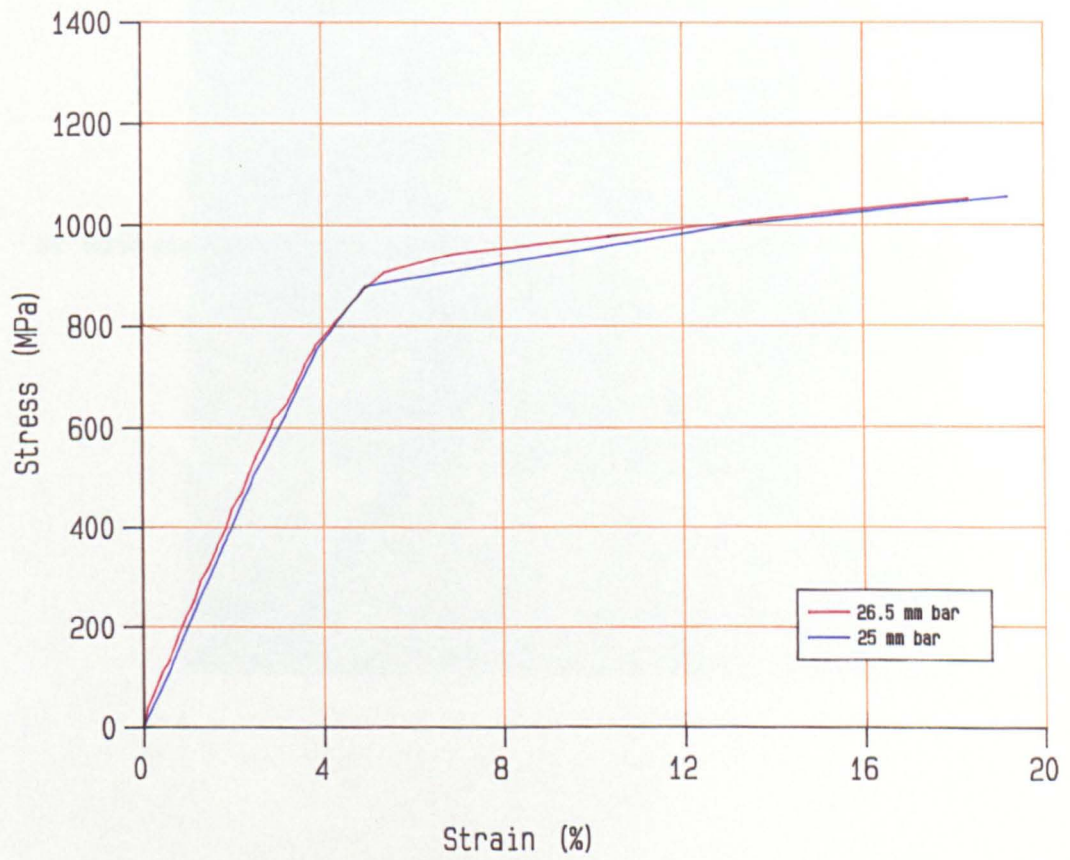


Fig. 4.21 Stress-strain Curve of the Prestressing Bars

**Plate 4.1 Prestressing Details of Bar Anchored to
Concrete Base**

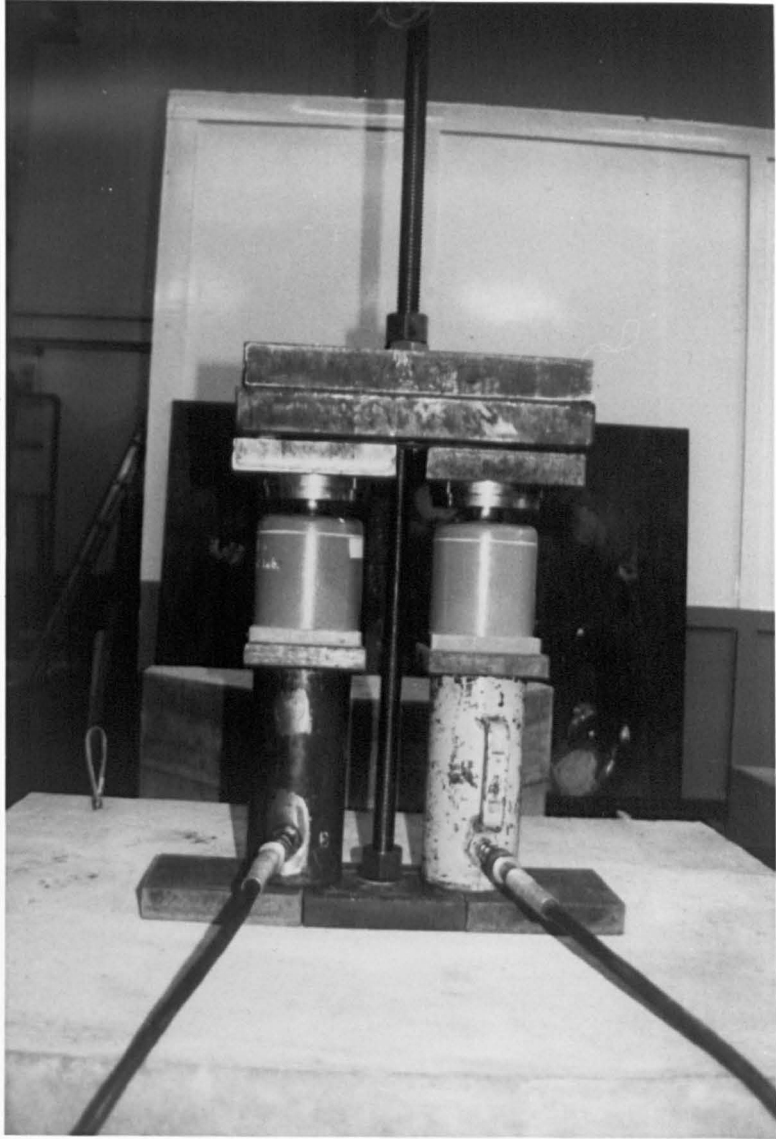


PLATE 4.1

Plate 4.2 During Construction of Diaphragm Wall

Plate 4.3 During Construction of Fin Wall

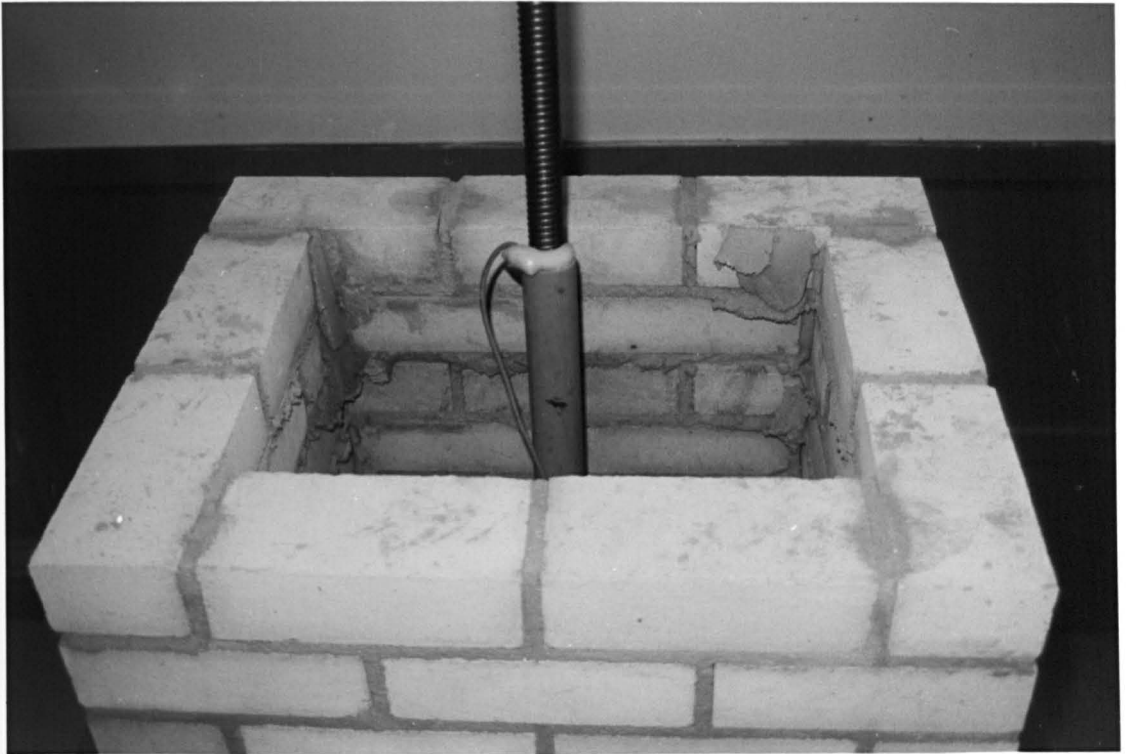


PLATE 4.2

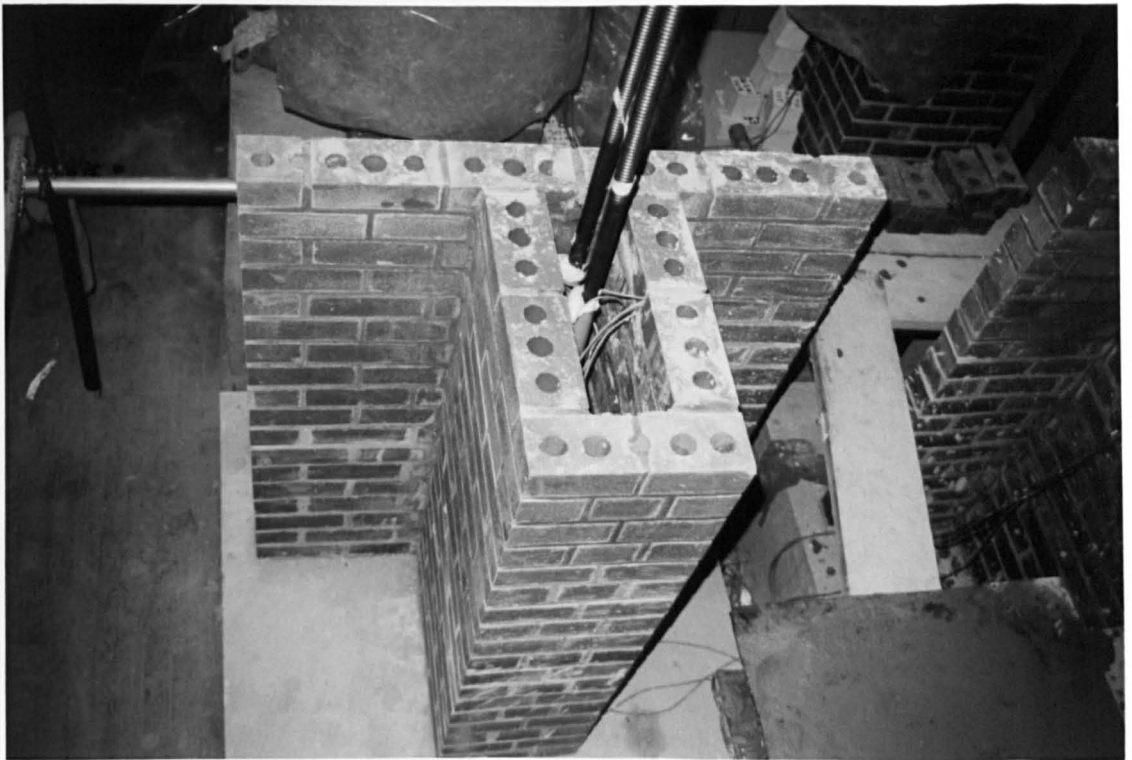


PLATE 4.3

**Plate 4.4 Prestressing Details of Bar at the top of
Concrete Capping Beam**



PLATE 4.4

Plate 4.5 Clay Brickwork under Test

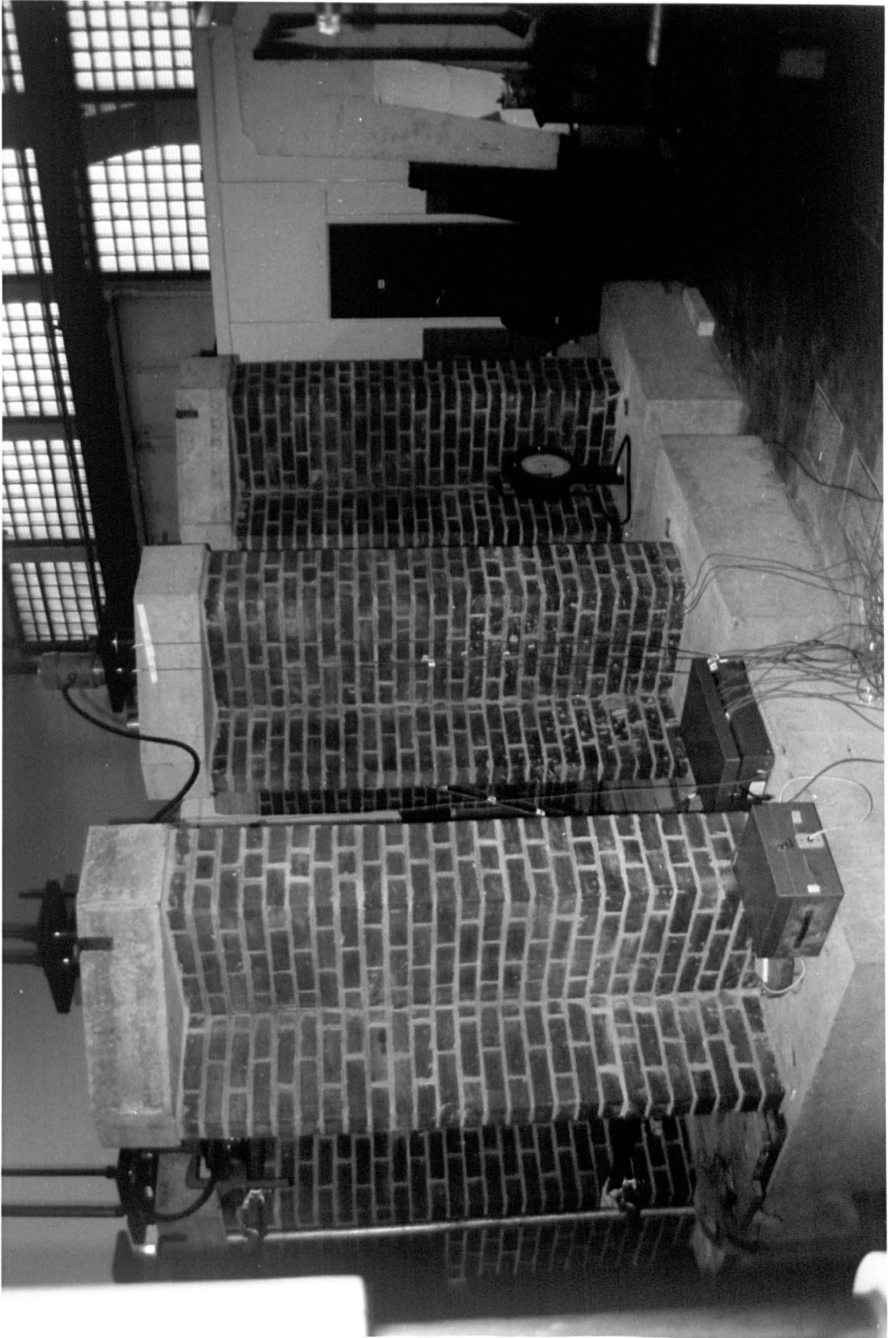


Plate 4.6 Calcium Silicate Brickwork under Test

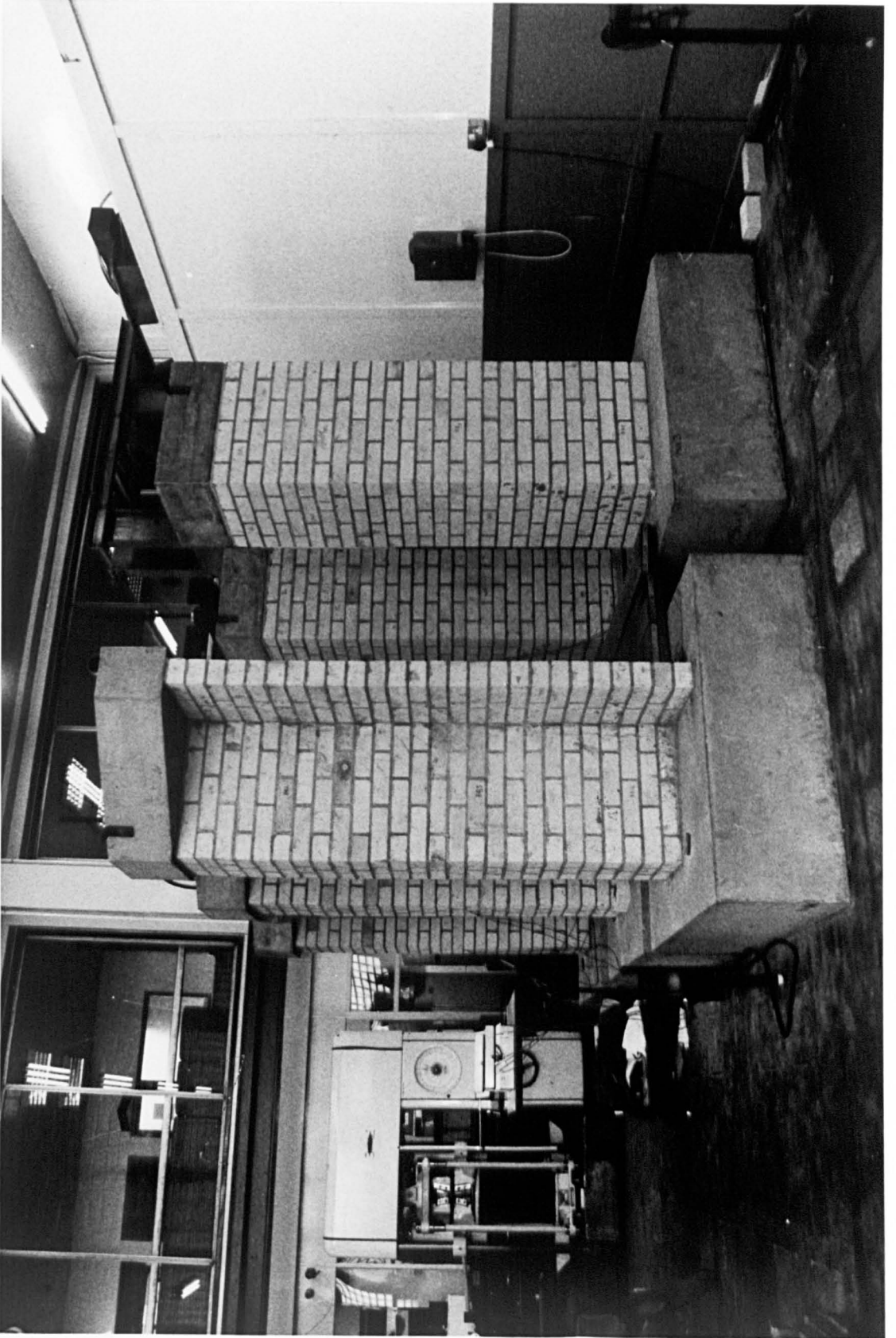


PLATE 4.6

Plate 4.7 Concrete Blockwork under Test



PLATE 4.7

Plate 4.8 Creep Tests on Masonry Units and Mortar Prisms



PLATE 4.8

CHAPTER 5

ANALYSIS AND DISCUSSION OF TEST RESULTS

5.1 Introduction

This chapter presents the observations and analysis of results for the tests described in Chapter 4. The properties of the masonry units and mortar prisms, determined from control tests, are tabulated in Chapter 4.

5.2 Brickwork

5.2.1 Elasticity

5.2.1 (a) Measured elasticity

Table 5.1 shows the average elasticity (secant) of the masonry walls determined from the measured initial strain on each face of the walls during loading. For all types of masonry, there is no indication that the elasticity of the brickwork is affected by the volume/exposed surface ratio (V/S) of the walls. These observations support previous findings that elasticity of brickwork is not affected by geometry (Lenczner 1978 and Amjad 1990).

As expected, due to the high compressive strength of clay units (103 MPa), clay brickwork had the highest elastic modulus compared to the calcium silicate and concrete block walls. The lower modulus of elasticity in calcium silicate and concrete block is due to the porous/permeable nature of their constituents.

The average modulus of elasticity of clay and calcium silicate brickwork is much less than their respective units compared with concrete blockwork. For example, for the clay fin walls, the ratio of unit /wall modulus was 1.60, whereas the corresponding ratio for the concrete block fin wall was 0.80 (Elastic moduli data is given in Table 5.7). While the elasticity of the brickwork walls is clearly influenced by the mortar, there is a smaller influence for blockwork. This is due to fewer mortar bed joints in blockwork than in brickwork for the same size of masonry member. For this investigation, it appears that elastic modulus of blockwork is roughly equal to the modulus of the block units, but this may not be true for other units.

5.2.1 (b) Elasticity by finite elements

Elasticity of the masonry walls was predicted by a linear elastic finite element method using Pafec (Program for Automatic Finite Element Calculations 1978) package. Pafec also computes creep of materials but its application is generally for mechanical engineering problems. In this research Pafec (1978) was used for comparing the elasticity of the masonry walls by applying individual deformations of the masonry units and mortar. The variables in this study were the types of masonry units with different compressive strength.

Basic assumption of the analysis

The analysis assumes that;

- a) the wall is thin and has a constant thickness,
 - b) stresses are constant throughout the thickness of the element,
- and c) the element is flat and carries load in its plane only.

The walls were analysed as 2-D plane stress element. The width of the walls was 665 mm in clay and calcium silicate brickwork, and 550 mm in concrete blockwork. The height of the walls was as in the experiments. Initially the walls were divided into a number of eight nodes isoparametric curvilinear quadrilateral elements. The elements were subjected to the same stress as the experimental brickwork. The elasticity of the walls was determined from the displacements output of the elements. Pafec (1978) determined the displacement of the elements by first expressing them in terms of in-plane nodal displacement matrices. Application of virtual work method results in a set of simultaneous equations (stiffness) which relate the nodal forces with the nodal displacement. The displacement of the elements is then solved by assembling and solving the equations for the entire wall.

Fig. 5.1 shows typical displacements in the masonry walls under 46% of its working stress. The elasticity using the finite elements method is compared to the measured values as in Table 5.1. Pafec predicts elasticity reasonably well in clay walls and within 20% in calcium silicate and concrete block walls, although the walls analysed were represented as a single-leaf wall. This confirms the previous observation that the elastic modulus of masonry is not influenced by geometry. The general prediction of elastic modulus is discussed in Chapter 6.

5.2.2 Creep of masonry walls

The average creep was determined by subtracting the average shrinkage and instantaneous (elastic) strains from the measured strains on the creep walls. Tables B.1, B.2 and B.3 of Appendix B show the strains of the clay, calcium silicate and concrete block walls measured at various positions. The average creep of the masonry walls was then plotted at each time interval as shown in Fig. 5.2 to 5.4. During these tests, the average temperature and humidity were 21°C and 40%, 18°C

and 45%, and 20°C and 45% for clay, calcium silicate and concrete block masonry, respectively (see Figs. 4.17 and 4.18).

All the masonry walls investigated in this test programme exhibited similar creep-time behaviour as concrete, i.e rapid increase initially and with a decreasing rate with time. Approximately 80% of the 120-day creep in the walls took place in the first 60 days after loading. Compared to the other walls, creep on different faces of the fin calcium silicate walls had the highest variation (10%).

The influence of geometry and masonry units on the average creep of the masonry walls is presented in the following sections.

5.2.2 (a) Influence of geometry

Figures 5.2 to 5.4 show that for all types of masonry, creep of the fin walls with a V/S ratio of 62 - 70 mm was higher than creep of the diaphragm walls with a V/S ratio of 81 - 85 mm. The fin walls generally exhibited 12 % higher creep than the diaphragm walls and the trend with geometry agrees with the findings of previous researchers (Abdullah 1989). The greater creep in the fin walls is due to its low value of V/S which means that, relatively, there is more exposed surface area for drying creep to take place in the masonry and the average drying path length for moisture diffusion is less. Since a greater drying is associated with a greater creep (as for concrete), the results of this investigation are as anticipated.

5.2.2 (b) Influence of masonry units

The influence of masonry units on specific creep is illustrated in Fig. 5.5 and Fig. 5.6 for the diaphragm and fin masonry walls, respectively. The trends indicate that creep is influenced by the type of masonry unit. Clay walls, constructed from units with a compressive strength of 103 MPa, exhibit less creep than walls constructed from calcium silicate and concrete block units. At 120 days, clay, calcium

silicate and concrete block fin walls undergo a specific creep of 83×10^{-6} , 160×10^{-6} and 150×10^{-6} per MPa, respectively. A lower creep was measured in the concrete block wall than the calcium silicate wall, although the compressive strength of calcium silicate units was greater (27.08 MPa) compared with the concrete block unit (14.87 MPa). However, a calcium silicate wall have three time as many bed joints as a concrete block wall, which therefore increase creep when comparing brickwork with concrete blockwork. Consequently, it can be concluded that for units of the same size, masonry units with high compressive strength exhibit a lower creep in masonry walls.

Creep of masonry occurs mainly due to mortar, the units offering resistance to creep. The stiffer the brick units the lower the creep of masonry and, generally, the stiffer the brick the greater the compressive strength.

5.2.2 (c) Ultimate creep

An estimate of the ultimate creep of the masonry walls was obtained using regression analysis of the Ross (1937) hyperbolic-time function, which was developed for concrete. This analysis has been used previously in determining ultimate deformations in masonry (Lenczner 1986a and Brooks et al 1990a). Previous researchers (Lenczner 1986a and Brooks et al 1990a) observed that the function underestimates short-term deformations but predicts long-term deformations reasonably well. The hyperbolic time function is:

$$c = \frac{t}{(a + bt)} \quad (5.1)$$

or
$$\frac{t}{c} = a + bt$$

where $c = \text{creep } (10^{-6})$;

$t = \text{time under load (days)}$;

$a = \text{constant};$

$b = \text{constant} = 1/C_u;$

and $C_u = \text{ultimate creep}.$

The analysis was carried out using the smoothed creep-time curves of Fig. 5.2 to 5.4. Initially, [time/creep] versus time curves were plotted at 20 day intervals. The plots give a straight line with a slope of 'b' and an intercept of ordinate 'a'. The ultimate creep was determined from a reciprocal of slope 'b'. The ultimate specific creep and the correlation coefficients, using the rectified hyperbolic equation are shown in Table 5.2. As expected the calcium silicate and concrete block diaphragm and fin walls exhibited a higher ultimate specific creep compared with the clay brickwork.

Attempts were also made to predict the ultimate creep specific by a logarithmic expression (Neville et al 1983). However, the expression only predicted short-term creep quite well (up to 60 days after loading), but the long-term values were underestimated.

The ultimate specific creep of diaphragm clay ($V/S=80$) and concrete block ($V/S=82$) walls were much lower than values reported by Abdullah (1989) for approximately the same V/S ratio (hollow piers). The differences could be due to the test conditions, because Abdullah (1989) tested masonry with bricks laid wet and the masonry was cured under polythene sheet until loading it at 28 days.

5.2.2 (d) Creep coefficient

The creep coefficients of the masonry walls are shown in Table 5.3. The creep coefficients were determined from the ratio of ultimate creep to the instantaneous strain at loading. Calcium silicate (2.2 - 2.4) and concrete block (2.34 - 2.53) walls exhibited higher values of creep coefficients compared to clay (1.49 - 1.55) walls.

For all types of masonry, fin walls have higher values of creep coefficients when compared to the diaphragm walls. This is due to the effect of geometry on creep as discussed in section 5.2.2.(a), the elastic strain being unaffected by geometry.

5.2.3 Shrinkage of masonry walls

The shrinkage of the masonry walls are given in Tables B.1, B.2 and B.3 of Appendix B. The measurements commenced on the same day as loading of the creep and prestress loss walls. All the masonry walls exhibited shrinkage with time, even the clay walls, as shown in Fig. 5.7 to 5.11. Compared with the other walls, the measured shrinkage on the different faces of the concrete block diaphragm walls had the highest variations (10%).

The effect of geometry and masonry units on shrinkage of the masonry walls is presented in the following sections.

5.2.3 (a) Influence of geometry

The average shrinkage-time curves of the masonry walls are shown in Fig. 5.7, Fig. 5.8 and Fig. 5.9 for clay, calcium silicate and concrete blocks walls, respectively. As expected the magnitude of the shrinkage was influenced by the masonry geometry, with fin walls showing a higher shrinkage than diaphragm walls. As for creep, the higher shrinkage in the fin walls can be explained by its lower value of V/S .

5.2.3 (b) Influence of masonry units

The influenced of masonry units on shrinkage is shown in Fig. 5.10 and 5.11. As for creep, the masonry walls built from high compressive strength

masonry units exhibited less shrinkage. This was due to the greater stiffness of the masonry units which restrains the shrinkage of the mortar joint.

The shrinkage of the clay wall was rapid initially and then slowed down after 60 days. The calcium silicate and concrete block walls undergo similar trends of shrinkage with time, but the rate of shrinkage of the walls was much higher especially at later stages.

5.2.3 (c) Ultimate shrinkage

Using the same hyperbolic-time function (Eq. 5.1) as for creep, the ultimate shrinkage was estimated for all the masonry types walls and tabulated in Table 5.4. There was no clear difference between the ultimate shrinkage of fin and diaphragm walls for all types of masonry. This implies that the geometry effect is smaller for long-term shrinkage of masonry. The ultimate shrinkage value of the calcium silicate diaphragm wall is higher than that of fin. This is due to the higher rate of shrinkage at later stages, but it should be emphasised that the ultimate values are based on relatively short-term test data. Longer term tests of several years are desirable.

For the same V/S ratio, the ultimate shrinkage of the diaphragm clay and concrete walls were higher than that reported by Abdullah (1989). Again, differences could be due to the tests conditions, as stated previously in section 5.2.2.(c).

5.2.4 Prestress loss of masonry walls

Generally good agreement was obtained between the strain recorded by the loadcell with the back-up strain as measured on the bar. The prestress loss of the diaphragm and fin prestressed masonry walls, initially loaded at 46% of its working stress, are shown in Figs. 5.12 to 5.14.

The measured prestress loss of the clay walls was up to 4% higher than that values measured by Curtin (1991) who carried out tests when the brickwork was several months old before prestressing; initially his brickwork was used for a reaction wall in a flexural strength test. This implies that Curtin's lower prestress loss was due to a reduced creep and shrinkage because of the greater age and also due to the effect of pre-loading. The present values of prestress loss of the clay walls are similar to those reported by Lenczner (1986).

The effect of geometry and the masonry units on prestress loss are discussed in the following section.

5.2.4 (a) Influence of geometry

The influence of geometry on prestress loss is illustrated in Figs. 5.12 to 5.14. For all the types of masonry the diaphragm walls have a lower prestress loss than the fin walls, by about 3 %. This was because of the corresponding lower time-dependent deformations of the diaphragm masonry walls. Hence, there is an influence of geometry as expressed in terms of the V/S ratio.

5.2 4 (b) Influence of masonry units

The effect of masonry units, clay, calcium silicate and concrete blocks on prestress loss in the prestressed diaphragm and fin masonry walls are illustrated in Fig. 5.15 and Fig. 5.16. The clay, calcium silicate and concrete block walls were initially stressed to 3, 1.57 and 2 MPa, respectively, and the clay walls exhibited a lower prestress loss compared to the prestressed calcium silicate and concrete block walls.

Again the pattern of prestress loss with unit type follows that of creep and shrinkage, viz. the lower the unit strength, the more the creep and shrinkage, and prestress loss.

5.2.4 (c) Measured strain on prestress loss walls

Figure 5.17 shows the measured strain-time curve of the prestressed clay walls under varying stress, which was due to the decrease of prestressing force on the walls as a result of creep, shrinkage and relaxation of the bars. Hence, the measured strain values on the prestressed walls were less than the sum of creep and shrinkage (Figs. 5.2 and 5.8). Due to the effect of geometry a higher strain was measured on the prestressed fin walls than on the prestressed diaphragm walls.

The corresponding measured strain-time curves for calcium silicate and concrete block walls are shown in Figs. 5.18 and 5.19, respectively. Similar trends were observed.

5.3 Mortar prisms

As stated earlier, the instantaneous and time-dependent deformations of partly sealed mortar prisms were determined in this study for the application of composite model theory to predict deformations in the masonry walls. The predicted deformations are compared to the measured deformations in Sections 6.2 and 6.3, of Chapter 6. The following sections present the test results.

5.3.1 Elasticity

The secant modulus of elasticity of the 75 x 75 x 200 mm mortar prisms was determined from the average strains resulting from applying the load in the creep test. Table 5.5 gives the results.

The mean modulus of elasticity varied between 6.94 to 10.04 GPa, even though the mix proportions and w/c ratio of the mortar remained constant throughout the test programme. The corresponding compressive strength of mortar is

shown in Table 4.5 in Chapter 4, and it can be seen that the variation is less than for the elastic modulus. Table 5.5 also indicates the standard deviations were quite high for the concrete blockwork mortar. When the standard deviation and Students t-test are considered, the variation of mean moduli was insignificant.

5.3.2 Creep

Figures 5.20 to 5.22 show the influence of geometry on the creep of partly sealed mortar prisms. For all the type masonry walls, mortar prisms for the fin walls exhibited higher creep than the diaphragm walls, which was the trend observed for the brickwork. Thus the simulated V/S ratio in the mortar prisms appeared to be satisfactory.

Figures 5.23 and 5.24 show the specific creep-time curve of the mortar prisms for the clay, calcium silicate and concrete block walls. The mortar prisms for both calcium silicate creep walls exhibited higher specific creep compared with the clay and concrete block walls. This could have been due to the lower compressive strength of mortar cubes for the calcium silicate walls (see Table 4.5). The actual measured strains are detailed in Appendix C.

5.3.2 (a) Ultimate creep

The ultimate creep of the partly sealed mortar prisms was determined using the same equation as for creep of brickwork i.e the Ross hyperbolic equation (Eq. 5.1). The ultimate creep and correlation coefficients of mortar prisms are as shown in Table 5.5. As expected the mortar prisms for the calcium silicate brickwork exhibited the highest ultimate specific creep compared with the clay and concrete block masonry. This is due to the lower compressive strength of mortar for calcium silicate brickwork.

5.3.3 Shrinkage

Figures 5.25 to 5.27 show the influence of geometry on shrinkage of mortar prisms was similar to that on creep of mortar, i.e a higher shrinkage for a lower V/S ratio.

Figures 5.28 and 5.29 compare the shrinkage-time curves of the partly sealed mortar prisms for each type of wall. For both the diaphragm and fin walls, the mortar prisms for the calcium silicate walls exhibited the greatest shrinkage. As for the explanation given for creep, this could have been due to the lower compressive strength. Appendix C shows the shrinkage measured on the mortar prisms, and the greatest variations occurred for the calcium silicate walls (20%).

5.3.3 (a) Ultimate shrinkage

The ultimate shrinkage of the partly sealed mortar prisms was determined using Ross hyperbolic equation (Eq. 5.1). Table 5.5 shows the ultimate shrinkage, constant 'a' and 'b', and correlation coefficients of the mortar prisms. As expected from the measured trends, the mortar prisms for the calcium silicate brickwork exhibit the highest ultimate shrinkage.

5.4 Masonry units

The deformations of the masonry units to be used in the application of the composite models theory in Chapter 6 are presented in the following sections.

5.4.1 Elasticity

Table 5.6 shows the elasticity of clay, calcium silicate and concrete block units when subjected to load between header faces. The bed-face modulus of the clay units were almost twice the header face modulus but there was no significant difference for the calcium silicate units. The reason for measuring the elasticity of the

header and bed face of masonry units was because elastic and time-dependent deformations tests were carried out with units loaded parallel to the bed face, which did not represent the actual loaded units in the masonry walls. To overcome this situation, the ratio relating elastic moduli between header and bed faces (E_{bx}/E_{by}) was required in order to adjust the header-face deformation to give the bed-face deformation as required for the composite model.

5.4.2 Creep

Figures 5.30 to 5.32 show the influence of geometry on the creep of the partly sealed masonry units was similar to that of shrinkage of the brickwork and of the partly sealed mortar prisms. Figures 5.33 and 5.34 compare the specific creep of the partly sealed unbonded masonry units for each type of wall. After 60 days of loading, all the masonry units exhibited creep at a decreasing rate and the magnitude of creep was insignificant in the clay units compared with the creep of the mortar prisms (Fig. 5.20 to 5.22). For the calcium silicate and concrete block units, the magnitude of creep was approximately 20% of the mortar creep.

The calcium silicate unit exhibited the greatest creep, and had the lowest strength, and therefore the general relationship between creep and strength seems to apply to units as well as mortar and concrete. The measured strains from which creep was calculated are given in Appendix C.

5.4.2 (a) Ultimate creep

Table 5.7 gives the ultimate creep, and correlation coefficients obtained by regression of the Ross hyperbolic equation (Eq. 5.1). The average ultimate creep of the clay units was about 3% of the average ultimate creep of the mortar prisms used for the clay walls, which suggests that clay units would hardly contribute to creep in the clay walls.

The average ultimate creep of the calcium silicate and concrete block units were about 20 % of the average ultimate creep of the mortar prisms used for the calcium silicate walls, i.e the same as the measured creep.

5.4.3 Shrinkage/moisture expansion

Figures 5.35 to 5.37 show that the influence of geometry on the shrinkage/moisture movement of masonry units was similar to that on shrinkage of the brickwork and mortar prisms.

For a given type of wall, Figs. 5.38 and 5.39 show ^{that} the clay units undergo a very small expansion instead of shrinkage. Calcium silicate and concrete block units undergo shrinkage with time but at a decreasing rate. However the magnitude of shrinkage of the units is negligible when compared to the corresponding shrinkage of mortar. The measured shrinkage are given in Appendix C, which shows that calcium silicate units had the highest variation (31%).

5.4.4 Ultimate shrinkage

Table 5.7 gives the results of the analysis by the rectified Ross hyperbolic shrinkage-time expression in order to estimate the ultimate shrinkage and moisture expansion (clay). Generally the trends of ultimate values with V/S ratio were the same as for the measured values.

5.5 Relaxation loss

Figure 5.40 shows the stress relaxation of the 25 mm and 26.5 mm bars over a period of 120 days under a constant strain. The maximum stress loss due to relaxation in the 26.5 mm and 25 mm bars was 4.5 and 3.5%, respectively. These values do not represent the actual prestress loss due to relaxation of the prestressing bars in the prestressed masonry because the prestress loss occurred under reducing

strain due to the time-dependent deformations of the masonry. The values can be corrected to represent the actual loss under varying stress by multiplying the loss by a factor suggested by Magura (1964).

Based on the relaxation tests (Fig. 5.40), the denominator in Eq. (3.14) was obtained by substituting the known variables. The average value of the denominator was calculated as 13.6, and thus the stress of the 25 mm and 26.5 mm bars expressed as Eq. (3.14) is as follows:

$$f_s(t) = -f_{si} \log_{10} 24t \frac{\left(\frac{f_{si}}{f_{sy}} - 0.55\right)}{13.6} \quad (5.2)$$

where f_s = the remaining stress at any time t after prestressing;

f_{si} = the initial stress;

f_{sy} = stress at 1% elongation;

and t = time after initial prestressing.

5.6 Individual Prestress Loss

Using the estimated ultimate creep (Section 5.2.2 (c)) and shrinkage (Section 5.2.3 (c)), the corresponding individual prestress loss was computed and shown in Table 5.8. The prestress loss due to relaxation in Table 5.8 was based on measured relaxation loss in Section 5.5. For calcium silicate and concrete block walls, shrinkage contributed the highest prestress loss compared to creep and relaxation. However, in clay brickwork creep contributed slightly more (by 1.5%) loss than shrinkage.

Eventhough calcium silicate walls (Figs. 5.13 to 5.14) exhibited higher prestress loss than concrete block walls during the first 120 days, there was no clear

difference in the total estimated ultimate prestress loss between the calcium silicate (22 - 23.5%) and concrete block (22.8 - 24.1%) walls.

5.7 Temperature and humidity

The variation of atmospheric temperature and humidity in the laboratory, during which strain measurements are taken, are shown in Figs. 4.17 and 4.18, respectively. The temperature and relative humidity varied between 17-26°C and 20-70%, respectively, during Test 1 (clay brickwork). The temperature decreased to about 10°C during Test 2 (calcium silicate brickwork) and later increased to a maximum of 24°C in Test 3 (concrete blockwork). The humidity varied between 25-62% and 25-55% in Test 2 and Test 3, respectively.

The variations in atmospheric temperature and humidity during Test 2 might have caused the difference in trend of creep and shrinkage of calcium silicate brickwork.

Table 5.1 Modulus of Elasticity of Clay, Calcium Silicate Brickwork and Concrete Blockwork (GPa)

Masonry Type	Secant Modulus of Elasticity (GPa)		
	Diaphragm*	Fin*	Pafec (1978)
Clay Brickwork	19.66 (1.1)	18.82 (1.5)	18.11
Calcium Silicate Brickwork	12.11 (2.18)	12.8 (1.54)	10.71
Concrete Blockwork	13.97 (5.3)	13.16 (1.05)	16.23

* - Measured values

() - standard deviation

Table 5.2 Ultimate Specific Creep of Clay, Calcium Silicate Brickwork and Concrete Blockwork

Masonry Type	Ultimate Specific Creep* (Microstrain/MPa)	
	Geometry	
	Diaphragm	Fin
Clay Brickwork	76 a = 0.064 b = 0.0044 R = 0.98	91 a = 0.045 b = 0.0037 R = 0.98
Calcium Silicate Brickwork	182 a = 0.114 b = 0.0035 R = 0.96	188 a = 0.079 b = 0.0034 R = 0.93
Concrete Blockwork	167 a = 0.095 b = 0.003 R = 0.99	192 a = 0.099 b = 0.0026 R = 0.98

* Ultimate Specific Creep = $1/(\text{Stress} \times b)$

R = Correlation coefficient

Table 5.3 Creep Coefficient of Clay, Calcium Silicate Brickwork and Concrete Blockwork

Masonry Type	Creep Coefficient	
	Geometry	
	Diaphragm	Fin
Clay Brickwork	1.49	1.55
Calcium Silicate Brickwork	2.20	2.40
Concrete Blockwork	2.34	2.53

Table 5.4 Ultimate Shrinkage of Clay, Calcium Silicate Brickwork and Concrete Blockwork

Masonry Type	Ultimate Shrinkage (Microstrain)	
	Geometry	
	Diaphragm	Fin
Clay Brickwork	179 a = 0.19 b = 0.0056 R = 0.99	204 a = 0.084 b = 0.0049 R = 0.98
Calcium Silicate Brickwork	418 a = 0.146 b = 0.0024 R = 0.92	400 a = 0.098 b = 0.0025 R = 0.90
Concrete Blockwork	500 a = 0.254 b = 0.002 R = 0.96	513 a = 0.207 b = 0.0195 Rb = 0.97

R = Correlation coefficient

Table 5.5 Deformation of Mortar Prisms as Sampled during Construction of the Masonry Walls

Masonry Types	Geometry	Strength MPa	Average Elasticity GPa	Specific Creep at 120 days (10^{-6})	Specific Ultimate Creep (10^{-6} /MPa)	Creep Coefficient	Creep Correlation Coefficient and values of 'a' and 'b'	Shrinkage at 120 days (10^{-6})	Ultimate Shrinkage (10^{-6})	Shrinkage Correlation Coefficient and values of 'a' and 'b'
Clay	Diaphragm	10.13 (0.72)	7.5 (0.70)	534 (67)	654	4.91	a = 0.041 b = 0.00149 R = 0.97	1400 (156)	2381	a = 0.0355 b = 0.00042 R = 0.95
	Fin	11.52 (1.28)	7.37 (0.9)	641 (98)	740	5.45	a = 0.024 b = 0.00135 R = 0.99	1650 (142)	2433	a = 0.03067 b = 0.00041 R = 0.98
Calcium Silicate	Diaphragm	10.42 (0.84)	7.78 (1.95)	675 (207)	781	6.08	a = 0.0302 b = 0.00128 R = 0.98	1630 (225)	2173	a = 0.025 b = 0.00046 R = 0.9
	Fin	9.66 (0.94)	6.94 (2.06)	701 (255)	813	6.32	a = 0.0177 b = 0.00123 R = 0.99	1893 (71)	2381	a = 0.0153 b = 0.00042 R = 0.9
Concrete Block	Diaphragm	12.27 (1.36)	10.04 (3.2)	662 (57)	736	7.4	a = 0.051 b = 0.00136 R = 0.99	1500 (150)	2179	a = 0.0253 b = 0.00046 R = 0.93
	Fin	13.04 (1.72)	9.56 (4.7)	653 (166)	787	7.52	a = 0.0337 b = 0.00127 R = 0.96	1640 (94)	2173	a = 0.03066 b = 0.00046 R = 0.94

() - Standard deviation
R - Correlation Coefficient

Table 5.6 Modulus of Elasticity of Masonry Unit Between Header and Bed Faces

Masonry Type	Secant Modulus of Elasticity (GPa)	
	Header Face	Bed Face
Clay Unit	17.49 (1.3)	29.0 (0.75)
Calcium Silicate Unit	13.38 (3.56)	15.17 (1.49)
Concrete Block	-	9.96 (.92)

() - standard deviation

Table 5.7 Deformations of Masonry Units

Masonry Types	Geometry	Strength MPa	Elasticity GPa (Header)	Specific Creep at 120 days ($10^{-6}/\text{MPa}$)	Specific Ultimate Creep ($10^{-6}/\text{MPa}$)	Creep Coefficient	Creep Correlation Coefficient and values of 'a' and 'b'	Shrinkage at 120 days (10^{-6})	Ultimate Shrinkage (10^{-6})	Correlation of Coefficient
Clay	Diaphragm Sample 1 Sample 2	103 (9.7)	17.77	17	20	0.34	a = 0.42 b = 0.051 R = 0.99	-18	-38	a = 0.36 b = 0.027 R = 0.85
			16.50	21				-22		
	Fin Sample 1 Sample 2		19.20	20	23	0.39	a = 0.023 b = 0.045 R = 0.99	-22.50	-35	a = 1.6 b = 0.029 R = 0.80
16.50	24	-27.50								
			Ave. = 17.49 (1.3)							
Calcium Silicate	Diaphragm Sample 1 Sample 2	26.08 (1.41)	13.23	150	152	2.3	a = 0.223 b = 0.0066 R = 0.9	270	284	a = 0.19 b = 0.0031 R = 0.95
			18.18	80				150		
	Fin Sample 1 Sample 2		12.61	121	152	2.3	a = 0.144 b = 0.0066 R = 0.99	230	324	a = 0.19 b = 0.0031 R = 0.90
9.50	134	230								
			Ave. = 13.38 (3.56)							

Table 5.7 Continue

Masonry Types	Geometry	Strength MPa	Elasticity GPa	Specific Creep at 120 days (10 ⁻⁶ /MPa)	Specific Ultimate Creep (10 ⁻⁶ /MPa)	Creep Coefficient	Correlation Coefficient and values of 'a' and 'b'	Shrinkage at 120 days (10 ⁻⁶)	Ultimate Shrinkage (10 ⁻⁶)	Correlation of Coefficient
Concrete Block	Diaphragm Sample 1 Sample 2	14.87 (1.14)	10.70	70	125	1.25	a = 0.282 b = 0.0084 R = 0.97	175 245	303	a = 0.214 b = 0.0033 R = 0.9
			9.80	128						
	Fin Sample 1 Sample 2		10.61 8.72	97 137	132	1.31	a = 0.14 b = 0.0076 R = 0.99	226 246	454	a = 0.24 b = 0.0022 R = 0.91
		Ave. = 9.96 (0.92)								

() - Standard deviation
R - Correlation Coefficient

Table 5.8 Ultimate Individual Prestress Loss of the Masonry Walls

Type of Masonry	Creep (%)		Shrinkage (%)		Relaxation (%)	Total Loss (%)	
	Diaphragm	Fin	Diaphragm	Fin		Diaphragm	Fin
Clay Brickwork	6.0	6.8	5.0	5.2	3.5-4.5	14.5	16.5
Calcium Silicate Brickwork	7.2	8.0	10.5	11.5	3.5-4.5	21.2	24
Concrete Blockwork	7.5	8.7	11.3	11.6	3.5-4.5	22.3	24.8

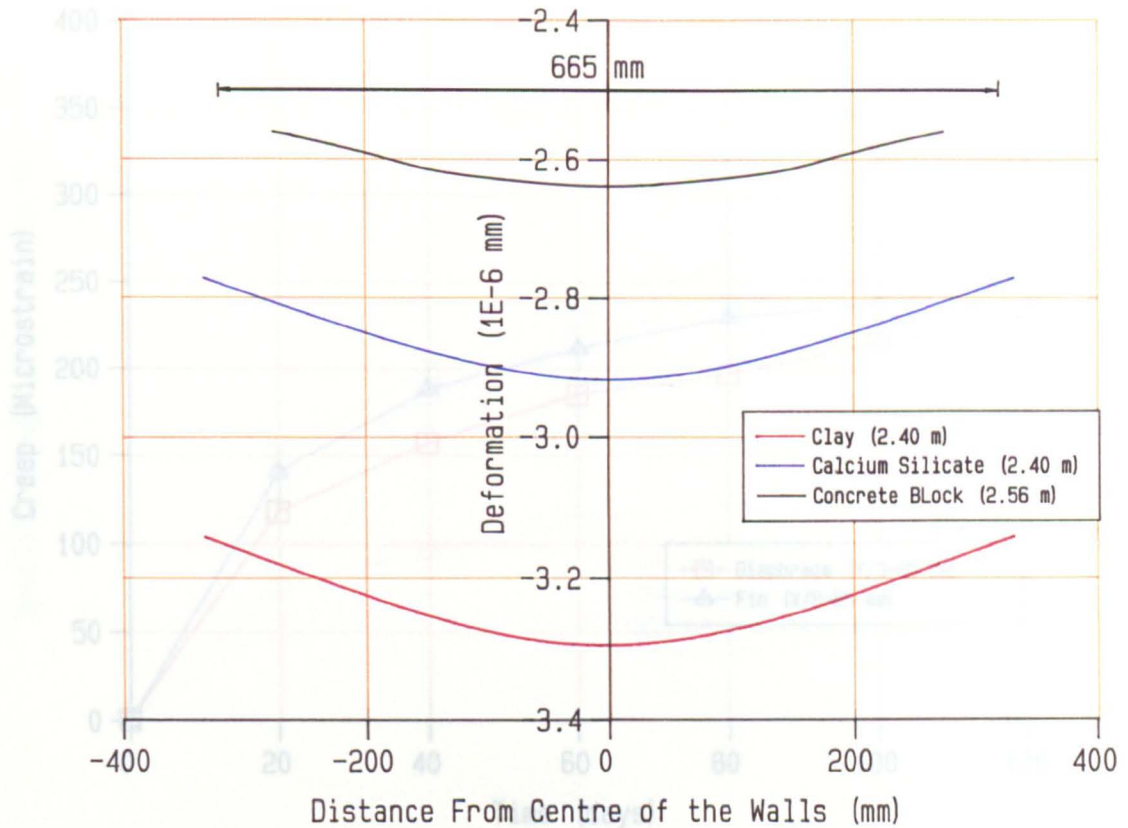


Fig. 5.1 Typical Displacement of Clay, Calcium Silicate and Concrete Block Walls by Pafec

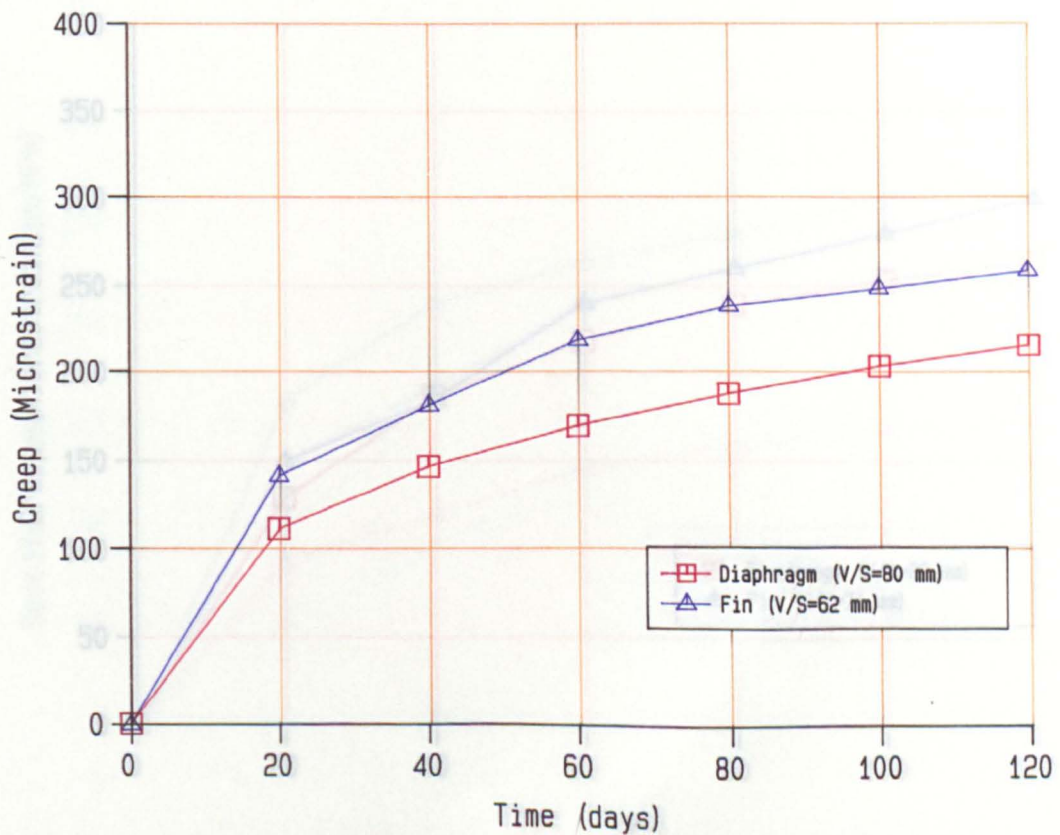


Fig. 5.2 Creep-time Curve of Clay Walls under 3 MPa Stress

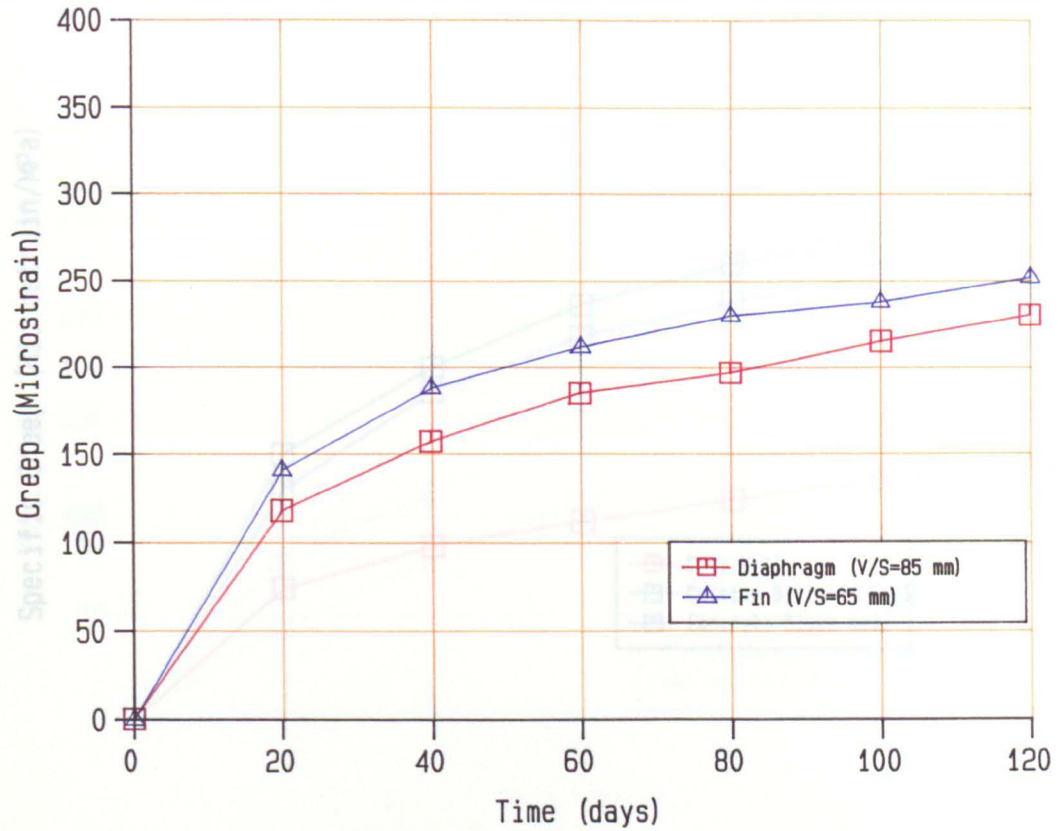


Fig. 5.3 Creep-time Curve of Calcium Silicate Walls under 1.57 MPa Stress

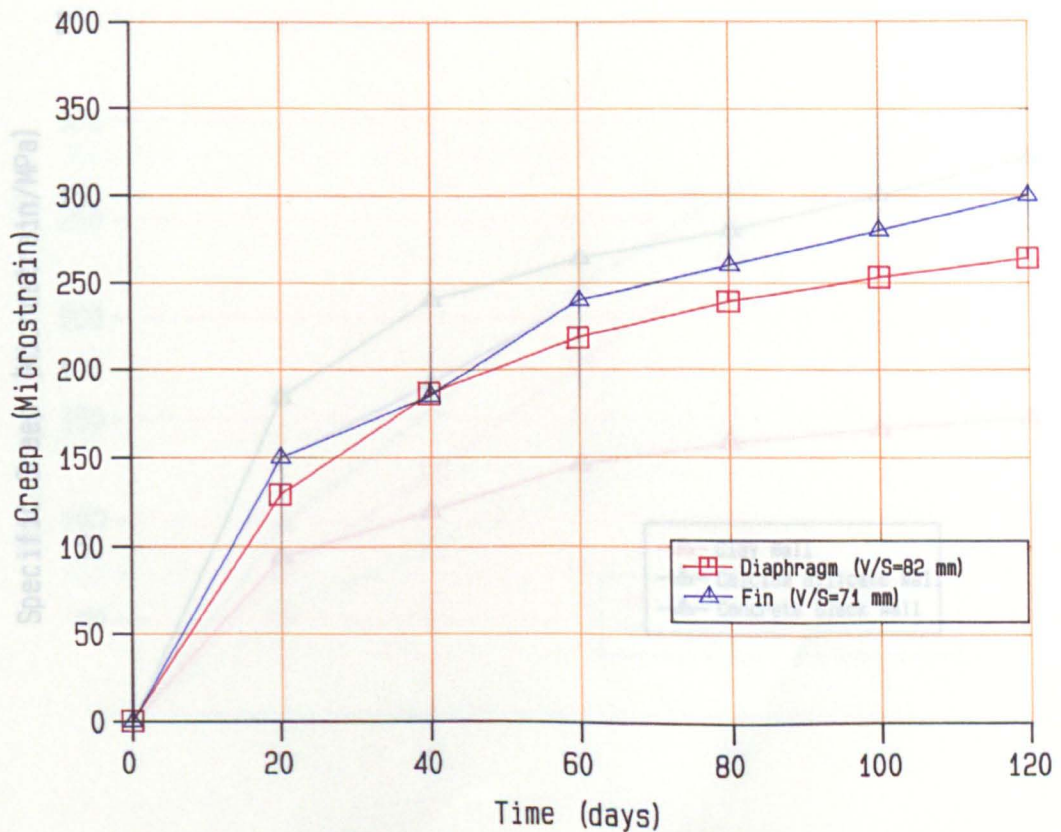


Fig. 5.4 Creep-time Curve of Concrete Block Walls under 2 MPa Stress

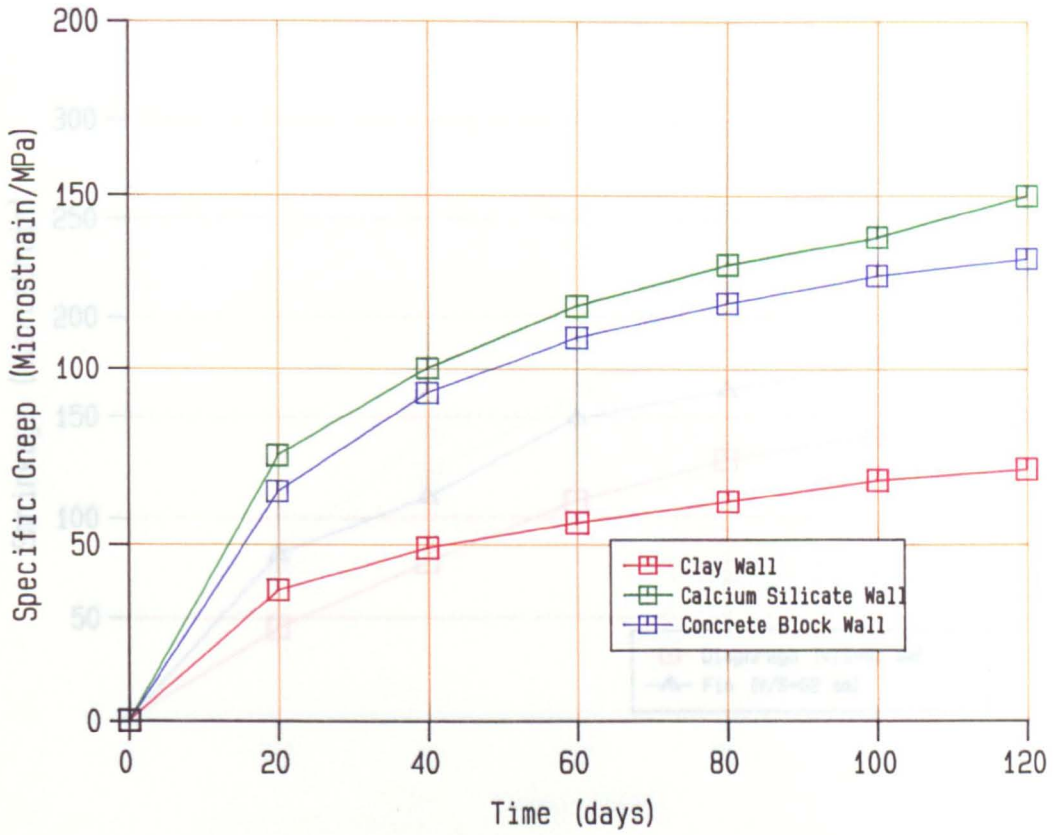


Fig. 5.5 Specific Creep-time Curve of Diaphragm Walls

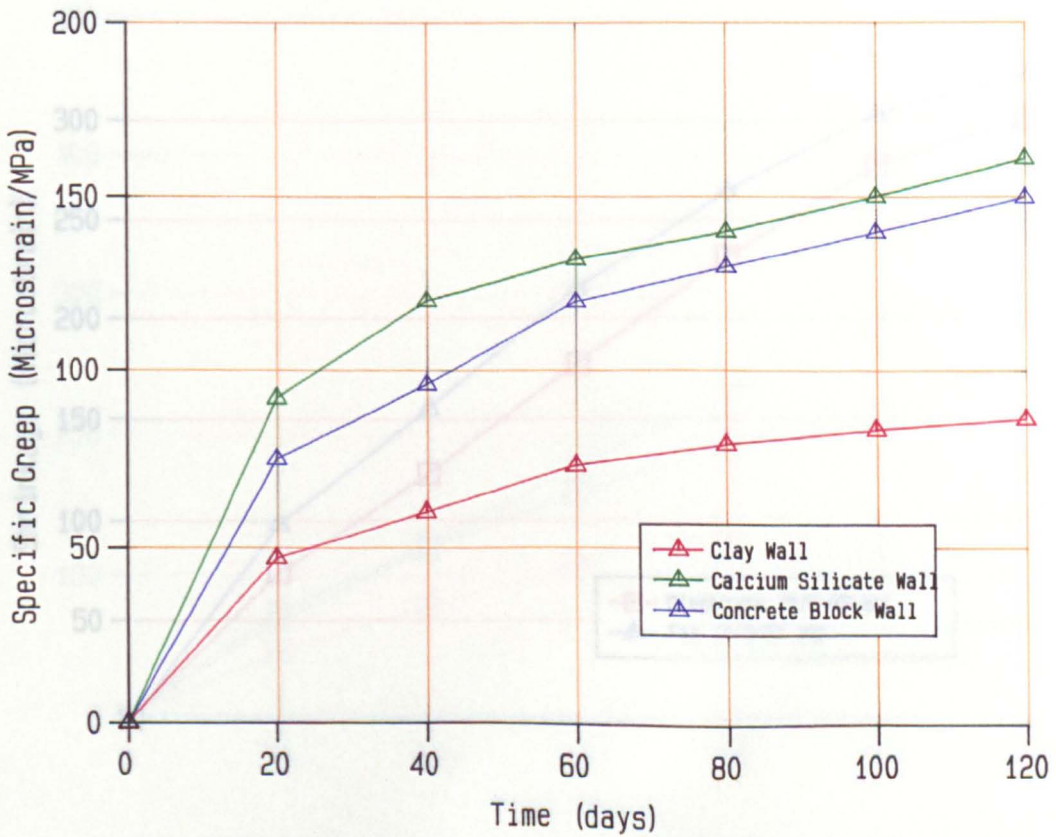


Fig. 5.6 Specific Creep-time Curve of Fin Walls

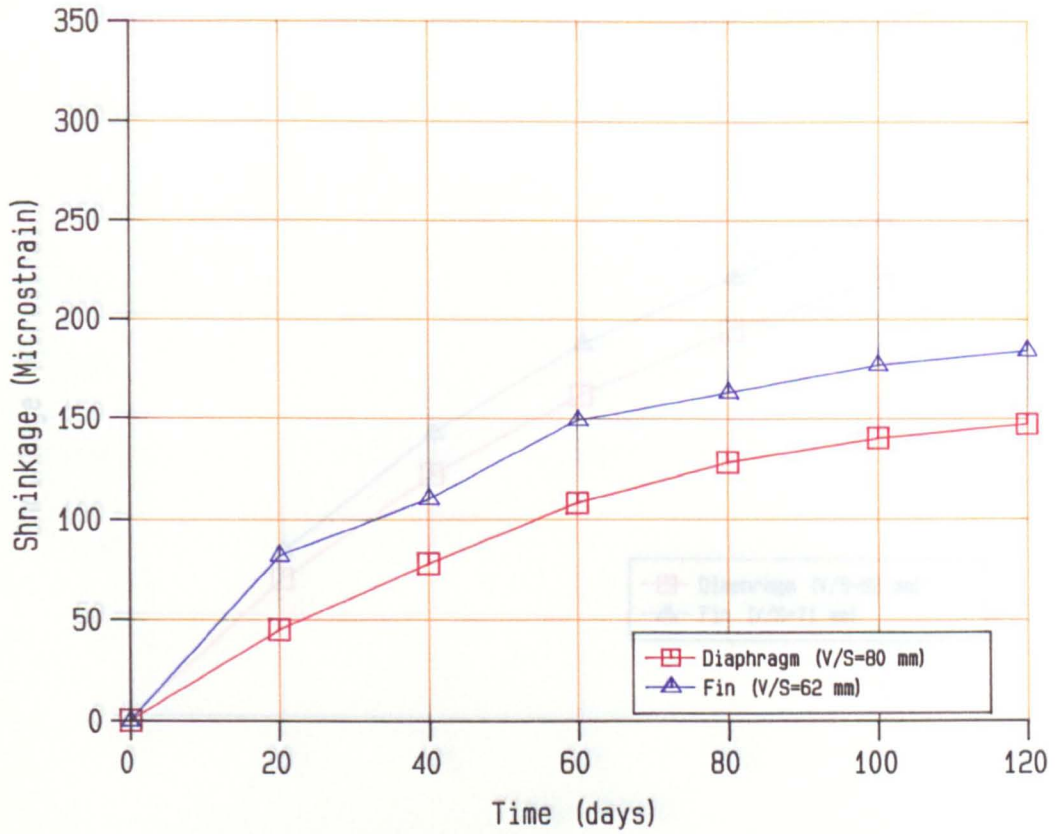


Fig. 5.7 Shrinkage-time Curve of Clay Walls

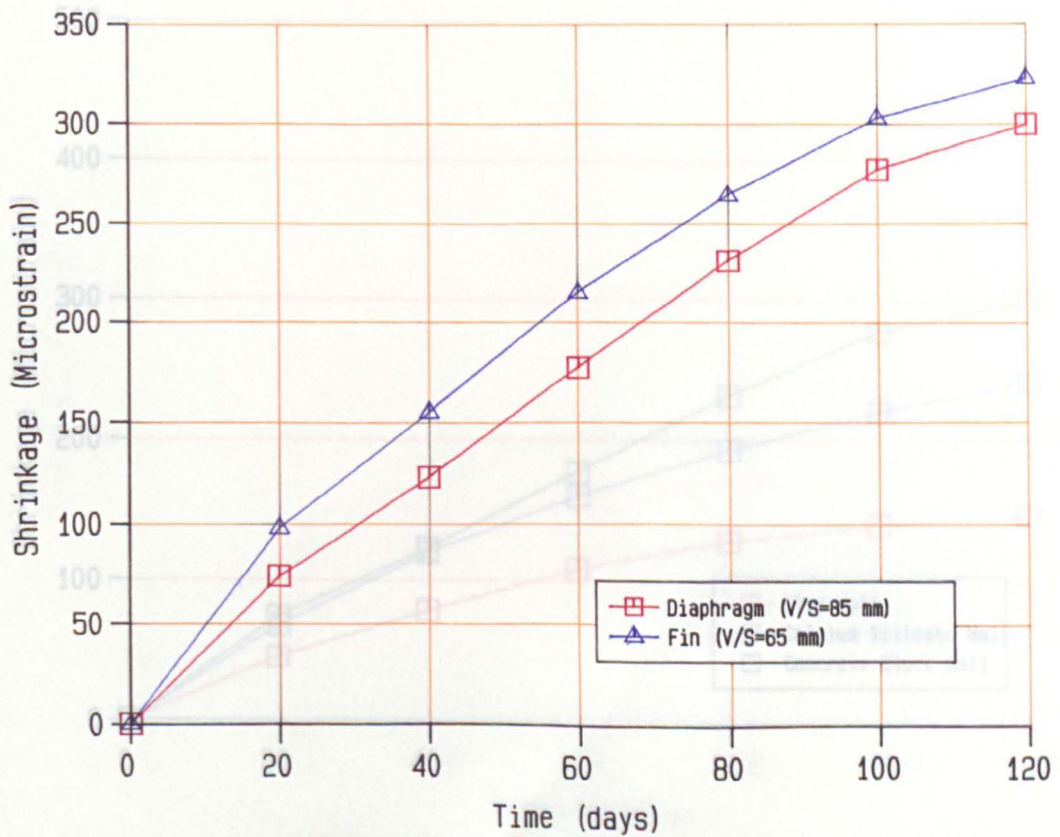


Fig. 5.8 Shrinkage-time Curve of Calcium Silicate Walls

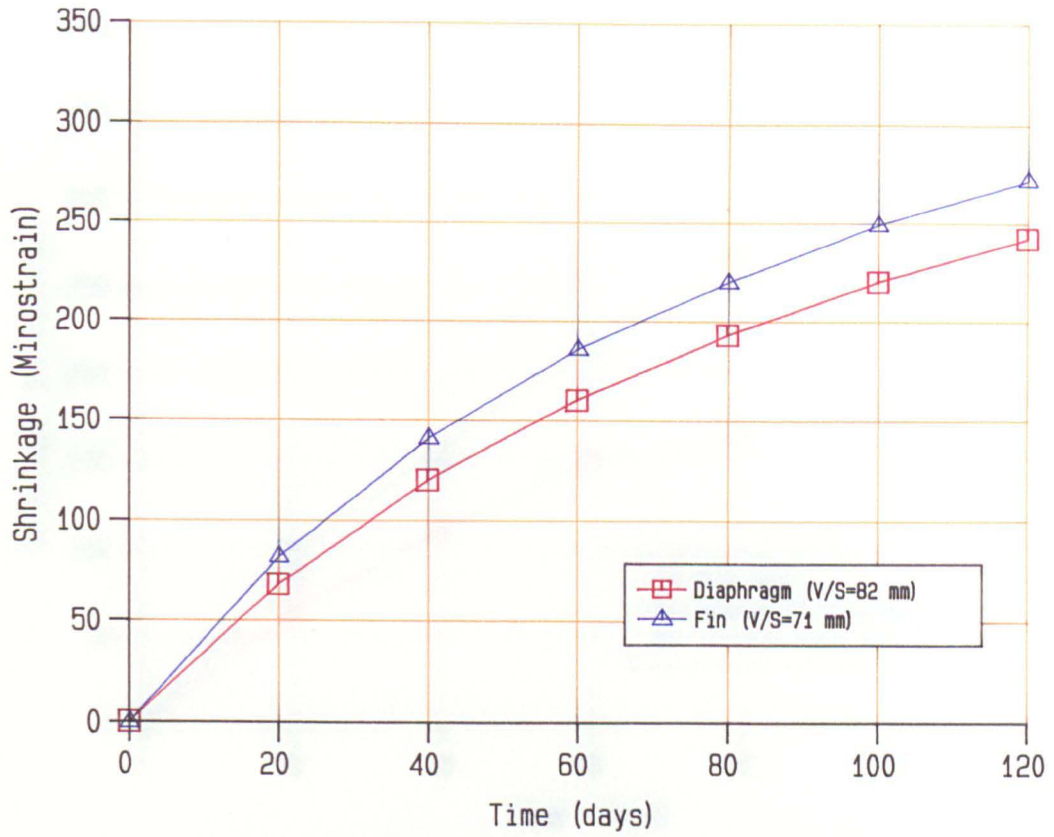


Fig. 5.9 Shrinkage-time Curve of Concrete Block Walls

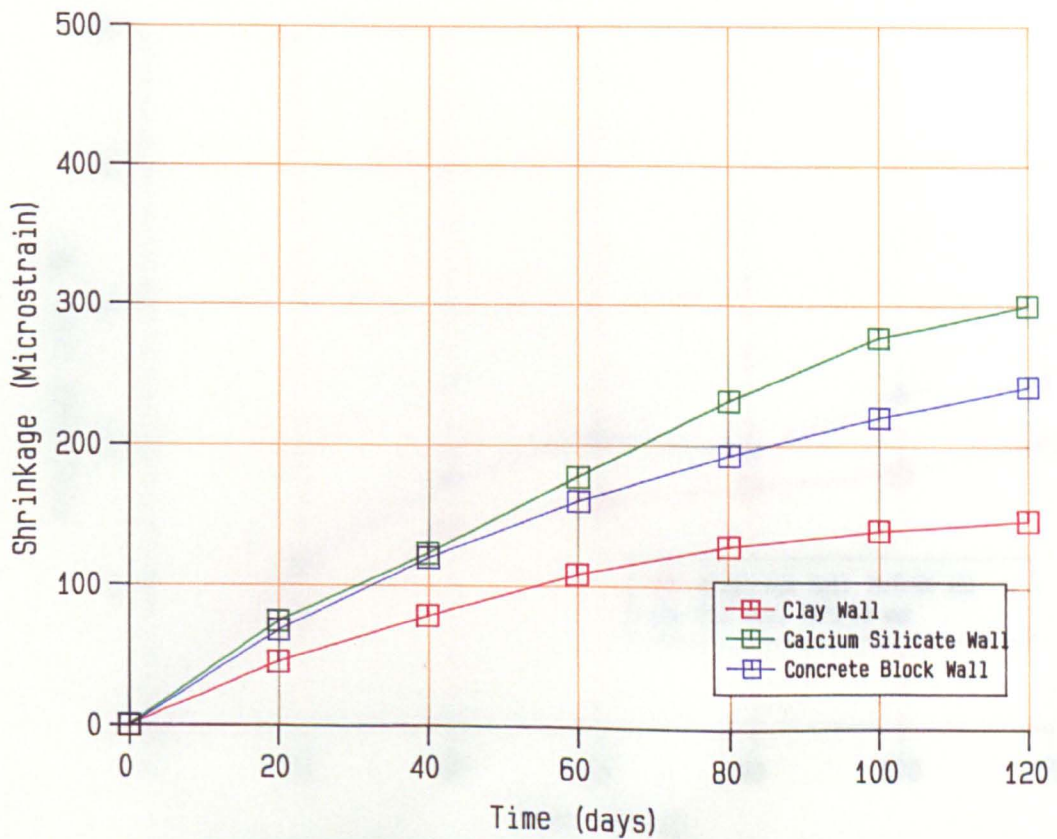


Fig. 5.10 Shrinkage-time Curve of Diaphragm Walls

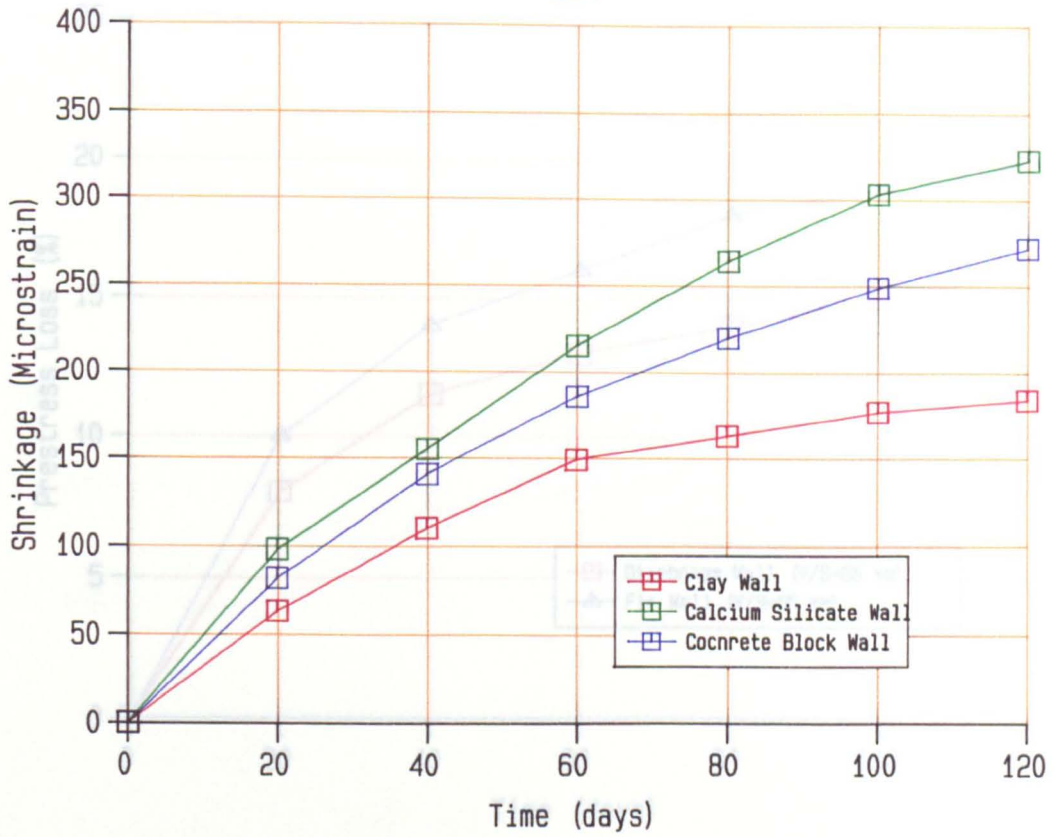


Fig. 5.11 Shrinkage-time Curve of Fin Walls

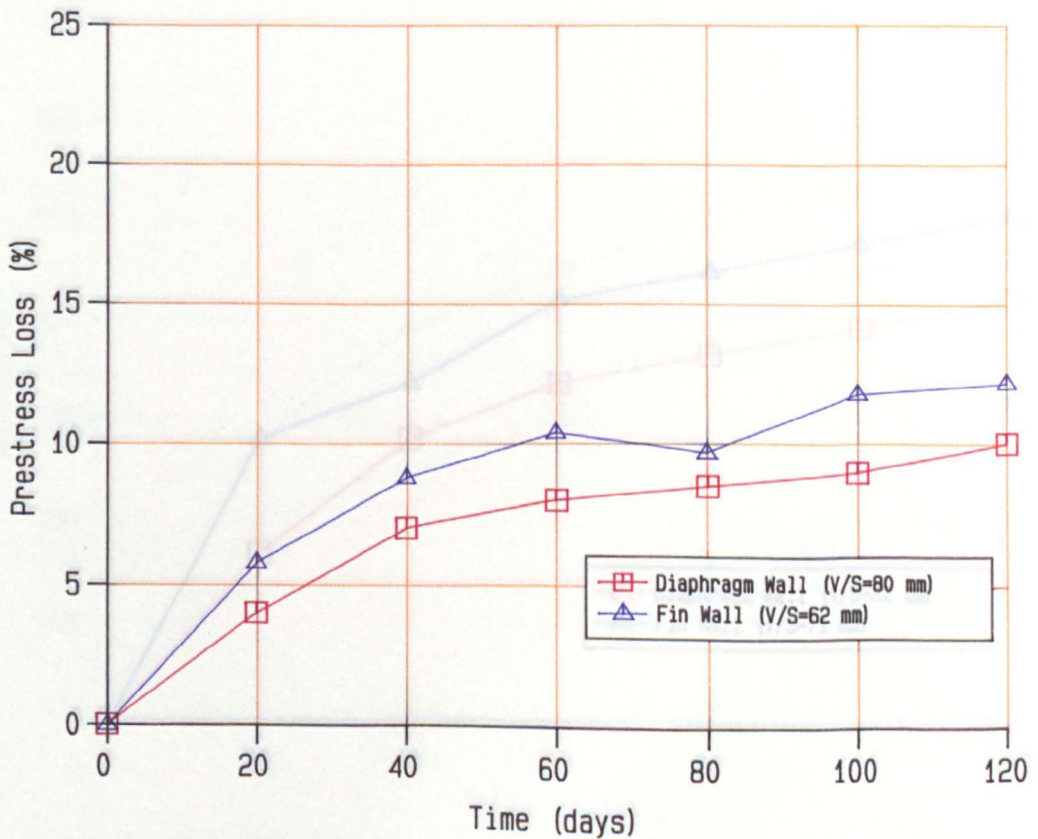


Fig. 5.12 Prestress Loss-time Curve of Clay Walls

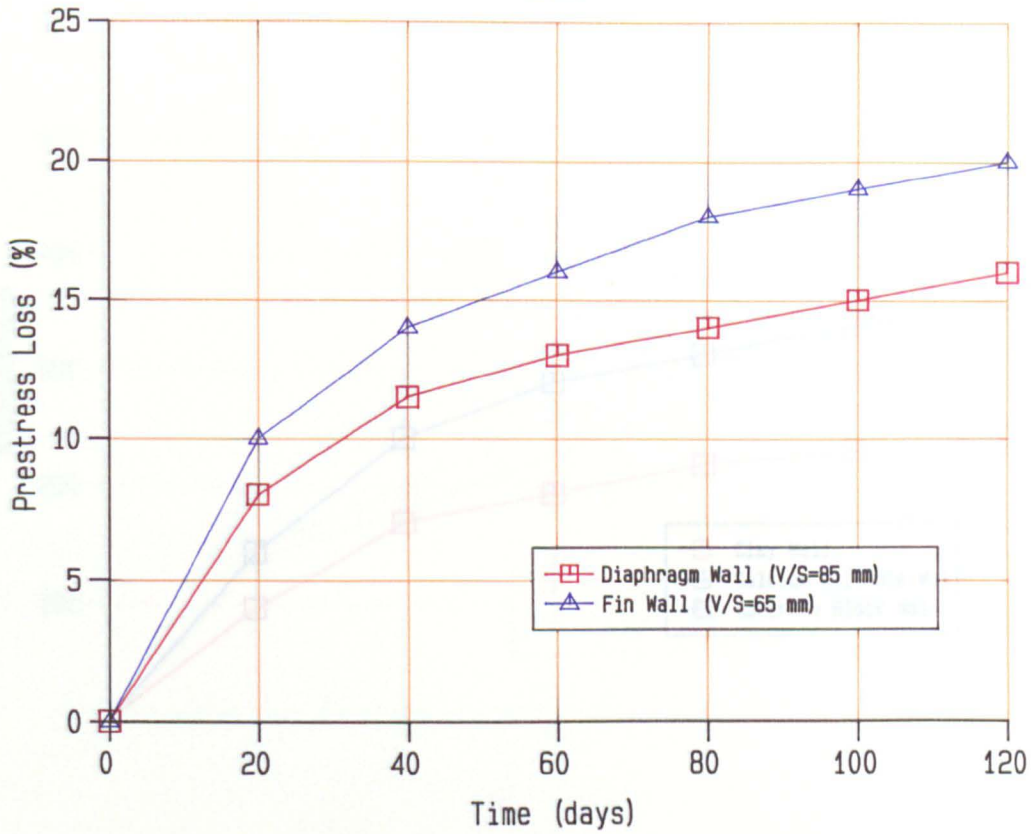


Fig. 5.13 Prestress Loss-time Curve of Calcium Silicate Walls

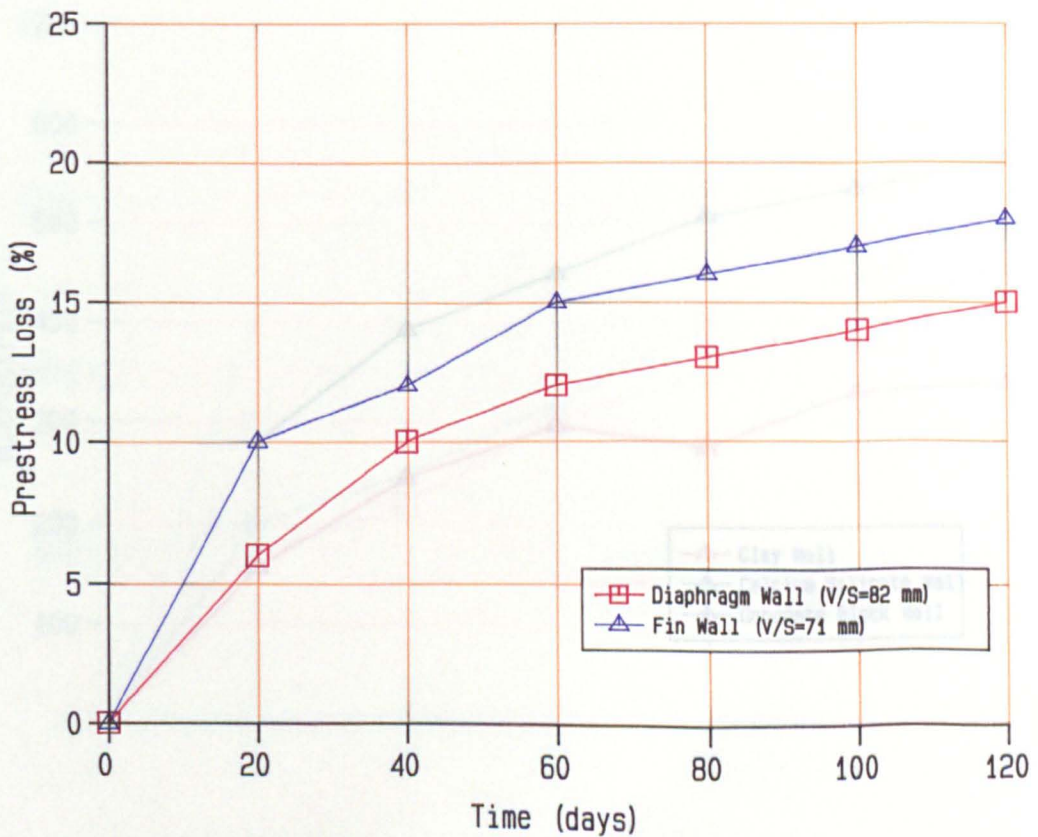


Fig. 5.14 Prestress Loss-time Curve of Concrete Block Walls

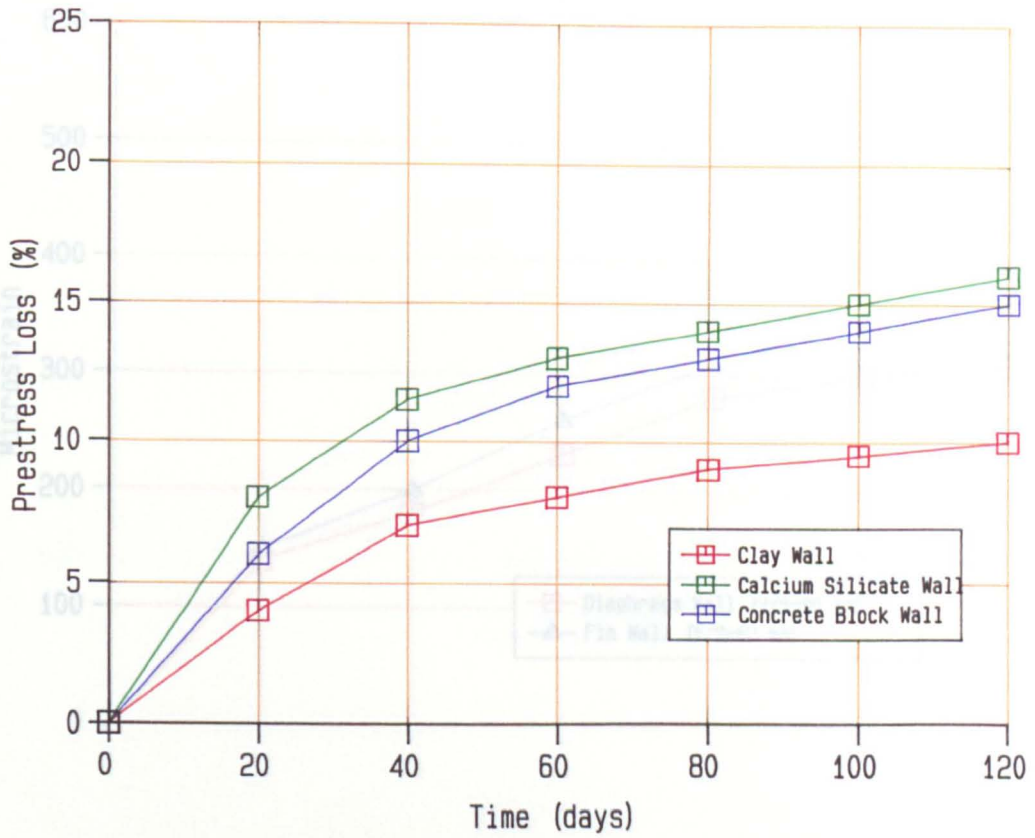


Fig. 5.15 Prestress Loss-time Curve of Diaphragm Walls

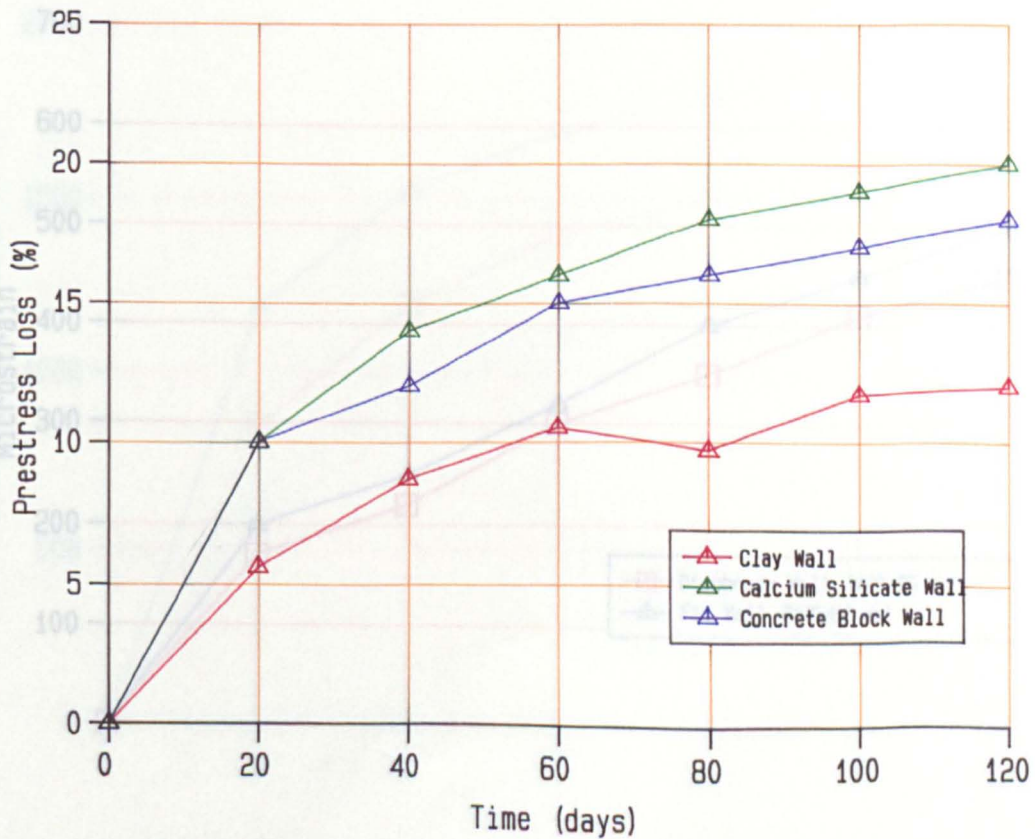


Fig. 5.16 Prestress Loss-time Curve of Fin Walls

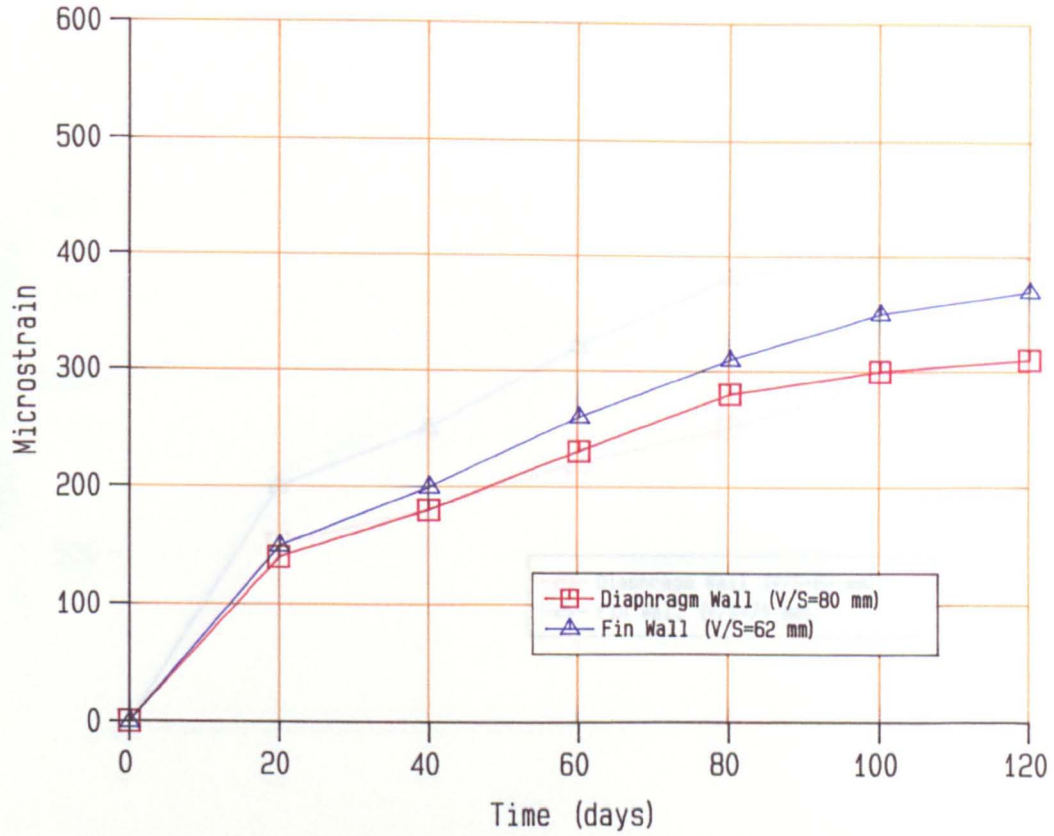


Fig. 5.17 Strain-time Curve of Prestress Loss Clay Walls

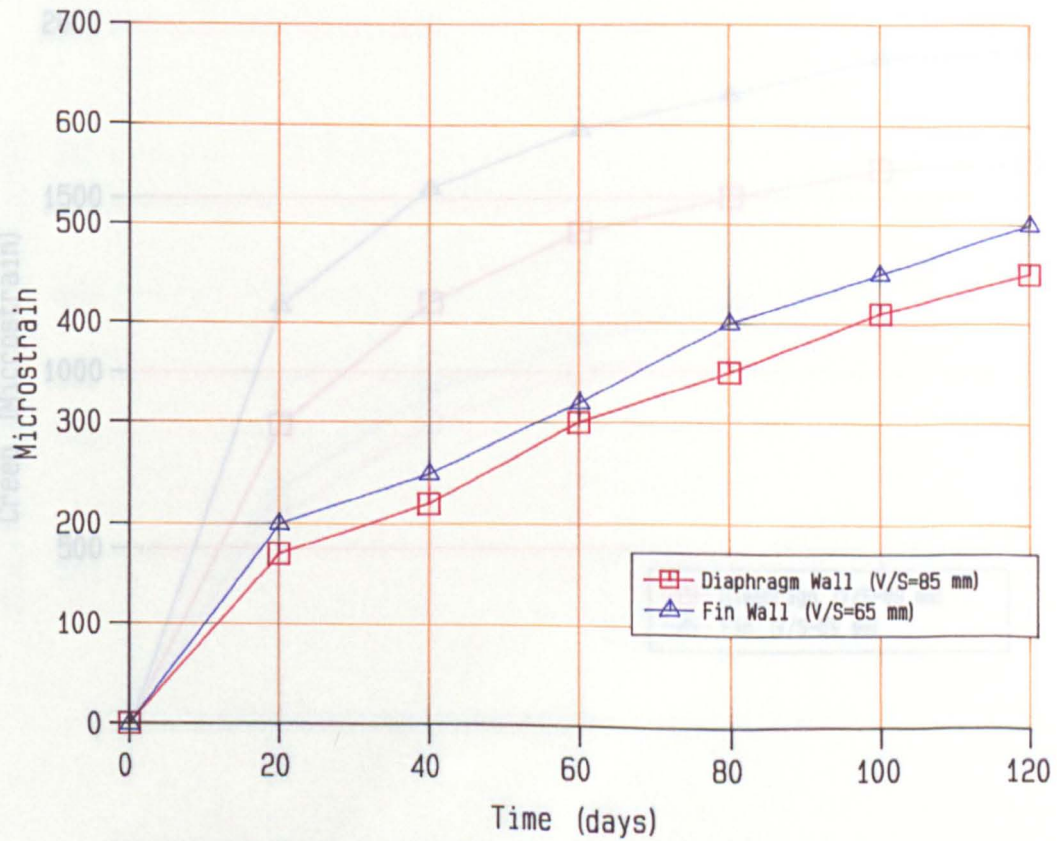


Fig. 5.18 Strain-time Curve of Prestress Loss Calcium Silicate Walls

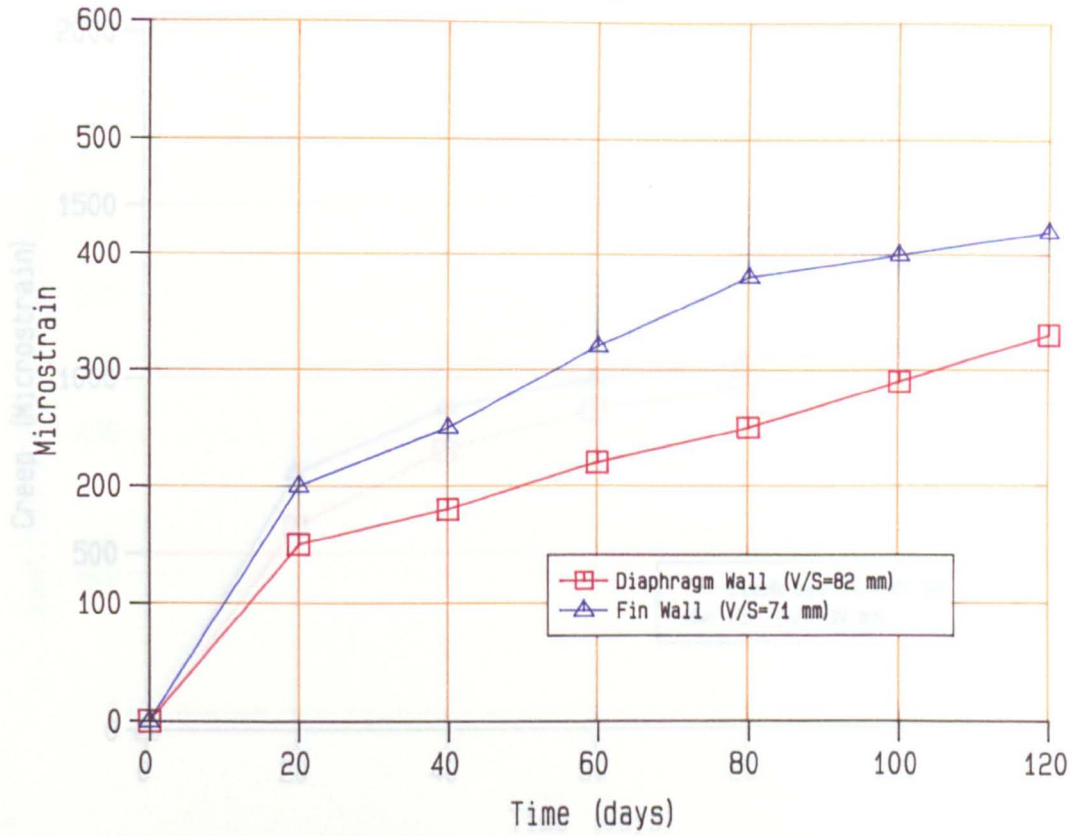


Fig. 5.19 Strain-time Curve of Prestress Loss Concrete Block Walls

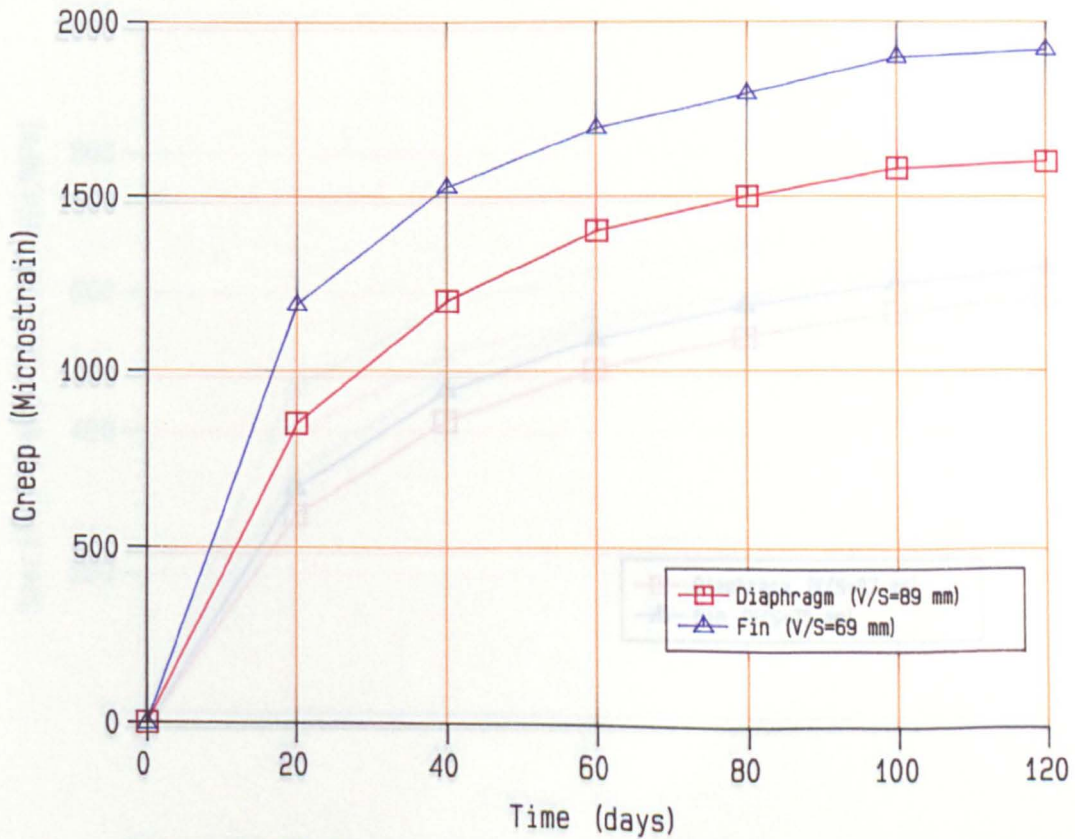


Fig. 5.20 Creep-time Curve of Mortar Prisms for Clay Walls under 3 MPa Stress

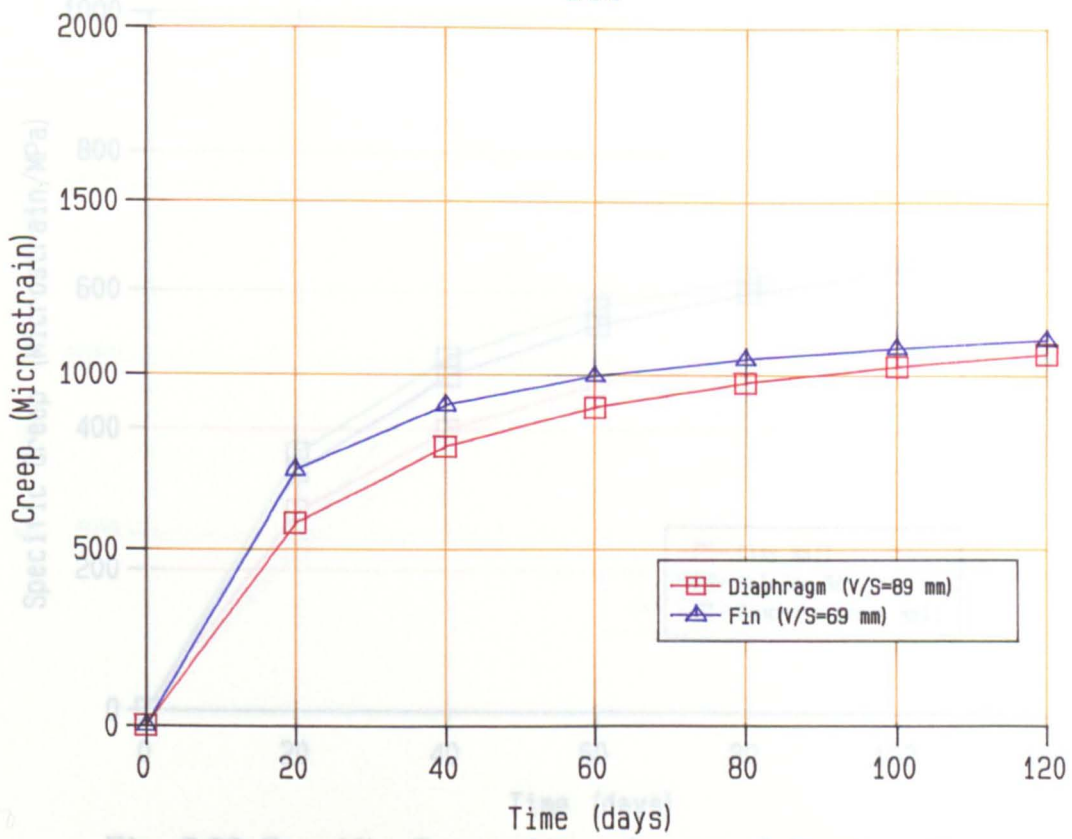


Fig. 5.21 Creep-time Curve of Mortar Prisms for Calcium Silicate Walls under 1.57 MPa Stress

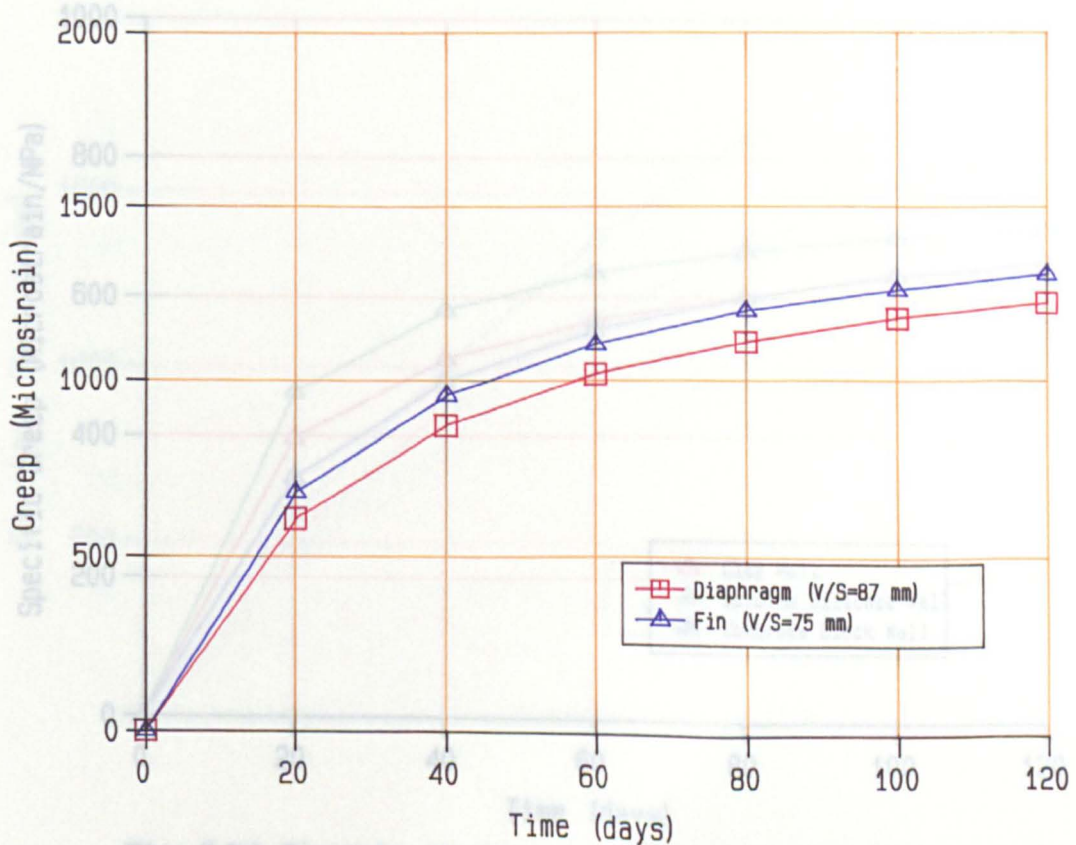


Fig. 5.22 Creep-time Curve of Mortar Prisms for Concrete Block Walls under 2 MPa Stress

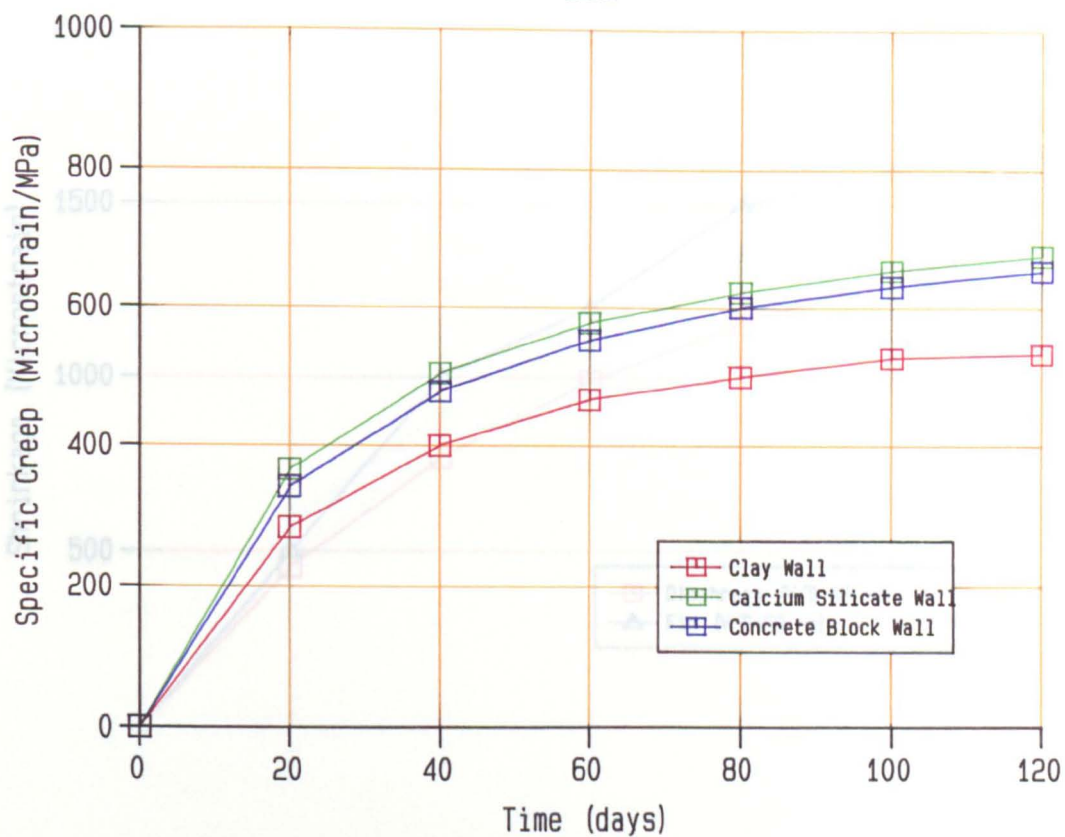


Fig. 5.23 Specific Creep-time Curve of Mortar Prisms for Diaphragm Walls

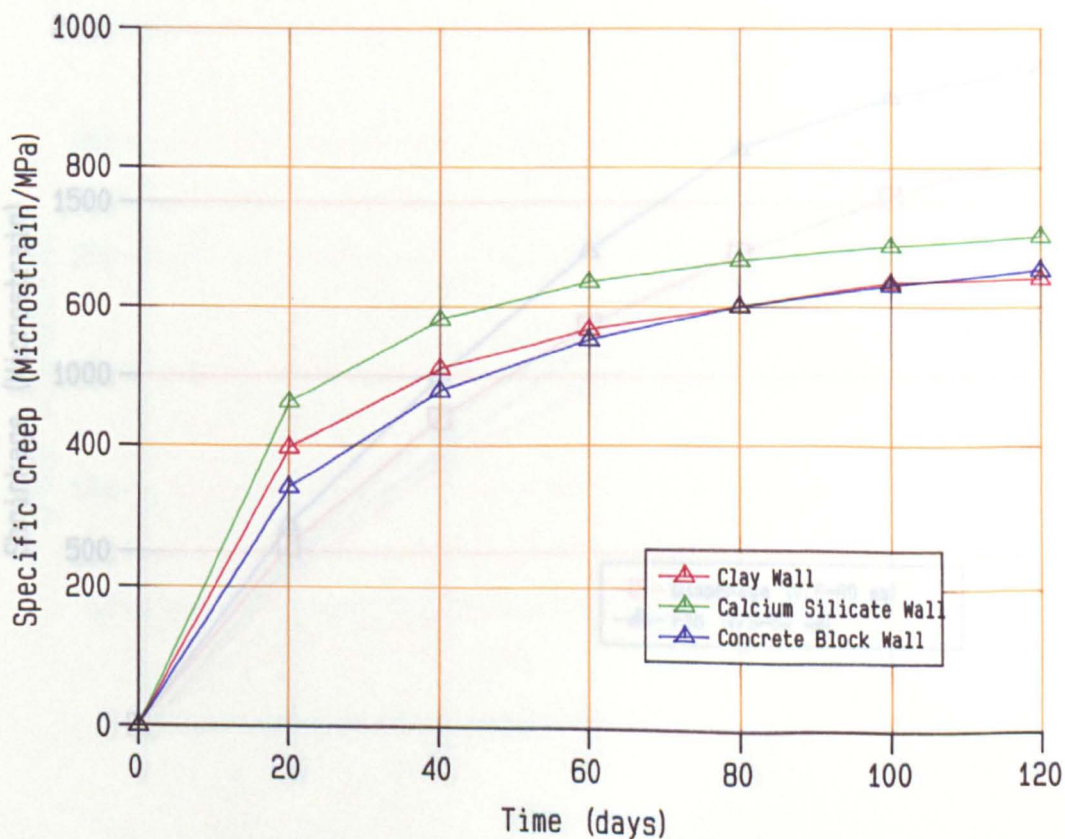


Fig. 5.24 Specific Creep-time Curve of Mortar Prisms for Fin Walls

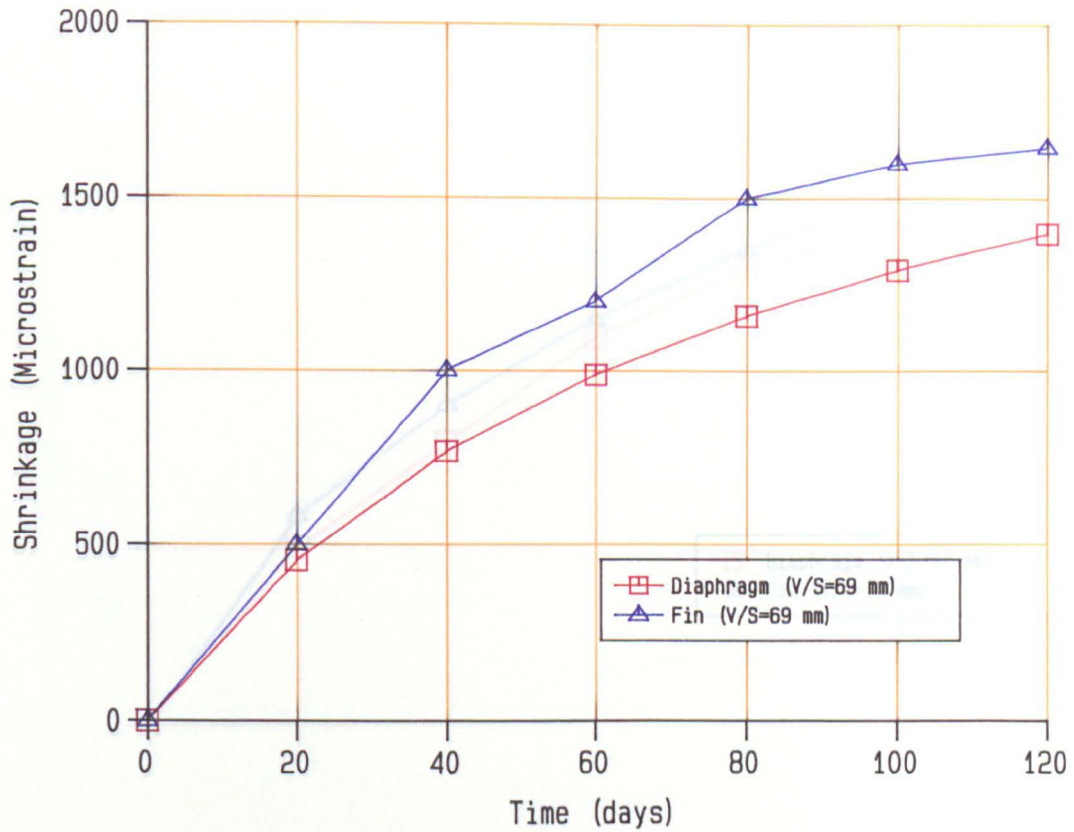


Fig. 5.25 Shrinkage-time Curve of Mortar Prisms for Clay Walls

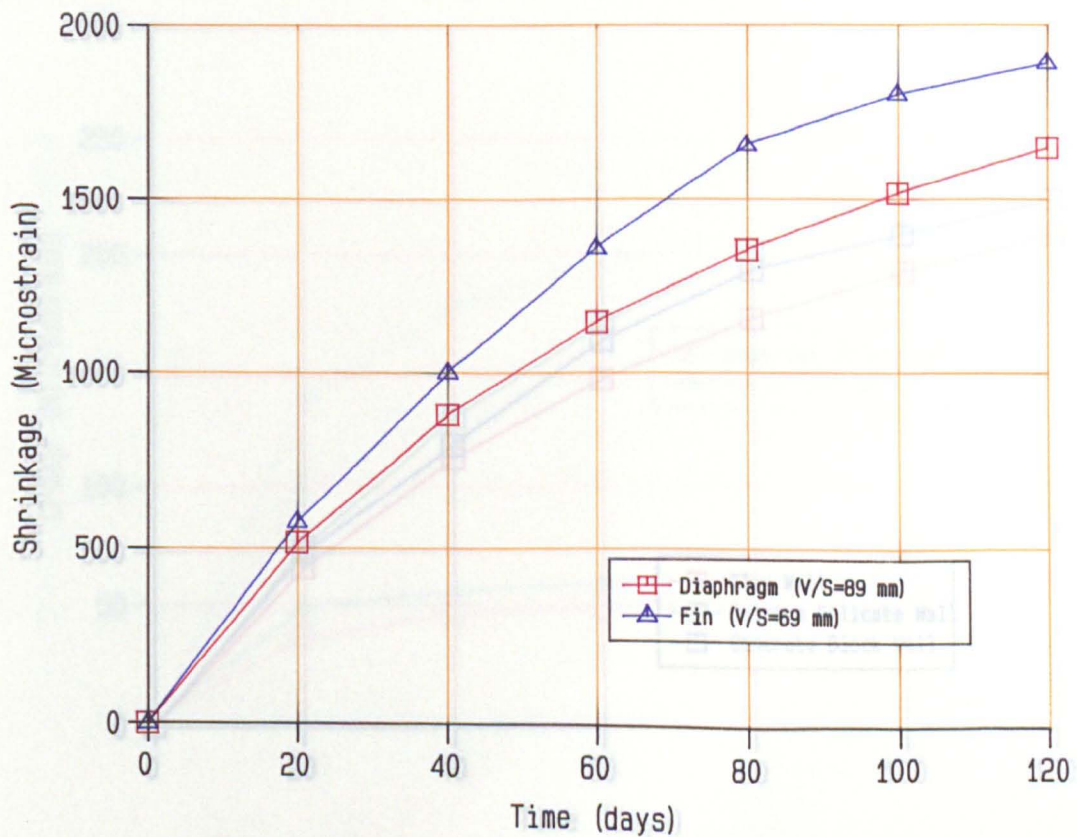


Fig. 5.26 Shrinkage-time Curve of Mortar Prisms for Calcium Silicate Walls

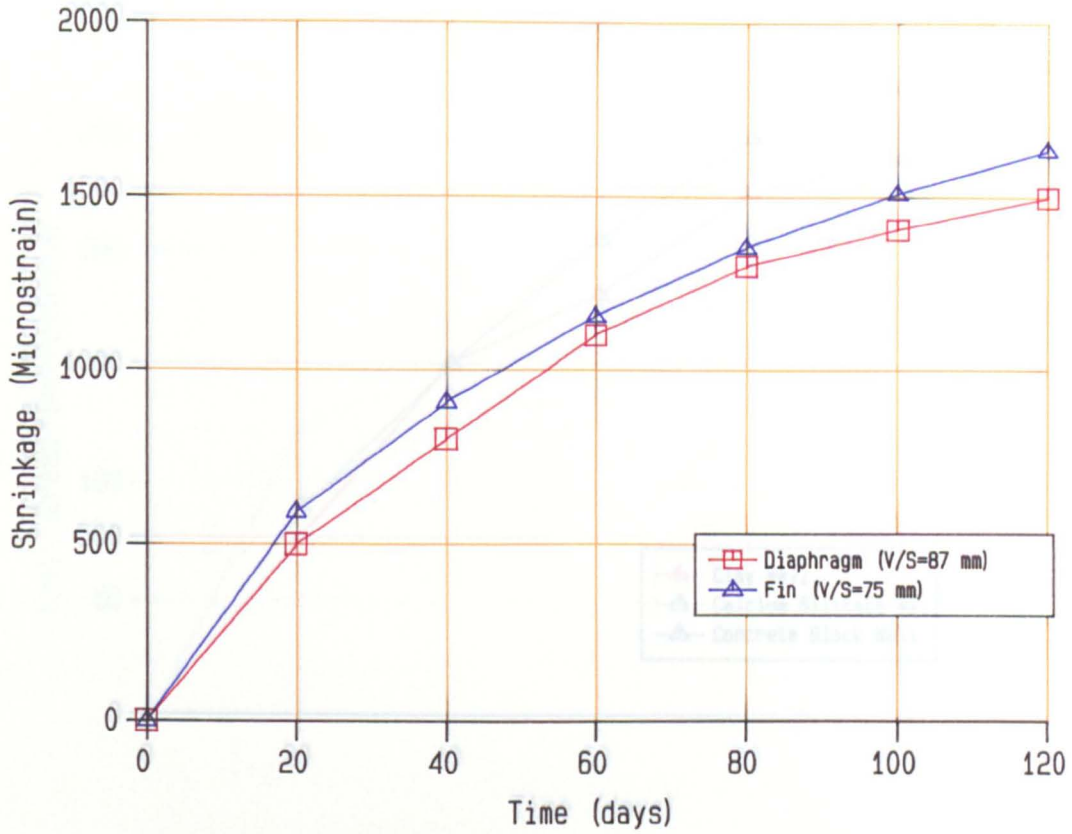


Fig. 5.27 Shrinkage-time Curve of Mortar Prisms for Concrete Block Walls

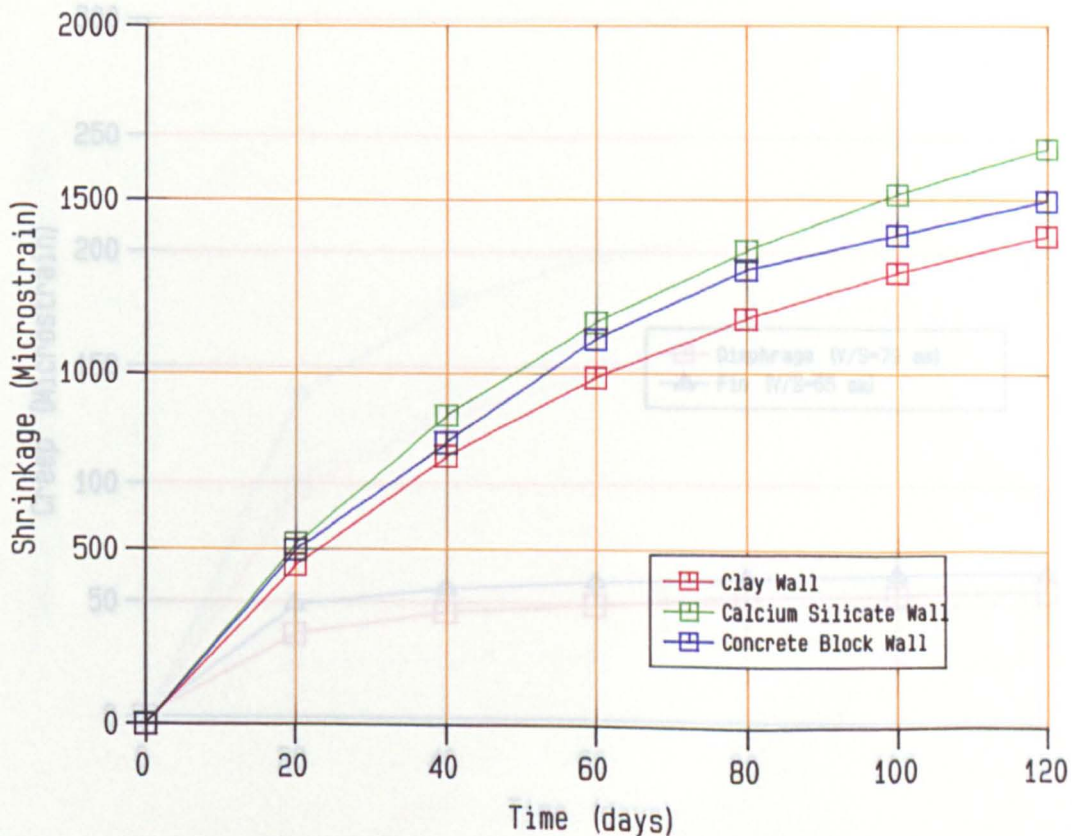


Fig. 5.28 Shrinkage-time Curve of Mortar Prisms for Diaphragm Walls

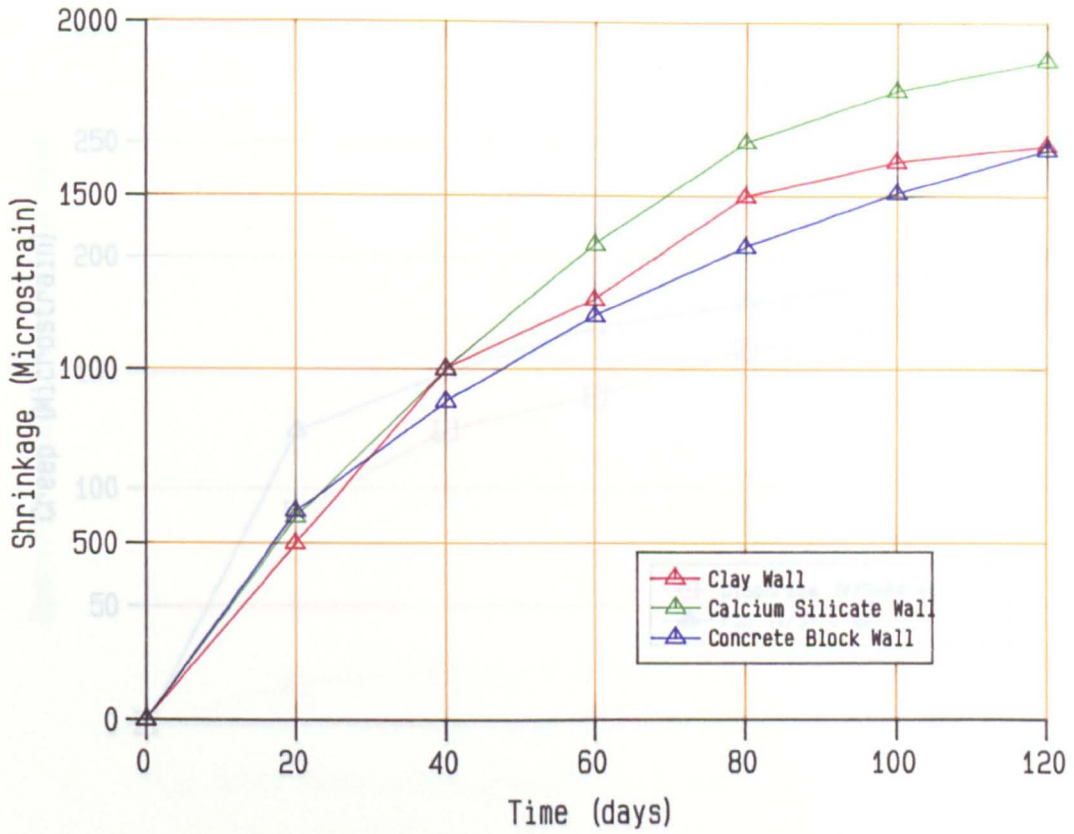


Fig. 5.29 Shrinkage-time Curve of Mortar Prisms for Fin Walls

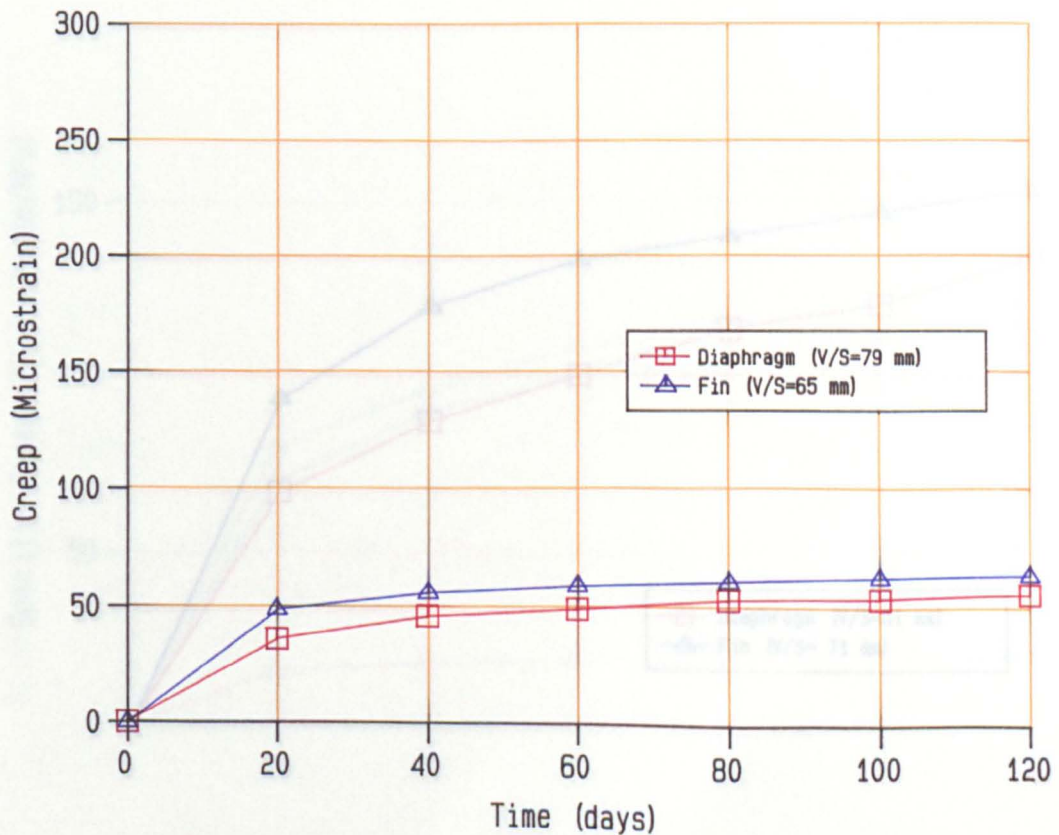


Fig. 5.30 Creep-time Curve of Clay Units under 3 MPa Stress

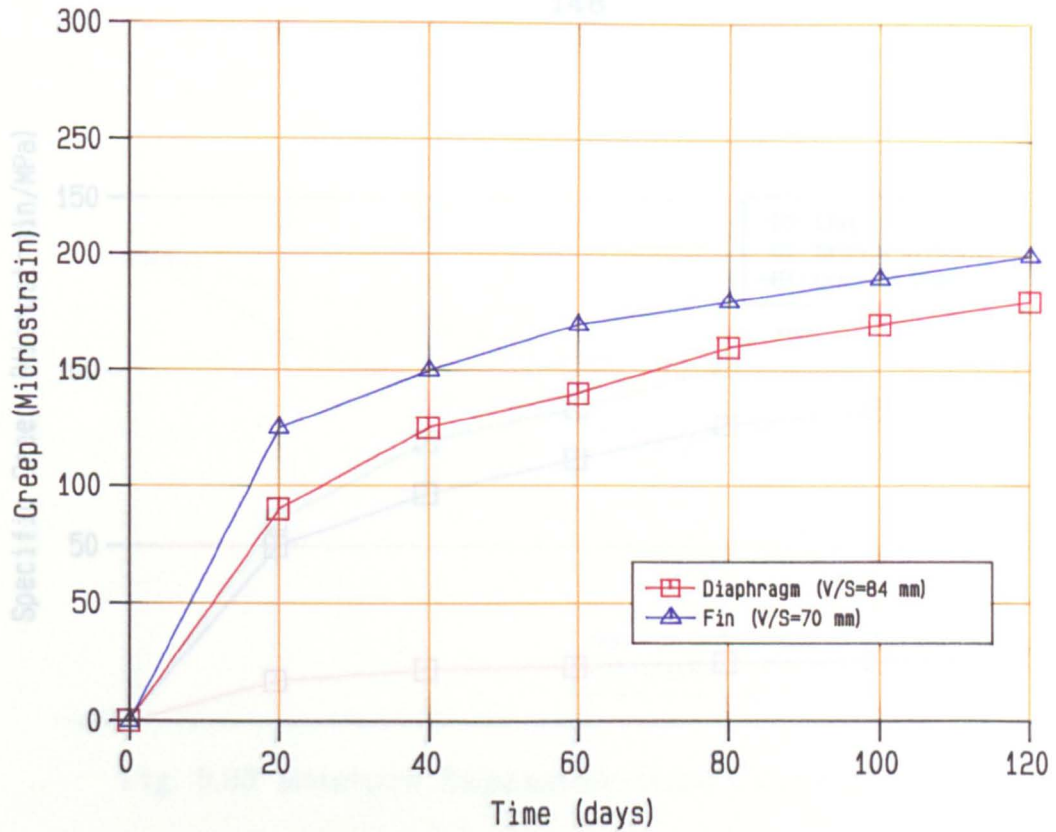


Fig. 5.31 Creep-time Curve of Calcium Silicate Units under 1.57 MPa Stress

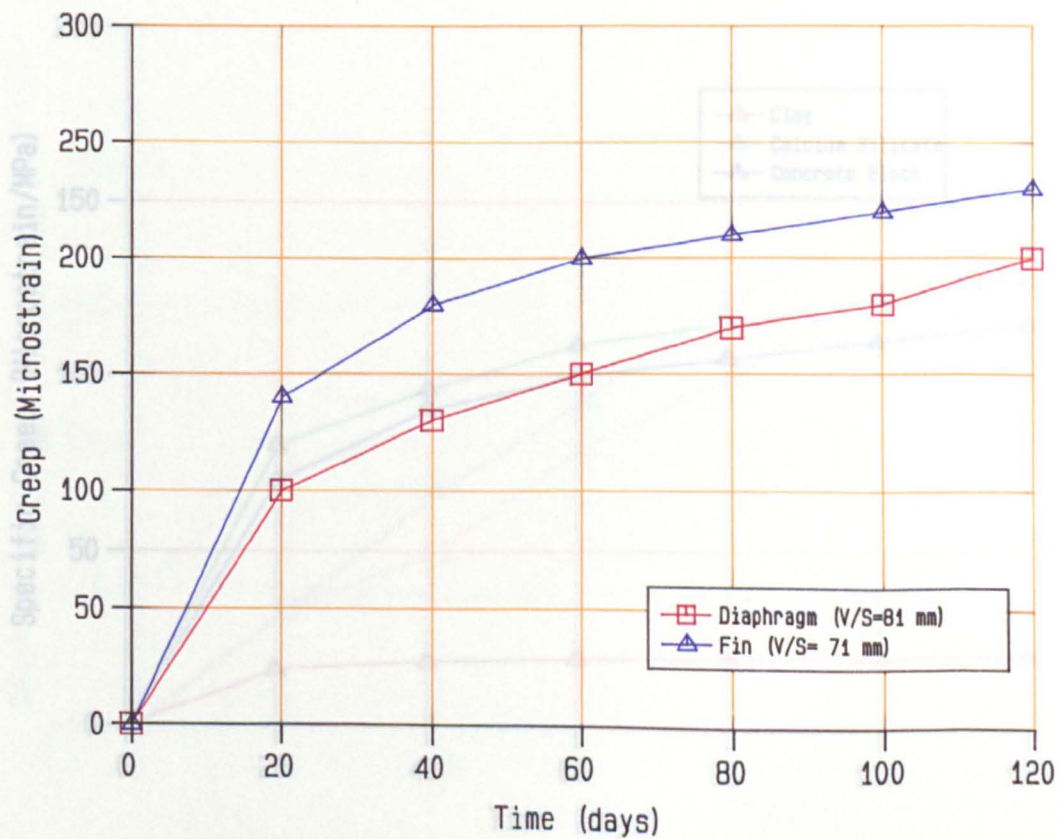


Fig. 5.32 Creep-time Curve of Concrete Block Units under 2 MPa Stress

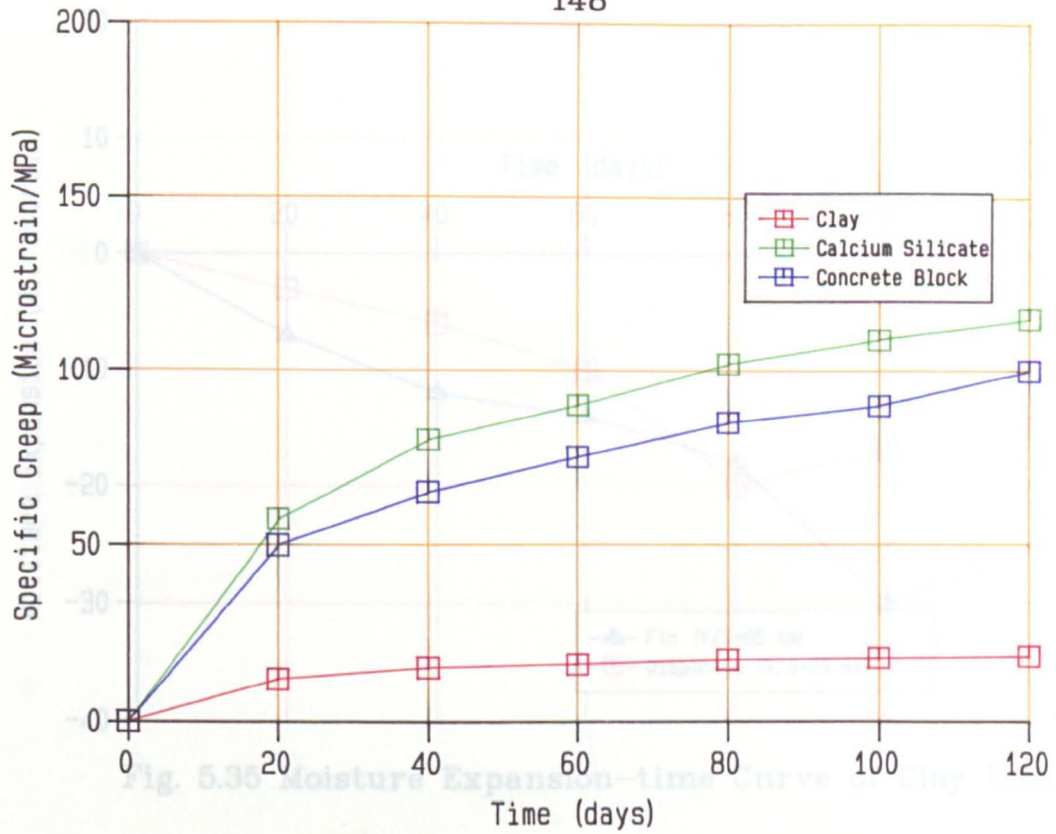


Fig. 5.33 Specific Creep-time Curve of Masonry Units for Diaphragm Walls

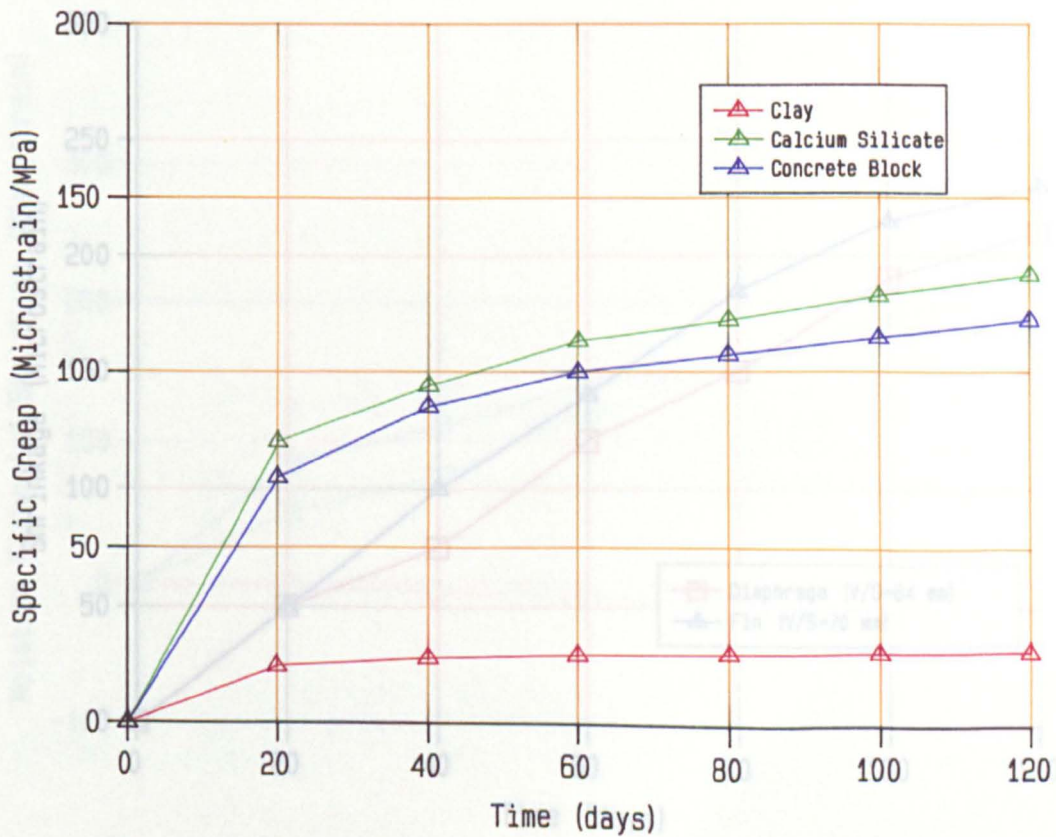


Fig. 5.34 Specific Creep-time Curve of Masonry Units for Fin Walls

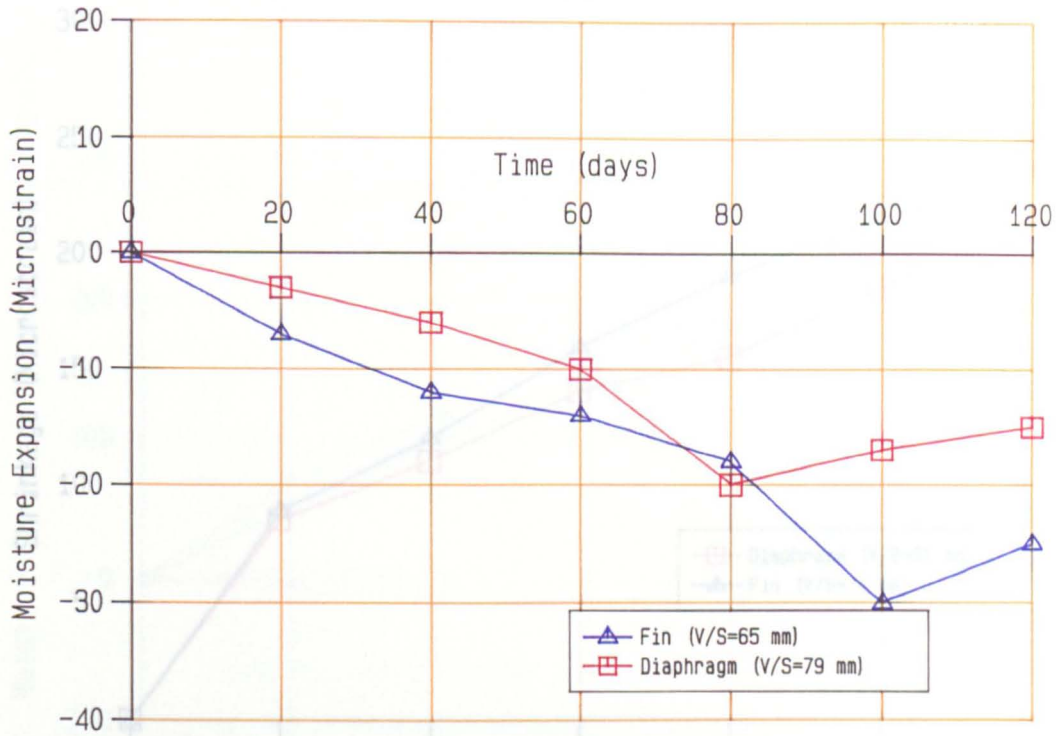


Fig. 5.35 Moisture Expansion–time Curve of Clay Units

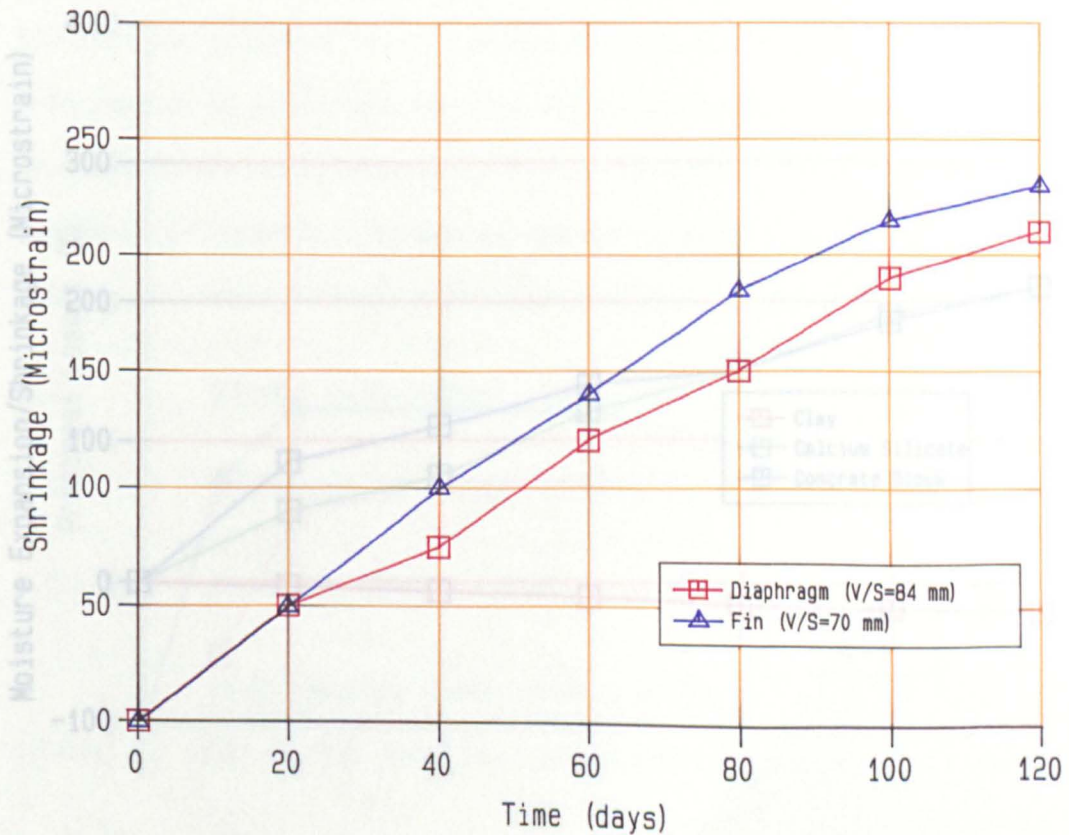


Fig. 5.36 Shrinkage–time Curve of Calcium Silicate Units

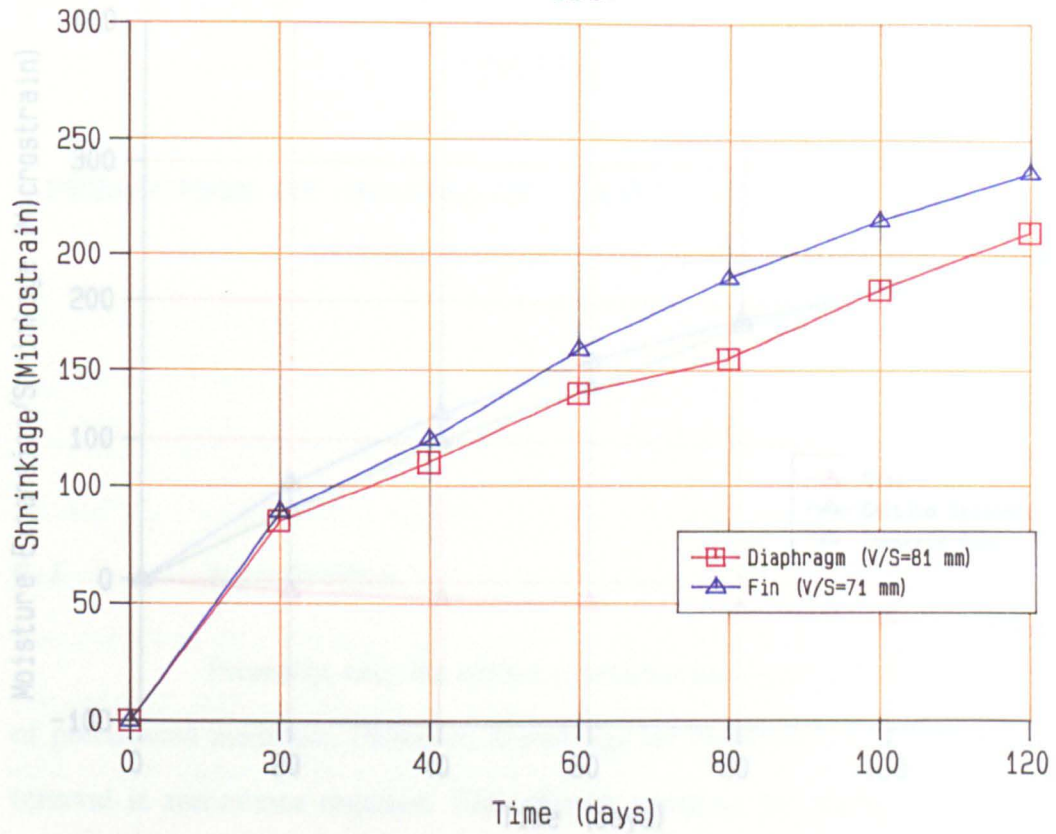


Fig. 5.37 Shrinkage-time Curve of Concrete Block Units

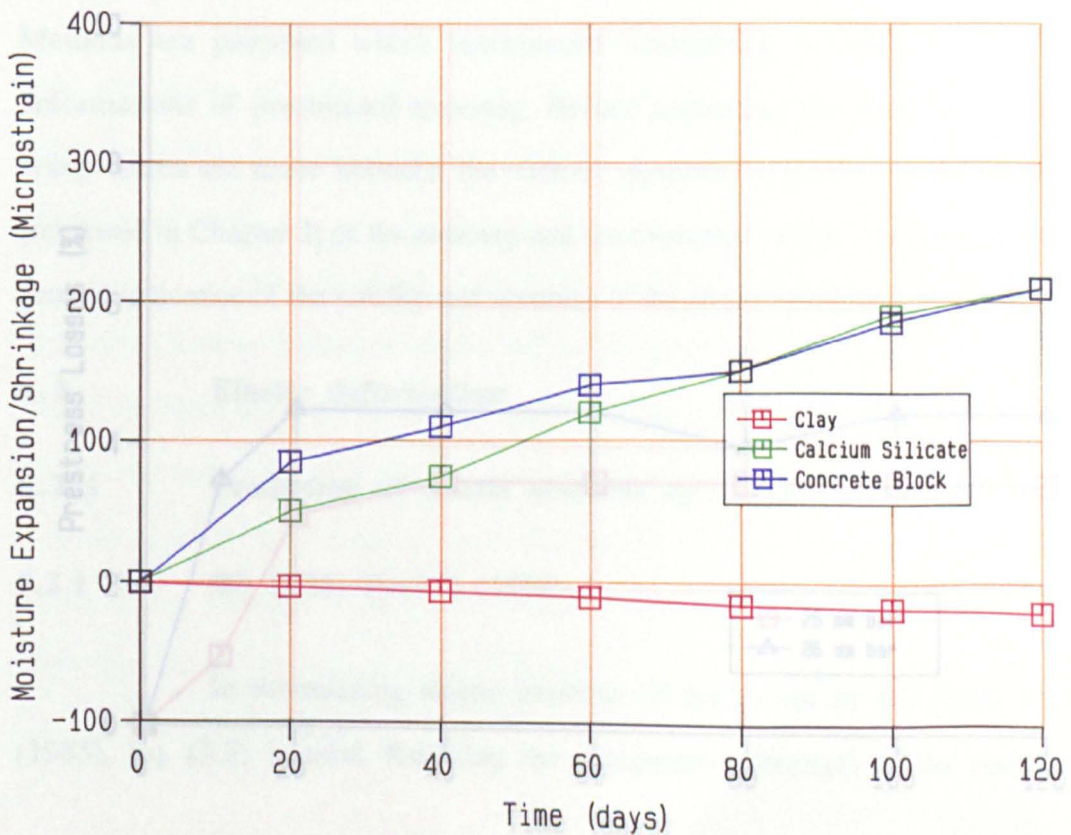


Fig. 5.38 Moisture Expansion/Shrinkage-time Curve of Masonry Units for Diaphragm Walls

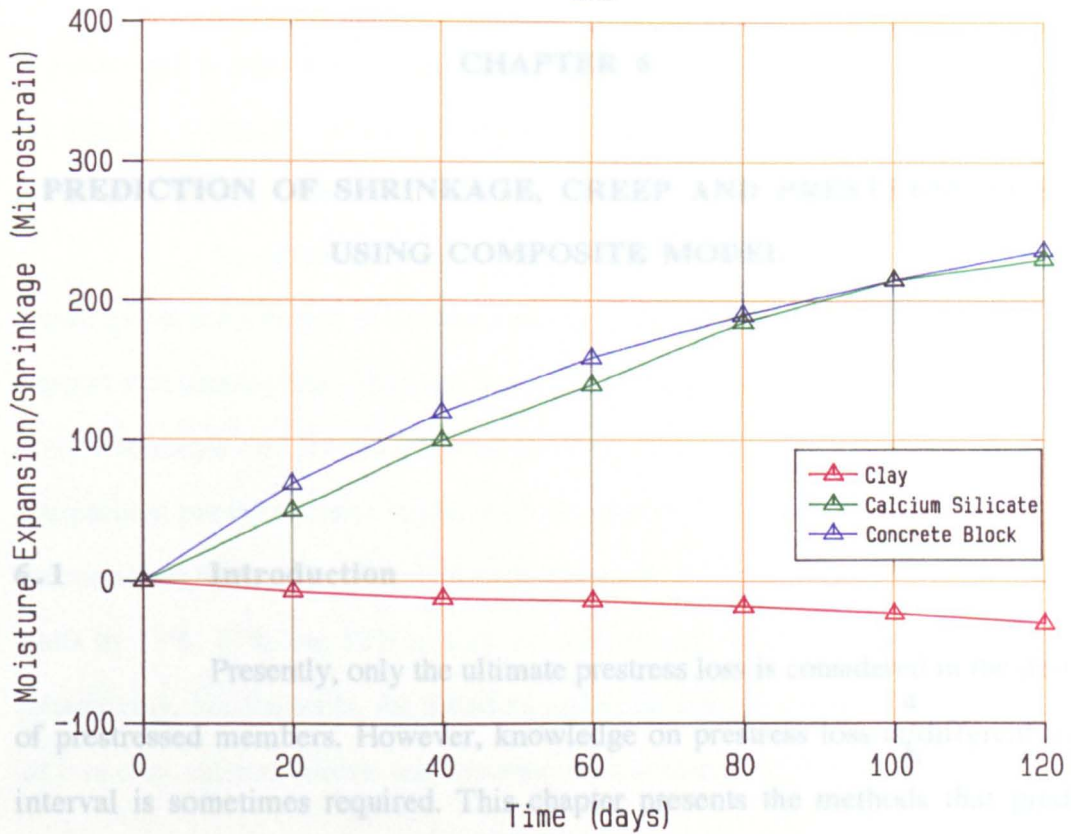


Fig. 5.39 Moisture Expansion/Shrinkage-time Curve of Masonry Units for Fin Walls

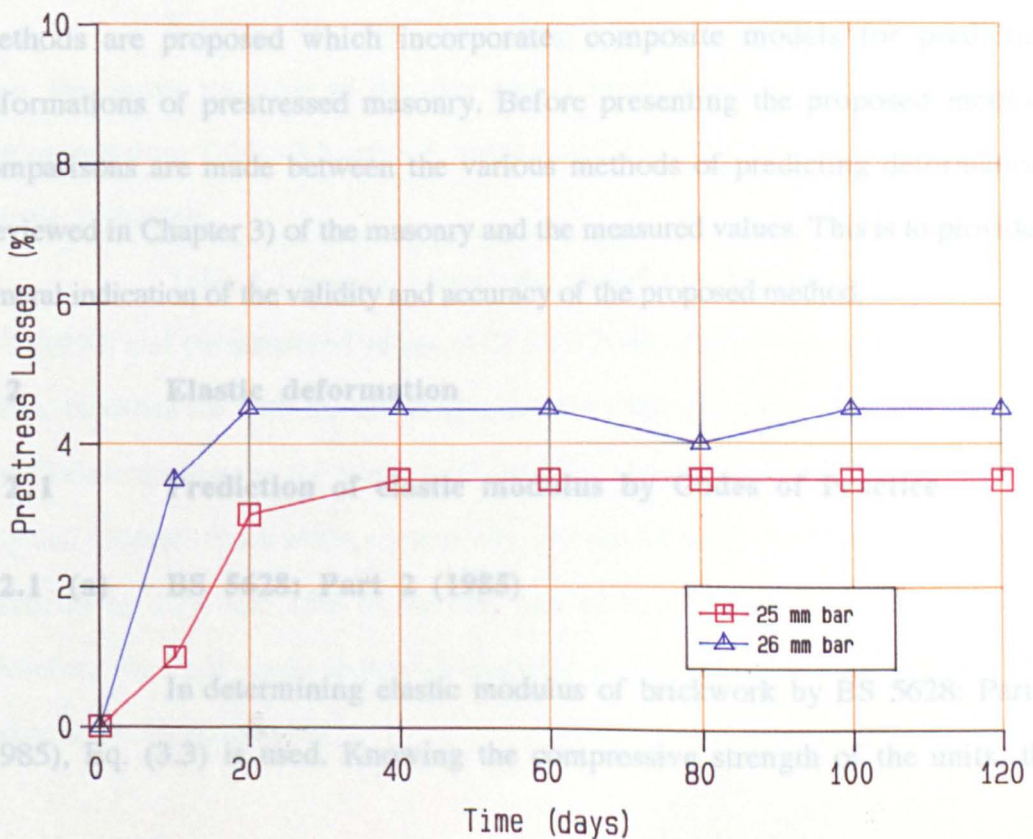


Fig. 5.40 Relaxation-time Curve of Prestressing Bars

CHAPTER 6

PREDICTION OF SHRINKAGE, CREEP AND PRESTRESS LOSS USING COMPOSITE MODEL

6.1 Introduction

Presently, only the ultimate prestress loss is considered in the design of prestressed members. However, knowledge on prestress loss at ^adifferent time interval is sometimes required. This chapter presents the methods that predict prestress loss at various times as well as the ultimate value. The prestress loss depends on the deformations of the masonry and relaxation of the prestressing bars. Methods are proposed which incorporate composite models for predicting deformations of prestressed masonry. Before presenting the proposed method, comparisons are made between the various methods of predicting deformations (reviewed in Chapter 3) of the masonry and the measured values. This is to provide a general indication of the validity and accuracy of the proposed method.

6.2 Elastic deformation

6.2.1 Prediction of elastic modulus by Codes of Practice

6.2.1 (a) BS 5628: Part 2 (1985)

In determining elastic modulus of brickwork by BS 5628: Part 2 (1985), Eq. (3.3) is used. Knowing the compressive strength of the units, the

characteristic compressive strength of masonry is obtained from Table 3.1. To obtain the elastic modulus, the characteristic compressive strength of the masonry is substituted into Eq. (3.3).

As stated in Chapter 3, BS 5628:Part 2 (1985) assumes no effect of geometry on deformation of masonry and the findings discussed in section 5.2.1.(a) support that assumption. Thus the Standard predicts a single value of elasticity for both diaphragm and fin walls investigated in this research. Table 6.1 shows the comparison between elastic modulus of the masonry by BS 5628:Part 2 (1985) and the measured values. The Standard underestimates the elastic modulus of diaphragm walls by 17%, 41% and 32% in clay, calcium silicate and concrete block masonry, respectively. For fin walls, the Standard underestimates elasticity by 9%, 44% and 28% in clay, calcium silicate and concrete block masonry, respectively.

6.2.1 (b) ACI 530-88/ASCE 5-88 (1990)

Knowing the compressive strength of the masonry unit and the mortar type, the elastic modulus of the clay and concrete block walls can be directly determined from Tables 3.2 and 3.3, respectively. No provision is given for calcium silicate brickwork.

Table 6.1 compares the elastic modulus of the masonry given by ACI 530 (1990) and the measured values. ACI 530 (1990) also predicts a single value of elastic modulus for both the diaphragm and fin walls investigated in this research. The Code overestimates the elastic modulus of diaphragm walls by 5% and 9% in the clay and concrete block walls, respectively. For the fin walls, the Code overestimates elasticity by 10% and 15% in the clay and concrete block walls, respectively. Therefore the Code seems to predict elasticity of masonry reasonably well for clay and concrete block masonry.

6.2.1 (c) Eurocode No 6 (1988)

Eurocode No 6 (1988) adopts a similar method as in BS 5628: Part 2 (1985) except that the characteristic compressive strength of masonry should be determined either experimentally or theoretically from an expression in terms of strength of unit and mortar (Eq. (3.4)).

Eurocode No 6 (1988) also predicts a single value of elastic modulus for both the diaphragm and fin walls investigated in this research. Table 6.1 compares the elastic modulus of the masonry by Eurocode No 6 with the measured values. The Code underestimates elastic modulus of the diaphragm walls by 7 %, 37% and 24% in the clay, calcium silicate and concrete block masonry, respectively. For the fin walls, the Standard underestimates elasticity by 3%, 41% and 19% in clay, calcium silicate and concrete block masonry, respectively. As in BS 5628: Part 2 (1985), Eurocode No 6 predicts elasticity reasonably well only in clay brickwork. The large differences between the elastic modulus measured in this test and the predicted values by the Standards in calcium silicate and concrete block walls cannot be explained, although this could be due to the methods being based on clay brickwork data alone.

6.2.2 Prediction of elastic modulus by previous researchers

Only the Lenczner (1986) and Brooks (1990) methods are considered in predicting elastic deformation of masonry. The model developed by Ameny (1983) is disregarded because it is restricted to certain types of full-bedded solid and face-shell bedded hollow concrete masonry. This means that the Ameny model is not really applicable to other types masonry with different types of bonds.

6.2.2 (a) Lenczner method (1986)

Equations (3.5) to (3.7) are used in predicting elastic modulus developed by Lenczner (1986). The elastic modulus of the masonry is determined directly from compressive strength of masonry units.

Again this method predicts a single value of elastic modulus for both the diaphragm and fin walls investigated in this research. Table 6.2 shows the method overestimates elastic modulus of the clay diaphragm and fin walls by 17% and 22%, respectively. However, this method underestimates elasticity of the calcium silicate diaphragm and fin walls by 52% and 55%, respectively. This method also underestimates elasticity of the concrete block diaphragm and fin walls by 68% and 66%, respectively. The large differences between the predicted elasticity of the calcium silicate and concrete block walls and the measured values are probably due to the empirical equations being based simply on clay brickwork test data.

6.2.2 (b) Brooks method (1990a)

For this method, elastic modulus of the masonry walls is obtained by direct substitution of the appropriate values of elastic modulus of the partly sealed unbonded brick units and the partly sealed mortar prisms into Eq. (3.8). In the prediction of elasticity of the clay walls, adjustment was made due to the difference in the elasticity between bed and header faces (anisotropy) of the clay units. The effect of anisotropy is presented in Section 5.4.1. No adjustments were made for the prediction of elasticity of the calcium silicate and concrete block walls, because Table 5.6 shows the calcium silicate units are isotropic. For the concrete block walls, no adjustments were made to the block units because the units were tested between bed face in the creep test.

Table 6.2 shows the predicted and measured elasticity of the masonry walls. Generally the predicted and measured elastic moduli of the clay and calcium silicate walls are in good agreement, i.e within 10 % of the measured values. However the model underestimates modulus of elasticity of the concrete block diaphragm and fin walls by 29 and 25 %, respectively.

A detailed discussion on the application of composite model was presented by Brooks (1990a). Appendix D shows a sample calculation of predicting elastic modulus of the clay diaphragm wall.

6.3 Creep

6.3.1 Creep of masonry by Codes of Practice

6.3.1 (a) BS 5628:Part 2 (1985)

BS 5628:Part 2 (1985) only predicts ultimate specific creep by multiplying the appropriate factor given in Section 3.4.1.(a) to the elastic strain (determined from Section 6.2.1 (a)) of the masonry walls. Table 6.3 compares the predicted and the estimated ultimate creep from extrapolation of experimental results of the masonry walls investigated in this research.

Based on a single value prediction, the Standard overestimates creep of the diaphragm walls by 21%, 20% and 89% in the clay, calcium silicate and concrete block walls, respectively. For fin walls, the Standard overestimates creep by 1%, 17% and 64% in the clay, calcium silicate and concrete block walls, respectively. However, if the measured elastic strain values were used, the Standard only overestimates creep of diaphragm and fin concrete block walls by 28% and 20%, respectively. It can be concluded that the Standard predicts creep quite well for the clay and calcium silicate walls but not for the concrete block walls.

6.3.1 (b) ACI 530-88/ASCE 5-88 (1990)

As with BS 5628 (1985), ACI 530 (1990) also predicts ultimate specific creep by multiplying the appropriate suggested coefficients of creep, in Section 3.4.1.(b), by the applied stress of the masonry walls. Table 6.3 compares the estimated ultimate creep of the masonry walls investigated in this test programme and the predicted creep by the Code.

The Code overestimates the ultimate creep of the diaphragm concrete block walls by twice as much as the estimated ultimate value extrapolated from test data, although only overestimates by 33% in the corresponding clay wall. For fin walls, the Code overestimates creep by 11% and 88% in the clay and concrete block walls, respectively. No provision is given for creep of calcium silicate brickwork.

6.3.1 (c) Eurocode No 6 (1988)

As with the previous two methods, Eurocode 6 (1988) also predicts ultimate specific creep and Table 6.3 shows the Code overestimates the ultimate creep of clay diaphragm wall by 8% and underestimates by 10% in the fin. The Code estimates creep reasonably well in the diaphragm and fin calcium silicate walls, i.e 8% and 5%, respectively. As in for the concrete block wall, the Code overestimates creep by 70% and 47% in the diaphragm and fin walls, respectively. The Code predictions follow the same pattern as the BS 5628: Part 2 (1985), reasonably well in the clay and calcium silicate walls but quite poor in the concrete block, because both standards suggest the same value of creep coefficients.

6.3.2. Prediction of creep by previous researchers

6.3.2 (a) Lenczner method (1986)

This method predicts creep in term of the creep ratio, which is determined using appropriate equations as given in Section 3.4.2.(a). The creep is then predicted by multiplying the creep ratio by the elastic strain (Section 6.2.2 (a)). The predicted creep is compared to the estimated ultimate creep values as in Table 6.4.

This method underestimates creep of the clay diaphragm wall by 18% and overestimates creep in fin wall by 1%. However, this method does not predict creep of calcium silicate and concrete block walls very well because the elastic modulus expressions (Section 3.3.2 (a)) had been based on clay brickwork. If the measured elastic strains were used, the method only underestimates creep by up to 16% in both the calcium silicate and concrete block walls.

6.3.2 (b) Brooks method (1987b)

In this method, creep is obtained in terms of specific creep. The specific creep is obtained by substituting the elastic and effective modulus of the brickwork to Eq. (3.12). The moduli of the masonry walls were determined using similar method as in Section 6.2.2.(b). Table 6.4 compares the predicted and estimated ultimate creep. The table shows that the predictions overestimate ultimate creep in the clay and calcium silicate walls by up to 39% and underestimate by 9% in the concrete block. For the same reason as in the prediction of elasticity of the clay walls, adjustments were made on to allow for anisotropy in predicting creep in clay walls.

Figure 6.1 compares the predicted creep of the clay walls to the measured values over a period of 120 days. This model predicts creep reasonably well in the diaphragm and fin clay walls (20%). However, the model overestimates creep by 25% and 23% in the diaphragm and fin calcium silicate walls, respectively (see Fig. 6.2). For the diaphragm and fin concrete block walls, the model overestimates creep by 4% and 9%, respectively (see Fig. 6.3).

6.4 Shrinkage

6.4.1 Prediction of shrinkage by Codes of Practice

6.4.1 (a) BS 5628:Part 2 (1985)

Table 6.5 gives the suggested maximum shrinkage strain of 500 microstrain for both the calcium silicate and concrete block walls. However, the Standard assumes no net moisture movement strain occurs in clay brickwork; although a shrinkage was measured between 147×10^{-6} to 184×10^{-6} .

The Standard overestimates shrinkage in calcium silicate and concrete block walls, viz. 20% and 25% for the diaphragm and fin calcium silicate walls, respectively, and by 3% for both the diaphragm and fin concrete block walls.

6.4.1 (b) ACI 530-88/ASCE 5-88 (1990)

The Code suggests a coefficient of irreversible moisture expansion of clay brickwork to be taken as 300×10^{-6} . As for concrete masonry, the coefficient of shrinkage is taken as 0.15-0.5 multiplied by the total linear drying shrinkage of the concrete masonry unit. As in BS 5628 (1985) the method fails to consider the type of mortar used.

Table 6.5 compares predicted moisture movement strain with the estimated ultimate creep values of the masonry walls investigated in this research. The Code estimates an expansion of 300×10^{-6} where as the average measured shrinkage of the diaphragm and fin clay brickwork is 147×10^{-6} and 184×10^{-6} , respectively. The Code underestimates shrinkage of the diaphragm and fin concrete block walls by up to 24%. No provision is given for shrinkage in calcium silicate brickwork.

6.4.1 (c) Eurocode No 6 (1988)

Clause 3.2.6.4 of Eurocode No 6 (1988) stipulates a moisture movement strain of -100 to 200×10^{-6} for clay masonry. A shrinkage of 200×10^{-6} is suggested for calcium silicate and concrete masonry. As for the other codes no allowance is made for the type of mortar.

Table 6.5 compares predicted moisture movement strain by Eurocode with the estimated ultimate creep values of the masonry walls investigated in this research. Compared with the range of moisture strain of -100 to 200×10^{-6} the estimated ultimate shrinkage of the diaphragm and fin clay walls fall within that range. When compared to the estimated ultimate shrinkage of the diaphragm and fin calcium silicate walls, the Code underestimates shrinkage of by 52% and 50%, respectively. The Code also underestimates shrinkage of both the diaphragm and fin concrete block walls by 60% .

6.4.2 Prediction of shrinkage by previous researchers

Only one method (Brooks 1987b) is available in predicting shrinkage of brickwork. In this method, appropriate expansion/shrinkage of the partly sealed unbonded masonry units and the partly sealed mortar prisms from tests results (Section 5.3.3 and 5.4.3) are substituted into Eq. (3.13). A detailed discussion on the

application of the composite model has been previously discussed by Brooks (1987b and 1990b). Table 6.5 compares the measured shrinkage of brickwork to the predicted values at 120 days. Appendix D shows a sample calculation predicting shrinkage in the clay walls.

Figure 6.4 compares the predicted shrinkage of the clay walls with the measured values over a period of 120 days. The predicted shrinkage of the diaphragm wall is in good agreement (3%) when compared to the fin wall (13%). However, the model does not predict shrinkage in the diaphragm and fin calcium silicate walls very well (see Fig. 6.5), there being overestimates of the diaphragm and fin calcium silicate walls by 40 % and 50 %, respectively. This is probably due to the water being absorbed by the units during laying the brickwork. As a result the partly sealed mortar prisms have higher water content than the mortar bed joint in the walls, and thus a higher shrinkage in the partly sealed mortar prisms is likely. Thus when the shrinkage of the partly sealed mortar prisms is applied to the model, an over estimation will occur. This logic is dealt with further in Chapter 7. Evidence of absorption by the unit after laying is shown in Plate 6.1.

Figure 6.6 compares the predicted shrinkage to the measured values for the diaphragm and fin concrete block walls. The predicted values are within 19 % and 15 % for the diaphragm and fin walls, respectively, and it is probable that unit water absorption also affected the prediction model.

6.5 Prestress loss

6.5.1 Prediction of prestress loss by Codes of Practice

Table 6.6 compares the estimated ultimate and the predicted prestress loss in the prestressed masonry walls by Codes of Practice. The relaxation loss of the bars are in accordance to BS 4486 (1980) as described in section 3.6.

6.5.1 (a) BS 5628: Part 2 (1985)

The Standard approach is based on a single value of creep coefficient and ultimate shrinkage depending on the type of masonry, i.e. clay, calcium silicate and concrete block masonry. The strength of unit and mortar are not considered. The method predicts prestress loss due to creep, shrinkage and relaxation, separately.

Using the predicted ultimate creep and shrinkage of the masonry walls, Table 6.3 and 6.5, the prestress loss in the masonry walls are as follows:

$$\text{Stress Loss} = \epsilon_{cr} \cdot E_s + \epsilon_{sh} \cdot E_s + R_{st} \quad (6.1)$$

where

E_s = elastic modulus of bar;

ϵ_{cr} = creep strain of masonry;

= c.f x elastic strain of masonry;

c.f = 1.5 for clay and calcium silicate brickwork, and

3.0 for concrete blockwork;

ϵ_{sh} = shrinkage strain (negligible for clay brickwork and

500×10^{-6} for calcium silicate and concrete block masonry);

and R_{st} = relaxation of steel at 1000 hours in accordance with BS 4486 (1980).

Using Eq. (6.1), the predicted prestress loss in the clay, calcium silicate and concrete masonry walls are tabulated in Table 6.6. The Standard overestimates prestress loss in the diaphragm and fin calcium silicate walls by 20% and 12%, respectively. For the diaphragm and fin concrete block walls, the Standard overestimates prestress loss by 33% and 27%, respectively. As for the clay

brickwork walls, the Standard underestimates prestress loss by 31% and 38% in the diaphragm and fin walls, respectively.

The Standard estimates prestress loss better (within 20%) if measured elastic strain for predicting creep, shrinkage and relaxation strain were used instead of the estimated values as shown in Table 6.7.

6.5.1 (b) ACI 530-88/ASCE 5-88 (1990)

No provision is given for predicting prestress loss of prestressed masonry. However the predicted deformations in Section 6.2 can be used to predict the prestress loss of prestressed masonry investigated in this research.

The prestress loss in the masonry walls due to creep and shrinkage is predicted by assuming the stress loss in the bar as follows;

$$\text{Stress Loss} = (C_{oc} \cdot f_{ave}) \cdot E_s + \epsilon_{sh} \cdot E_s + R_{st} \quad (6.2)$$

where E_s = elastic modulus of bar;

E_{mw} = elastic modulus of masonry;

f_{ave} = average prestress on masonry at transfer;

C_{oc} = creep coefficient of masonry (Section 6.3.1 (b));

R_{st} = relaxation of prestressing bar;

and ϵ_{sh} = shrinkage/moisture expansion strain (Section 6.4.1 (b)).

Using Eq. (6.2), prestress loss predicted by ACI 530 (1990) is shown in Table 6.6. The Code estimates a stress gain instead of a loss in the clay wall. Since no provision is given for the deformations of calcium silicate brickwork, no prediction of prestress loss was possible. As in the case of concrete blockwork walls, this method overestimates prestress loss in both the diaphragm and fin walls by 25%.

6.5.1 (c) Eurocode No 6 (1988)

No provision is given for predicting prestress loss in prestressed masonry. However, as in Section 6.5.1 (b), the predicted deformations in Section 6.2 was used to predict the prestress loss in the prestressed walls investigated in this research. Stress loss in the bar;

$$\text{Stress Losses} = \epsilon_{cr} \cdot E_s + \epsilon_{sh} \cdot E_s + R_{st} \quad (6.3)$$

where E_s = elastic modulus of bar;

ϵ_{cr} = creep strain (as in Section 6.5.1 (a));

R_{st} = relaxation of prestressing bar;

and ϵ_{sh} = shrinkage/moisture expansion strain (-100 to 200×10^{-6} for clay brickwork and 200×10^{-6} for calcium silicate and concrete block masonry).

Using Eq. (6.3), the prestress loss predicted by Eurocode No 6 is shown in Table 6.6. This method predicts the prestress loss reasonably well in concrete block walls, i.e within 20%, but underestimates prestress loss in clay and calcium silicate brickwork by up to 33%.

6.5.2 Prediction of prestress loss by Previous Researchers

6.5.2 (a) Lenczner method (1986)

Lenczner (1986) presented a method that predicts time-dependent prestress loss due to creep and shrinkage only; excluding relaxation loss in the prestressing bar. The method is based on the predicted creep coefficient and the measured shrinkage of the walls.

Figure 6.7 and 6.8 show the predicted prestress loss for the clay masonry walls using Eq. (3.1). The method predicts prestress loss very well in clay brickwork. For diaphragm and fin calcium silicate masonry, the method underestimates the prestress loss by 25% and 40% respectively. However the method predicts prestress loss up to 33% and 41 % in the diaphragm and fin concrete block walls respectively. Table 6.8 compares measured prestress loss to the estimated values when measured creep, shrinkage and relaxation strains were used, and as expected better estimations were obtained in all the masonry types.

6.5.2 (b) Tatsa method (1973)

This method predicts prestress loss due to creep and shrinkage by taking into account of the deformations of the masonry unit and mortar. However the method had only been verified on post-tensioned concrete blockwork. Using Eq. (3.2), based on measured deformation values, the method overestimates prestress loss by 13 % and 5% for the diaphragm and fin concrete block walls (Figs. 6.11 and 6.12), respectively. Comparisons could not be carried out on clay and calcium silicate brickwork due to lack of data.

6.6 Methods of predicting prestress loss in prestressed concrete

Two methods, developed for prestressed concrete, are considered for predicting prestress loss. These methods are based on Dilger (1983) and Abeles (1966). The method developed by Dilger takes into account the effect of varying stress by incorporating ^{an} aging coefficient but the Abeles (1966) method ignores the effect of varying stress. When applied to prestressed concrete, both methods require estimates of creep and shrinkage which can be obtained from Standard methods of prediction. Since there are no equivalent methods for masonry, creep and shrinkage are obtained from the composite models.

6.6.1 Dilger method (1983)

This method is given by Eq. (3.16), the creep coefficient and shrinkage strain being those determined using the composite modelling. The creep coefficient is expressed in terms of creep at time t divide by elastic strain at loading, i.e.

$$\text{Creep coefficient } (\phi) = \epsilon_c(t) / \epsilon_i(t_0)$$

where $\epsilon_c(t)$ = creep at time t

and $\epsilon_i(t_0)$ = elastic strain at loading = $(\frac{\sigma_w}{E_{wy}})$

From composite modelling the specific creep at time t ;

$$C_s = \frac{1}{E'_{wy}} - \frac{1}{E_{wy}}$$

thus creep at time t , $C = \sigma_w (\frac{1}{E'_{wy}} - \frac{1}{E_{wy}})$

where σ_w = applied stress

Therefore the creep coefficient can be expressed as

$$\begin{aligned} (\phi) &= \frac{\sigma_w (\frac{1}{E'_{wy}} - \frac{1}{E_{wy}})}{(\frac{\sigma_w}{E_{wy}})} \\ &= (\frac{E_{wy}}{E'_{wy}} - 1) \end{aligned} \quad (6.4)$$

where E_{wy} = elastic modulus of masonry (Eq. (3.8));

and E'_{wy} = effective elastic modulus of masonry.

The effective elastic modulus of masonry (E'_{wy}) can be determined as below;

$$\frac{1}{E'_{wy}} = \frac{b_y C}{H} \left[\frac{A_w}{E'_{by} A_b + E'_m A_m} \right] + \frac{m_y (C + 1)}{H} \frac{1}{E'_m} \quad (6.5)$$

where E'_{wy} = effective elastic modulus of masonry;

E'_{by} = effective elastic modulus of elasticity of unit;

E'_m = effective elastic modulus of elasticity of mortar ;

H = height of masonry;

C = number of courses;

$C + 1$ = number of mortar courses;

b_y = depth of unit,

m_y = height of mortar joint;

A_w = cross sectional area of masonry ;

A_b = cross-sectional area of bricks;

and A_m = cross-sectional area of vertical mortar joints = $A_w - A_b$.

Based on Eq. (3.16), the stress loss can be expressed as

$$\delta f_s (t) = \frac{n_o f_o \left(\frac{E_{wy}}{E'_{wy}(t,t_o)} - 1 \right) + \epsilon_{sh}(t,t_o) E_s + f'r(t)}{1 + \rho n_o (1 + y_1^2 / r^2) (1 + \chi \left(\frac{E_{wy}}{E'_{wy}(t,t_o)} - 1 \right))} \quad (6.6)$$

Appendix D shows a sample calculation using this method. Figures 6.7 to 6.12 compare the predicted prestress loss to the measured values for all the masonry walls.

Attempts were also made to estimate prestress loss by substituting measured creep, shrinkage and relaxation strains in Eq. (6.6). Table 6.8 gives the estimated prestress loss using the measured strains.

6.6.2 Abeles method (1966)

The expression for this method can be found in Section 3.7.2, and involves substituting the predicted creep and shrinkage into Eq. (3.17) at the required time. The predicted creep and shrinkage are determined from the composite model expressions presented in Sections 6.3.2.(b) and 6.4.2.(a). Appendix C shows a sample calculation using this method. Comparison between the predicted prestress loss to the measured values are given in Fig. 6.7 to 6.12. As in Dilger method (1983), prestress loss was obtained using the measured strains and the estimated loss are shown in Table 6.8.

6.7 Comparison of the proposed method of predicting prestress loss of brickwork with the experimental results and previous researchers

Figure 6.7 compares the predicted prestress loss with the measured values of the prestressed clay diaphragm walls. Dilger method (1983), which includes an aging coefficient, predicts prestress loss more accurately (+ 30%) than Abeles (1966). Abeles (1966) overestimated prestress loss up to 46% in the diaphragm walls. The Lenczner method (1986) predicts prestress loss in the prestressed clay diaphragm walls very well ($\pm 5\%$).

Figure 6.8 compares the predicted prestress loss with the measured values for the clay fin walls. Dilger et al. (1983) and Abeles (1966) methods overpredict prestress loss by 25% and 36%, respectively. The Lenczner method (1986)

overpredicts prestress loss in the clay fin wall for the first 80 days but then predict it reasonably well.

Figure 6.9 compares the predicted prestress loss with the measured values for the prestressed calcium silicate diaphragm walls. The Dilger et al. (1983) and Abeles (1966) methods overestimated prestress loss by 35% and 50%, respectively.

Figure 6.10 compares the predicted prestress loss with the measured values for the prestressed calcium silicate fin walls. The Dilger (1983) and Abeles (1966) methods overpredict prestress loss by 13% and 25%, respectively.

Figure 6.11 compares the predicted prestress loss with the measured values in the prestressed concrete block diaphragm walls. Once again, Dilger et al. (1983) and Abeles (1966), both methods overpredict prestress loss up to 25%. The Tatsa (1973) method overestimates prestress loss in the concrete block diaphragm wall by 13%.

Figure 6.12 compares the predicted prestress loss with the measured values in the prestressed concrete block fin wall. The Dilger et al. (1983) and Abeles (1966) methods overestimate prestress loss up to 20%. However Tatsa (1973) method predicts prestress loss in the concrete block fin wall very well ($\pm 5\%$).

As expected Dilger (1983) method predicted prestress loss accurately ($\pm 10\%$) when measured strains were used.

6.8 Conclusions

Lenczner and Tatsa methods gave good predictions of prestress loss in clay and concrete block masonry, respectively. Even though the use of (height of member/length of bar) ratio in Lenczner method would reveal the best method in estimating prestress loss in clay walls, however the method tends to underestimate prestress loss in other types of masonry units even if measured creep, shrinkage and

relaxation strains were used (Table 6.8). This is due to the method being merely based on clay brickwork. Method developed by Tatsa (1973) does not predict prestress loss well in other types of masonry because the method was based on concrete block masonry only.

BS 5628: Part 2 (1985) and Eurocode No 6 (1988) give better estimation of prestress loss in the calcium silicate and concrete block walls, respectively, compared to other national standards.

Generally all the methods give reasonably good agreement with measured prestress loss if the measured strains were known. This means that most of the methods are suitable for predicting prestress loss, the only problem is lack of data to give better prediction of creep and shrinkage.

For practical and design purposes, ultimate prestress loss of clay brickwork can be assumed as 20% which agrees with values recommended by Curtin (1989). As for calcium silicate and concrete block walls, an ultimate value of 30% can be used.

Table 6.1 Modulus of Elasticity of Clay, Calcium Silicate Brickwork and Concrete Blockwork Predicted by Codes of Practice

Masonry Type	Geometry	Measured (GPa)	BS 5628 (1985) (GPa)	ACI-530 (1990) (GPa)	Eurocode (1988) (GPa)
Clay Brickwork	Diaphragm	19.66	16.38	20.68	18.2
	Fin	18.82			
Calcium Silicate Brickwork	Diaphragm	12.11	7.11	NA	7.6
	Fin	12.8			
Concrete Blockwork	Diaphragm	13.97	9.54	15.17	10.6
	Fin	13.16			

Table 6.2 Modulus of Elasticity of Clay, Calcium Silicate Brickwork and Concrete Blockwork Predicted by Previous Researchers

Masonry Type	Geometry	Measured (GPa)	Brooks (1990a) (GPa)	Lenczner (1986) (GPa)
Clay Brickwork	Diaphragm	19.66	20.36	23.05
	Fin	18.82	20.2	
Calcium Silicate Brickwork	Diaphragm	12.11	11.96	5.82
	Fin	12.8	11.65	
Concrete Blockwork	Diaphragm	13.97	9.98	4.46
	Fin	13.16	9.93	

Table 6.3 Ultimate Specific Creep of Clay, Calcium Silicate Brickwork and Concrete Blockwork Predicted by Codes of Practice

Masonry Type	Geometry	Creep ($10^{-6}/\text{MPa}$)		BS 5628 (1985) ($10^{-6}/\text{MPa}$)	ACI-530 (1990) ($10^{-6}/\text{MPa}$)	Eurocode No 6 (1988) ($10^{-6}/\text{MPa}$)
		120 days	Ultimate *			
Clay Brickwork	Diaphragm	72	76	92	101	82
	Fin	86	91			
Calcium Silicate Brickwork	Diaphragm	143	183	220	NA	198
	Fin	161	188			
Concrete Blockwork	Diaphragm	132	167	315	360	283
	Fin	150	192			

*Based on extrapolation of test data

Table 6.4 Ultimate Specific Creep of Clay, Calcium Silicate Brickwork and Concrete Blockwork Predicted by Previous Researchers

Masonry Type	Geometry	Creep ($10^{-6}/\text{MPa}$)	Brooks (1990a) ($10^{-6}/\text{MPa}$)	Lenczner (1986) ($10^{-6}/\text{MPa}$)
Clay Brickwork	Diaphragm	76	106	62
	Fin	91	120	90
Calcium Silicate Brickwork	Diaphragm	183	245	166*
	Fin	188	250	158*
Concrete Blockwork	Diaphragm	167	164	157*
	Fin	192	175	167*

* based on measured strain

**Table 6.5 Predicted Shrinkage of Clay, Calcium Silicate
Brickwork and Concrete Blockwork**

Masonry Type	Geometry	Shrinkage (10 ⁻⁶)		Brooks (1990a) (10 ⁻⁶)		BS5628 (1985) (10 ⁻⁶)	ACI-530 (1990) (10 ⁻⁶)	Eurocode No 6 (1988) (10 ⁻⁶)
		120 days	Ultimate	120 days	Ultimate	Ultimate	Ultimate	Ultimate
Clay Brickwork	Diaphragm	147	179	175	303	0	-300	-100 to 200
	Fin	184	204	210	306			
Calcium Silicate Brickwork	Diaphragm	300	418	421	563	500	NA	200
	Fin	323	400	480	627			
Concrete Blockwork	Diaphragm	242	500	280	404	500	300	200
	Fin	272	513	313	582			

Table 6.6 Predicted Ultimate Prestress Loss of Clay, Calcium Silicate Brickwork and Concrete Blockwork by Codes of Practice*

Masonry Type	Geometry	Estimated Prestress Loss (%)	BS 5628 (1985) (%)	ACI-530 (1990) (%)	Eurocode No 6 (1988) (%)
Clay Brickwork	Diaphragm	14.5	9.94	-4	10.42
	Fin	16.5	10.3	-3	11.07
Calcium Silicate Brickwork	Diaphragm	21.2	25.4	NA	17.1
	Fin	24	26.9		17.5
Concrete Blockwork	Diaphragm	22.3	29.6	18.50	20.8
	Fin	24.8	31.48		21.8

* Using estimated creep and shrinkage strain

Table 6.7 Predicted Ultimate Prestress Loss of Clay, Calcium Silicate Brickwork and Concrete Blockwork by Codes of Practice*

Masonry Type	Geometry	Estimated Prestress Loss (%)	BS 5628 (1985) (%)	ACI-530 (1990) (%)	Eurocode No 6 (1988) (%)
Clay Brickwork	Diaphragm	14.5	14.2	14.0	14.2
	Fin	16.5	16.45	17.00	16.45
Calcium Silicate Brickwork	Diaphragm	21.2	19.75	21.00	19.75
	Fin	24	20	22.00	20
Concrete Blockwork	Diaphragm	22.3	19.7	22.5	19.7
	Fin	24.8	20	24.5	20

* Using measured elastic strain and shrinkage

Table 6.8 Predicted Prestress Loss of Clay, Calcium Silicate Brickwork and Concrete Blockwork by Previous Researchers at 120 days*

Masonry Type	Geometry	Measured (%)	Lenczner (1986) (%)	Tatsa (1973) (%)	Dilger** (1983) (%)	Abeles (1966) %
Clay Brickwork	Diaphragm	10	10	NA	13.5	14.2
	Fin	12.5	13.1		14.72	16.69
Calcium Silicate Brickwork	Diaphragm	17	16.27	NA	20.5	22.75
	Fin	20	17		22.00	24.00
Concrete Blockwork	Diaphragm	15	13	17	17.41	18.6
	Fin	17.5	13	18	17.6	19.07

* Using measured elastic strain and shrinkage

** Aging coefficient of 0.5 was used

Table 6.9 Estimated Ultimate Individual Prestress Loss of the Masonry Walls by Composite Modelling

Type of Masonry	Creep (%)	Shrinkage (%)	Relaxation (%)
Clay Brickwork	9.2	8	3.5 - 4.5
Calcium Silicate Brickwork	10	16.0	3.5 - 4.5
Concrete Blockwork	9.5	15	3.5 - 4.5

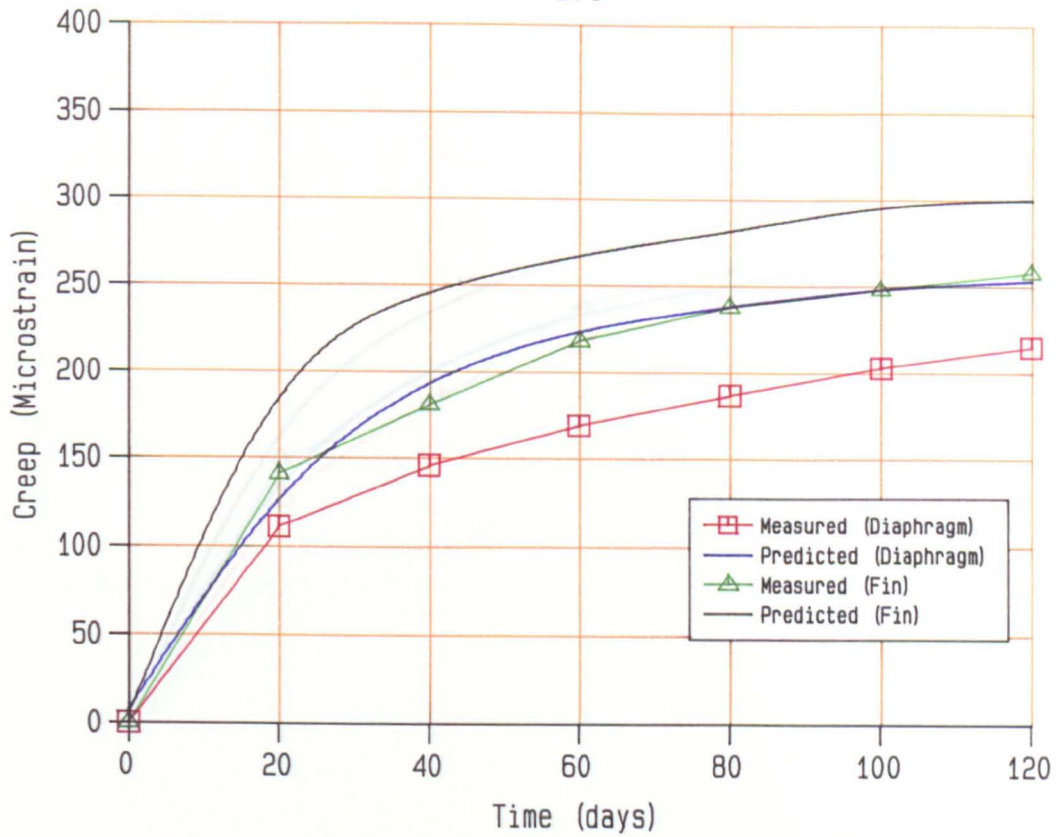


Fig. 6.1 Measured and Predicted Creep in Clay Walls

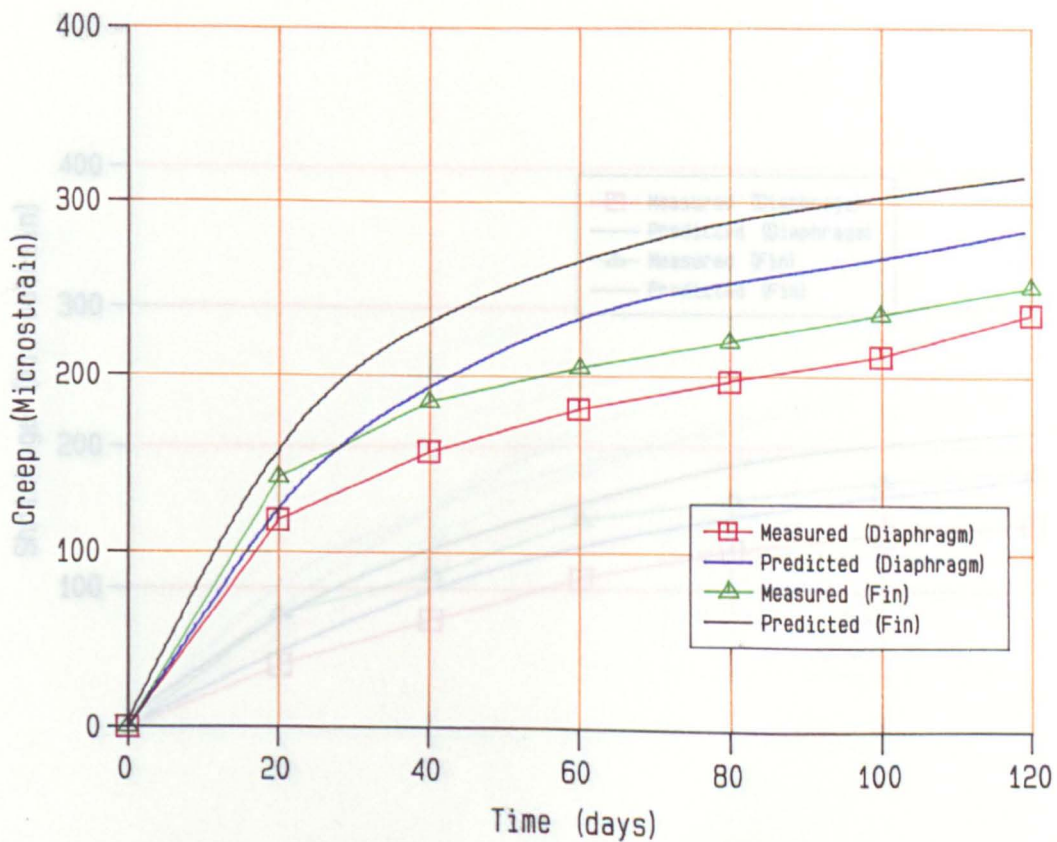


Fig. 6.2 Measured and Predicted Creep in Calcium Silicate Walls

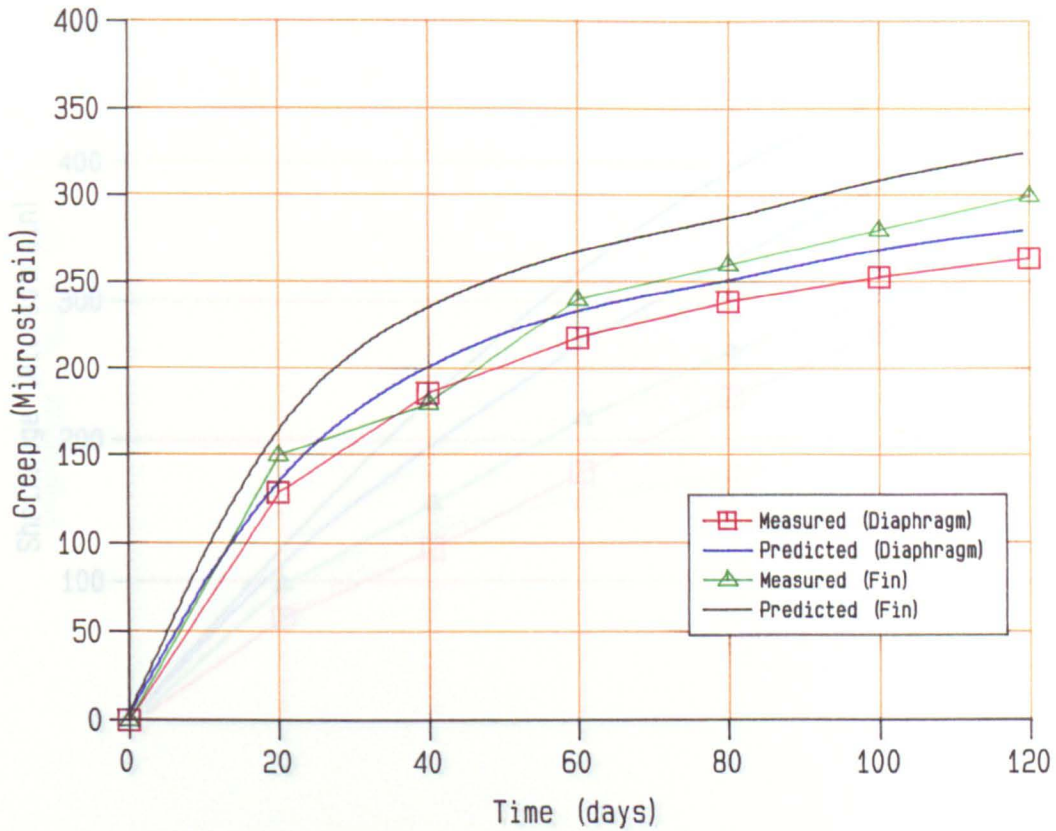


Fig. 6.3 Measured and Predicted Creep in Concrete Block Walls

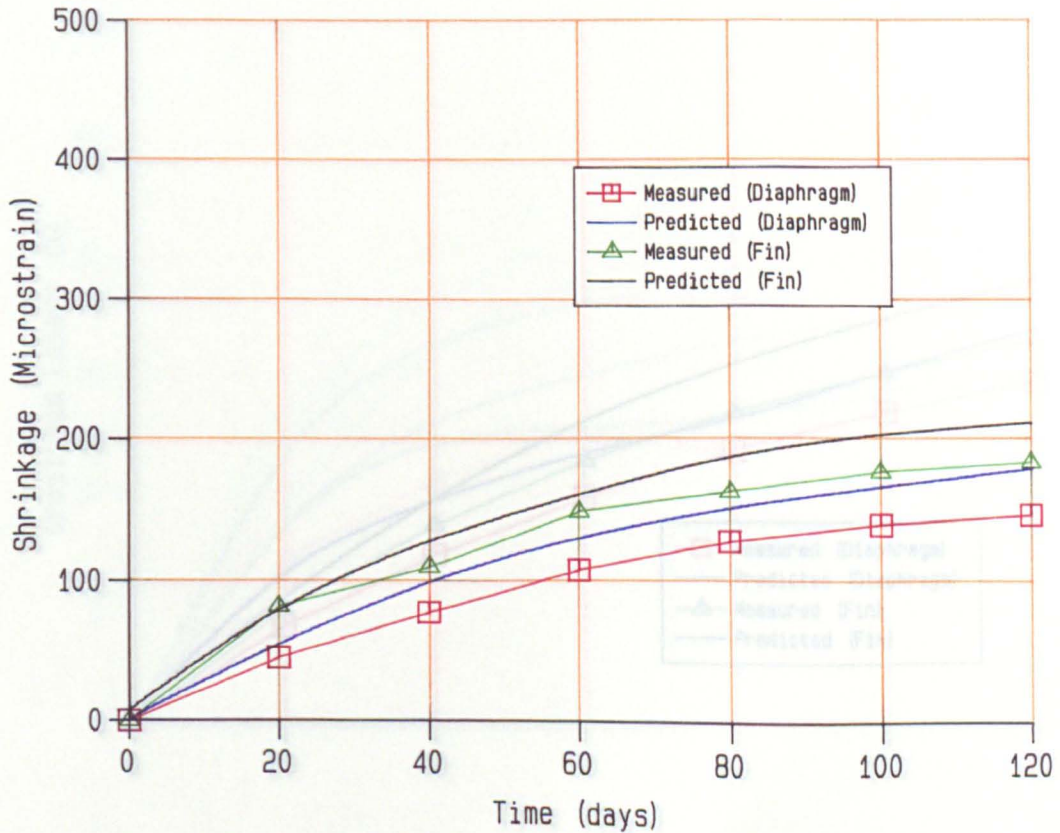


Fig. 6.4 Measured and Predicted Shrinkage-time Curve in Clay Walls

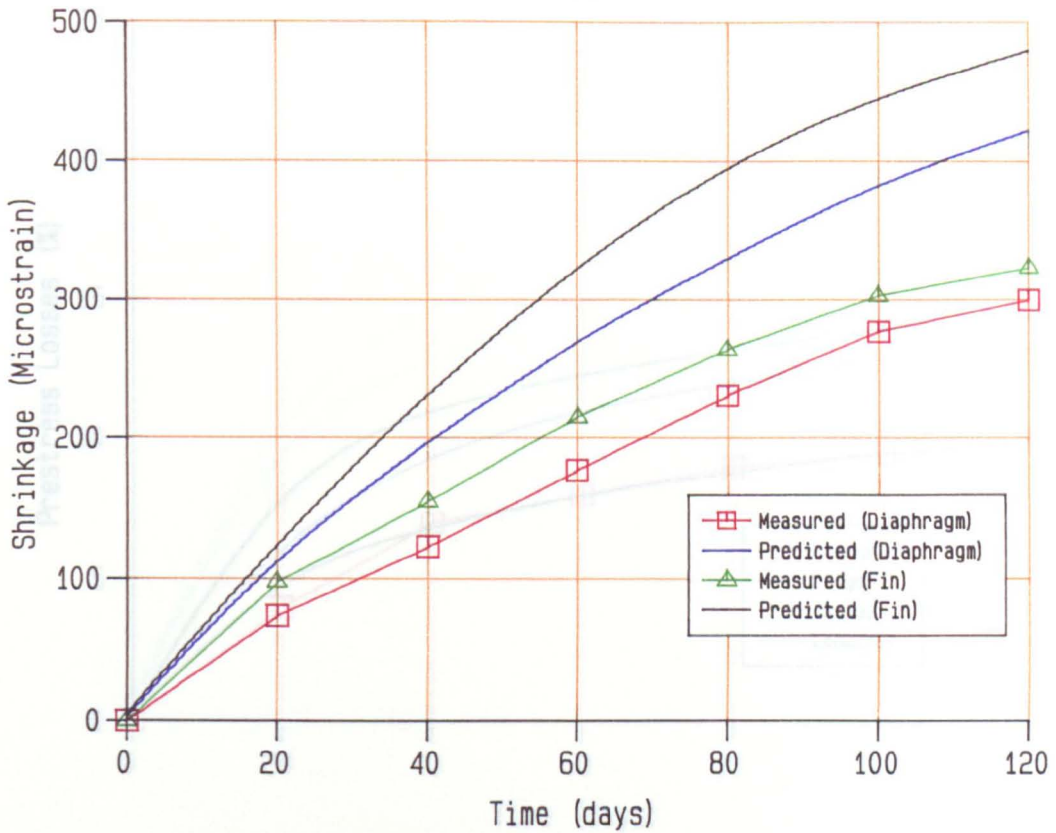


Fig. 6.5 Measured and Predicted Shrinkage–time Curve of Calcium Silicate Walls

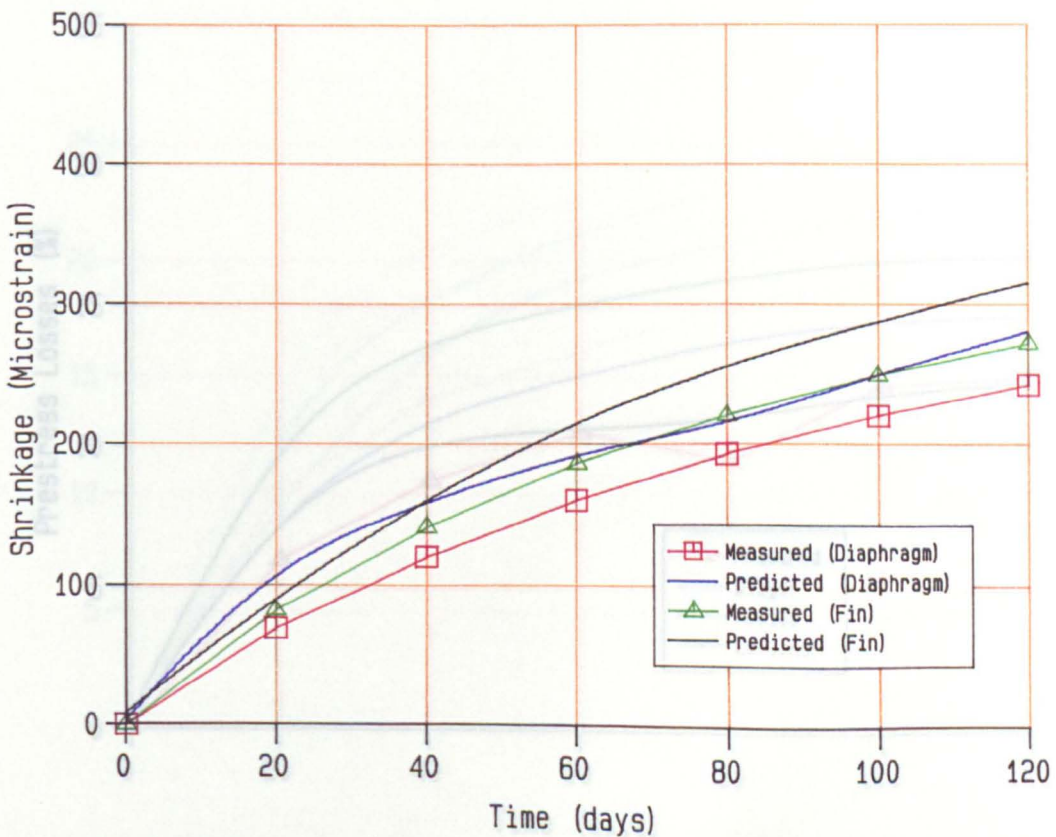


Fig. 6.6 Measured and Predicted Shrinkage–time Curve of Concrete Block Walls

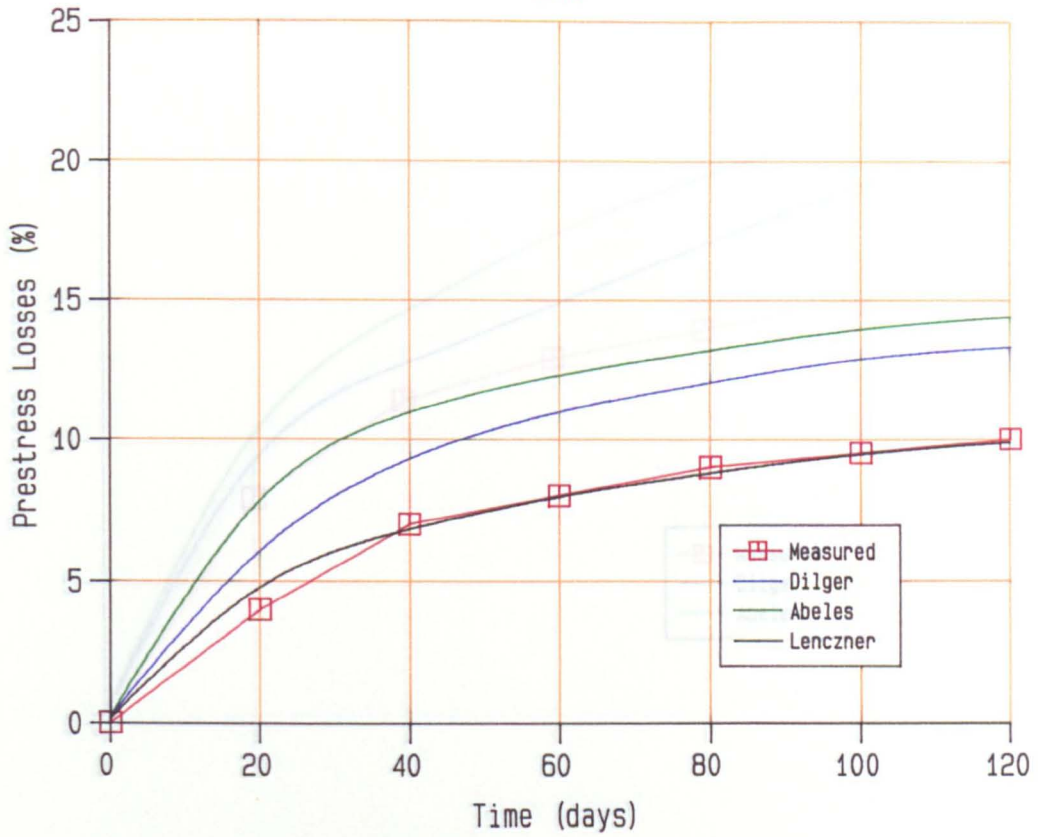


Fig. 6.7 Measured and Predicted Prestress Loss-time Curve of Clay Diaphragm Walls

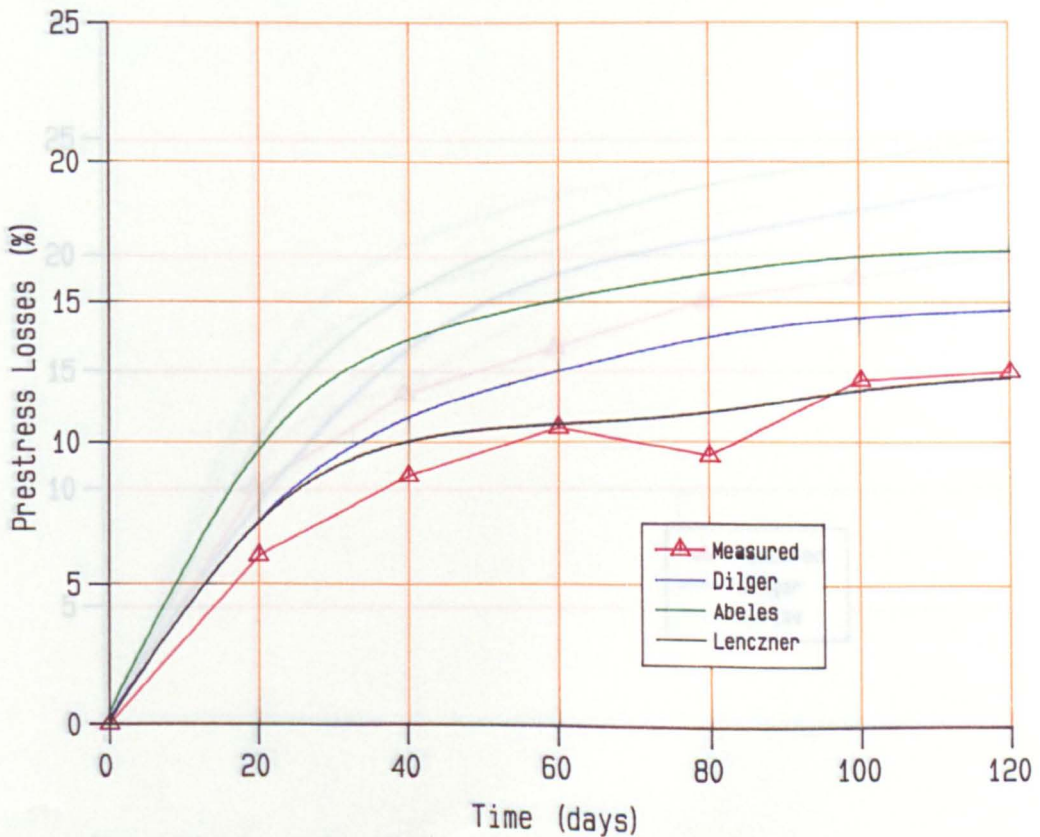


Fig. 6.8 Measured and Predicted Prestress Loss-time Curve of Clay Fin Wall

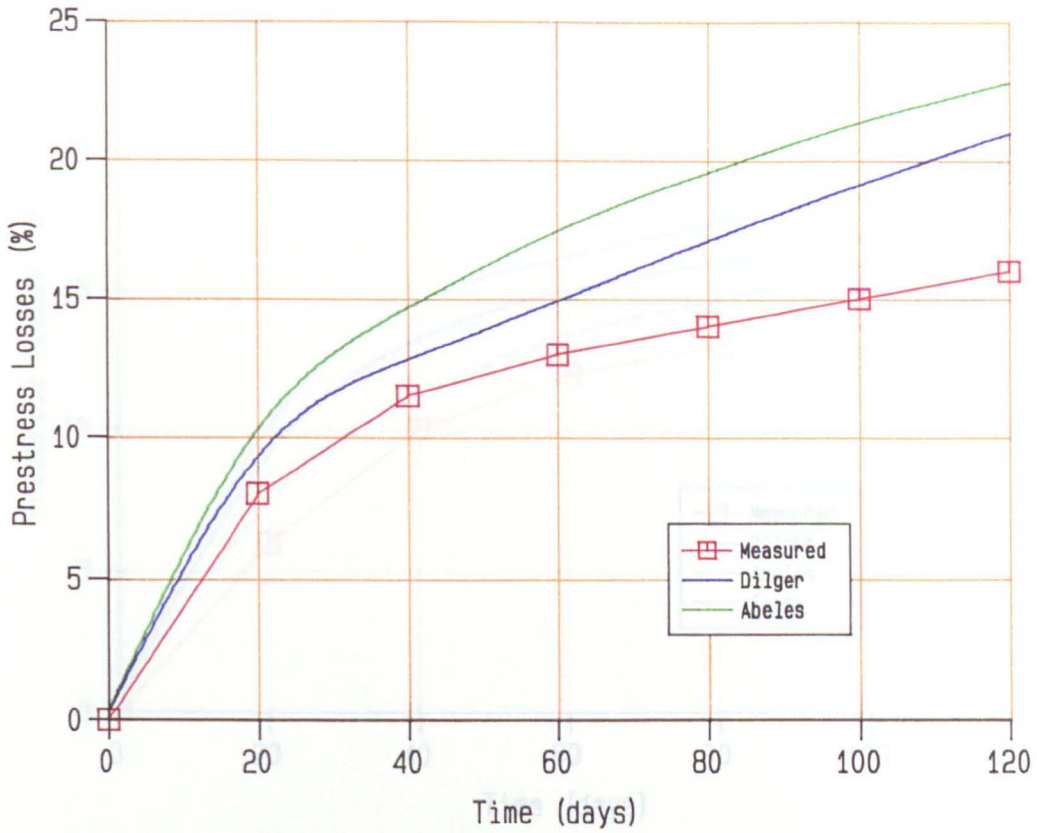


Fig. 6.9 Measured and Predicted Prestress Loss-time Curve of Calcium Silicate Diaphragm Wall

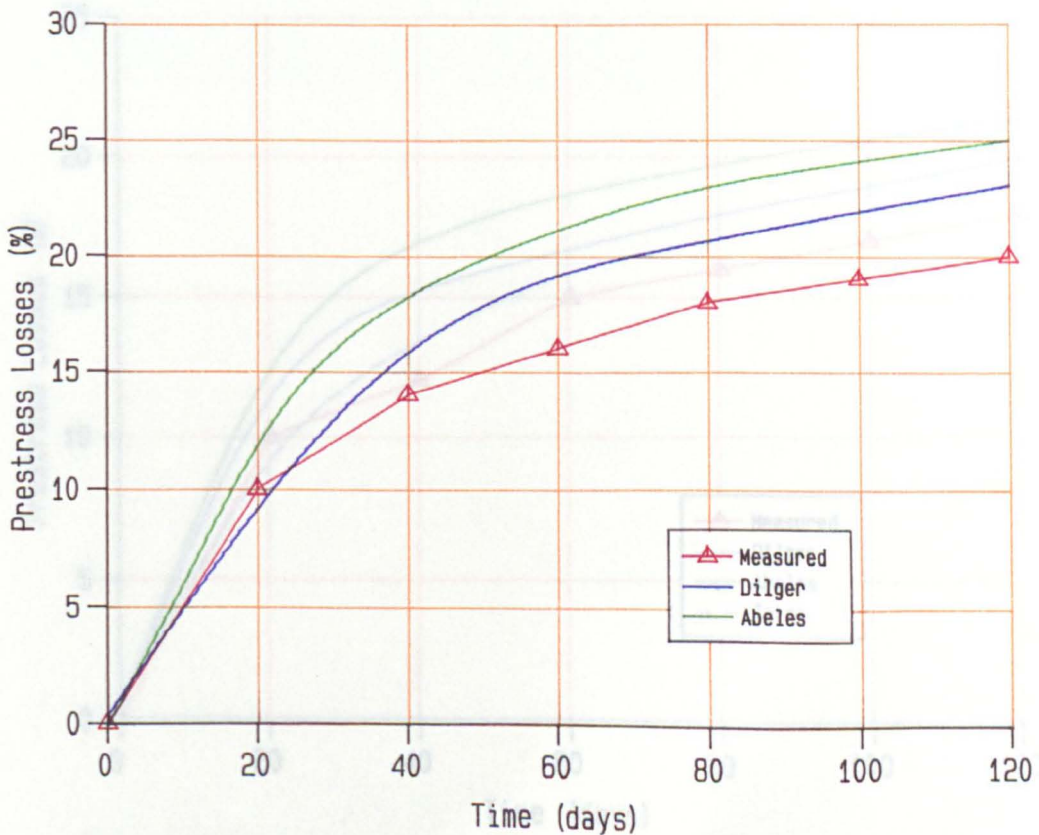


Fig. 6.10 Measured and Predicted Prestress Loss-time Curve of Calcium Silicate Fin Wall

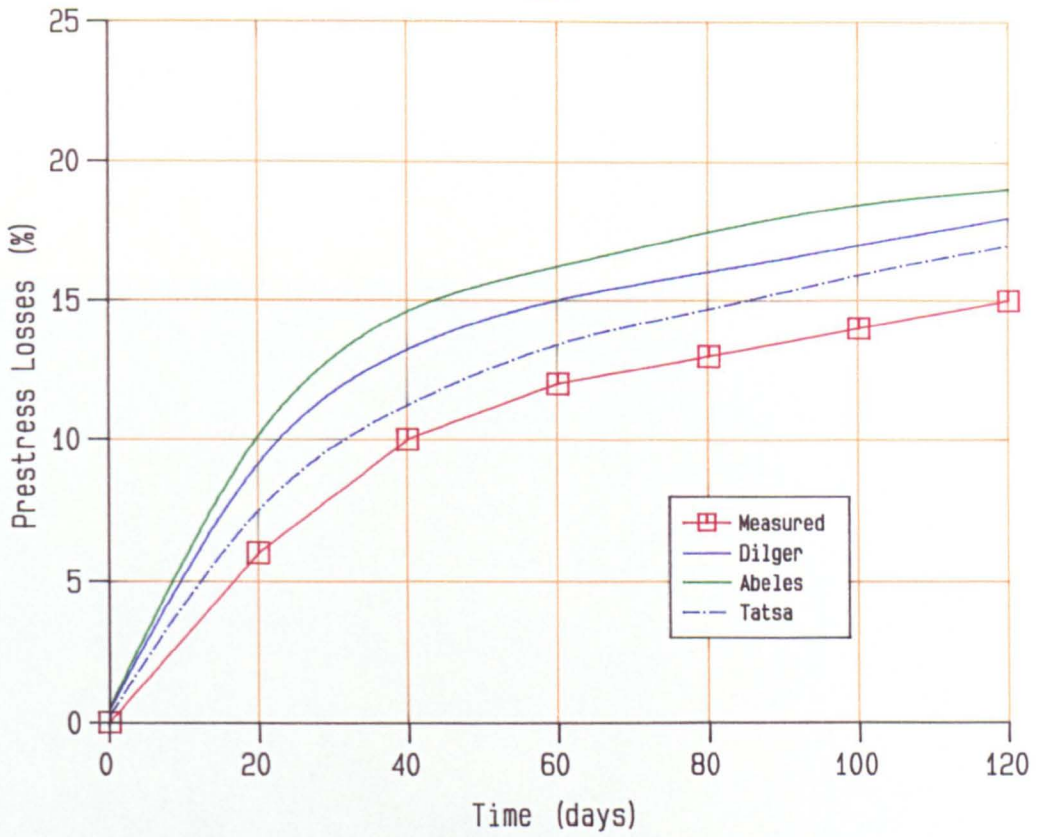


Fig. 6.11 Measured and Predicted Prestress Loss-time Concrete Block Diaphragm Wall

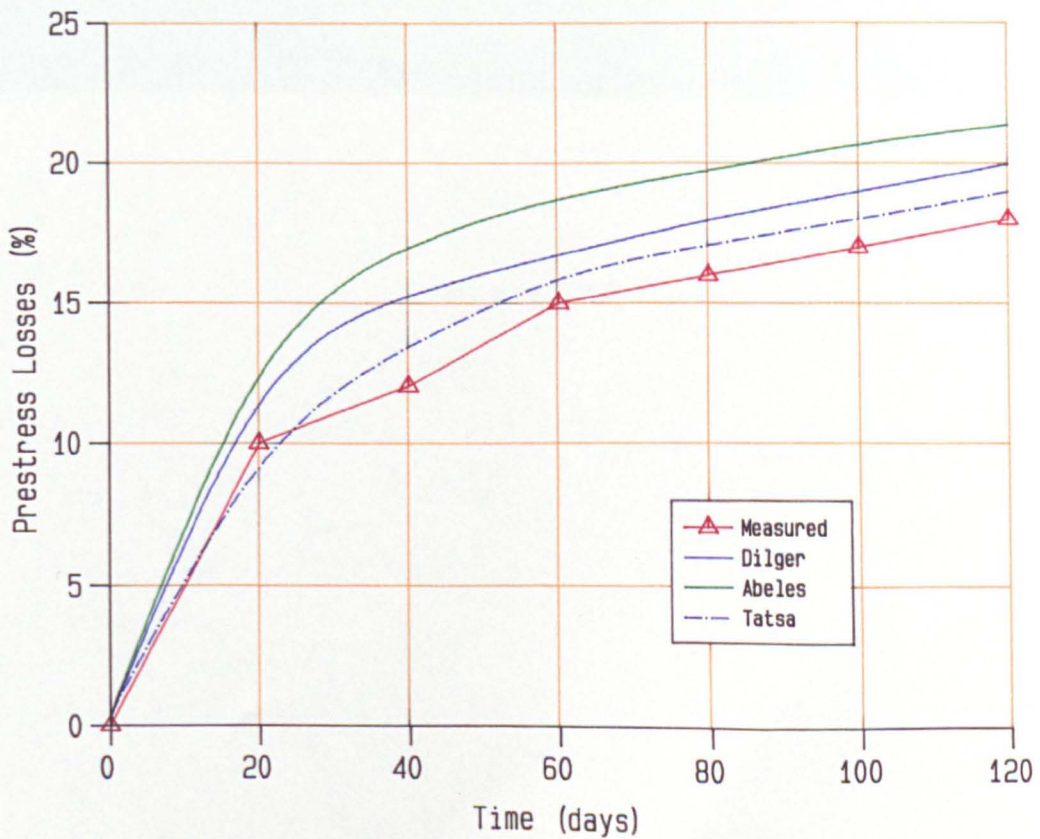


Fig. 6.12 Measured and Predicted Prestress Losses-time Curve of Concrete Block Fin Wall

**Plate 6.1 Migration of Water from Mortar to Calcium
Silicate Units During Laying**



PLATE 6.1

CHAPTER 7

IMPLICATIONS OF UNIT WATER ABSORPTION ON PREDICTION OF MASONRY DEFORMATION AND PRESTRESS LOSS

7.1 Introduction

Previous research (Brooks 1990a, Bingel 1984 and Abdullah 1989) had shown that for docked units the long-term deformation, creep and shrinkage, could be predicted reasonably accurately by composite modelling. However, in this investigation, predictions were rather poor for the calcium silicate and concrete block masonry. This chapter describes the findings from additional tests carried out to investigate this poor prediction. The tests were mainly to study the effect of high water absorption masonry units, laid dry, on moisture movement and resulting strain in the unit and mortar joint, both during and after curing.

Since no external drying is taking place during curing, the overall moisture content is the same during this period. However, the moisture content in the masonry unit is probably higher than before construction. Even though the overall moisture content is the same when the masonry is first exposed for drying, the shrinkage and creep potential of the brickwork may be reduced because moisture movement, from the fresh mortar joint to the masonry unit, may tend to lower the water/cement ratio of the mortar. Reduction in the water/cement ratio of mortar joint would tend to reduce the creep and shrinkage of the brickwork on exposure to the environment.

The water absorbed by the unit would not appreciably affect the shrinkage of the unit because it is in the form of 'free water' which only affects reversible

shrinkage, and this is usually small compared with irreversible shrinkage due to loss of adsorped water.

7.2 Experimental details

7.2.1 Control tests

Three control tests were carried out on each type of masonry unit: an initial rate of suction test, a standard water absorption test (BS 3921 1985) and a modified unit water absorption test. A detailed description of the modified water absorption test is presented in Section 7.2.1 (c).

7.2.1 (a) Initial rate of suction

The suction test carried out on each type of masonry unit was in accordance with BS 3921 (1985). The test was carried out by weighing the units, 10 units for each type of masonry, before and after immersing in 3 mm depth of water for 60 seconds.

7.2.1 (b) Standard water absorption

The standard water absorption test was carried out in accordance with BS 3921 (1985). Although there is no provision for a water absorption test for concrete block units, a test similar to that of clay and calcium silicate units was carried out on the concrete block. A 24-hour cold immersion test was carried out instead of the 5-hour boiling test. According to BS 3921 (1985), the 24-hour cold immersion test results are always lower than the 5-hour boiling test. As in the initial rate of suction test, 10 units were used for each type of masonry.

Initially the units were oven dried until a constant weight was achieved. The oven dried masonry units were then immersed in water for 24 hours before they were weighed again. The water absorption was obtained from:

$$\text{Water Absorption} = \frac{100 (\text{wet mass} - \text{dry mass})}{\text{dry mass}}$$

7.2.1 (c) Modified water absorption

A short-term modified water absorption test was carried out by monitoring the weight of one unit of a 2-course bonded masonry sample before and 0.5,1,3,5,10 and 24 hours after laying. Six sets of 2-course masonry samples were laid for each type of masonry. All the specimens were kept in separate polythene sheets immediately after laying to prevent moisture loss to the environment and to prevent moisture movement between the specimens.

To prevent bonding between the mortar and the masonry unit to be weighed, a layer of polythene mesh was used. Plate 7.1 shows the arrangement of the 2-course masonry. At the same time, the overall weight of the 2-course masonry sample was monitored before and at each time of weighing. This was to confirm that there was no loss of moisture to the surrounding environment during the test period.

For the concrete block unit, a single unit was capped with mortar and covered with glass instead of another block because of the limited capacity of the weighing balance being used. As for the clay and calcium silicate units, a layer of polythene mesh was used to prevent bonding between mortar and concrete block. Plate 7.2 shows the concrete block during the water absorption test.

7.2.2 Long-term test

Two sets of tests were carried out on each type of masonry: shrinkage and modified water absorption. The water absorption and shrinkage tests were carried out up to 70 and 140 days, respectively. Table 7.1 shows the compressive strength of mortar used for each type of masonry. Another test was carried out to compare the shrinkage and creep of mortar prisms with the original, and with a reduced water/cement ratio, the prisms being partly sealed to correspond with the calcium silicate tests discussed in Chapter 4.

7.2.2 (a) Modified water absorption

The procedure for the long-term modified water absorption test was similar to the short-term (24 hours) modified water absorption test but the period of tests was extended up to 70 days. The weight of the units was monitored at 1,3,7,14,21,30,40,50,60 and 70 days. A total of 10 sets of 1-course (concrete block) and 2-course (clay and calcium silicate) masonry were laid for each type of masonry. All the masonry samples were stored in a controlled environment with a temperature of $21 \pm 1^\circ\text{C}$ and a relative humidity of $65 \pm 5\%$, the samples being covered with polythene sheet for the first 21 days.

7.2.2.(b) Shrinkage

For the shrinkage tests of the clay and calcium silicate masonry, four 3-course masonry sets were laid. Two sets of the masonry were laid from dry units and the other two sets from docked units.

Individual shrinkage measurements of the masonry units and the mortar prisms as in Chapter 4 were carried out. The masonry units and the mortar

prisms were sealed according to the V/S of the masonry (Table 7.2). Two mortar prisms were sampled from each type of masonry. No measurements were made on unbonded concrete blocks between header faces because the shrinkage measurements in Chapter 4 were between bed faces. Plate 7.3 shows the arrangement for the shrinkage test using clay and calcium silicate masonry. Shrinkage measurements were taken at the same times interval as in water absorption tests. For shrinkage of the concrete block, 2-course masonry was laid as shown in Plate 7.4.

7.2.2 (c) Reduced water/cement ratio of mortar prisms

Creep and shrinkage tests, similar to those of the diaphragm and fin calcium silicate walls in Chapter 4, were carried out on 8 partly sealed mortar prisms. Another set of creep and shrinkage tests were also carried out on mortar prisms with a reduced water/cement (w/c) ratio. The reason for carrying out this test was to study the effect of migration of moisture from mortar to masonry units during construction on creep and shrinkage.

From the known mortar mix, water/cement ratio and weight of mortar joint from the water absorption test, the effective water/cement ratio (w/c) of mortar joint after 24 hours was determined from the following equation;

$$w/c = \frac{(W_O - WA)}{C_{ce}} \quad (7.1)$$

where W_O = mass of water in mortar = $\frac{W/C_O \times \text{mass of mortar joint}}{6 + W/C_O}$;

WA = water absorbed by the units from modified water absorption test;

C_{ce} = mass of cement;

and W/C_O = original water/cement ratio.

For the 2-course masonry with $1:\frac{1}{2}:4\frac{1}{2}$ mortar mix, the mass of the mortar joint was 591 gm, the mass of cement was 81.3 gm, and the water absorption

(WA) was 26 gm. Hence with an original water/cement ratio of 1.27, the reduced water/cement ratio of 0.95 was determined from Eq. (7.1).

The amount of water absorbed by the units was obtained at the end of the short-term modified water absorption test, i.e 24 hours after laying. At this time the cement had set and all the water was not in its 'free form'.

7.3 Measurements

7.3.1 Modified unit water absorption

For both the short and long-term water absorption test of the clay and calcium silicate masonry, a weighing balance with maximum capacity of 10 kg was used, while a balance with maximum capacity of 25 kg was used for water absorption test of concrete block. Both balances had an accuracy of ± 1 grammes.

7.3.2 Shrinkage

The overall shrinkage of the clay and the calcium silicate masonry was measured using a 200 mm Demec gauge. The shrinkage of the unbonded unit (between header faces) and the mortar prisms were measured using a 150 mm Demec gauge. The vertical shrinkage of the individual bonded units was measured using a surface-mounted 50 mm acoustic vibrating wire gauge (VWG). The gauges were fixed to the units surfaces by an epoxy adhesive to special end mounting blocks.

The vibrating wire gauge measures a change of strain of ± 1 microstrain, the change of strain ($\delta\epsilon$) being:

$$(\delta\epsilon) = 4 \times 10^{-10} \left(\frac{1}{T_1^2} - \frac{1}{T_2^2} \right)$$

where T_1 and T_2 are periods of frequency

Measurements were made before laying and then at 1,3,7,14,21,30,40,50,60 and 70 days after laying.

For the concrete blocks, a 400 mm Demec gauge was used to measure the overall strain. The individual block units were monitored using a 200 mm Demec gauge. Figure 7.1 shows the positions of the Demec studs and the vibrating wire gauge on the clay, calcium silicate and concrete block masonry.

7.3.3 Reduced water/cement ratio of mortar prisms

Creep and shrinkage tests of the partly sealed mortar prisms were carried out using the apparatus abscribed in Chapter 4, the strains being measured using 150 mm Demec gauge.

7.4 Test results

7.4.1 Short-term water absorption

7.4.1.(a) Initial suction rate

The initial suction rate test is a measure of surface porosity of masonry units which absorb water from the mortar by capillary action and thus possibly affects the bond between the units and mortar (Garrity 1993). Table 7.3 shows the results of the initial suction test of the masonry units. Concrete had the highest suction rate compared with the clay and calcium silicate units. This could be due to the presence of large pores in the concrete block but the pore-size distribution may also be a factor.

7.4.1.(b) Standard water absorption

The water absorption test is a measure of the overall porosity of masonry units and is normally expressed in terms of the percentage increase in mass. Table 7.3 shows the results of the standard water absorption test for all the masonry

units. As expected (because of the higher initial suction rate), the calcium silicate units (11.32%) exhibit a higher water absorption compared with the clay units (3.72%). However, that trend of behaviour was not applicable to concrete block units because they had a water absorption of 8.83%, while showing the greatest suction rate. This could be due to the higher air void/unit weight ratio in calcium silicate units when compared to concrete block units, since units with a higher air void/unit weight ratio tend to have higher water absorption

7.4.1 (c) Modified water absorption test

Figure 7.2 shows the water absorbed by the masonry units over a period of 24 hours. All the units show similar trends of water absorption: rapid initially and then at a reducing rate after 3 hours. Clay units absorbed the least amount of water compared with both calcium silicate and concrete block units. Even in terms of the percentage increase in mass, the clay had the least water absorption (0.35%) compared with the concrete block (0.65%) and calcium silicate (1%) units. The difference in percentage increase in mass in this test when compared to the standard method (Fig. 7.3) is partly due to the units being oven dried in the standard method. A higher percentage of water being absorbed by the units in the standard water absorption test was also partly due to a higher exposed surface area of absorption (immersed completely) of the units in the standard water absorption test. In the modified water absorption test, only one surface (bed face) was available for absorption of moisture.

7.4.2 Long-term water absorption tests

7.4.2 (a) Modified water absorption

Figures 7.4 to 7.6 show the long-term water absorption of all the masonry units. An overall weight of 99% of the original weight were measured on all

the water absorption specimens during curing, which indicates a negligible water loss to the atmosphere during this period. Thus any moisture movement occurred between the mortar and the masonry units only.

Figure 7.4 shows that clay units absorbed about 0.3% of water after 1 day of laying and then lost water for the next 7 days. Between 7 and 21 days, some moisture from the mortar was absorbed back by the units. On exposure to the surrounding air at 21 days, there was a delay before the unit started to lose moisture. After 30 days all the initial water absorbed was dissipated.

The calcium silicate units absorbed about 0.6% of water from mortar after 1 day of laying (Figure 7.5) and then lost water for the next 13 days. Over the next seven days, the units absorbed back some of the moisture from the mortar joint. On exposure to the surrounding air at 21 days, moisture was lost immediately for the first 9 days. After 9 days of exposure, the units appear to absorb moisture again for the next 10 days before losing moisture for the remaining test period.

The concrete block units exhibited a similar pattern of moisture movement to the calcium silicate units (Fig. 7.6). The block unit absorbed about 0.55% of water one day after laying and then lost water for the next 20 days. On exposure to the surrounding air at 21 days, the block continued losing moisture till the end of the test.

7.4.2 (b) Shrinkage

Mortar prism

Figure 7.7 shows the shrinkage of the part-sealed mortar prisms for each batch of mortar used in the modified water absorption test. When compared with the shrinkage of the mortar prisms in Chapter 4, the trends of shrinkage of the prisms for the clay and concrete block masonry are similar. However the shrinkage of the mortar prism for the calcium silicate brickwork in Chapter 4 is considerably higher

than in Fig. 7.7. This could be due the lower compressive strength of mortar used for calcium silicate walls in Chapter 4 which suggests a potential for higher shrinkage.

Masonry units

Figure 7.8 compares the shrinkage of bonded and unbonded clay units measured between header and bed faces. During curing, the bonded docked unit undergoes shrinkage which suggests the mortar is taking water for hydration. On the other hand, the bonded dry unit undergoes expansion due to water absorption from the mortar. When exposed to the surrounding air, the docked and dry units exhibit similar shrinkage, i.e when measured from the age of 21 days.

Figure 7.8 also suggests a significant difference between bed and header face shrinkage (after curing) of the dry unbonded clay unit, which has implications for the composite model where deformations were measured between header faces. However, the header face shrinkage is only slightly less than the 'actual' shrinkage of the bonded dry bed face unit.

Figure 7.9 compares the shrinkage of calcium silicate units measured between header and bed faces. During curing, there is little moisture movement strain except in the case of the bonded dry unit which undergoes expansion due to water absorption. On exposure to the surrounding air, the bonded dry unit exhibits less shrinkage than the bonded docked unit, there being little difference between the bed and header face shrinkage of the unbonded units. However, the 'actual' shrinkage of the bonded dry unit is greater than the unbonded unit shrinkage which is used in the composite model.

The shrinkage results for the concrete block units (Fig. 7.10) are similar in behaviour to the calcium silicate units, i.e the bonded dry unit exhibits less shrinkage than the bonded docked unit on exposure to drying at 21 days. Compared with unbonded shrinkage, the 'actual' dry bonded shrinkage is slightly greater.

Masonry

Figures 7.11 to 7.13 compare shrinkage-time curves of the clay, calcium silicate and concrete block masonry built from docked and dry units. All the masonry made with docked units exhibited a higher shrinkage compared with masonry made from dry units. For the masonry constructed from dry units, the mortar joint never recovers all the moisture that has been absorbed by the dry units during curing. As a result, the shrinkage potential of masonry made from dry units is reduced even though the overall moisture content in the masonry is the constant during the curing period. On exposure to the surrounding air, the higher moisture content of the docked bonded unit would be expected to have a greater shrinkage than the dry bonded unit as confirmed in Figs. 7.12 and 7.13. In the case of clay units (Fig. 7.11), there is no significant difference between the docked and dry units, previous researchers have indicated that dry units can sometimes undergo shrinkage more than docked units. The absorbed water may be in the form of 'free' water which does not contribute significantly to shrinkage.

Mortar joint

The shrinkage of the mortar joint in the masonry was determined by deducting the shrinkage of masonry units from the total masonry shrinkage using the following equation:

$$\epsilon_{\text{smortar}} = \frac{(DL_{\text{mas}} \times \epsilon_{\text{smas}} - (DL_{\text{mas}} - n \times m) \times \epsilon_{\text{sunits}})}{n \times m} \quad (7.2)$$

where DL_{mas} = length of the Demec gauge used to measure the overall strain on the masonry (mm);

m = depth of mortar joint (mm) (varied from 10 mm to 20 mm);

n = number of mortar joints;

ϵ_{sunits} = average strain of the units (see Fig. 7.1 (a) and (b));

ϵ_{smas} = average measured strain on the masonry (see Fig. 7.1 (a) and (b));

and $\epsilon_{\text{smortar}}$ = strain of the mortar.

For clay and calcium silicate masonry, Eq. (7.2) becomes:

$$\epsilon_{\text{smortar}} = \frac{(200 \times \epsilon_{\text{smas}} - (200 - 2 \times m) \times \epsilon_{\text{sunits}})}{2 \times m} \quad (7.3)$$

For the concrete block masonry, the corresponding equation is as follows:

$$\epsilon_{\text{smortar}} = \frac{(400 \times \epsilon_{\text{smas}} - (400 - 1 \times m) \times \epsilon_{\text{sunits}})}{1 \times m} \quad (7.4)$$

Figure 7.14 compares the shrinkage of the mortar joint, in masonry made from docked and dry units, to the shrinkage of the partly sealed mortar prism for clay masonry. The shrinkage of the mortar joint in masonry 'laid dry' exhibits less shrinkage compared with the mortar prisms (26%). The reduction in the shrinkage of the mortar joint in masonry 'laid dry' can be attributed to the reduced water/cement (w/c) ratio caused by the unit absorption.

Figure 7.15 compares the shrinkage of the mortar joint to the shrinkage of the partly sealed mortar prisms for the calcium silicate masonry. There is little difference between the shrinkage of the mortar joint in 'docked' masonry and the partly sealed mortar prisms (10%). Due to the lower effective water/cement ratio, the shrinkage of the mortar joint in the masonry 'laid dry' exhibits less shrinkage when compared with the partly sealed mortar prisms (80%). It is also noticeable that during curing, the mortar joint exhibits shrinkage, as a result of transfer of moisture to units. Due to the vertical and horizontal restraint by the bond, shrinkage of the mortar joint in the masonry 'laid dry' during curing could lead to bond cracking and as a result could affect the elastic load deformation of masonry.

Figure 7.16 compares the shrinkage of the mortar joint with the shrinkage of the partly sealed mortar prisms for 2-course concrete block masonry. As for the calcium silicate masonry, there is not much difference^{ce} between the docked unit masonry shrinkage in the mortar joint and the partly sealed mortar prisms (9%). However, the shrinkage of the mortar joint in the masonry 'laid dry' exhibits less shrinkage when compared to the partly sealed mortar prisms (70%).

It will be recalled that the reason for partly sealing mortar prisms was to simulate the mortar in the masonry i.e to have the same volume/exposed surface (V/S) ratio. Therefore, the shrinkage of the partly sealed prisms should be the same as the shrinkage of the 'docked' mortar joint. Figures 7.14 to 7.16 show a small difference. Therefore it can be concluded that from the limited tests carried out, the V/S ratio simulation gives a reasonable approximation of the mortar joint shrinkage when the units are docked.

Figures 7.17 and 7.18 show the shrinkage ratio of the bonded/unbonded units, and the bed mortar joint/mortar prisms over a period of 120 days. The ratios can be used to re-predict the shrinkage by the composite model. The mortar shrinkage ratio is more significant than for the units since most of the shrinkage takes place in mortar bed joint. For mortar used with the dry units, the ratio is actually a shrinkage reduction factor for the mortar prisms.

***Relation between creep and shrinkage of mortar prisms,
and water absorbed by units***

Figure 7.19 shows the relationship between the shrinkage reduction factor of mortar prisms (see Fig. 7.18) and the percentage standard water absorption for each type of masonry. From a practical point of view, it is desirable to relate the shrinkage reduction factor to the standard water absorption which is normally supplied by the manufacturers, rather than the modified water absorption. The

shrinkage factors were obtained from the average ratio of shrinkage of bonded mortar bed joint (laid dry)/mortar prism as given in Table 7.4. The shrinkage reduction factor is defined as :

$$\frac{\text{shrinkage of the bonded mortar joint}}{\text{shrinkage of the mortar (unbonded) prism}}$$

Figure 7.19 also shows that the shrinkage reduction factor of mortar prisms decreases as the unit standard water absorption increases: theoretically shrinkage reduction factor of unity represents zero unit water absorption. Table 7.4 also compares the average ratio of shrinkage of bonded mortar bed joint (docked)/mortar prism with the average ratio of shrinkage of the bonded mortar bed joint (laid dry)/mortar prism in all the masonry. As expected, the average ratio of shrinkage of bonded mortar bed joint (docked)/mortar prism is higher than that laid dry. In the masonry made from docked units there was no moisture movement between the mortar bed joint and the units and, consequently, the mortar bed joint made with docked units has higher moisture content than that of the mortar bed joint made with dry units. Higher moisture content generally results in higher shrinkage due to more moisture escaping from the external surface.

The corresponding shrinkage enlargement factor for masonry units is in Fig. 7.20. The enlargement factor is defined as:

$$\frac{\text{shrinkage of the bonded dry unit}}{\text{shrinkage of the unbonded dry unit between headers}}$$

for the clay and calcium silicate units, and

$$\frac{\text{shrinkage of the bonded dry unit}}{\text{shrinkage of the unbonded dry unit between bed faces}}$$

for the concrete block unit.

The influence of the unit standard water absorption being the opposite of that of mortar prisms because shrinkage enlargement factor reduces with a decrease in percentage water absorption. The shrinkage enlargement factor of the bonded units (laid dry)/unbonded in Table 7.4 is greater than unity in all the masonry due to the higher moisture content in the bonded units at the time of exposure to the environment. For the same reasons, the shrinkage enlargement factor for the docked units is greater than for the dry units.

Re-prediction of creep and shrinkage by composite model

Using the information presented in this Chapter, the deformations of the masonry walls tested in Chapter 4 were re-predicted by adjusting the original creep and shrinkage data (unbonded) to allow for the unit water absorption. The adjustment to the shrinkage and creep was as follows:

(a) Shrinkage

The shrinkage of the partly sealed mortar prisms was reduced by a shrinkage reduction factor according to the unit water absorption (Fig. 7.19).

The shrinkage of the calcium silicate and concrete block units were increased by the factors shown in Fig. 7.20; no adjustment was made to the clay unit, because the factor was close to unity.

(b) Creep

From the specific creep-shrinkage curves of Figs. 7.21 to 7.25, the adjusted creep was obtained from the adjusted shrinkage. For example, Fig. 7.21 shows the adjustment procedure for the final creep (C_{fr}) of the mortar prisms (clay

diaphragm wall) obtained from the final adjusted shrinkage (S_{fr}), where $S_{fr} = 0.74 \times$ original shrinkage (S_f), giving final creep of 472×10^{-6} .

Detailed calculations of the re-prediction of creep of the walls is shown in Appendix E. Figures 7.26 to 7.31 compare the prediction of creep with and without the adjustment factors, with the measured values. As expected the re-prediction values gives better estimates, i.e a difference of 5%.

Detailed calculations of the re-prediction of shrinkage of the walls are also shown in Appendix E. As for creep, the re-predicted shrinkage for all the masonry types give better estimations compared with the original predictions (see Figs.7.32 to 7.37).

Re-prediction of prestress loss

Using the adjusted creep and shrinkage values, the re-estimations of prestress loss of the post-tensioned masonry walls tested in Chapter 4 are shown in Figs. 7.38 to 7.43. As for creep and shrinkage, the re-prediction of prestress loss gives a better estimate for all the masonry types. Detailed calculations of the re-prediction of prestress loss are given in Appendix E. The accuracy of prestress loss is improved by an average of 50%, 79% and 60% for the post-tensioned clay, calcium silicate and concrete block walls, respectively.

7.4.2 (c) Reduced water/cement ratio of mortar prisms

Using Eq. (7.1), the actual water/cement ratio used in the calcium silicate walls was found to be reduced by 25% due to absorption of single unit. Therefore, for the 2-course masonry, the actual water/cement ratio would be reduced by 50%. However, a mortar mix with a high reduction of the water/cement ratio was judged to be unreasonable, and so the mortar prisms were made with the 25 %

reduced water/cement ratio. As stated earlier, the reason for this test was to demonstrate the effect of a reduced water/cement ratio on creep and shrinkage of mortar. The reduced and original water/cement ratio of mortar cubes had a mean compressive strength of 17.09 (standard deviation = 4.8) and 12.55 (standard deviation = 0.64) MPa, respectively. Appendix F shows the creep and shrinkage of these mortar prisms.

Creep

Figure 7.44 shows the creep of the partly sealed mortar prisms for the original and reduced water/cement ratio tests. As expected, for both diaphragm and fin walls, the creep of mortar prisms with a reduced water/cement ratio is about 40% lower than creep of mortar with original water/cement ratio. However, the trend of the creep in both mortar prisms were similar i.e rapid initially and slower after 60 days.

Figures 7.46 and 7.47 show the effect of water/cement ratio on the creep of mortar prisms for calcium silicate walls at intervals of 20 days. The creep of mortar increases with an increase in the water/cement ratio because the strength is lower; according to Neville and Brooks (1993) creep is approximately inversely proportional to strength. While the creep in these tests is greater than that deduced from the modified water absorption/shrinkage tests on the masonry, the effect of a reduction in effective water/cement ratio on creep is clearly demonstrated. The attempted simulations of a reduction in the water/cement ratio does not appear to be correct probably because of compaction: the mortar prisms were fully compacted but the mortar joint would remain more porous after removal of moisture through absorption.

Shrinkage

Figure 7.45 shows the shrinkage of the partly sealed mortar prisms for the original and the reduced water/cement ratio test. The shrinkage of mortar prisms with the reduced water/cement ratio is about 20% lower than the shrinkage of mortar with original water/cement ratio. The low water/cement ratio results in lower shrinkage potential (see Figs. 7.48 to 7.49) because cement paste structure is 'stronger' so that moisture is held more firmly within the pores structure and also due to less of moisture escaping.

7.5 Summary on the effects of unit water absorption on prediction of deformation of masonry.

Test results presented in this chapter demonstrate the importance of unit absorption on the accuracy of predicting deformation of masonry by composite model. The results explain why the composite model over predicts deformation of masonry presented in Chapter 6. This means that the assumption, i.e shrinkage in mortar joint is the same as in mortar prisms, made in the prediction of composite model is only valid if the units are docked first. For the masonry laid dry, the shrinkage of the unbonded mortar prism to be used for predicting the shrinkage of the masonry has to be reduced, and that reduction of shrinkage can be as much as 80% for units with high water absorption characteristics. The same situation applies to creep. It is interesting to note that BS 5628:Part 3 (1985) recommends that brick units with initial suction rate greater than 1.5 kg/(mm².min) should be docked first before laying. If the brick units are not docked, the mortar consistency should be adjusted by increasing the water/cement ratio.

Reduction of the water/cement ratio in mortar results in a higher strength and thus lower the creep and shrinkage potential of masonry. Moreover, the reduction in w/c ratio could also increase the modulus elasticity of the masonry provided self-

compaction (due to its weight) of the masonry, during initial curing, occurs. On the other hand, too much reduction in the w/c ratio at an early stage could also cause the mortar to become too porous and thus lower its compressive strength and the modulus of elasticity of masonry. This could happen if, especially in a hot weather, the masonry is not cured properly. As a result, poor bond between the mortar joint and the masonry units could occur.

Table 7.1 Compressive Strength of Mortar used for Water Absorption and Shrinkage Test

Masonry Type	Compressive Strength (MPa)
Clay	9.63 (± 2.5)
Calcium Silicate	11.74 (± 1.8)
Concrete Block	12.1 (± 1.1)

() Standard deviation

Table 7.2 Volume/exposed Surface Ratios of the Masonry, Masonry Units and Mortar Prisms.

Masonry Type	Volume (10^5 mm^3)			Exposed surface area (10^4 mm^2)			V/S (mm)			Total Sealed length** x (mm)	
	Mas.*	Brick	Mortar	Mas.*	Brick	Mortar	Mas.*	Brick	Mortar	Brick	Mortar
Clay	44.5	40.1	4.41	15.9	14.6	1.27	28	27.5	35	-24	-2.5
Calcium Silicate	47.4	43	4.41	15.9	14.6	1.27	30	29	35	-25	-2.5
Concrete block	198	194	0.04	53	52	1.08	37	37	41	-12	-3

Mas.* = masonry
** see Fig. 4.19

Table 7.3 Initial Suction Rate and Standard Water Absorption

Masonry Type	Initial Suction Rate Test (kg/mm ² .min)	Standard Water Absorption Test (% increase in mass)
Clay Unit	.27 (± 0.15)	3.72 (± 0.83)
Calcium Silicate Unit	0.5 (± 0.11)	11.32 (± 0.68)
Concrete Block Unit	7.98 (± 0.72)	8.83 (± 0.21)

() Standard deviation

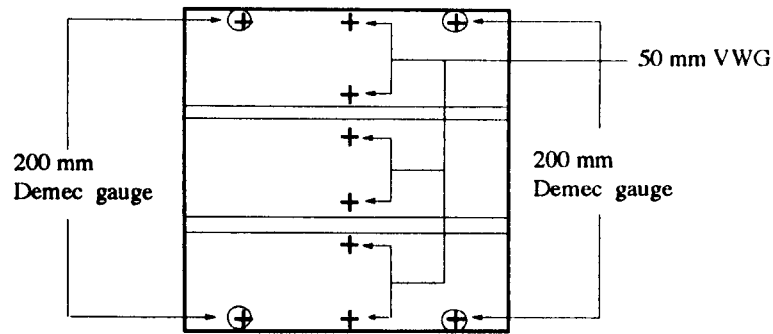
Table 7.4 Average Shrinkage Factors of Masonry Units and Mortar Prisms

Masonry Type	Mortar (bonded/unbonded*)		Unit (bonded/unbonded**)	
	Docked	Dry	Docked	Dry
Clay	0.8 (0.1)	0.7 (0.1)	1.9 (1.0)	1.1 (0.8)
Calcium Silicate	0.88 (0.1)	0.2 (0.1)	2.3 (0.5)	1.4 (0.1)
Concrete Block	1.1 (0.4)	0.3 (0.08)	5.24 (0.95)	1.3 (0.1)

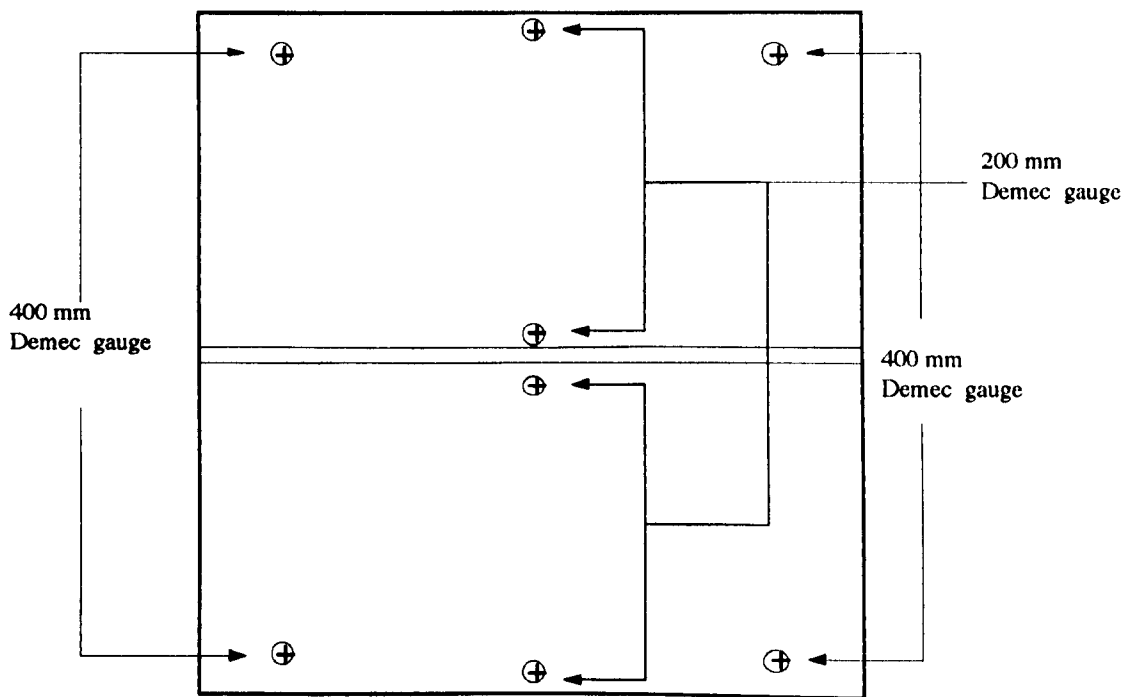
* Unbonded mortar prisms

** Dry unbonded unit

() Standard deviation



(a) Positions of Demec Studs and Vibrating Wire Gauges on Clay and Calcium Silicate Masonry



(b) Positions of Demec Studs on Concrete Block Masonry

Fig. 7.1 Positions of Demec Studs and Vibrating Wire Gauges on Clay, Calcium Silicate and Concrete Block Masonry

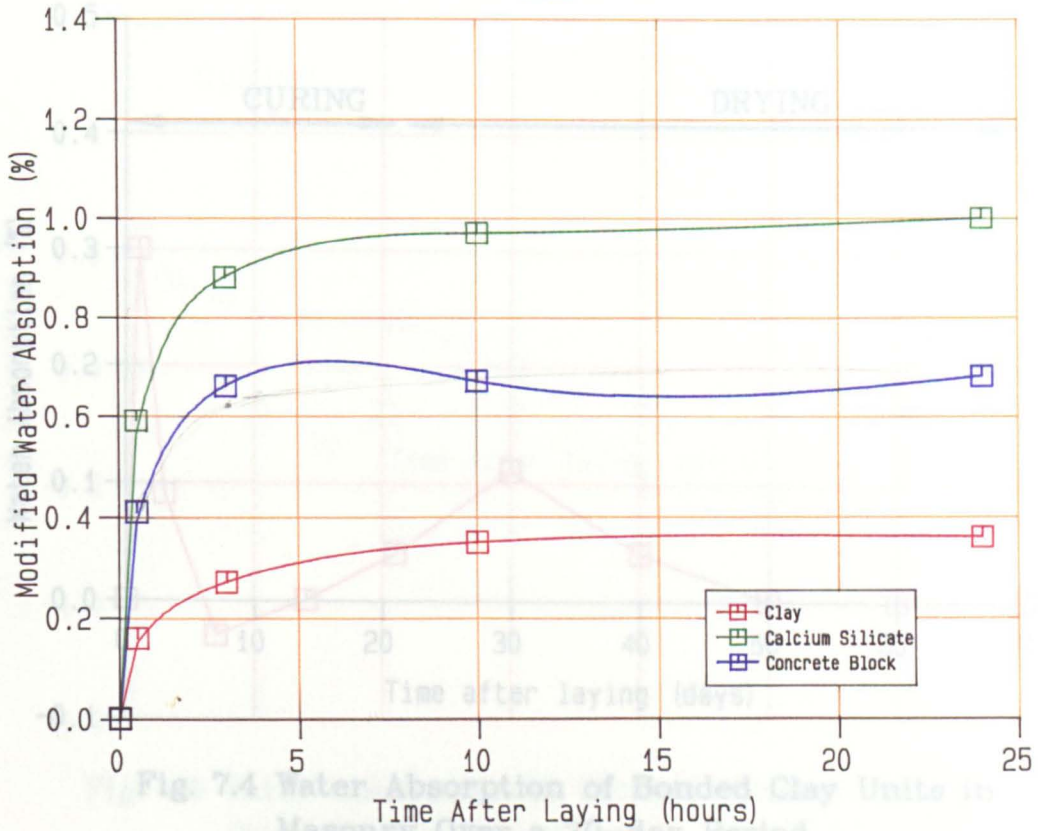


Fig. 7.2 Water Absorption of Bonded Units in Masonry Over a 24-hour Period

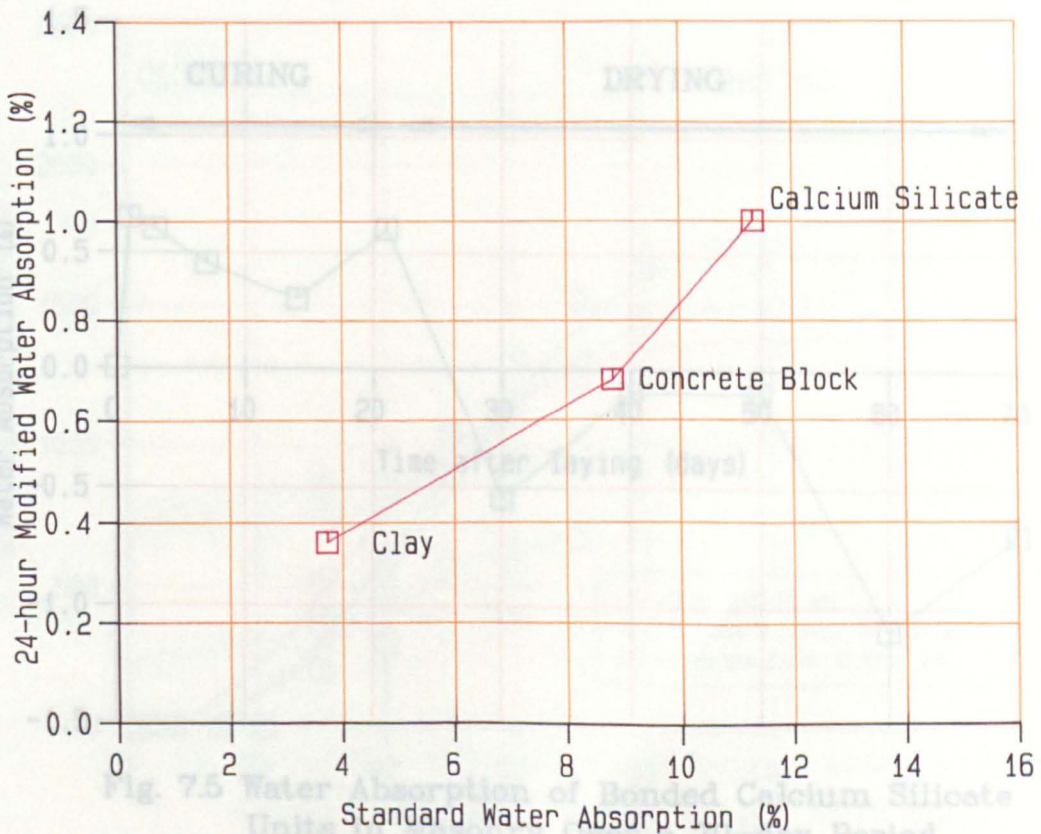


Fig. 7.3 Modified Water Absorption in Relation to the Standard Water Absorption

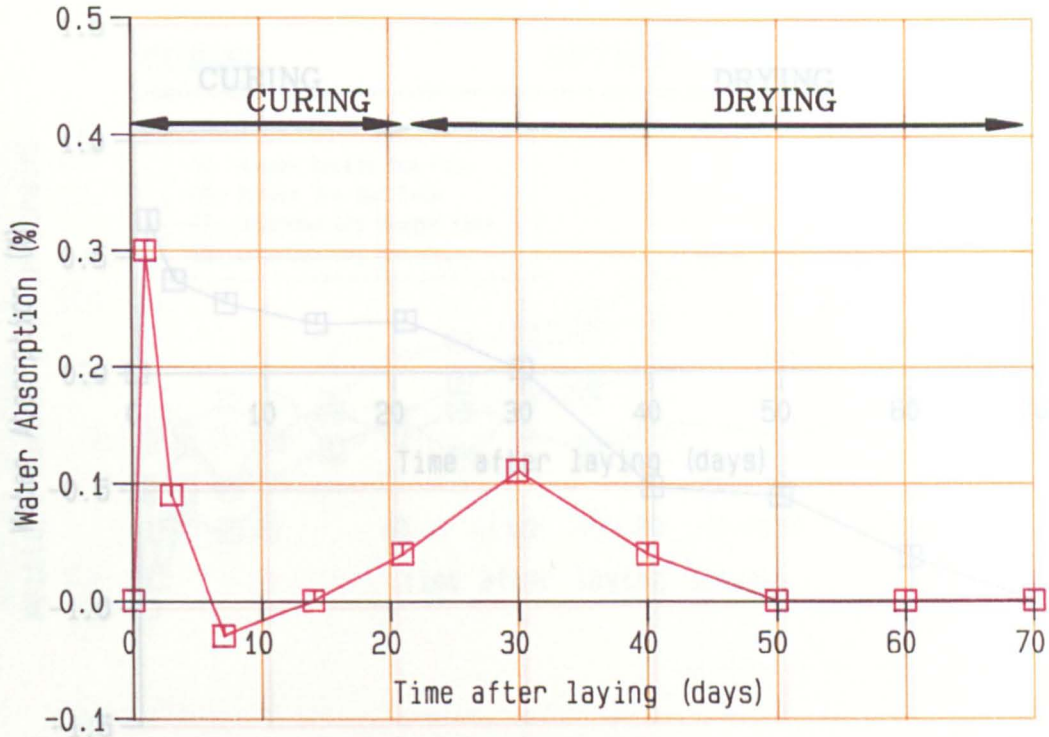


Fig. 7.4 Water Absorption of Bonded Clay Units in Masonry Over a 70-day Period

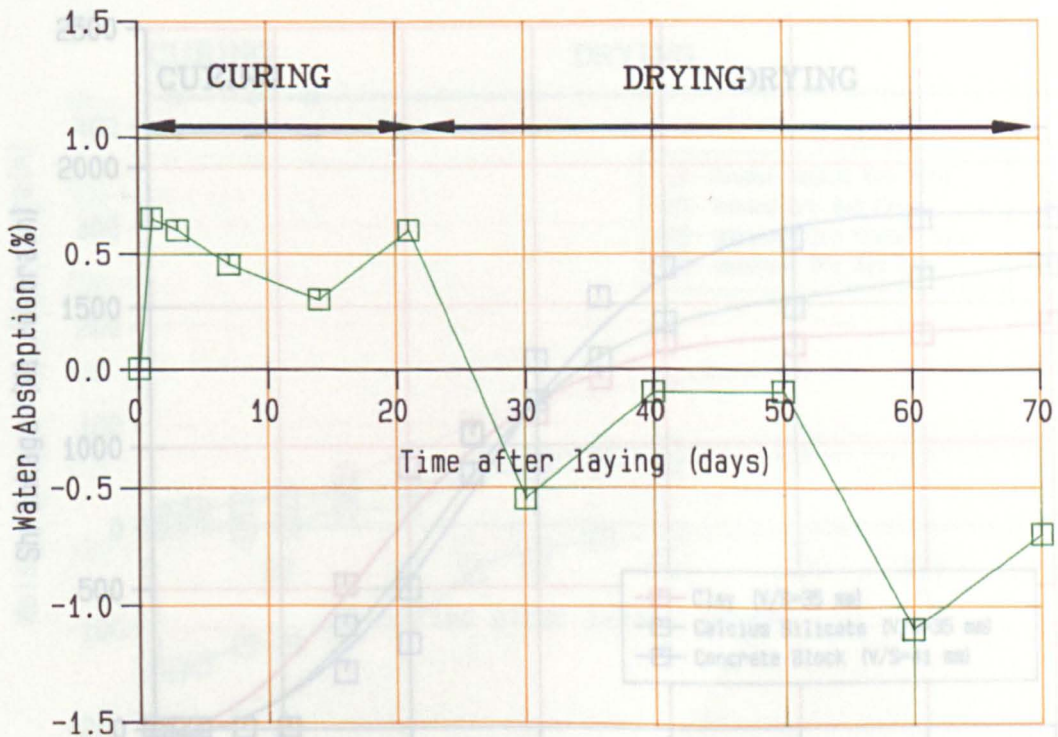


Fig. 7.5 Water Absorption of Bonded Calcium Silicate Units in Masonry Over a 70-day Period

Fig. 7.7 Shrinkage-time Curve of Mortar Prisms, Partly Sealed to Different V/S ratios

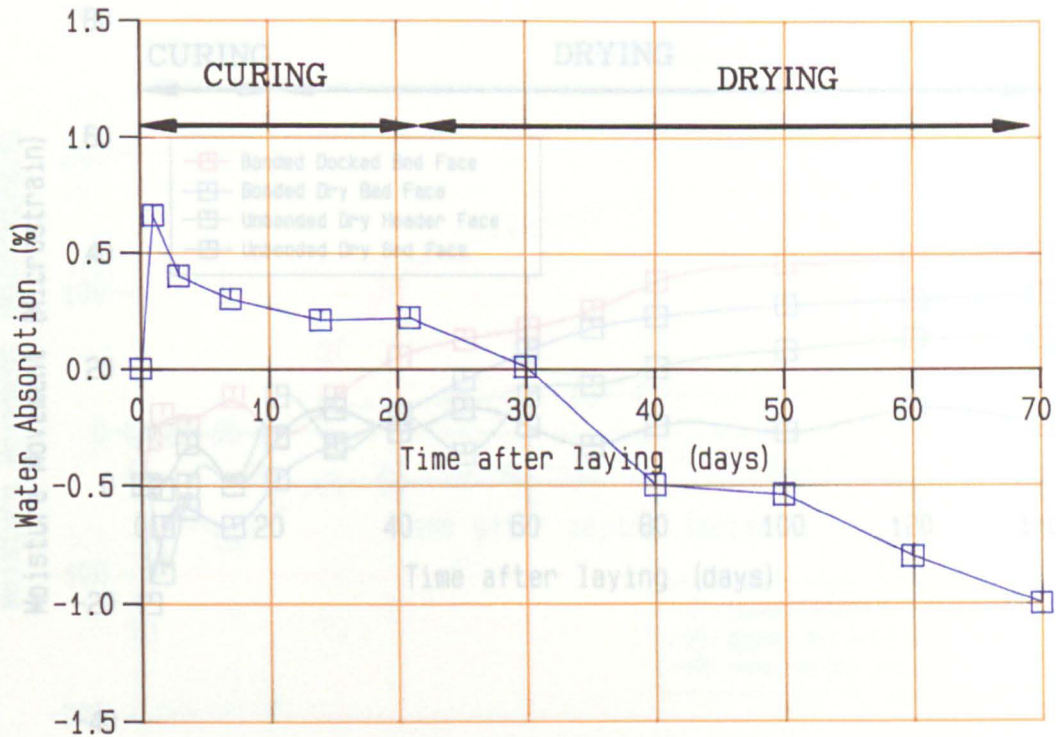


Fig. 7.6 Water Absorption of Bonded Concrete Block Unit Over 70-day Period

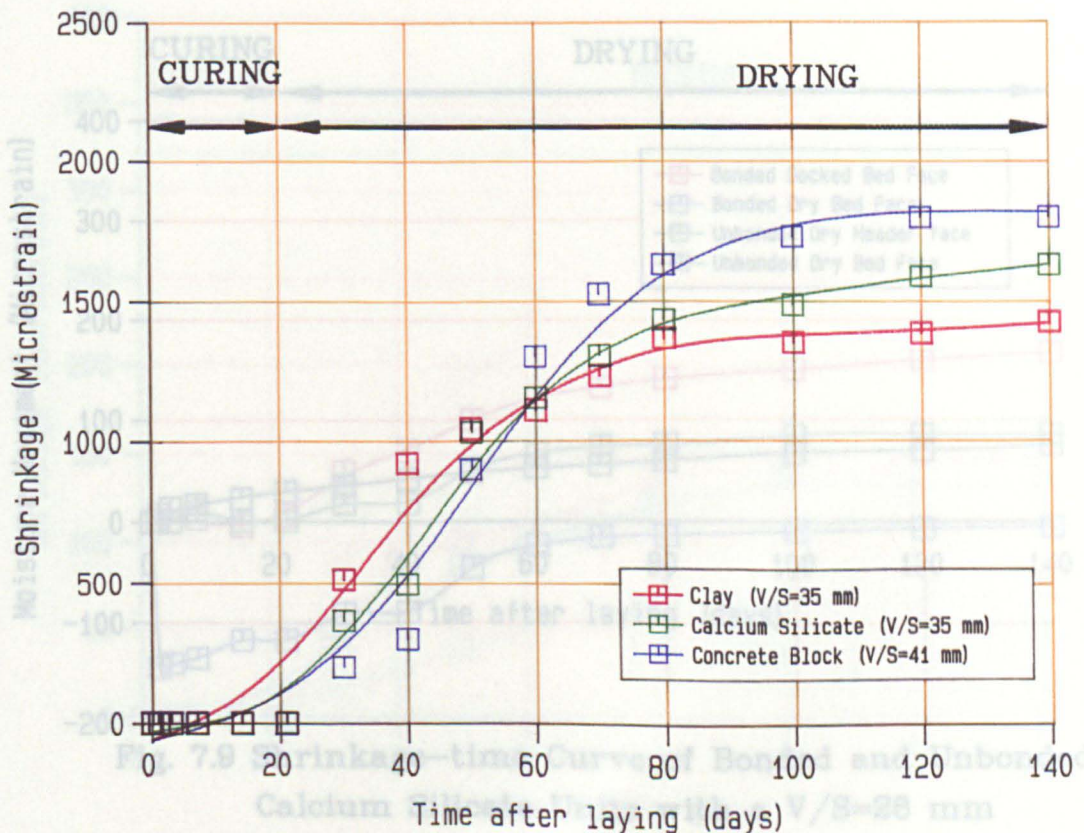


Fig. 7.7 Shrinkage-time Curve of Mortar Prisms, Partly Sealed to Different V/S ratios

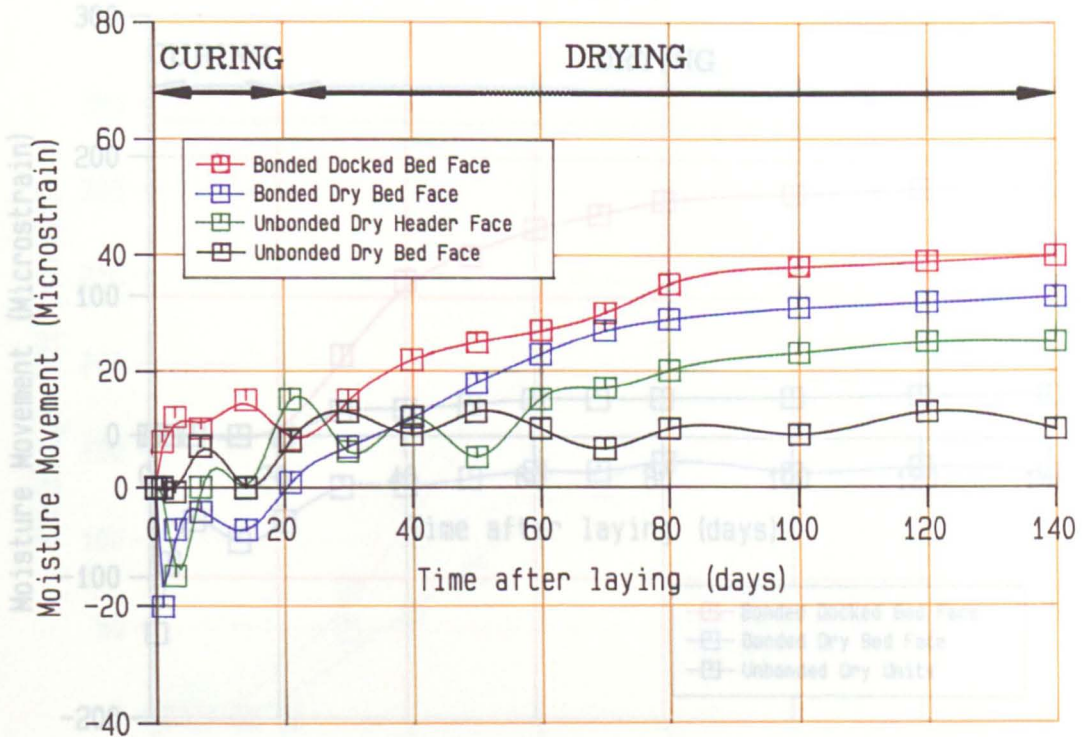


Fig. 7.8 Moisture Movement-time Curve of Bonded and Unbonded Clay Units with a $V/S=28$ mm

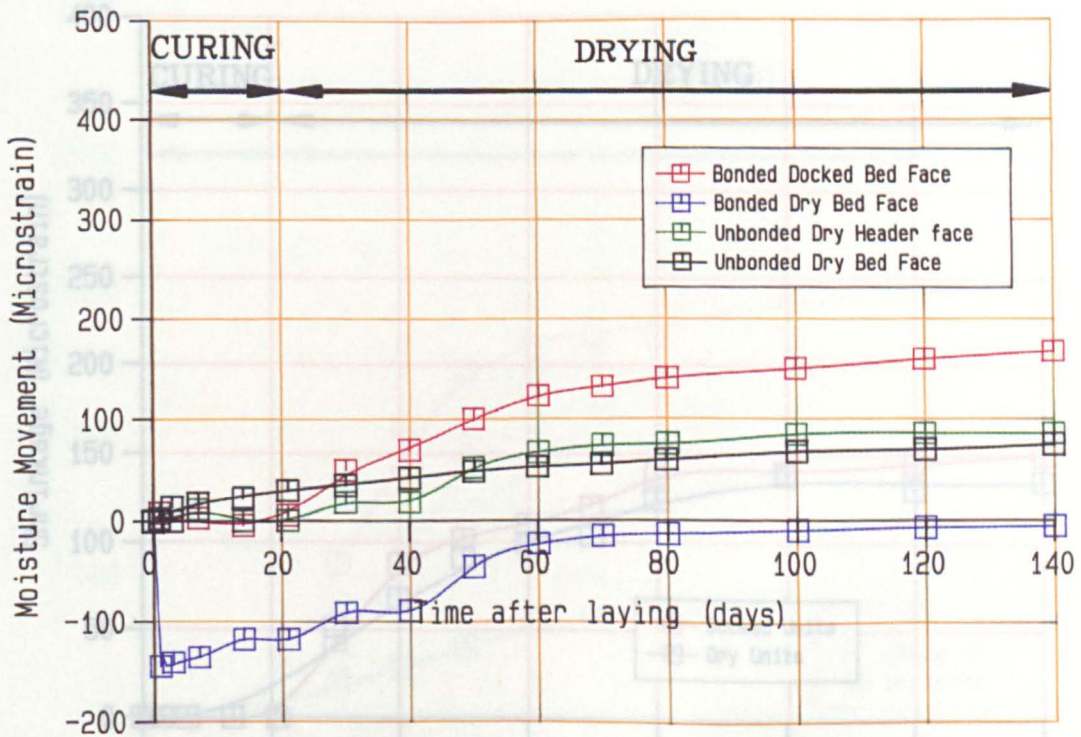


Fig. 7.9 Shrinkage-time Curve of Bonded and Unbonded Calcium Silicate Units with a $V/S=28$ mm

Fig. 7.11 Shrinkage-time Curve of 3-Course Clay Masonry with a $V/S=25$ mm

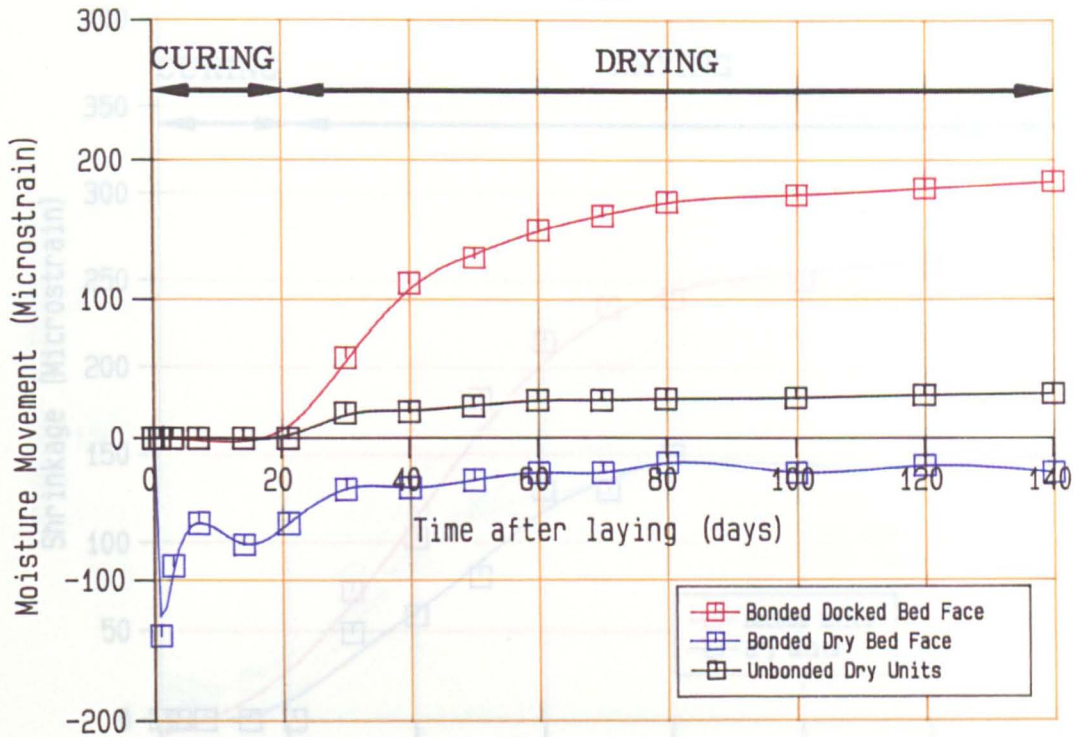


Fig. 7.10 Shrinkage-time Curve of Bonded and Unbonded Concrete Block Units with a $V/S=37$ mm

Fig. 7.12 Shrinkage-time Curve of 3-Course Calcium Silicate Masonry with a $V/S=30$ mm

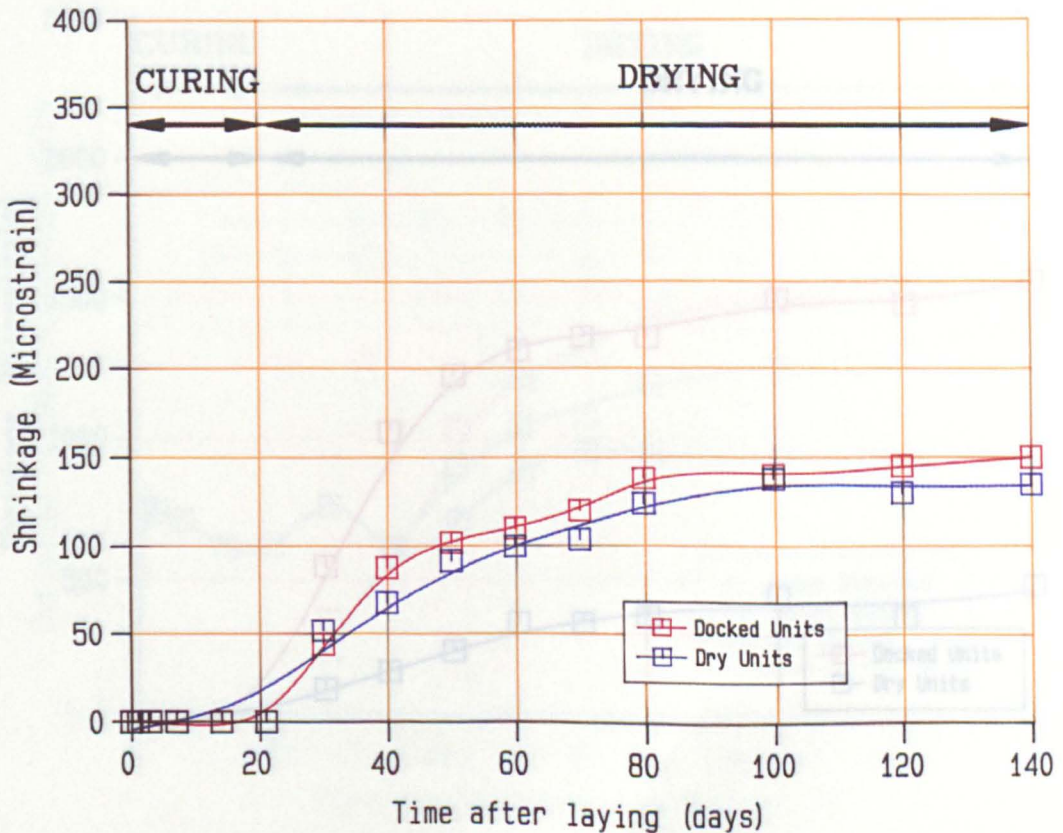


Fig. 7.11 Shrinkage-time Curve of 3-Course Clay Masonry with a $V/S=25$ mm

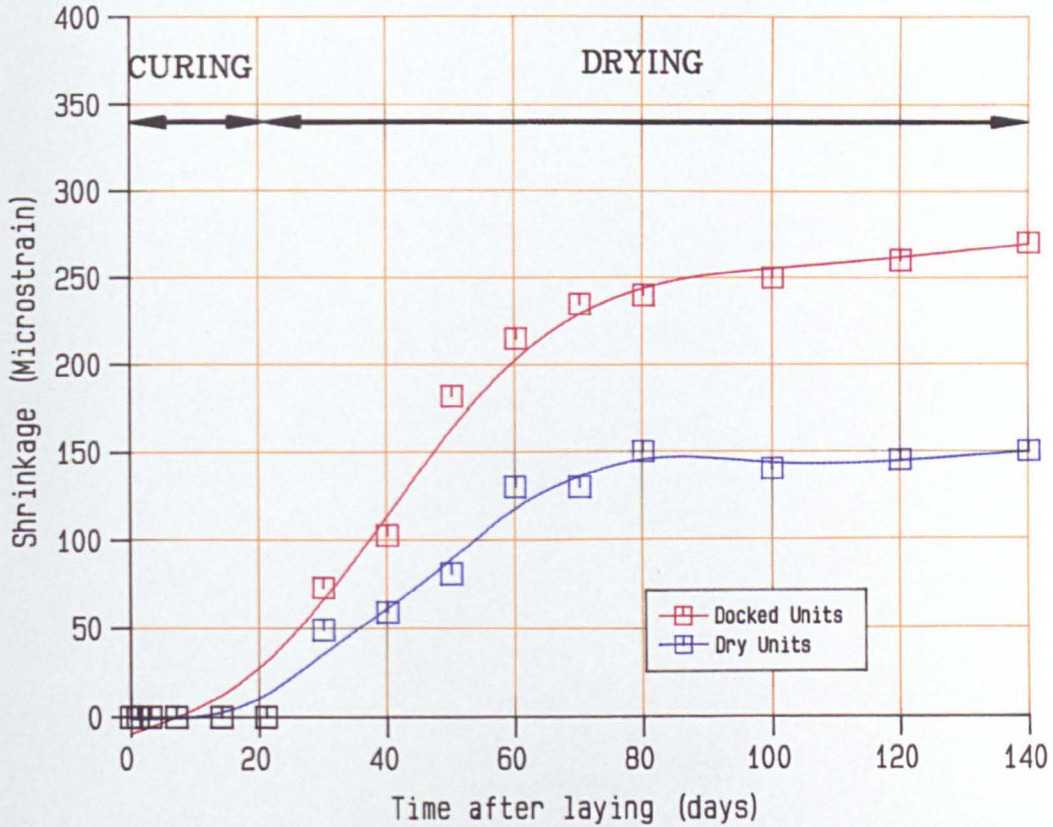


Fig. 7.12 Shrinkage-time Curve of 3-Course Calcium Silicate Masonry with a V/S=30 mm

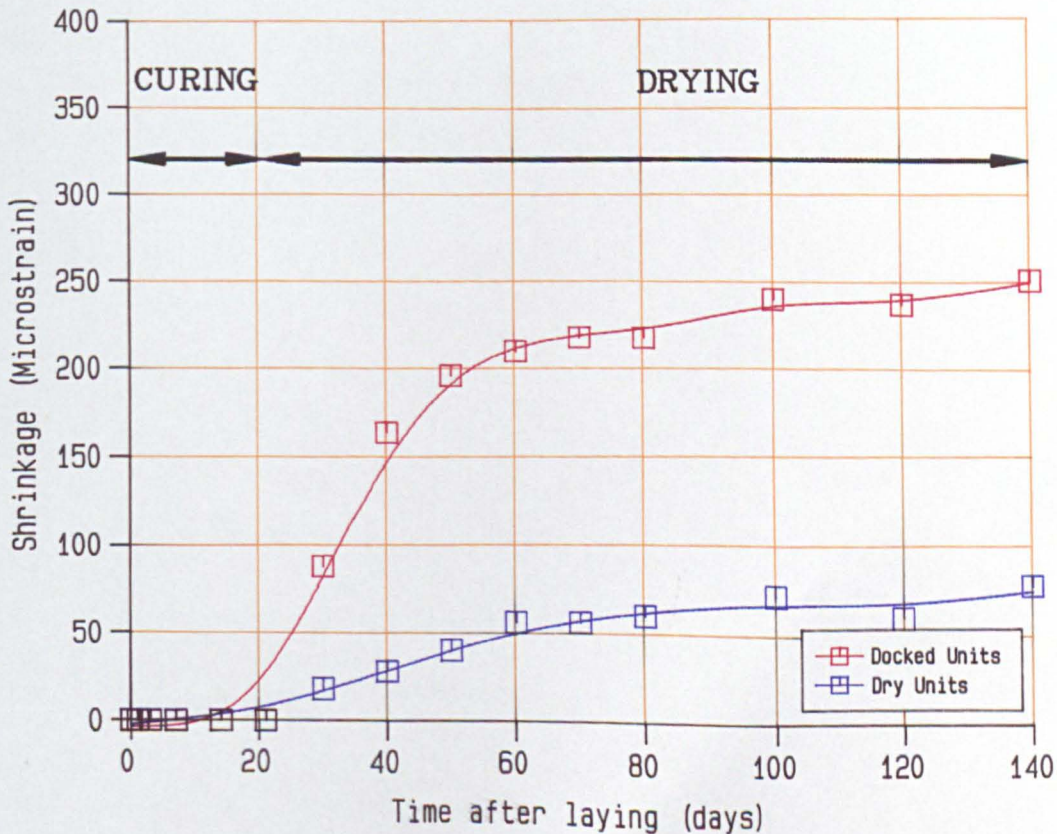


Fig. 7.13 Shrinkage-time Curve of 2-Course Concrete Block Masonry with a V/S=37 mm

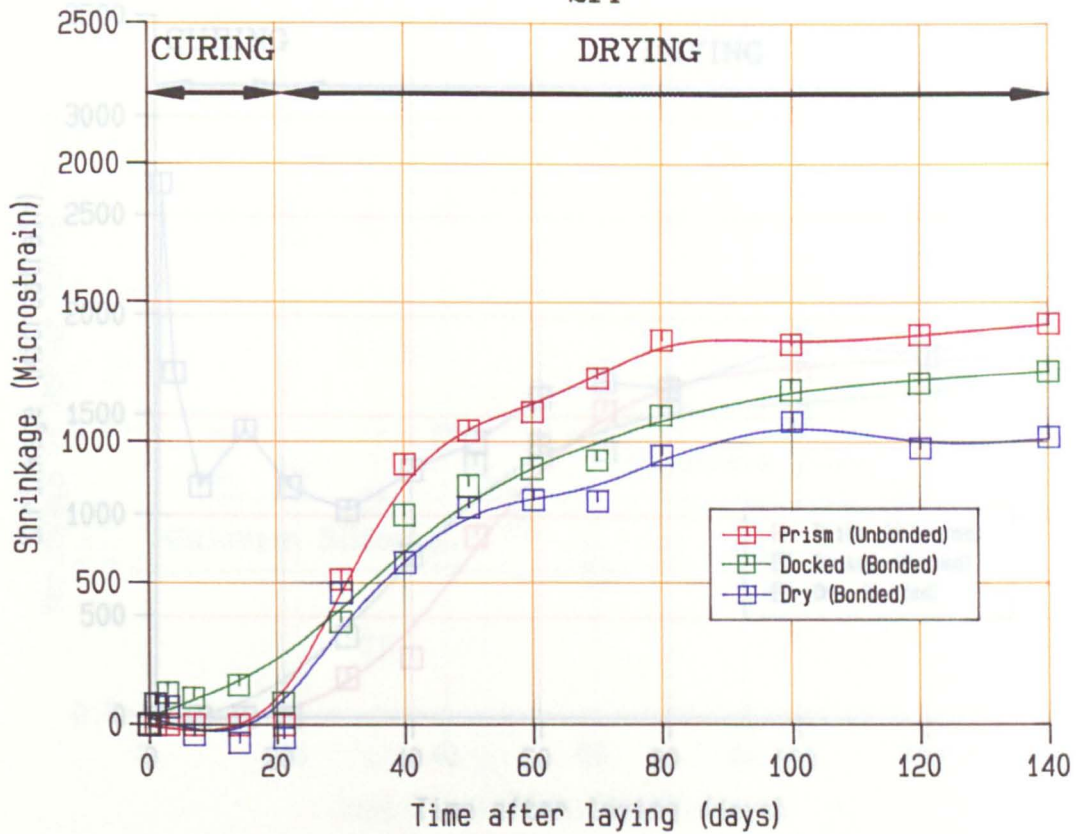


Fig. 7.14 Shrinkage-time Curve of Mortar in 3-Course Clay Masonry

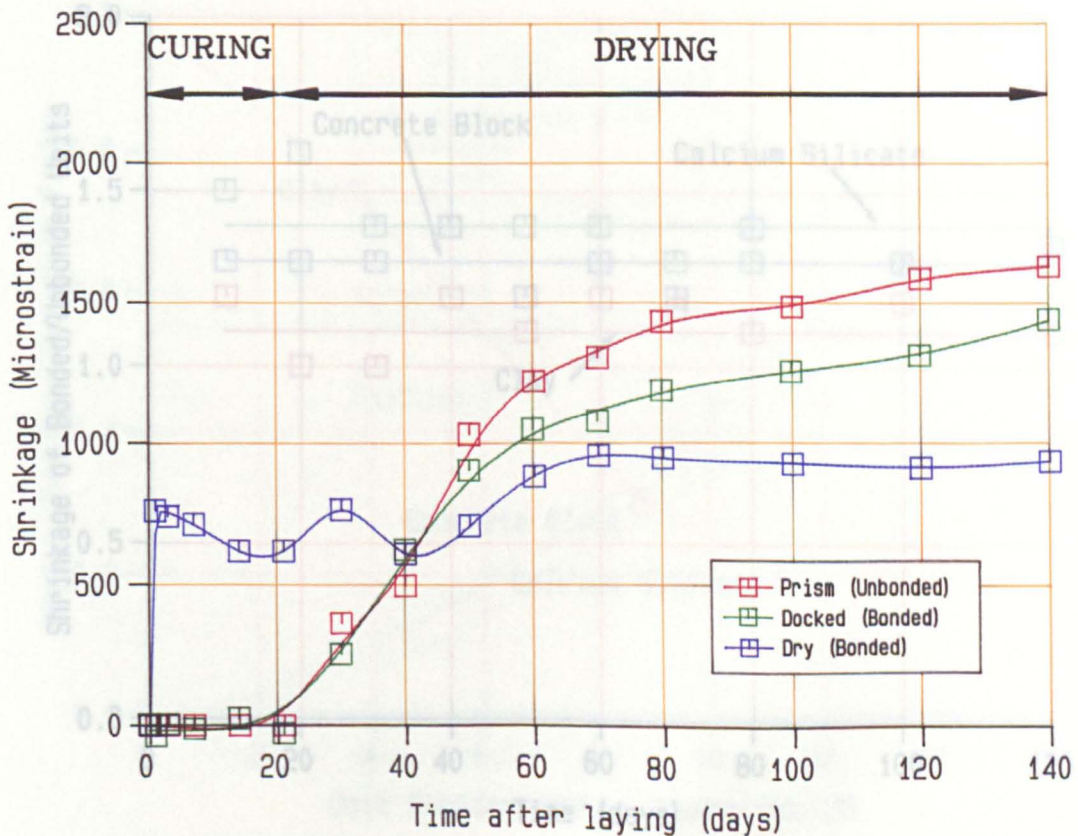


Fig. 7.15 Shrinkage-time Curve of Mortar in 3-Course Calcium Silicate Masonry

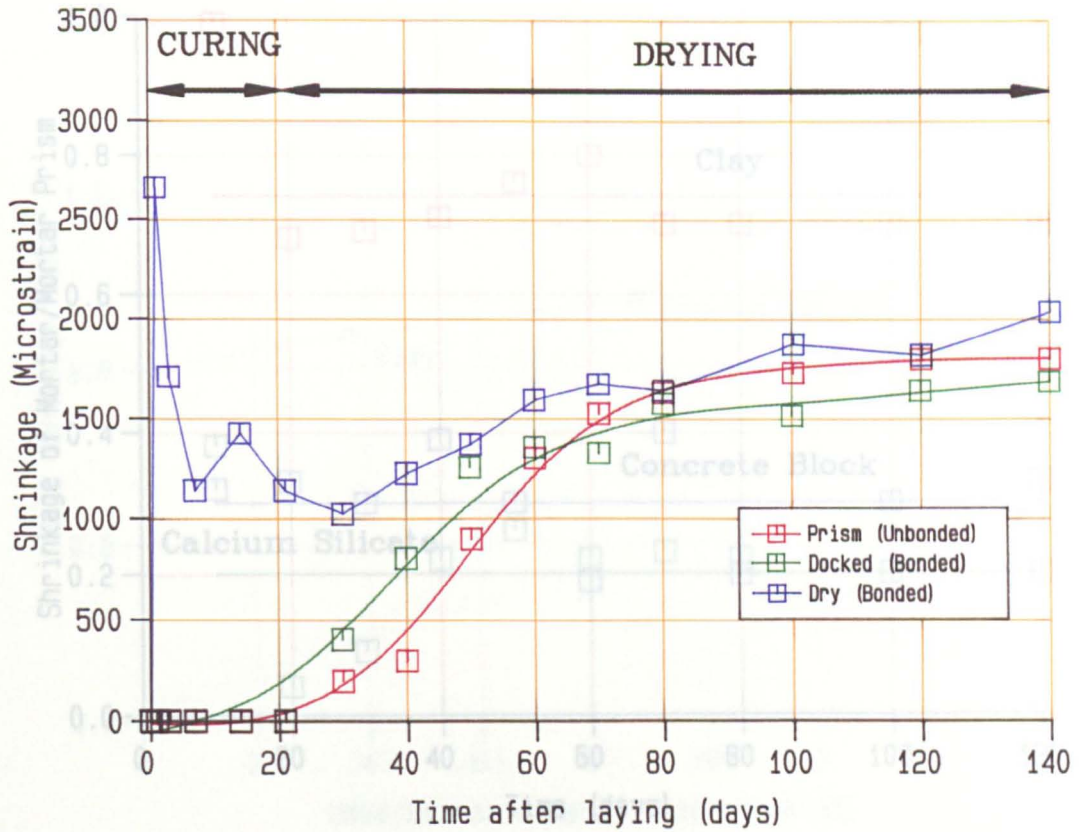


Fig. 7.16 Shrinkage-time Curve of Mortar in 2-Course Concrete Block Masonry

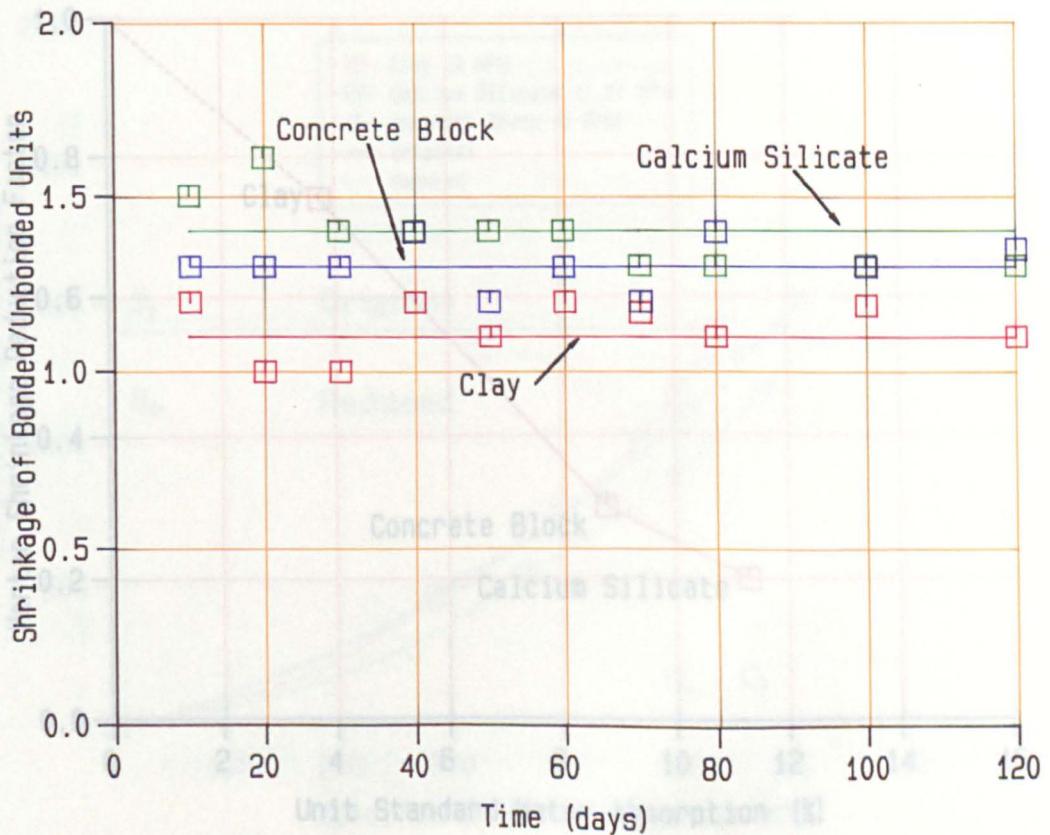


Fig. 7.17 Shrinkage of Bonded/unbonded Ratio-time Curve of Masonry Units

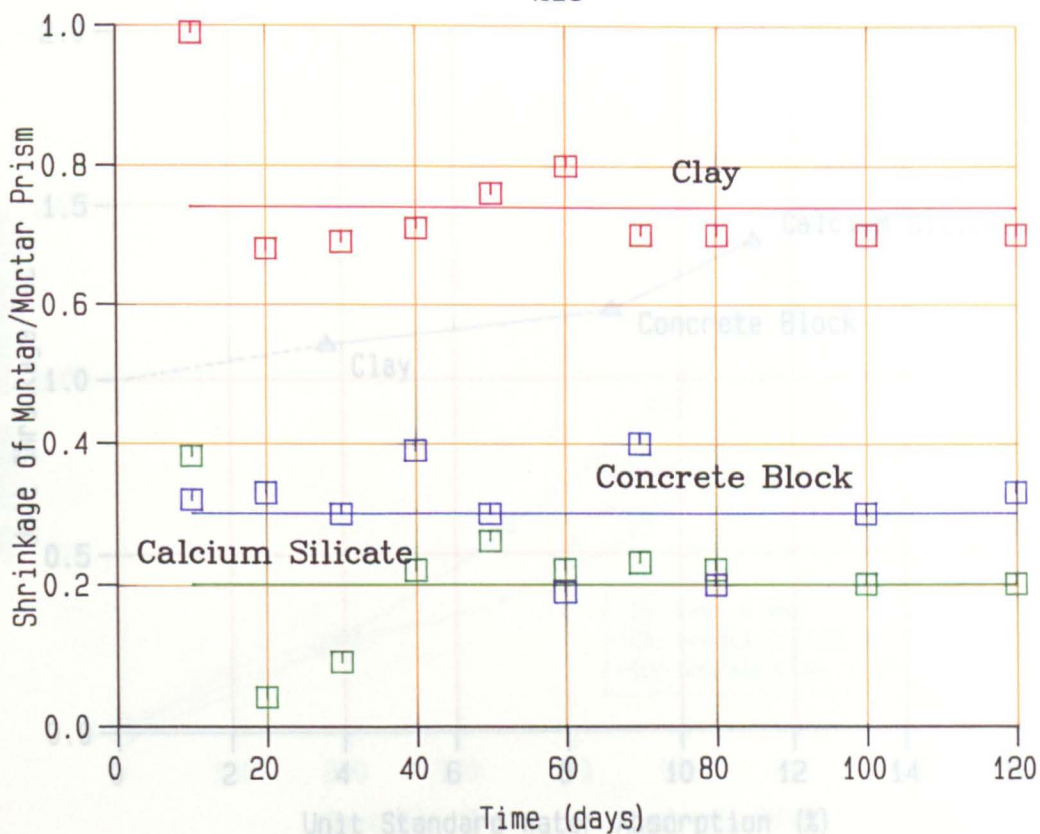


Fig. 7.18 Shrinkage of Mortar/Mortar Prism-time Curve

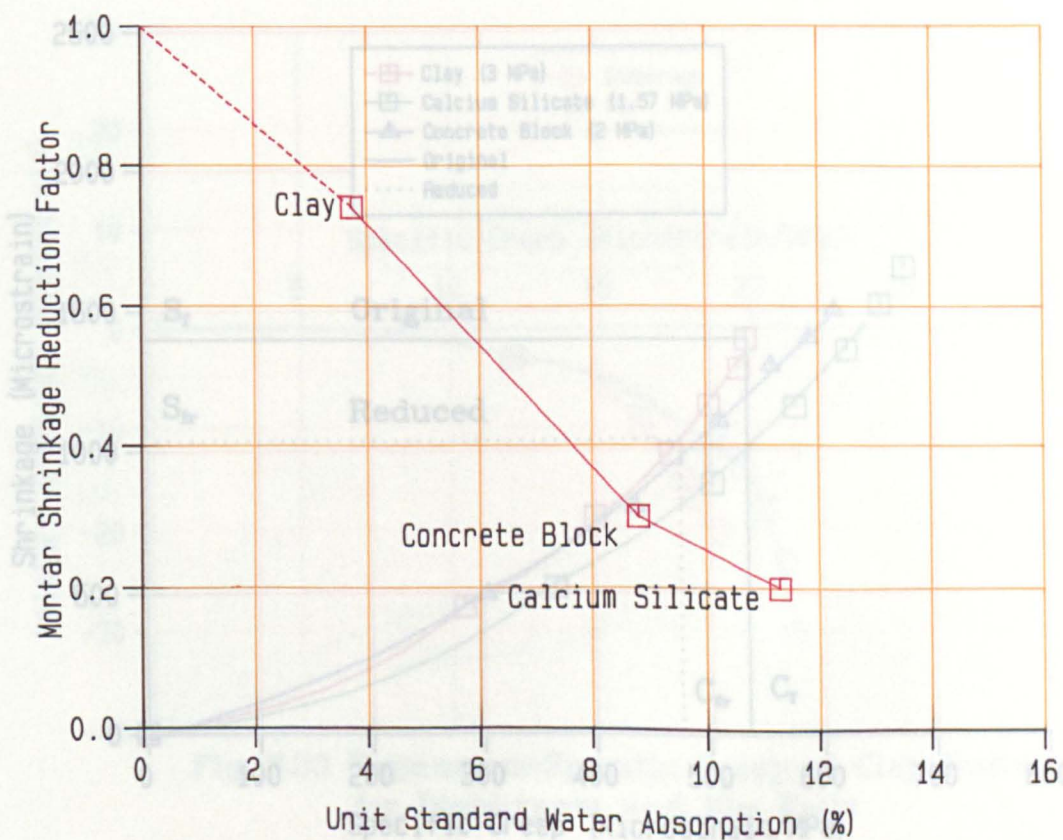


Fig. 7.19 Shrinkage Reduction Factor of Mortar-Water Absorption for Masonry Made from Dry Units

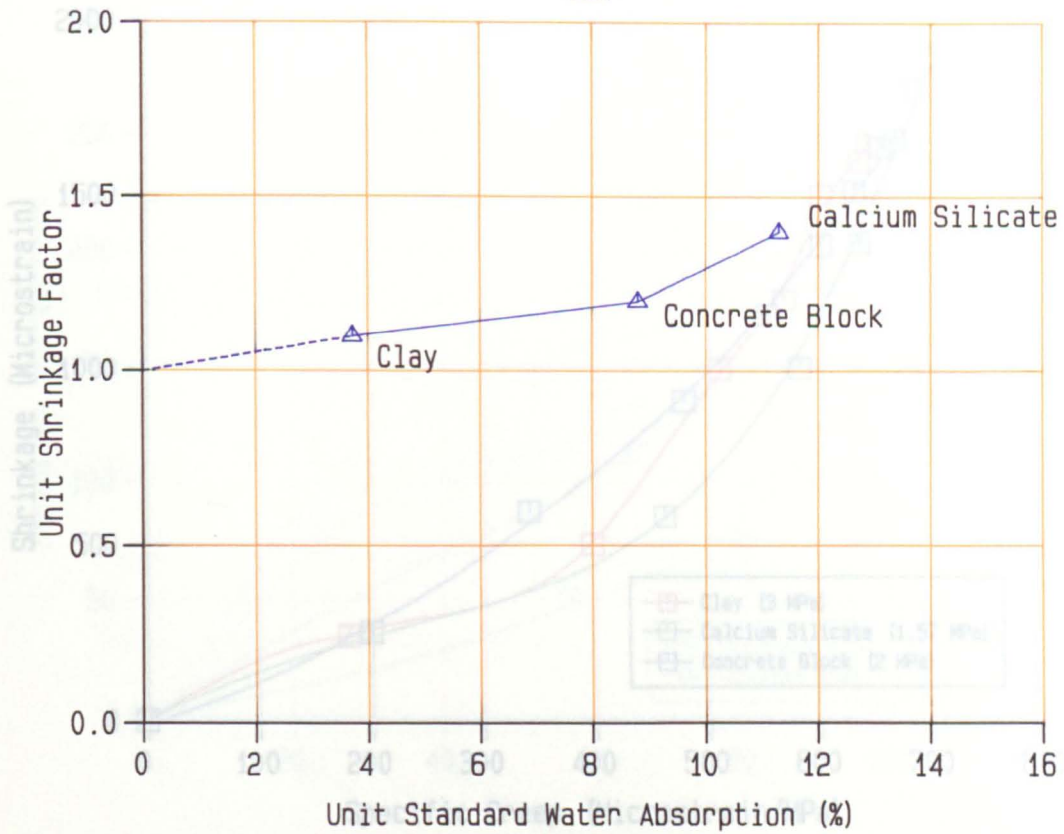


Fig. 7.20 Shrinkage Enlargement Factor of Masonry Units – Water Absorption for Masonry Made with Dry Units

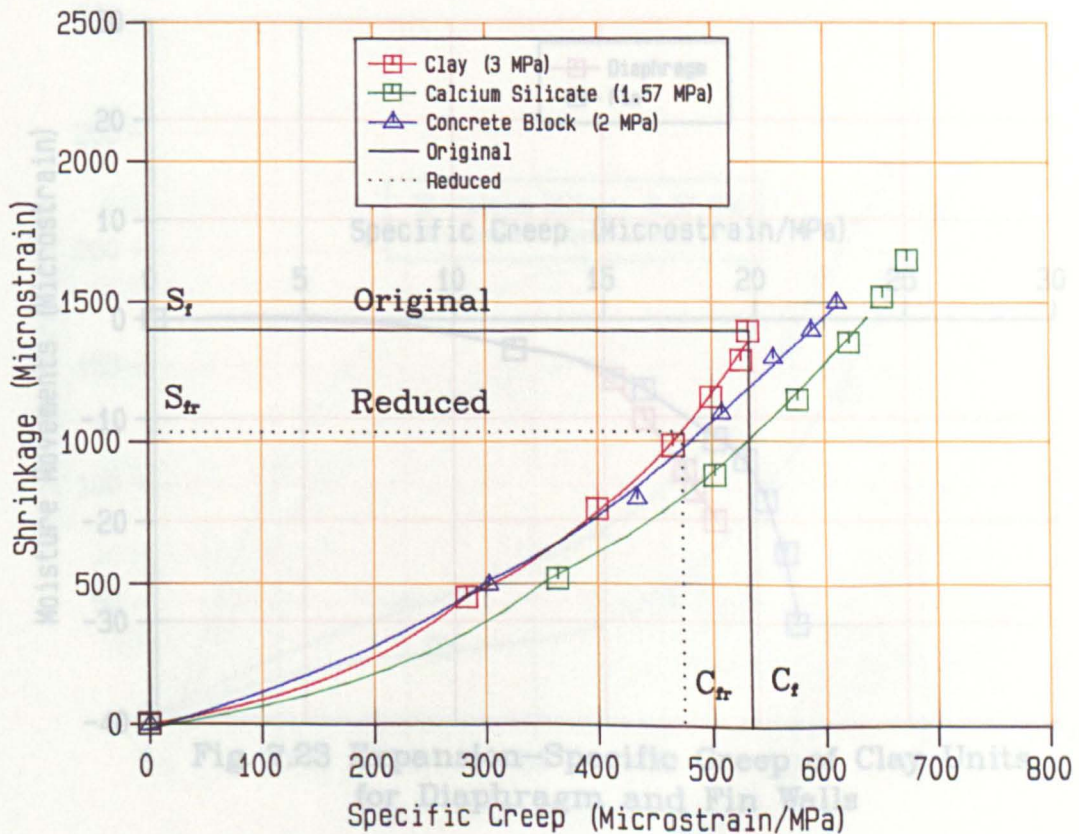


Fig. 7.21 Shrinkage–Specific Creep of Mortar Prisms for Diaphragm Walls

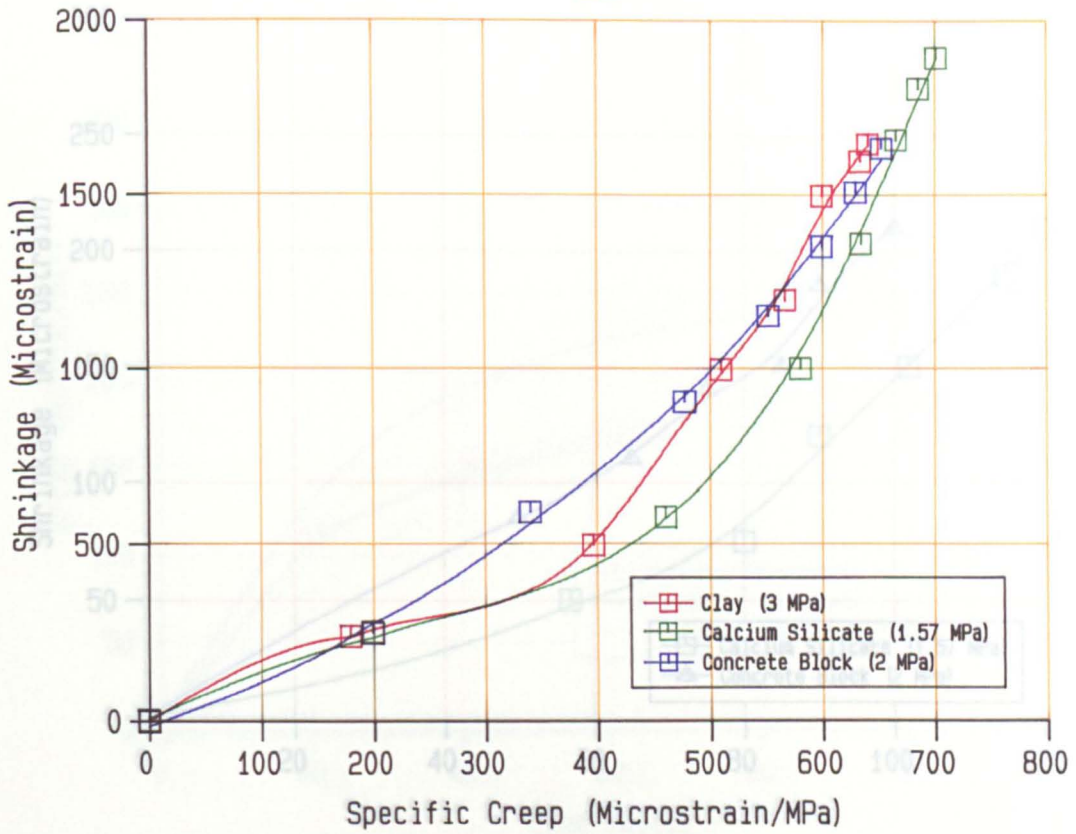


Fig.7.22 Shrinkage-Specific Creep of Mortar Prisms for Fin Walls

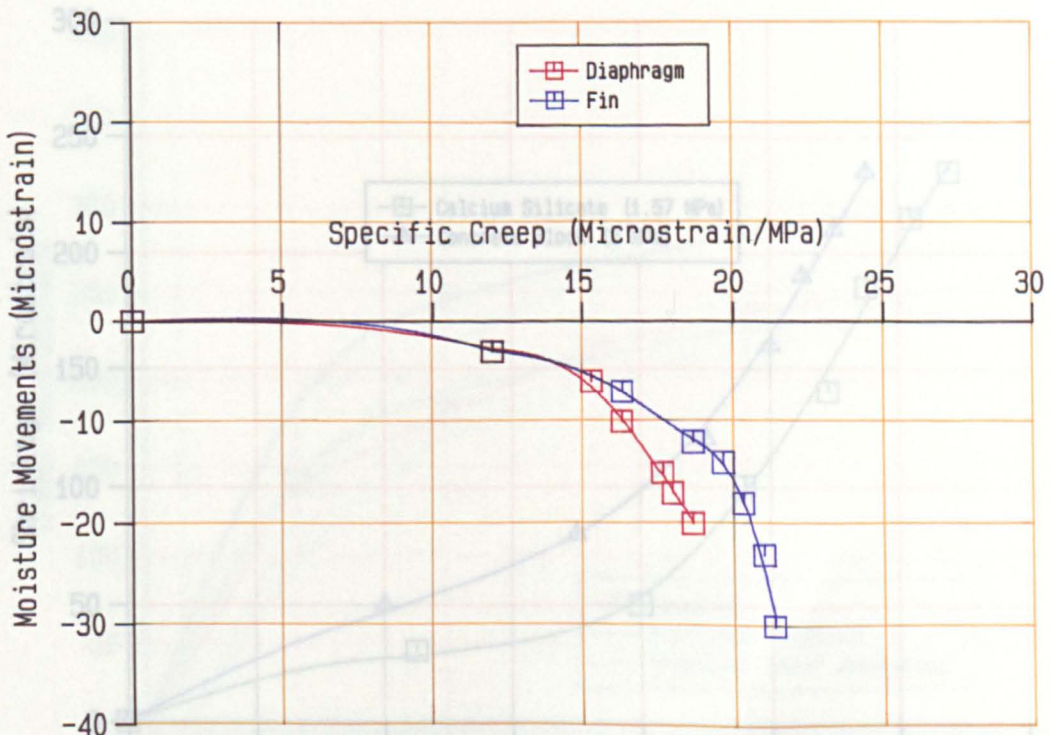


Fig. 7.23 Expansion-Specific Creep of Clay Units for Diaphragm and Fin Walls

Fig. 7.25 Shrinkage-Specific Creep of Masonry Units for Fin Walls

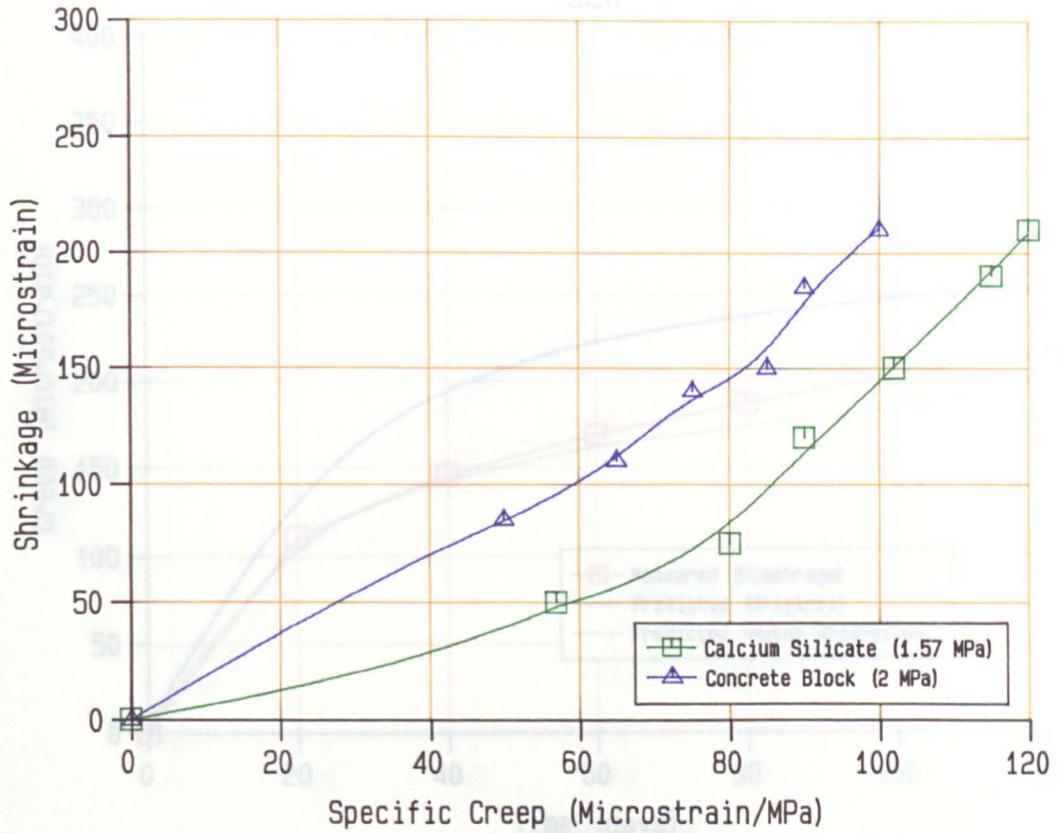


Fig. 7.24 Shrinkage-Specific Creep of Masonry Units for Diaphragm Walls

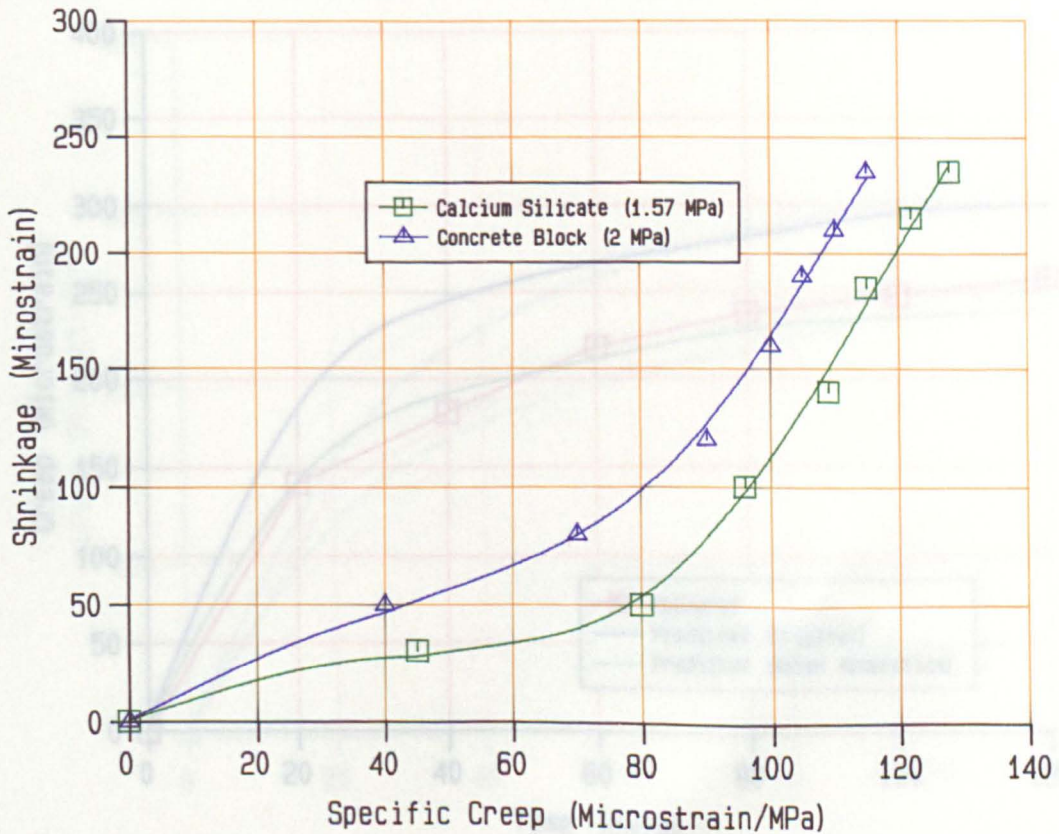


Fig. 7.25 Shrinkage-Specific Creep of Masonry Units for Fin Walls

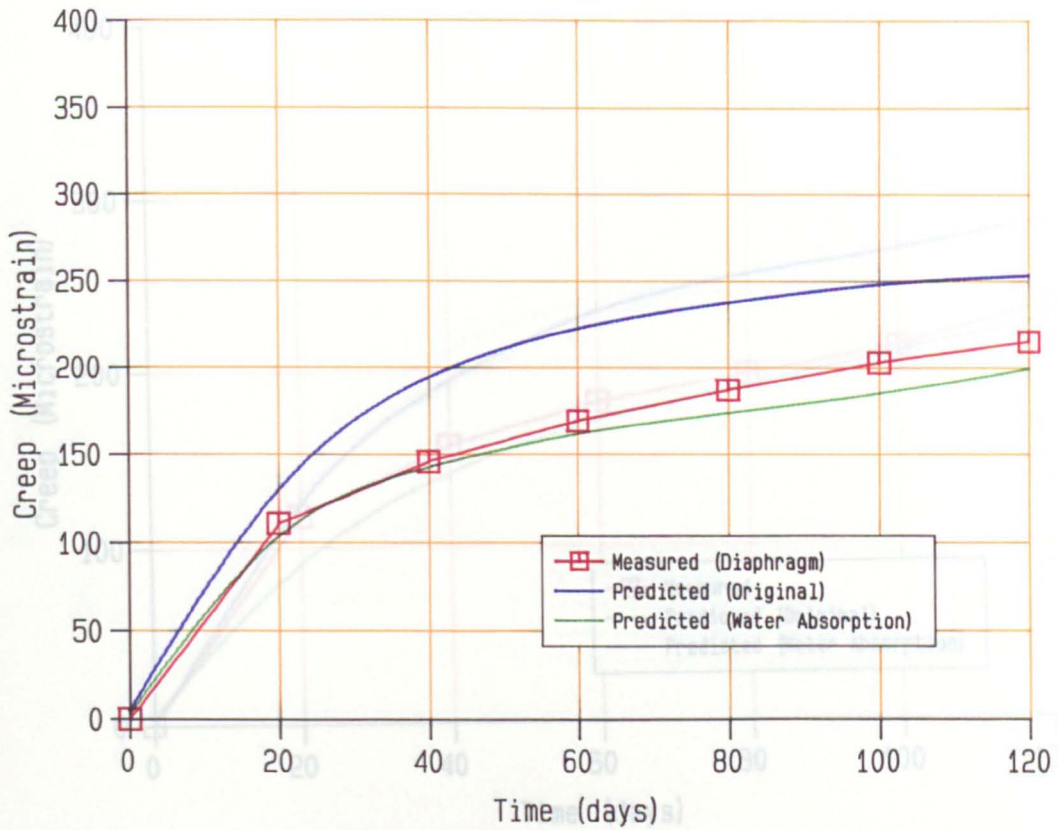


Fig. 7.26 Measured and Predicted Creep-time Curve of Diaphragm Clay Walls

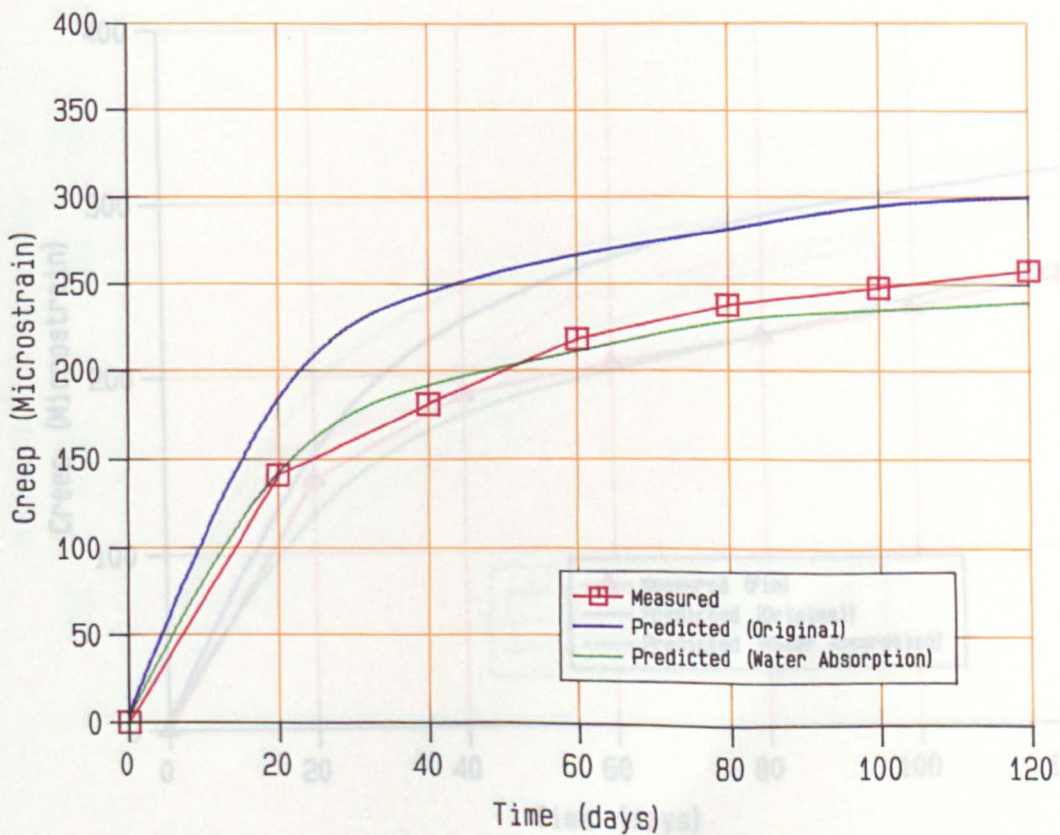


Fig. 7.27 Measured and Predicted Creep-time Curve of Fin Clay Walls

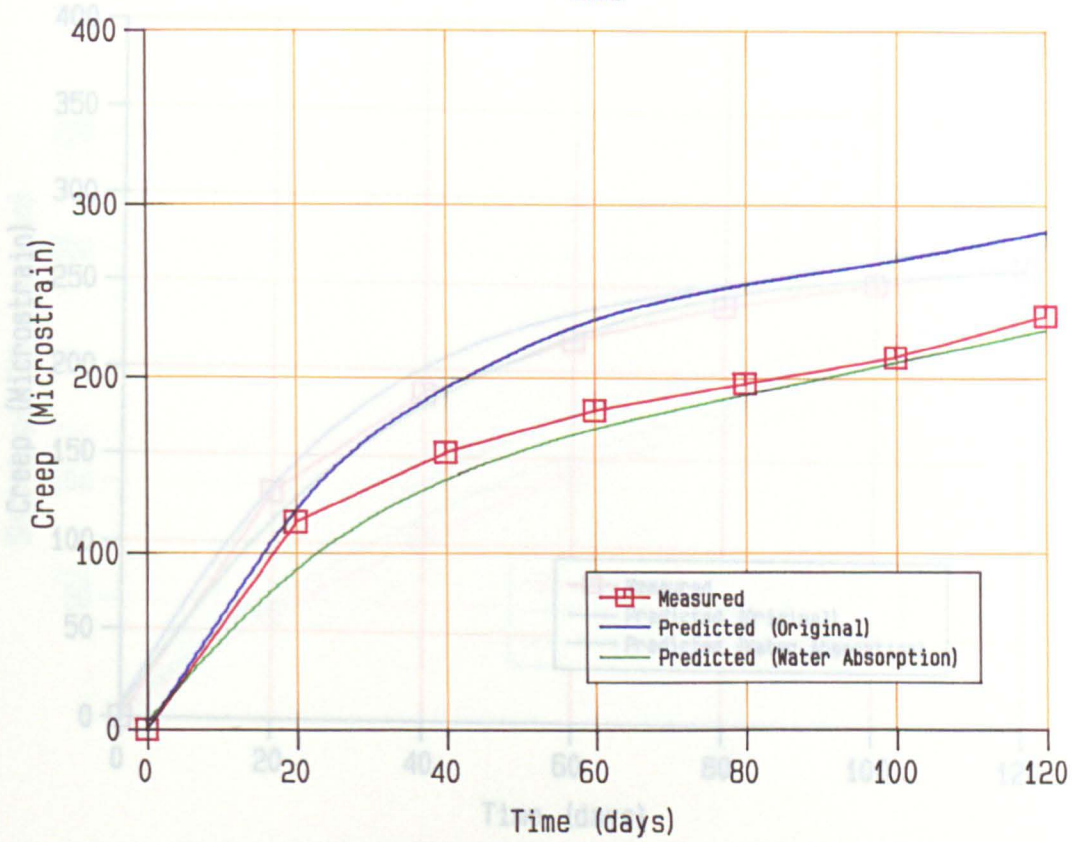


Fig. 7.28 Measured and Predicted Creep-time Curve of Diaphragm Calcium Silicate Walls

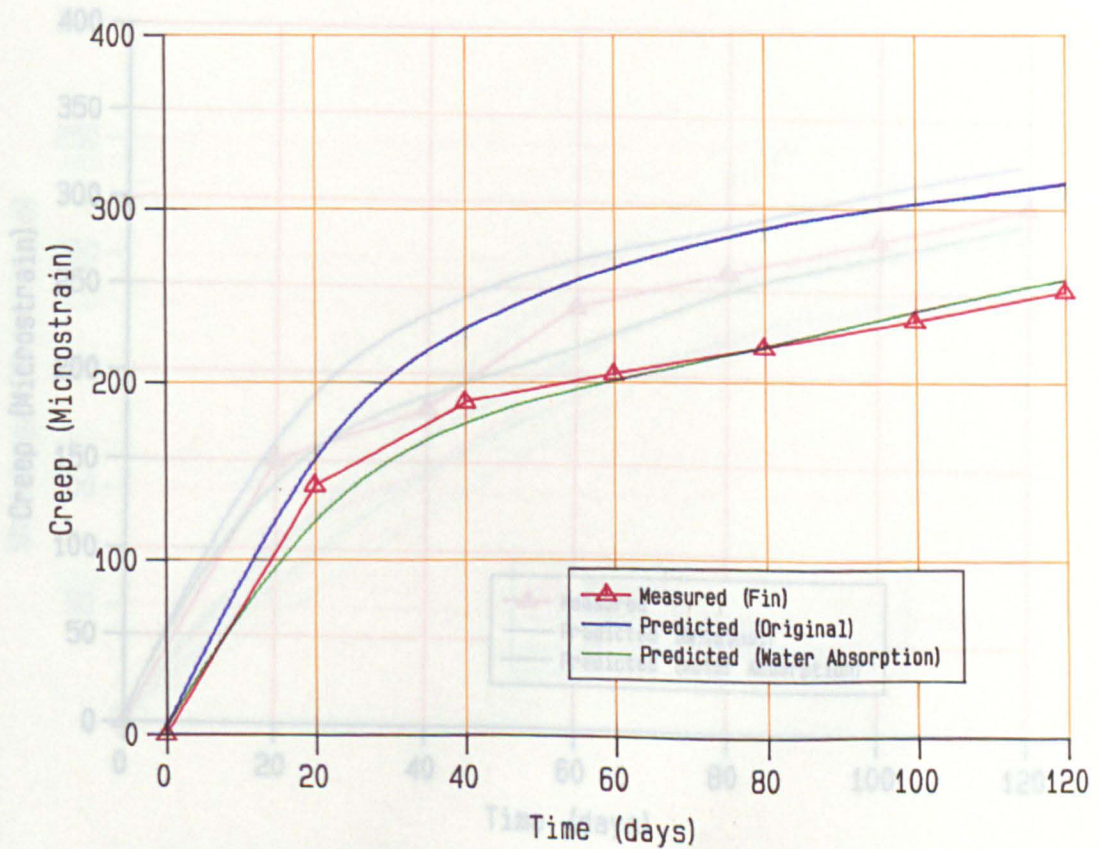


Fig. 7.29 Measured and Predicted Creep-time Curve of Fin Calcium Silicate Walls

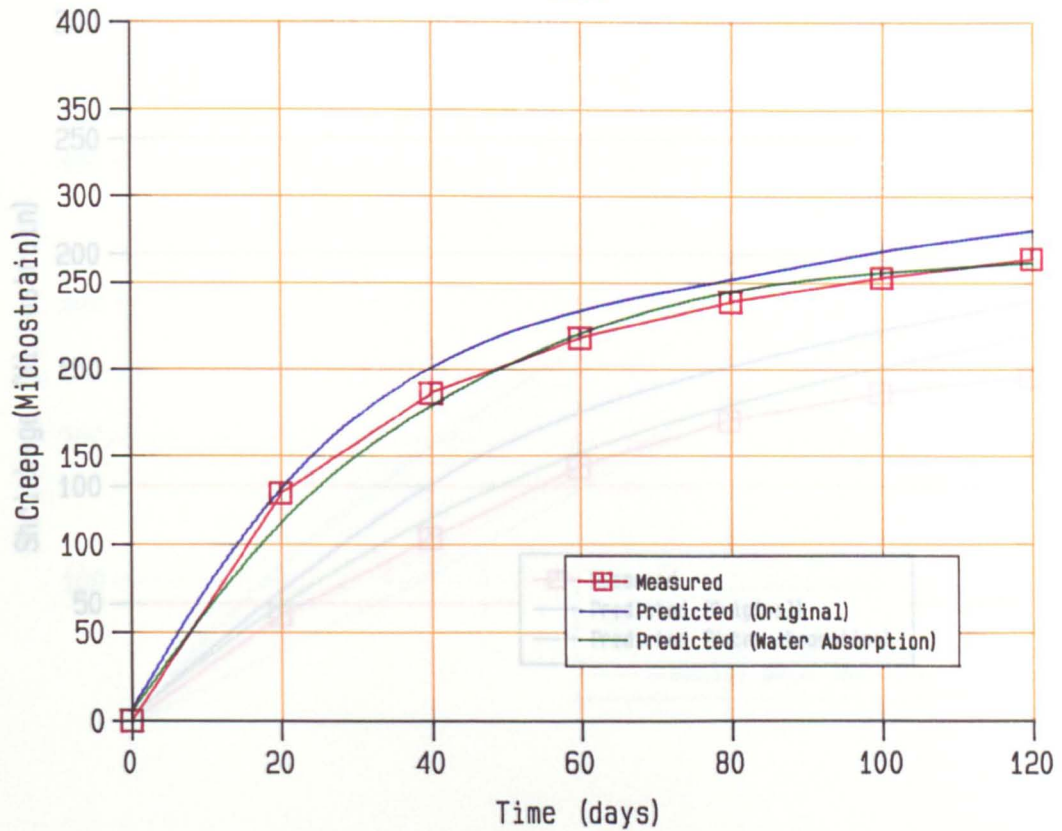


Fig. 7.30 Measured and Predicted Creep-time Curve of Diaphragm Concrete Block Walls

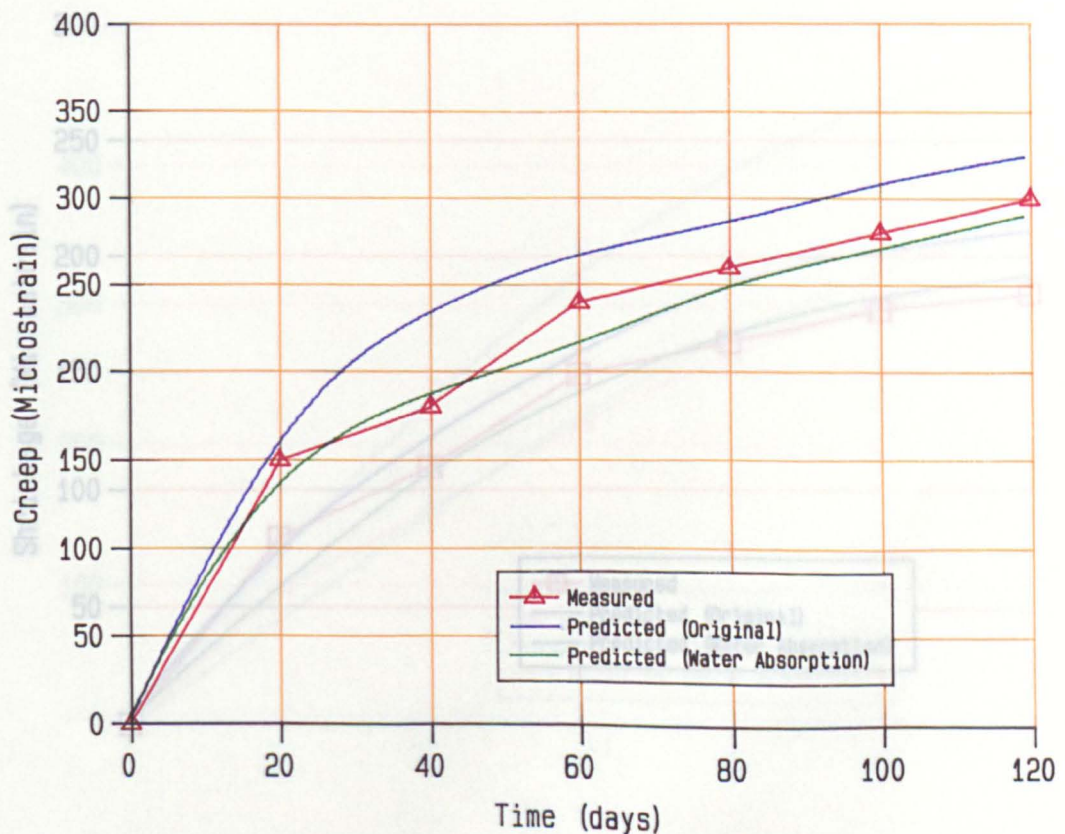


Fig. 7.31 Measured and Predicted Creep-time Curve of Fin Concrete Block Wall

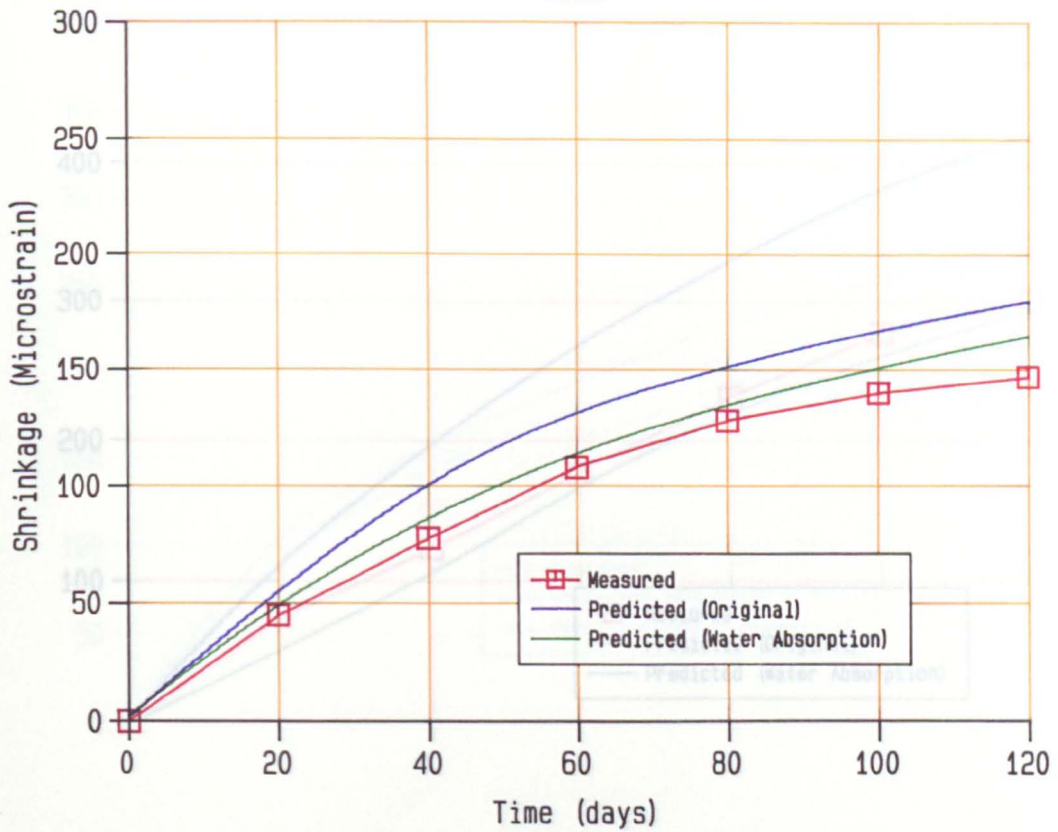


Fig. 7.32 Measured and Predicted Shrinkage-time Curve of Diaphragm Clay Wall

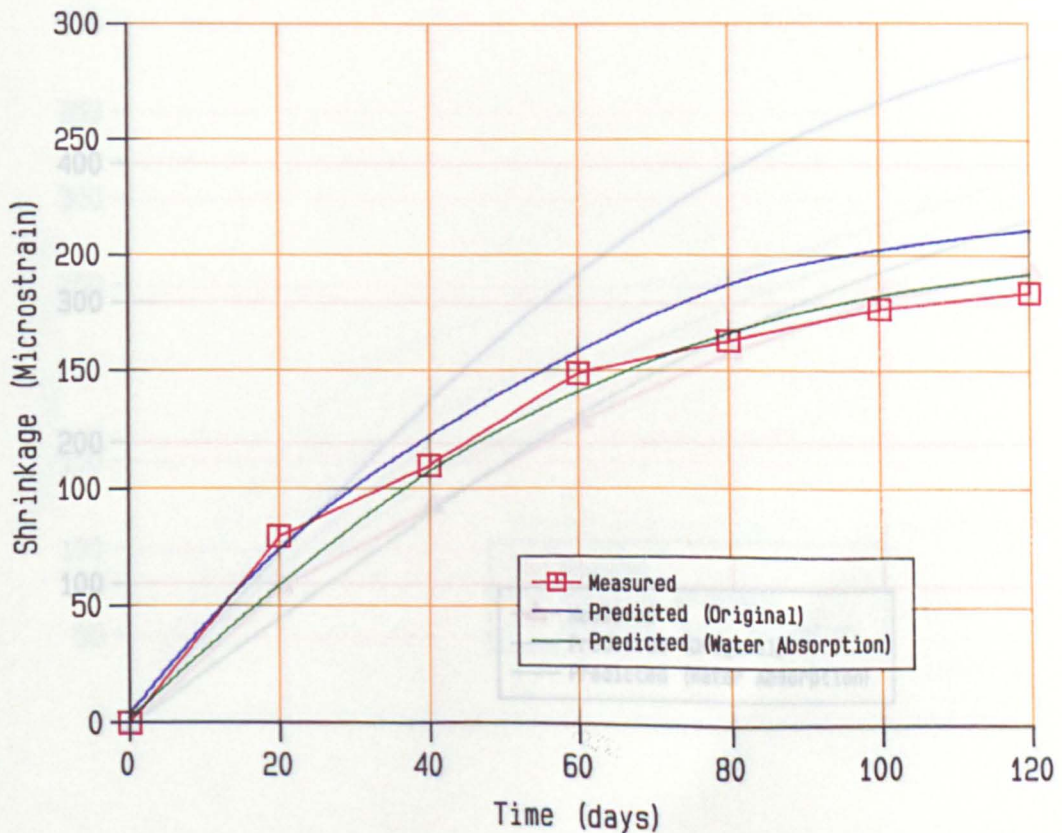


Fig. 7.33 Measured and Predicted Shrinkage-time Curve of Fin Clay Walls

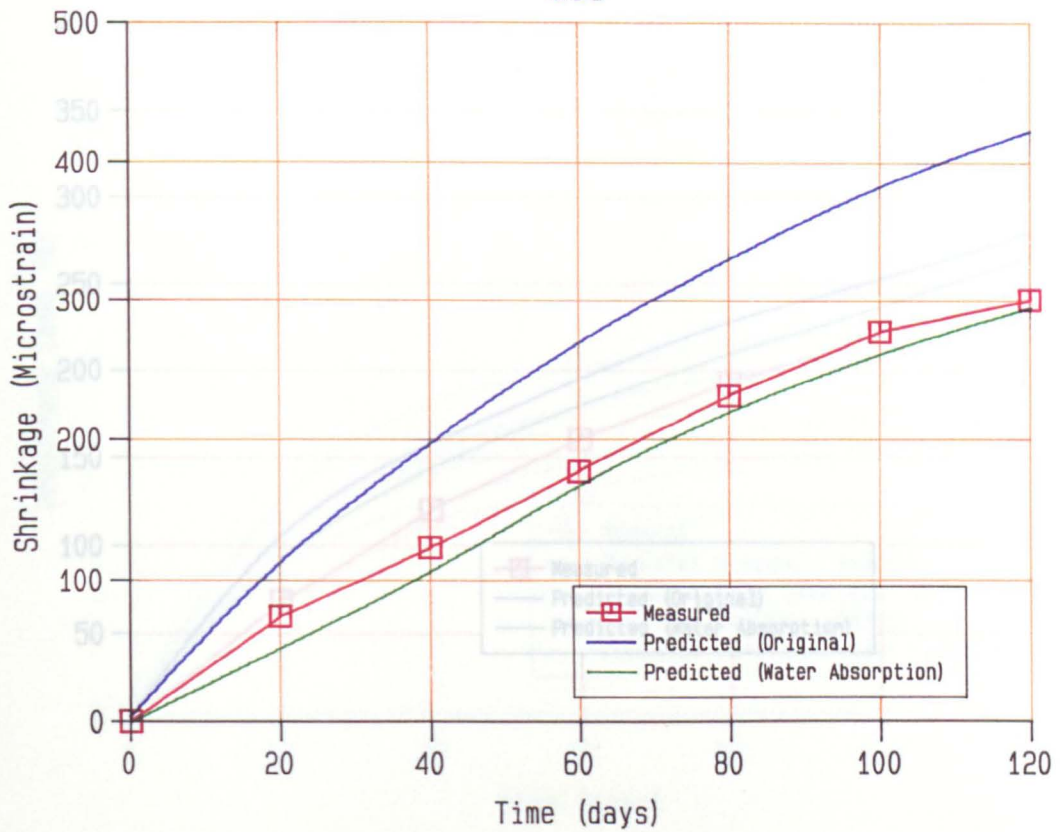


Fig. 7.34 Measured and Predicted Shrinkage-time Curve of Diaphragm Calcium Silicate Wall

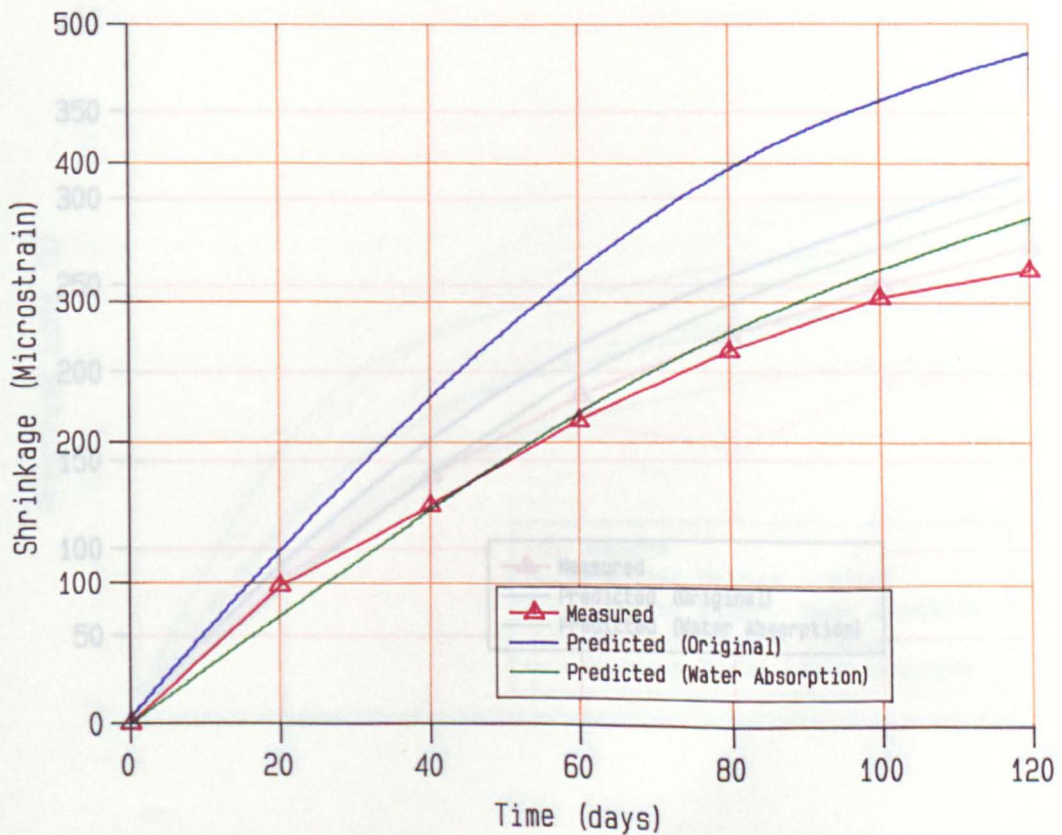


Fig. 7.35 Measured and Predicted Shrinkage-time Curve of Fin Calcium Silicate Wall

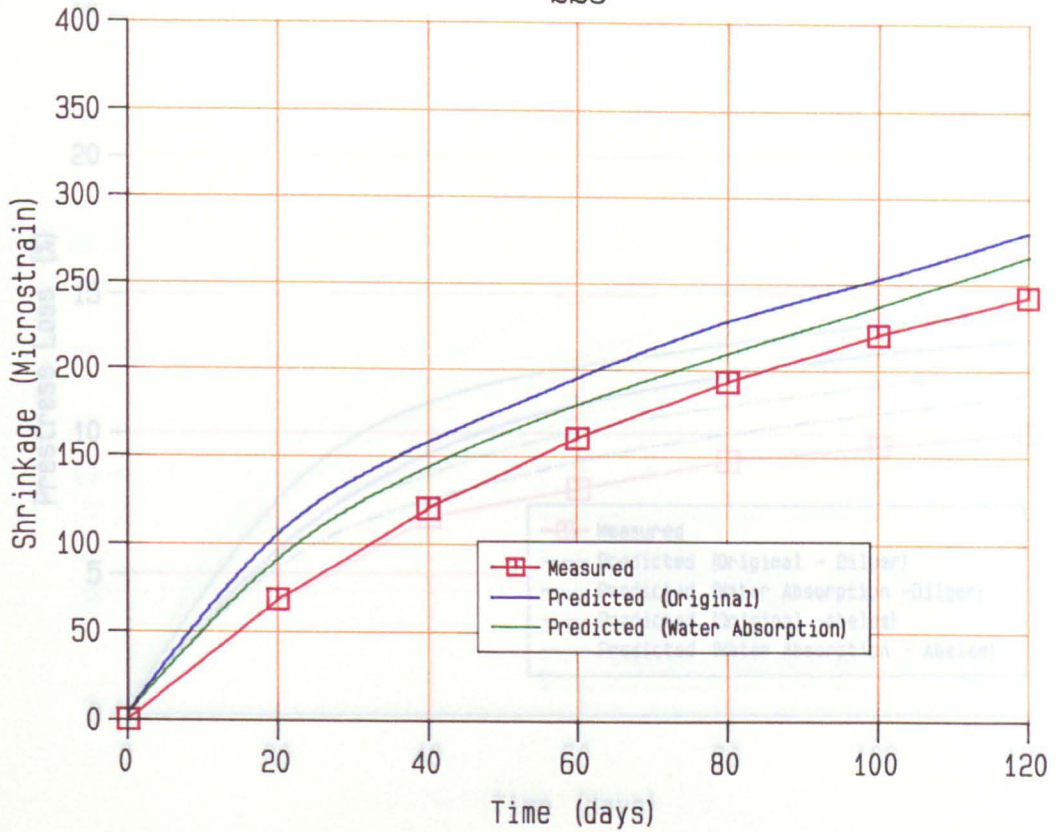


Fig. 7.36 Measured and Predicted Shrinkage-time Curve of Diaphragm Concrete Block Wall

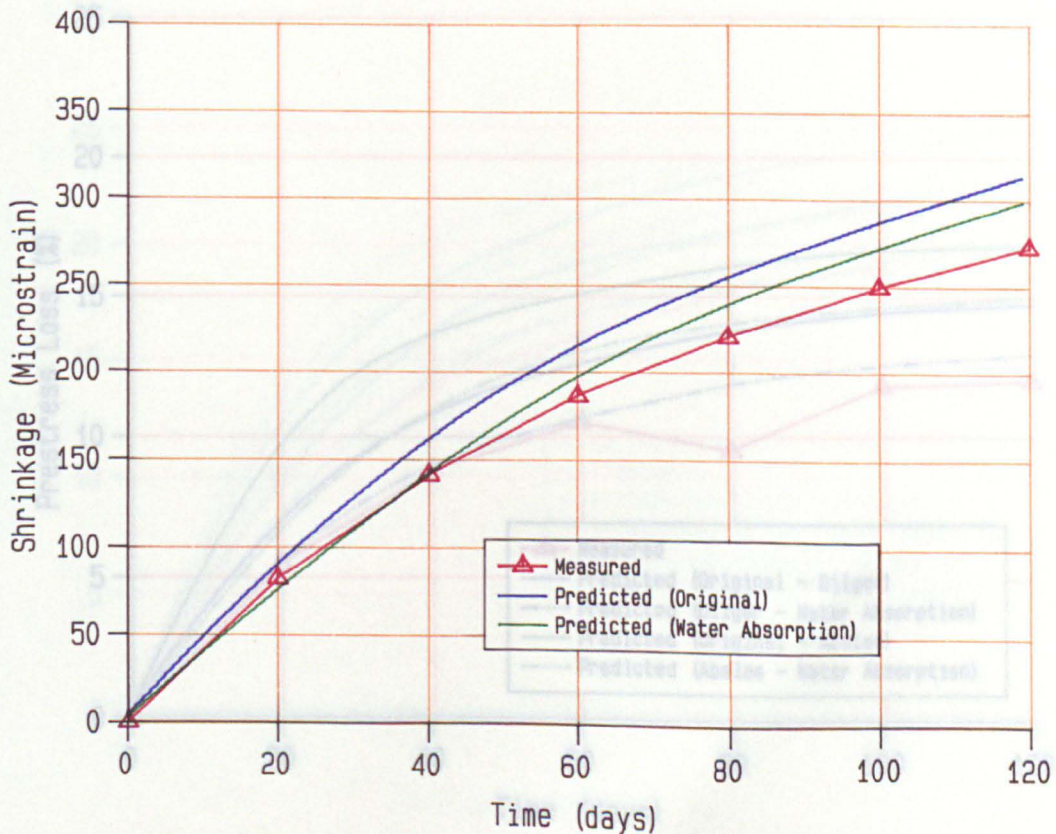


Fig. 7.37 Measured and Predicted Shrinkage-time Curve of Fin Concrete Block Wall

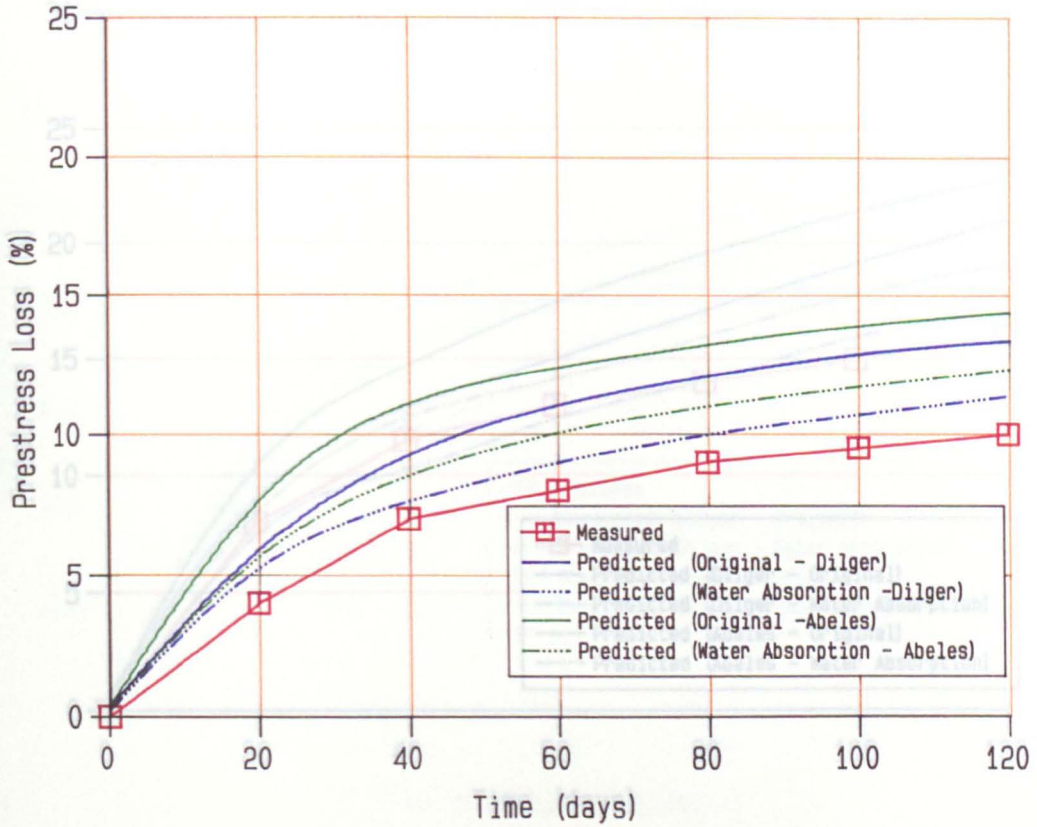


Fig. 7.38 Measured and Predicted Prestress Loss-time Curve in Clay Diaphragm Walls

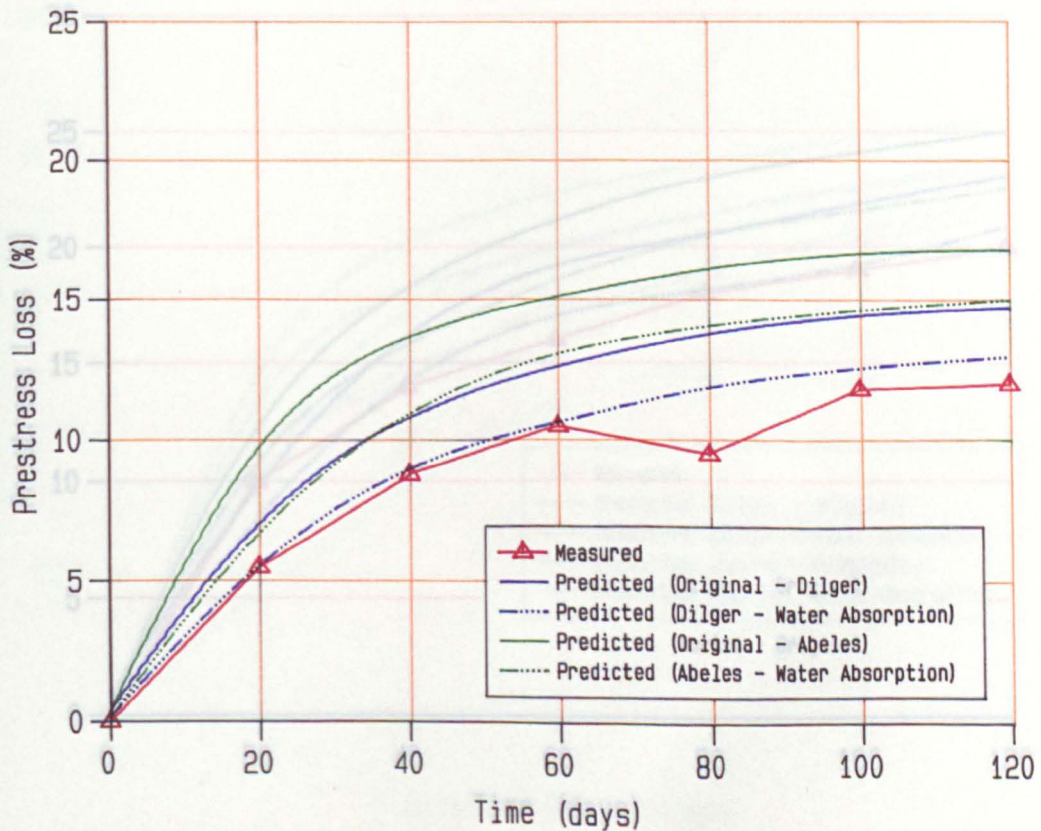


Fig. 7.39 Measured and Predicted Prestress Loss-time Curve of Clay Fin Wall

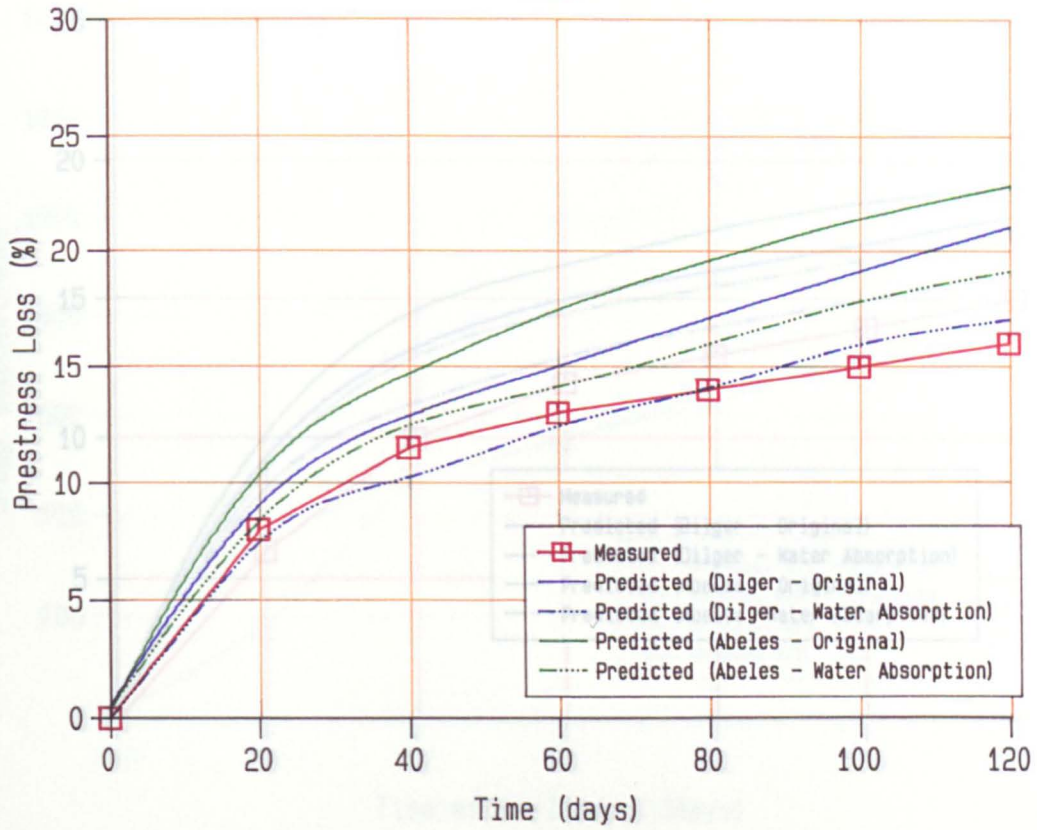


Fig. 7.40 Measured and Predicted Prestress Loss-time Curve of Calcium Silicate Diaphragm Wall

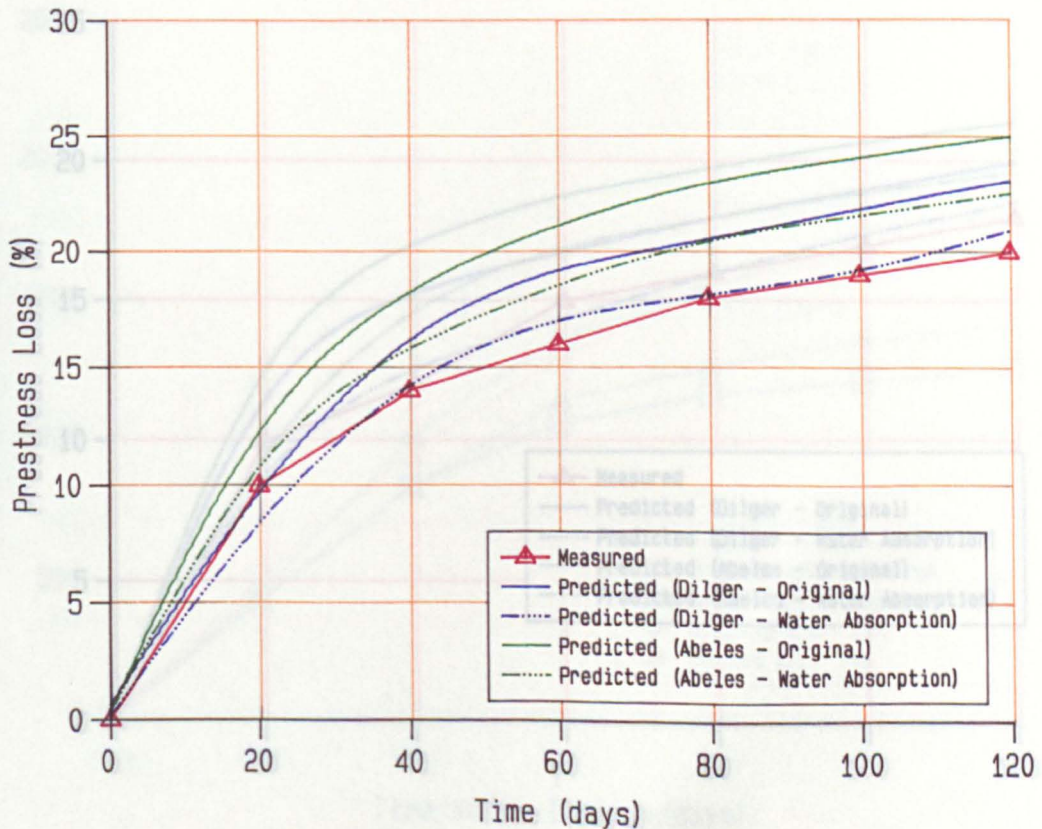


Fig. 7.41 Measured and Predicted Prestress Loss-time Curve of Calcium Silicate Fin Wall

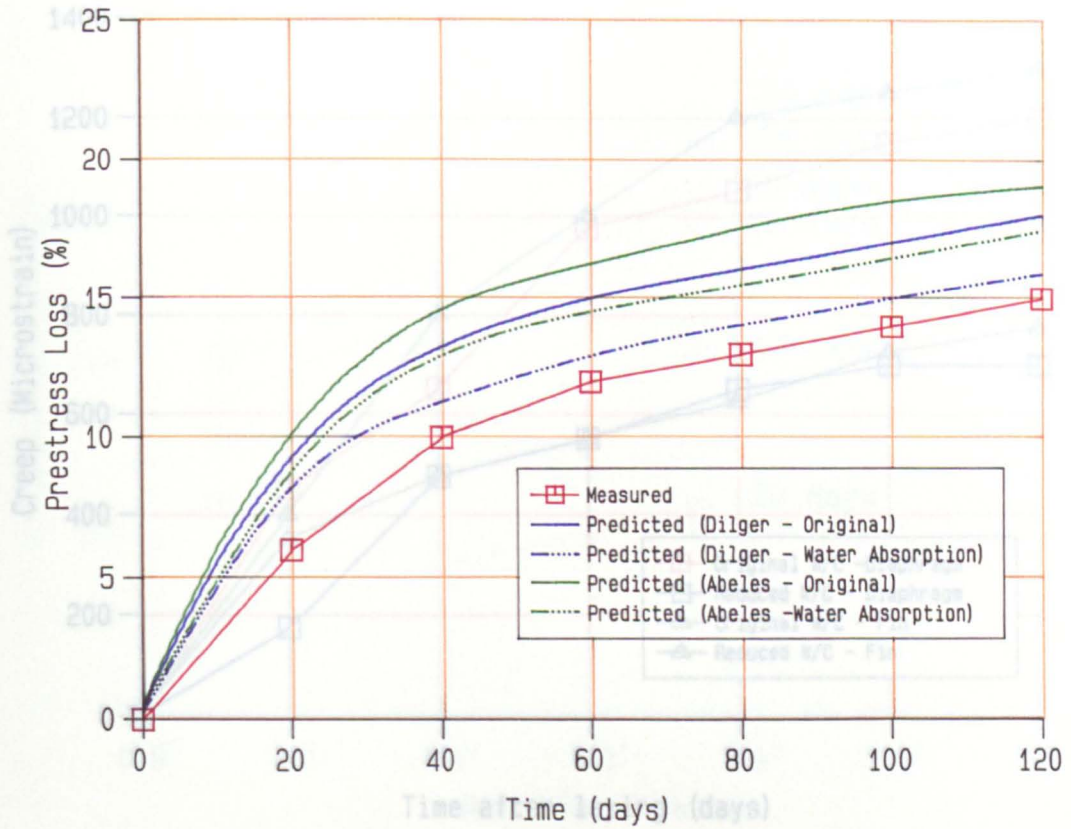


Fig. 7.42 Measured and Predicted Prestress Loss-time Curve of Concrete Block Diaphragm Wall

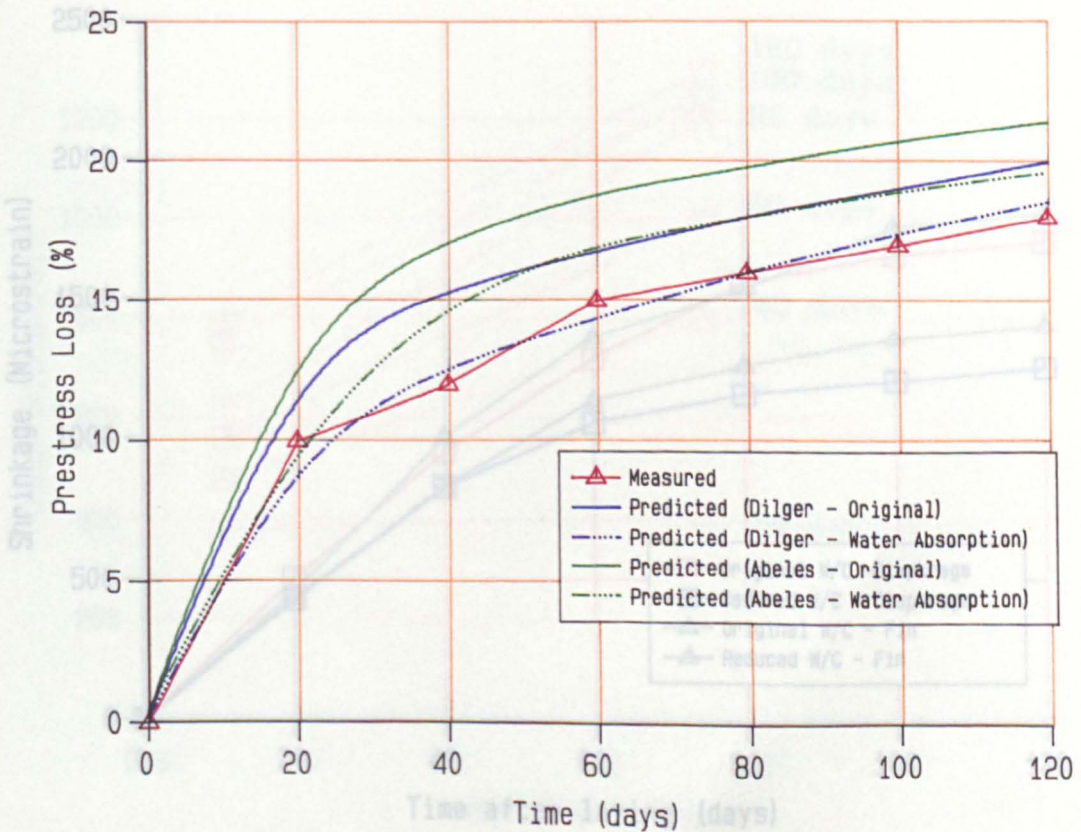


Fig. 7.43 Measured and Predicted Prestress Loss-time Curve of Concrete Block Fin Wall

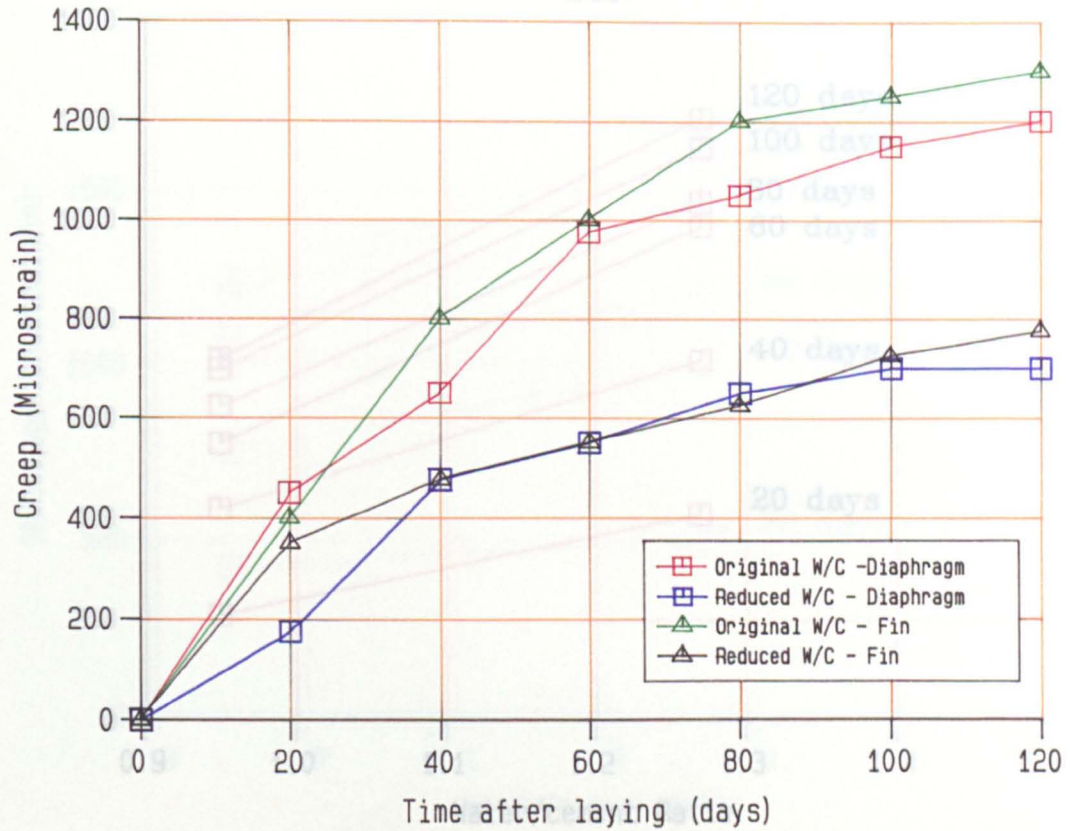


Fig. 7.44 Creep-time Curve of Mortar with Original and Reduced Water/cement Ratio

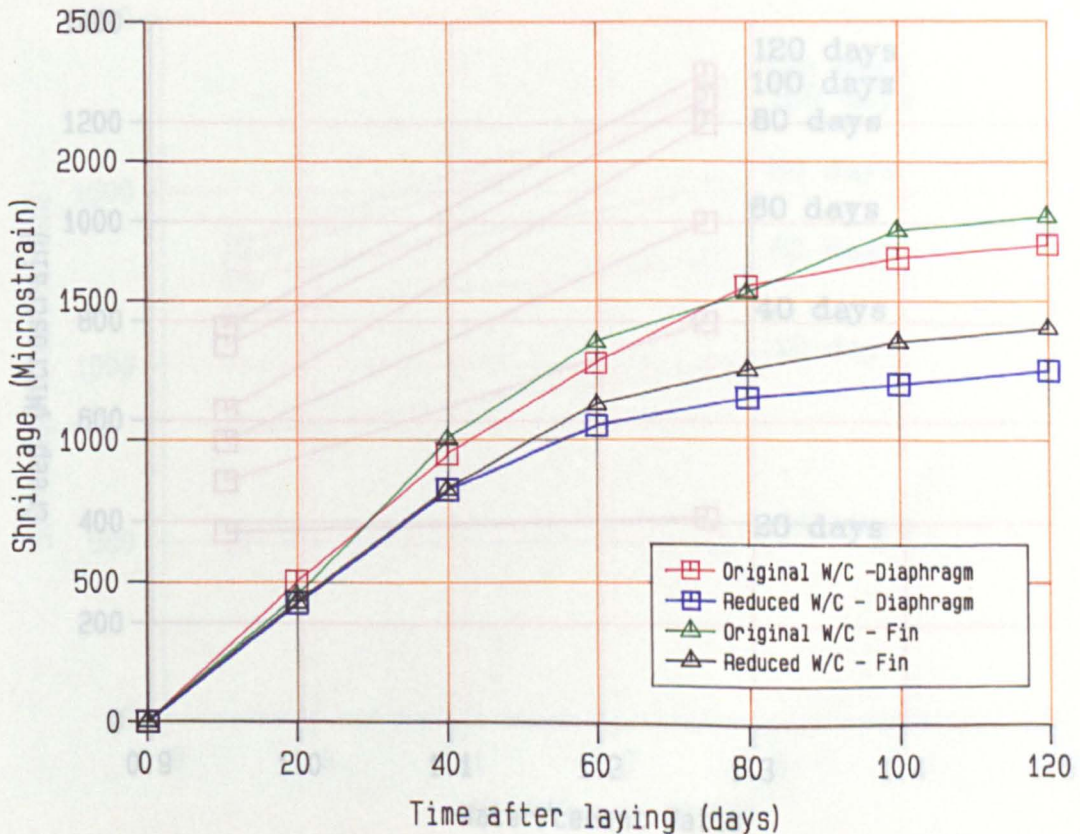


Fig. 7.45 Shrinkage-time Curve of Mortar with Original and Reduced Water/cement Ratio

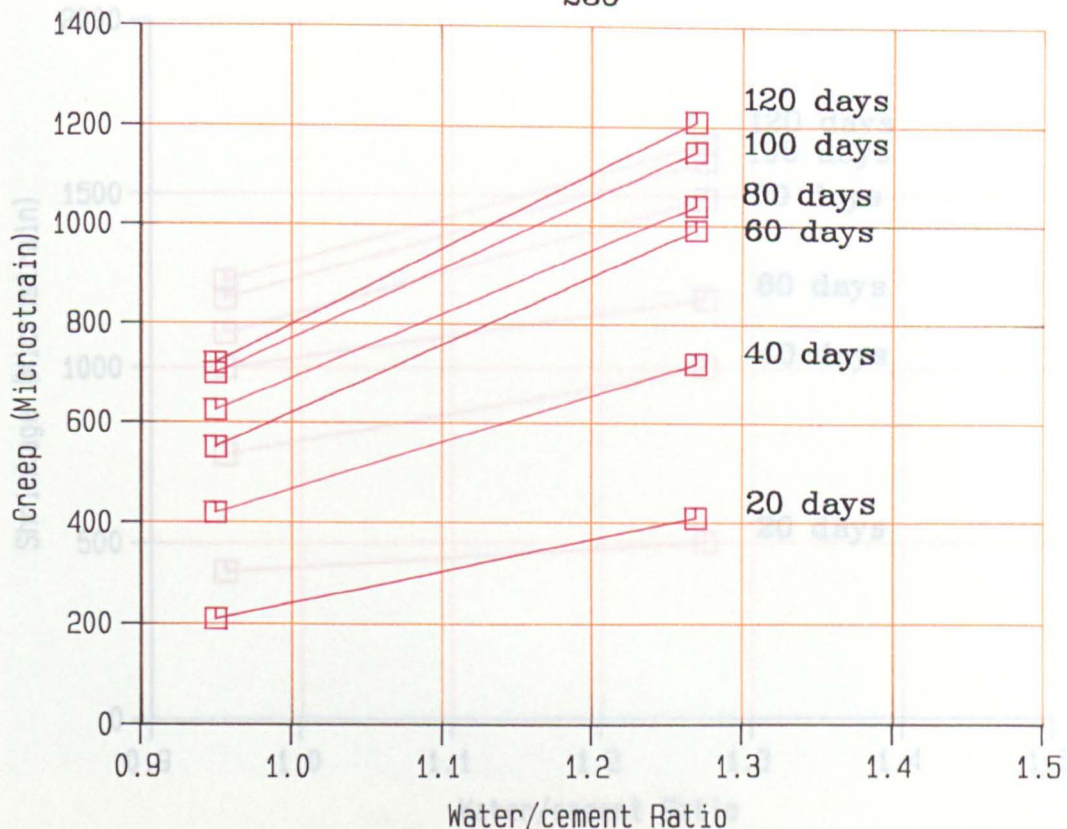


Fig. 7.46 Creep-water/cement Ratio of Mortar Prisms for Calcium Silicate Diaphragm Wall

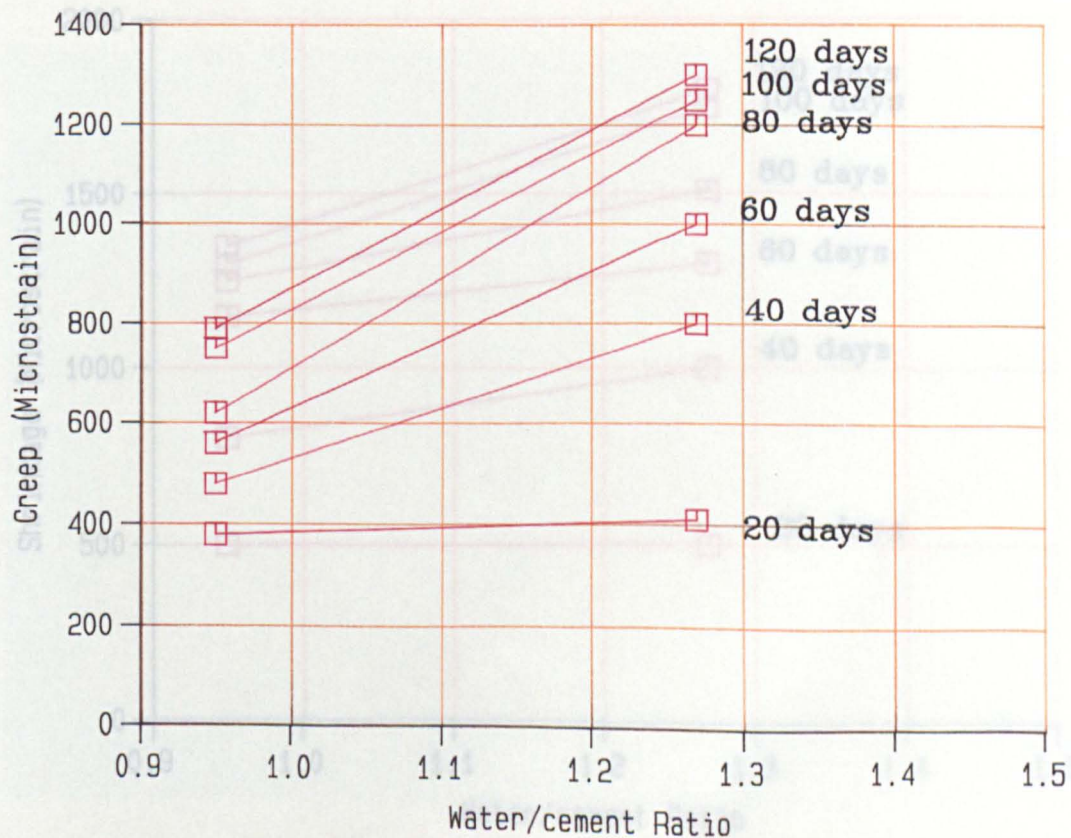


Fig. 7.47 Creep-water/cement Ratio of Mortar Prisms for Calcium Silicate Fin Wall

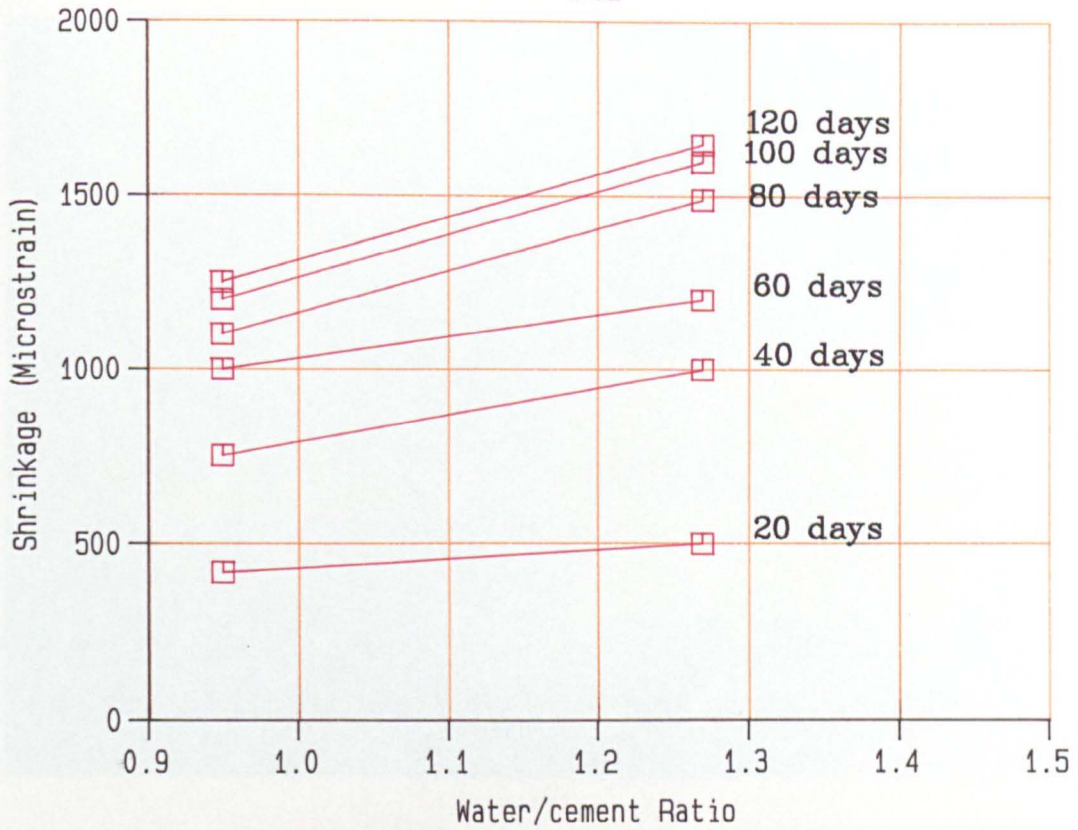


Fig. 7.48 Shrinkage–water/cement Ratio of Mortar Prisms for Calcium Silicate Diaphragm Wall

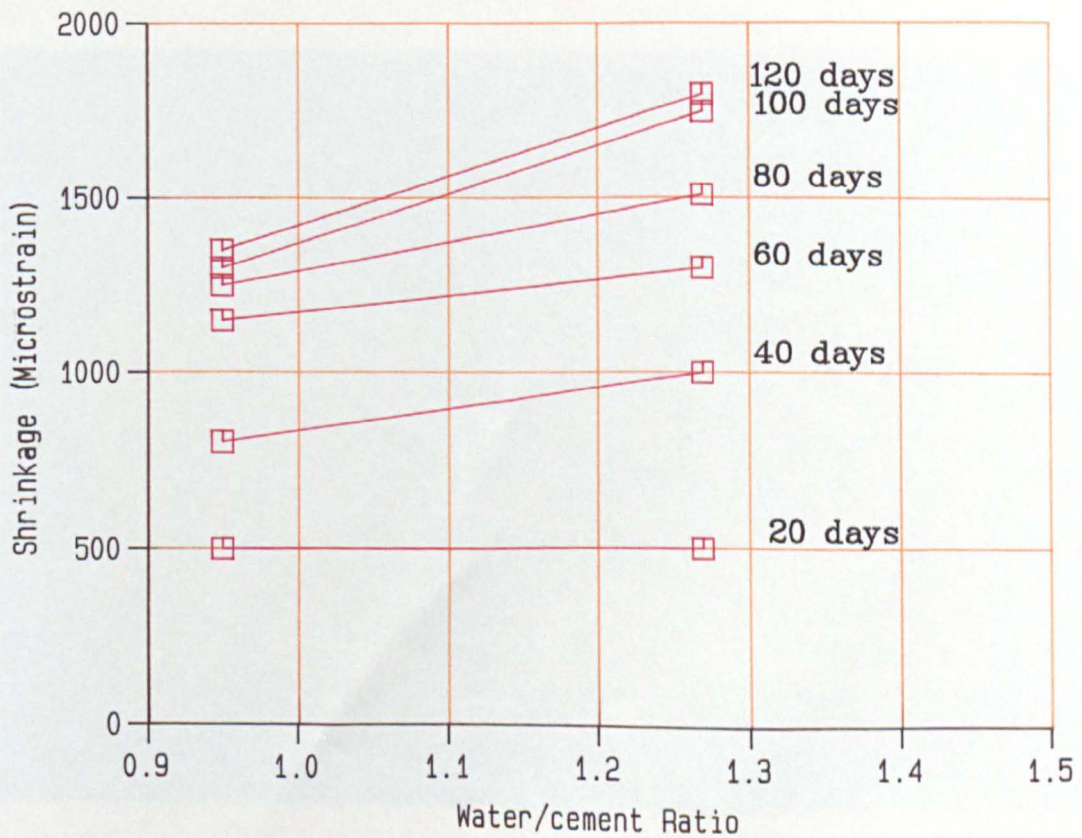


Fig. 7.49 Shrinkage–water/cement Ratio of Mortar Prisms for Calcium Silicate Fin Wall

**Plate 7.1 Two-course Clay and Calcium Silicate Masonry
for Modified Water Absorption Test**

**Plate 7.2 Concrete Block Unit for Modified Water
Absorption Test**

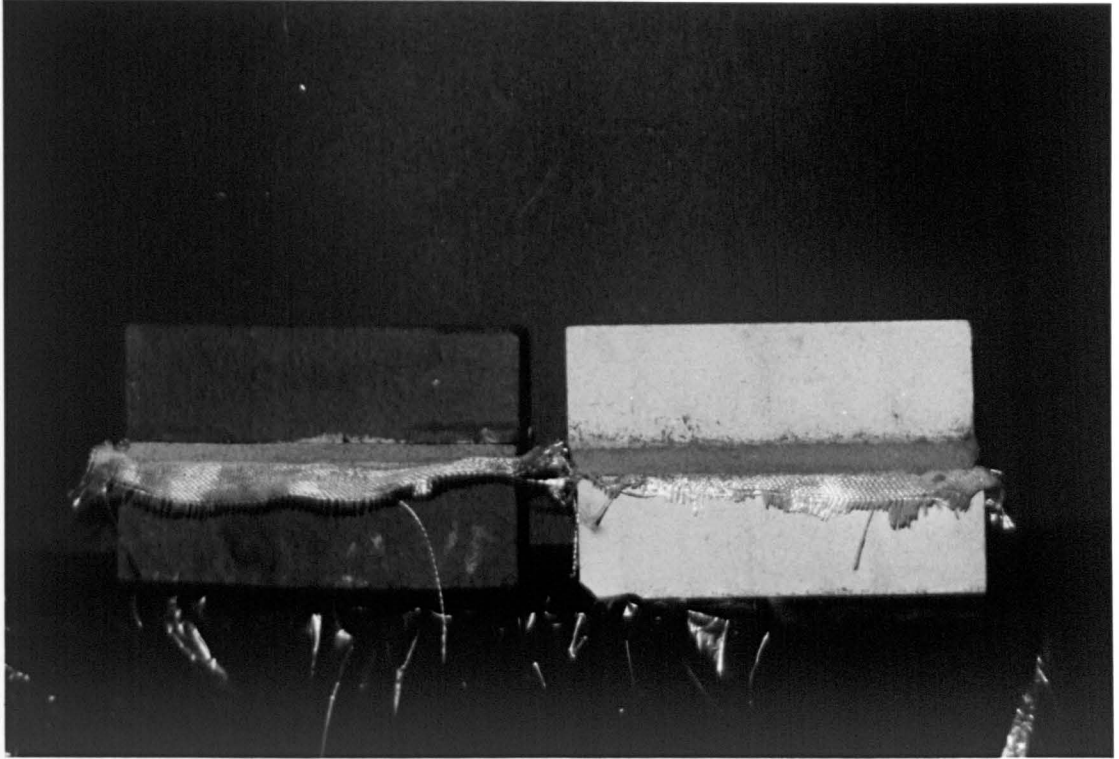


PLATE 7.1

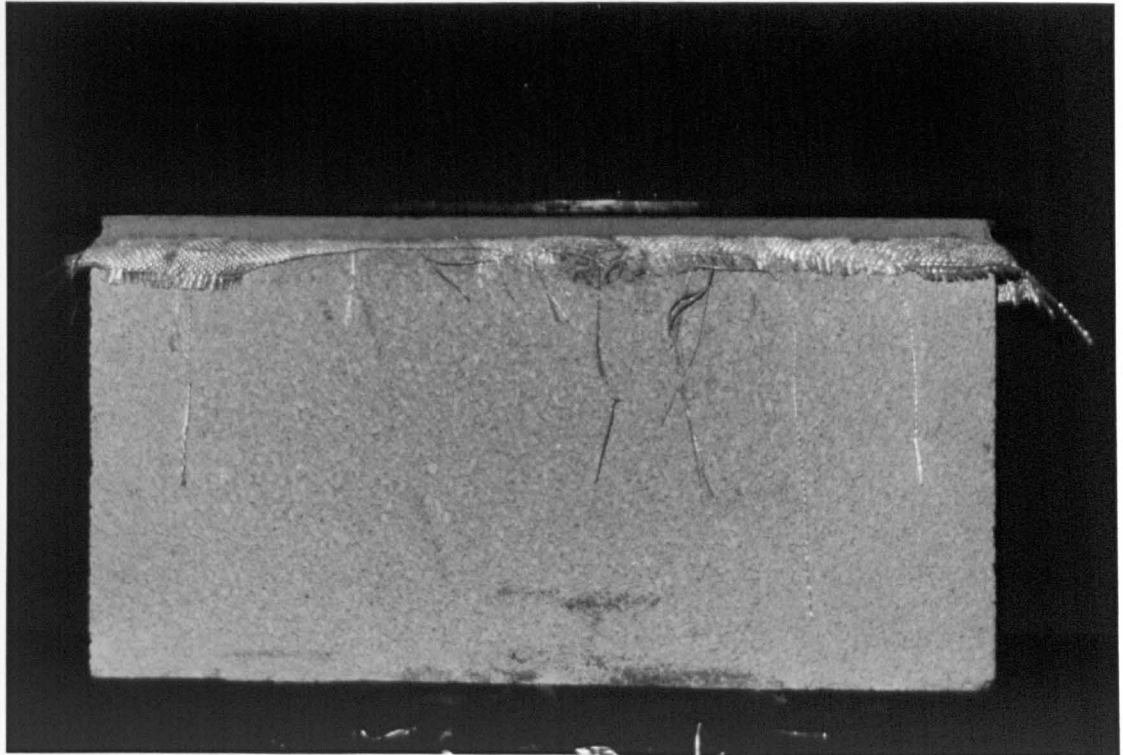


PLATE 7.2

**Plate 7.3 Three-course Clay and Calcium Silicate Masonry
for Shrinkage Test**

**Plate 7.4 Two-course Concrete Block Masonry for
Shrinkage Test**

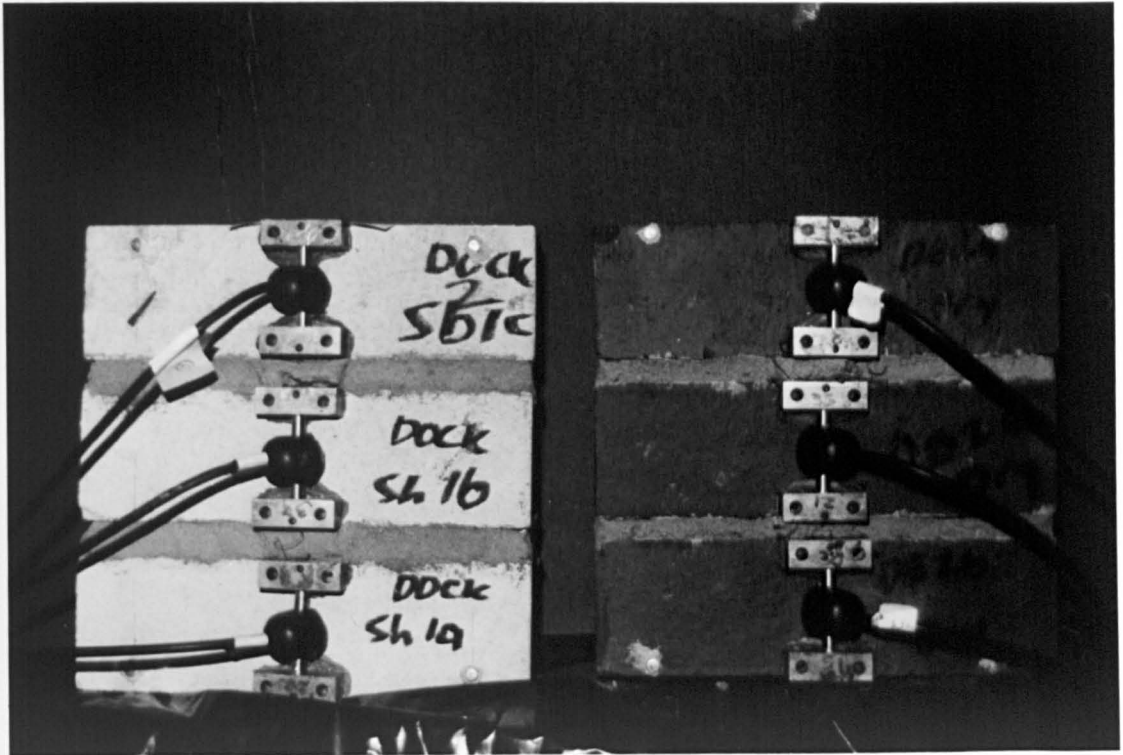


PLATE 7.3

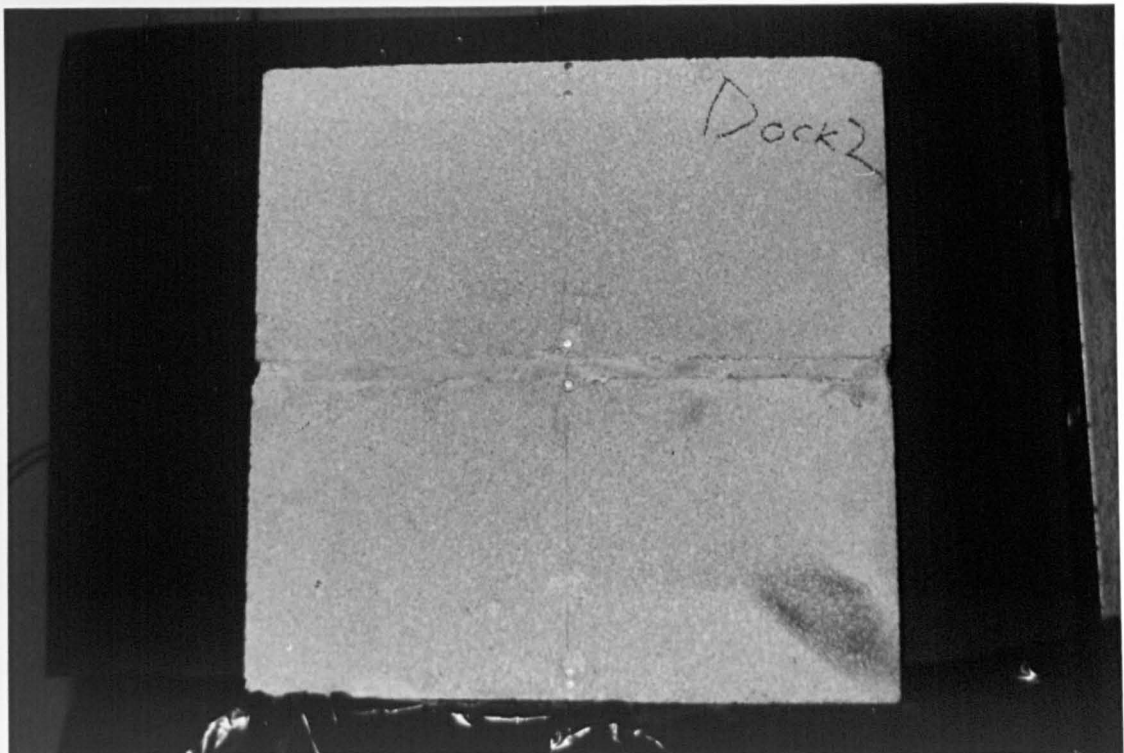


PLATE 7.4

CHAPTER 8

CONCLUSIONS AND RECOMMENDATIONS FOR FURTHER RESEARCH

8.1 Introduction

This chapter compares the experimental and analytical findings for time-dependent deformations in prestressed masonry. The investigation was carried out on post-tensioned clay, calcium silicate and concrete block walls. For each type of masonry three diaphragm and three fin walls were built to determine prestress loss (decreasing load), creep (constant load) and shrinkage (zero load). The eighteen full scale walls were constructed with grade (ii) mortar.

A composite model for masonry, based on Brooks (1987a), was incorporated into methods developed for prestressed concrete to predict prestress loss for post-tensioned masonry. In order to validate the composite model, short and long-term tests were carried out on unbonded masonry units and mortar prisms.

The implications of high water absorption units, laid dry, on the prediction of deformation of masonry were also investigated. Based on the findings from this investigation, suggestions for future research are presented.

8.2 Prestress loss

- 1- Prestress loss was affected by the shape and the size of the cross-section which was expressed in terms of the volume/exposed surface ratio (V/S).

Prestress loss decreased with an increased in the V/S ratio, and diaphragm walls exhibited a lower prestress loss than fin walls.

- 2- Prestressed masonry members constructed from high compressive strength units exhibited a lower prestress loss.
- 3- The diaphragm and fin calcium silicate masonry walls exhibited a higher prestress loss than the concrete block masonry walls which had a higher prestress loss than the clay walls.
- 4- In all the masonry studied in this investigation, most of the prestress loss in the post-tensioned masonry walls took place during the first 60 days after loading. After 60 days of loading, prestress loss continued at a decreasing rate.
- 5- Post-tensioned clay, calcium silicate and concrete block diaphragm walls exhibited prestress loss of 10%, 17% and 15 %, respectively (Figs. 5.12 to 5.14), after a period of 120 days. The corresponding prestress loss of clay, calcium silicate and concrete block fin walls were 12.5%, 20% and 17.5%, respectively.
- 6- Based on extrapolation of test data, the total ultimate prestress loss of the clay, calcium silicate and concrete block diaphragm walls were 14.5%, 21.2% and 22.3%, respectively. As for the clay, calcium silicate and concrete block fin walls, the total ultimate prestress loss were 16.5%, 24% and 24.8%, respectively

7- In the clay, calcium silicate and concrete block fin walls, the ultimate prestress loss due to creep was 6.8%, 8.0% and 8.7%, respectively (Table 5.8). As for the clay, calcium silicate and concrete block diaphragm walls, the the ultimate prestress loss due to creep was 6.0%, 7.2% and 7.5%, respectively.

The ultimate prestress loss due to shrinkage in the clay, calcium silicate and concrete block fin walls was 5.2%, 11.5% and 11.6%, respectively (Table 5.8). The corresponding prestress loss due to shrinkage in the clay, calcium silicate and concrete block diaphragm walls was 5%, 10.5% and 11.3 %, respectively. However, prestress loss due relaxation was found to be about 3.5 to 4.5% (Table 5.8).

8.3 Creep and shrinkage

1- As for prestress loss, creep and shrinkage of the masonry walls were found to be affected by the shape and the size of the cross-section which was expressed in terms of the V/S ratio. Creep and shrinkage of the masonry decreased with an increase in the V/S ratio and diaphragm walls exhibited a lower creep and shrinkage than fin walls .

2- During the first 120 days, the diaphragm and fin walls constructed from clay units exhibited a lower specific creep than that of walls constructed from calcium silicate and concrete block units. However, the specific creep of the calcium silicate diaphragm and fin walls exhibited a higher specific creep than that of concrete block walls (Figs. 5.5 and 5.6).

As for the shrinkage, similar trends as in the specific creep were observed (Figs. 5.10 and 5.11).

- 3- The estimated ultimate creep coefficients from extrapolation of experimental results of the clay, calcium silicate and concrete block diaphragm walls investigated in this research were 1.49, 2.2 and 2.34, respectively (Table 5.3). The corresponding estimated ultimate creep coefficients of the clay, calcium silicate and concrete block fin walls were 1.55, 2.40 and 2.53, respectively.
- 4- Based on extrapolation of test data, the estimated ultimate shrinkage of the clay, calcium silicate and concrete block diaphragm walls were 179×10^{-6} , 400×10^{-6} and 500×10^{-6} , respectively (Table 5.4). As for the clay, calcium silicate and concrete block fin walls, the estimated ultimate shrinkage were 204×10^{-6} , 418×10^{-6} and 516×10^{-6} , respectively.

8.4 Composite modelling

- 1- An initial application of the composite model developed by Brooks (1987a) to predict the deformation of masonry constructed with dry units resulted in overestimations of creep by 25% and shrinkage by 35% (Figs. 6.1 to 6.7). When allowances were made for the unit water absorption, the composite model gave creep and shrinkage satisfactory predictions (see Section 8.4 -4).
- 2- Shrinkage of the mortar bed joint in masonry (calcium silicate and concrete block) built with units laid dry exhibited only about 20-30% of the shrinkage of unbonded mortar prisms (Figs. 7.15 and 7.16). However, the shrinkage of the mortar bed joint in masonry built with docked units was within (\pm) 15% of the shrinkage of an unbonded mortar prism which was partly sealed to the V/S ratio of the the masonry mortar joints.

- 3- In Chapter 7 a method has been developed to allow for unit water absorption on creep and shrinkage of unbonded unit and mortar specimens. The method gives factors for the change in creep and shrinkage in terms of a standard water absorption. For the units laid dry, creep and shrinkage enlargement factors occur, while creep and shrinkage reduction factors occur for the mortar joints.
- 4- When adjusted creep and shrinkage data for the unbonded mortar prisms and masonry units were incorporated into the composite model, the corresponding creep and shrinkage of the masonry walls were predicted satisfactorily i.e within $\pm 5\%$ in both cases (Figs. 7.26 to 7.37).
- 5- When the composite model (with adjusted creep and shrinkage data to allow for unit water absorption) was incorporated into existing methods developed for predicting loss in prestressed concrete, the post-tensioned masonry loss ($\pm 10\%$) were predicted satisfactorily (Figs. 7.39 to 7.43) as described below.

8.5 Comparison between the ultimate values obtained by extrapolation of the experimental results and prediction methods

- 1- BS 5628: Part 2 (1985) underestimates the modulus of elasticity (Table 6.1) of clay, calcium silicate and concrete block walls by up to 17%, 47% and 32%, respectively. Shrinkage of the calcium silicate walls is overestimated by up to 25% and underestimated by up to 3% for concrete block walls (Table 6.5); although the Standard implies that shrinkage of clay brickwork is negligible, a shrinkage was measured between $147 - 184 \times 10^{-6}$. Although creep was predicted satisfactorily ($\pm 20\%$) in clay and calcium silicate

brickwork, it was found to overestimate creep by up to 89% in the concrete block masonry (Table 6.3).

BS 5628: Part 2 (1985) predicted prestress loss (Table 6.6) reasonably well (12 to 33%) in calcium silicate and concrete block masonry but for clay brickwork the prestress loss was generally found to be underestimated (38%).

- 2- ACI-530 (1990) predicts modulus of elasticity reasonably well (+ 15%) for clay brickwork and for concrete blockwork (Table 6.1). The Code predicts creep reasonably well (+22%) in the clay brickwork walls but not in the concrete block walls that is with an overestimation of at least 88% (Table 6.3). As in the BS 5628, the ACI-530 (1990) also implies that clay brickwork does not undergo shrinkage although a shrinkage between $147 - 184 \times 10^{-6}$ was measured in this research. For the concrete block walls, the Code overestimates shrinkage by 24%. When the Code creep and shrinkage values were used to predict prestress loss in clay brickwork, the Code predicts a gain of 3.5% as compared to the average measured loss of 15.5% (Table 6.6). In the case of concrete blockwork the Code predicts prestress loss within 25%.

- 3- Eurocode No 6 (1988) predicts the modulus of elasticity reasonably well for clay ($\pm 5\%$) and concrete block masonry (- 24%) but not for the calcium silicate (- 41%) brickwork (Table 6.1). The Code also predicts creep reasonably well ($\pm 10\%$) for clay and calcium silicate brickwork walls but overestimates for concrete blockwork by up to 69% (Table 6.3). As for the shrinkage, the Code underestimates by 40% to 60% in all the masonry walls (Table 6.5). When the Code values for creep and shrinkage were used to predict prestress loss for all the walls, estimates were found to be reasonable i.e within 33% (Table 6.6).

- 4- The Lenczner method (1986) predicts modulus of elasticity and creep satisfactorily for clay brickwork (+ 22%). The method was developed specifically for clay masonry and it was found to underestimate the elastic modulus and creep of calcium silicate and concrete block masonry by 68% (Table 6.2). However, the method predicts creep of calcium silicate brickwork and concrete blockwork reasonably well (- 20%) when the actual elastic strains were used (Table 6.4). Loss of prestress for the clay brickwork was predicted reasonably well (+ 5%), while loss of prestress for calcium silicate brickwork and concrete blockwork was underestimated by up to 24% (Table 6.8).

- 5- The composite model (Brooks method 1987a) satisfactorily predicts modulus of elasticity ($\pm 10\%$) of clay and calcium silicate brickwork but for concrete blockwork (- 30%) it was underestimated (Table 6.2). This was due to the moisture movement from the mortar joint to the high water absorption block that tends to reduce the elastic modulus of the unit. Prediction of creep, shrinkage and prestress loss are referred to in Section 8.4

- 6- Using estimated (from composite modelling) creep and shrinkage, Dilger method (1983) predicts prestress loss more accurately (+ 30%) than Abeles (1966) which overestimated by up to 46% (Figs. 6.7 to 6.12). Even when the measured creep, shrinkage and relaxation were used to predict prestress loss for all the walls tested, the Dilger method ($\pm 10\%$) predicts more accurately than Abeles method ($\pm 20\%$)

- 7- The Tatsa method (1973), specifically developed for concrete block masonry (Table 6.8), overestimates prestress loss by 13% and 5% for the diaphragm and fin walls, respectively.

8.6 Suggestions for future research

- 1- Investigations into creep, shrinkage and prestress loss of other types of masonry with different types of units and mortar should be carried out to cover the large range of masonry products available.
- 2- The effect of incremental prestressing at different ages on prestress loss of post-tensioned masonry should be investigated, particularly the application of post-tensioning in stages from an early age. In post-tensioned prestressed concrete, this technique is used to minimise losses due to creep and shrinkage.
- 3- Measurements of prestress loss on full scale retaining walls exposed to severe weather conditions (relative humidity, temperature, freezing, thawing and diurnal effects) need to be carried out. The severe weather conditions will affect long-term creep, shrinkage and prestress loss (gain/loss). In extreme conditions, diurnal effects could sometimes reduce the level of prestress particularly in low strength units where creep and shrinkage are greater.
- 4- The effect of non-prestressing steel on prestress loss of post-tensioned masonry needs to be investigated. Some prestressed masonry retaining walls use high yield non-prestressing steel for additional reinforcement in perforated bricks.

- 5- The effect of unit water absorption units, laid dry and docked, on elasticity, creep and moisture movement strain of masonry should be studied on other types of masonry so that 'standard' adjustment factors can be established for the unbonded properties required by the composite model approach. The modified water absorption test developed in this investigation (Chapter 7) can be used for this purpose.

- 6- Further tests on creep, shrinkage and prestress loss need to be carried ^{out} for a longer duration, especially with calcium silicate brickwork which exhibited a higher deformation rate after prolonged loading than clay brickwork and concrete blockwork.

REFERENCES

REFERENCES

1. **Abdullah C. S.** 1989 *Influence of geometry on creep and shrinkage of clay, calcium silicate bricks and concrete blockwork*. Phd Thesis, University of Leeds, 291 pp.
2. **Abeles P. W.** 1966 *Introduction to prestressed concrete*, vol. 2, Concrete Publications Limited , London .
3. **ACI-530-88/ASCE-5-88.** 1989 *Building Code Requirements for Concrete Masonry Structures*. ACI Manual of Concrete Practice Part 5.
4. **Al-Khaja W. A.** 1986 *Time-dependent Losses in Post-tensioned Prestressed Concrete*, Phd Thesis, University of Leeds, 317 pp.
5. **Ameny P, Loov R. E and Shrive N. G.** 1983 Prediction of elastic behaviour of masonry. *The Int. J. Masonry Construction*, Vol. 3, No. 1 pp 1-9.
6. **Ameny P, Loov R. E and Shrive N. G.** 1984 Models for long term deformation of brick. *Masonry Int.* Vol. 1, pp 27-28.
7. **Amjad M. A.** 1990 Elasticity and strength of masonry, units and mortar, Phd Theses, University of Leeds, 253 pp.
8. **Baker L. R. and Jessop E. L.** 1982 Moisture movement in concrete masonry : a review. *The International Journal of Masonry Construction* 2(2) pp 75-82.
9. **Brick Development Association** 1988 *BDA Design Note 10*. Designing for Movement in Brickwork, 11 pp.
10. **Bingel P. R.** 1984 Moisture Movement in Brickwork and Blockwork. MSc. Thesis, Dept. of Civil Eng., Leeds University, 160 pp.

11. **Branson D. E.** 1977 *Deformation of Concrete Structures*, McGraw Hill, 546 pp.
12. **British Standard of Institution:** BS 187: 1978. *Specifications for calcium silicate bricks*, BSI London.
13. **British Standard of Institution:** BS 882: 1992 1201. *Aggregates from natural sources for concrete* , BSI London.
14. **British Standard of Institution:** BS 915: 1972 *High Alumina cement*, BSI London.
15. **British Standard of Institution:** BS 1200: 1976. *Building sands from natural sources*, BSI London 1976.
16. **British Standard of Institution:** BS 1881; Part 3: 1970. *Methods of testing concrete*, BSI London 1970.
17. **British Standard of Institution:**BS 3921: 1985. *Clay bricks and blocks*, BSI London 32 pp.
18. **British Standard of Institution:** 1980 BS 4486 *Specification for hot rolled and hot rolled and processed high tensile alloy steel bars for the prestressing of concrete* BSI, London.
19. **British Standard of Institution:** BS 4551: 1980. *Methods of testing mortars, screeds and plasters*. BSI London 1980.
20. **British Standard of Institution:** 1985 BS 5628 : Part 2:1985. *Structural Use of Reinforced and Prestressed Masonry*. BSI .

21. **British Standard of Institution:** 1985 BS 5628 : Part 3:1985. *Materials and Components, Design and Workmanship* BSI .
22. **British Standard of Institution:** BS 6073: Part 1: 1981:..*Specifications for precast concrete masonry units*, BSI London
23. **British Standard of Institution:** 1985 BS 8110 : Part :1985, *Structural use of concrete*, BSI London.
24. **Brooks J. J.**1986a Composite Model for Predicting Elastic and Long term Movements in Brickwork Walls. *Proc. Brit. Mas. Soc.* 1, pp 20-23.
25. **Brooks J. J.** 1986b Time-Dependent Behaviour of Calcium Silicate and Fletton Clay Brickwork Walls. *British Masonry Society Proc.* No. 1, pp 17-19.
26. **Brooks J. J.** 1987a Composite Modelling of Elasticity and Creep of Masonry. *Civil Engineering Dept. Report*, University of Leeds, 24 pp.
27. **Brooks J. J.** 1987b Composite Modelling of Moisture and Thermal Movement Masonry. *Civil Engineering Dept. Report*, University of Leeds, 21 pp.
28. **Brooks J. J.** 1990 Composite Modelling of Masonry Deformation. '*Material and Structures* , RILEM, PARIS, pp 241-251.
29. **Brooks J.J. and Abdullah C. S.** 1988 Composite Modelling Prediction of the geometry effect on Creep and Shrinkage of Clay Brickwork. *Proc. 8IBMAC.* Ed. J.W. deCourcy, London Elsevier Applied Science, pp 316-323.
30. **Brooks J. J. and Abdullah C. S.** 1990a Creep and drying shrinkage of concrete blockwork. *Magazine of Concrete Research*, 42 No. 150, March, pp 15-22.

31. **Brooks J. J. and Abdullah C. S.** 1990b Composite Modelling of the geometry influence on creep and shrinkage of calcium Silicate Brickwork. *British Masonry Society Proc.* No. 4, pp 36-38.
32. **Brooks J. J. and Forth J. P.** 1992a Influence of Unit Type on Creep and Shrinkage of Single Leaf Clay Brickwork, *International Masonry Conference (3rd), London, October 1992*
33. **Brooks J.J. and Forth J.P.** 1992b Effect cross-section geometry on long-term deformation of clay of brickwork, *International Masonry Conference (3rd), London, October 1992*
34. **Brooks J.J. and Bingel P. R.** 1985 Influence of size on moisture movements in unrestrained masonry, *Masonry International*, No 4 March, pp 36-44.
35. **Curtin W. G., Shaw G. and Beck J. K.** 1982a *Design of Reinforced and Prestressed Masonry* . Published by Thomas Telford London.
36. **Curtin W. G., Shaw G., Beck J. K and Bray W.** 1982b *Structural Masonry Designers' Manual*. Granada Publishing Limited.
37. **Curtin, W.G.** 1987 Site Testing and Lab Research fo the Design Development of Prestressed Brickwork. *Proc. Ints. Civil Engineer Symp. Practical Design of Mas. Structures*. London 23-24 Sept., pp 237-253.
38. **Curtin W. G., Shaw G., Beck J. K and Howard J.** 1989 *Design of Post-tensioned Brickwork*. Brickwork Development Association, 72 pp.

39. **Curtin, W.G.** 1986 An Investigation of Structural Behavior of Post-tensioned Brick Diaphragm Walls. *The Structural Engineer* Vol. 64B: Number 4 Dec., pp 77-84.
40. **Curtin W.G and Howard J.** 1991 Research on Prestressed Cantilever Diaphragm walls. *The Structural Engineering* 19 March, Vol. 69 No 6, pp 105-112.
41. **Eurocode 6** 1988 Common Unified Rules for Masonry Structure, Commission of the European Communities.
42. **Foster D.** 1991 Development and Applications of Reinforced and Prestressed masonry. *Reinforced and Prestressed Masonry*. Published by Construction Series, First Edition, pp 1-20.
43. **Foster D. and Johnson G.D.** 1982 Design for movement in clay brickwork in the U.K *Proc. of the Brit. Ceramic Soc.* NO 30(7), pp 1-12.
44. **Foster D.** 1970 Design and construction of prestressed brickwork water tank in West HWH, Speed KH (eds) *Proc. 2nd Int. Brick Mas. Conference*. Stoke-on-Trent. April , pp 287-294.
45. **Garrity S. W.** 1993 *Masonry Earth Retaining Walls*, University of Bradford, pp 1.1-3.60.
46. **Ghali A. and Favre R.** 1986 *Concrete Structures: Stresses and Deformations.*, Chapman and Hall, 352 pp
47. **Glodowski R. J. and Lorenzetti J. J.** 1972 A method for predicting Prestress losses in Prestressed Concrete Structure. *Journal of PCI*, Vol. 17, No 2, March-April.

48. **Hansen T. C. and Mattock A. H.** 1966 *Influence of size and shape of member on shrinkage and creep of concrete*, ACI Journal, Proceeding 63, 2, Feb., pp 267-289.
49. **Harvey R. J and Lenczner D** 1993 *Creep prestress losses in concrete masonry*, Proc. of the 5th International RILEM Symposium, Barcelona
50. **Hendry A. W., Sinha B. P. and Davies S.R.** 1987 *Load Bearing Brickwork Design*. 2nd edition by Ellis Horwood Series in Civil Engineering, 185pp.
51. **Jessop E L.** 1980 Moisture, thermal elastic and creep properties in masonry : State of the art report. In Suter G T, Keller, H(eds) *Proceedings of the 2nd Canadian Masonry Symposium*, Ottawa June, pp 505-520.
52. **Johnson G. D.** 1984 *Creep and shrinkage in stresses clay brickwork*. Phd Thesis, University of Wales Institute of Science and Technology, 291 pp.
53. **Lenczner D.** 1970 Creep in Brickwork. *Proc. 2nd International Conf. on Brick Masonry*, 8IBMAC, Stoke-on-Trent, Brit. Ceramic Society, pp 44-49.
54. **Lenczner D.** 1972 *Elements of loadbearing Brickwork*, Pergamon Press, pp 113.
55. **Lenczner D.** 1978a The Effect of Strength and Geometry on the Elastic and Creep Properties of Masonry Members, *Proc. North American Mas. Conf. University of Colarado-Boulder* , pp 23.1-23.15.
56. **Lenczner D.** 1978b Creep in Brickwork and Blockwork in Cavity Walls and Piers, *Proc. British Ceramic Society, Loadbearing Brickwork* (6), No 27, pp 53-66.

57. **Lenczner D.** 1981 Brickwork: a guide to creep. *The International Journal of Masonry Construction*, 1, No. 4, pp 127-133.
58. **Lenczner D.** 1985 The loss of prestress in Post-Tensioned Brick Masonry Members. *Mas. Int.*, No. 5, July, pp 9-12.
59. **Lenczner D.** 1986a Creep and Prestress Losses in Brick Masonry. *The Structural Engineer* Vol. 64B/No. 3 Sep., pp 56-62.
60. **Lenczner D.** 1986b In-Situ Measurement of Creep Movement in a Brick Masonry Tower Block. *Mas. International* Vol. 8, pp 12-20.
61. **Lenczner D. and Davis P.** 1988 Creep Loss of Prestress in Post-Tensioned Brickwork Walls with Previous Stress History. *Proc. of the Brit. Mas.*, No. 2 Sep., pp 5-7.
62. **Lenczner D** 1988 Creep in Brickwork Walls at High and Low Stress/Strength Ratio, Proc. 8th IBMAC, Dublin, pp 324 -333.
63. **Lenczner D.** 1990 Creep in Brickwork I-section Walls and Solid Piers. *Proc. of Brit. Masonry*, No. 4, pp 34-35.
64. **Magura D. D, Sozen M. A and Siess C. P.** 1964 A study of stress relaxation in prestressed concrete. *Journal of the PCI*, Vol. 9, No 2 April , pp 13-57.
65. **Neville A. M. and Brooks J. J.** 1993 *Concrete Technology*. Longman Scientific & Technical, 438 pp.
66. **Neville A. M., Dilger W. and Brooks J. J.** 1983 *Creep of plain and Structural Concrete*. Construction Press, 361 pp.

67. **PAFEC Ltd** 1978 *PAFEC75 Theory and Results*, Nottingham.
68. **Prestress Concrete Institute** 1975 *Committee on Prestress Losses*, PCI Journal, vol. 20, no. 4, Jul/August, pp 108-126.
69. **Phipps M. E.** 1991 Prestressed masonry walls. *Reinforced and Prestressed Masonry*. Concrete Design and Construction Series, pp 125-159.
70. **Phipps M. E and Montague T. I.** 1976 The Design of Prestressed Concrete Blockwork Diaphragm Walls. *Aggregate Concrete Block Association* . 21 pp.
71. **Roberts J. J., Edgell G. J. and Rathone A. J.** 1986 *Handbook to BS 5628: Part 2*, Viewpoint Publications, 197 pp
72. **Ross A. D.** 1937 Concrete Creep Data, *The Structural Engineer*, 15, N0.8, pp 314 -326.
73. **Shrive N. G.** 1988a Post-tensioned Masonry - Status and Prospects. *Annual Conference*, Calgary, Canada, pp 679-696.
74. **Shrive N. G.** 1988b Effects of Time Dependent Movements in Composite and Post-tensioned Masonry, *Masonry International*, Vol. 2, No 1, pp 25-29.
75. **Shrive N. G and England G. L.** 1981 Elastic, Creep and Shrinkage Behaviour of Masonry. *Int. Journal of Masonry Construction*, Vol. 1, No 3, pp 103-109.
76. **Shrive N. G.** 1990 Materials and material properties. *Reinforced and Prestressed Masonry*. Concrete Design and Construction Series, pp 25-51.
77. **Sutherland R. J. M.** (1982) *The future for prestressed masonry*. 6th I.B.M.O Sixth International Brick Masonry Conference, pp 582-593.

78. **Tatsa E., Yishai O. and Levy M.** 1973 Loss of Steel Stresses in Prestressed Concrete Blockwork Walls. *The Structural Engineer*, Vol. 51 No 5 May, pp 172-182.
79. **Taneja R., Shrive N. G and Huizer A.** 1986 Losses of Prestressed in Post-tensioned Hollow Masonry Walls, *Proc. ASCE, Advances in Analysis of Masonry Structures*, pp 79-93.
- 80 **VSL International.** *Post-tensioned Masonry Structure*. Published by VSL International Ltd, Berne Switzerland, 34 pp.
81. **Warren D. and Lenczner D.** 1981 A Creep-time Function for Single-leaf Brickwork Walls, *The International Journal of Masonry Construction* Vol. 2 (1)
82. **Wass R. J. and Turner D. J.** 1969 A Prestressed Clay Masonry (Jonhson) ed; *Designing, Engineering and constructing with masonry Products* .Gulf, Houston, Texas, pp 200-209.

APPENDICES

APPENDIX A

A.1 - Prestress Loss due to creep, shrinkage and thermal effect

Consider Class B Engineering Clay Bricks with compressive strength of 70 MPa, with grade (ii) mortar.

Characteristic strength (f_k) = 15.1 MPa (BS 5628 Part 2 1985)

Elastic modulus of masonry (E_m) = $0.9 f_k$ GPa = 13.6 GPa

Assume working stress of 3 MPa,

therefore the elastic strain = $3 \text{ MPa} / 13.6 \text{ GPa}$
 $= 221 \times 10^{-6}$

Creep (BS 5628 Part 2 1985) = $1.5 \times$ elastic strain
 $= 1.5 \times 221 \times 10^{-6} = 332 \times 10^{-6}$

Neglect shrinkage (BS 5628 Part 2 1985)

Thermal (-20 to 65 °C) = Coeff. of thermal (BDA 1988) \times range of temperature
 $= 8 \times 10^{-6}/^\circ\text{C} \times 85 \text{ }^\circ\text{C} = 680 \times 10^{-6}$

Ultimate tensile stress of Macalloy bar = 1030 MPa

Working stress of Macalloy bar = $0.7 \times 1030 \text{ MPa} /$ factor safety of prestressing steel
 $= 0.7 \times 1030 \text{ MPa} / 1.15$
 $= 627 \text{ MPa}$

Prestress loss due to creep = $\frac{(\text{Creep} \times \text{Elastic modulus of steel})}{\text{Working stress of steel}}$

$$= \frac{332 \times 10^{-6} \times 165 \times 10^3}{627}$$

$$= \frac{54.78}{627}$$

$$= 8.73 \%$$

No prestress loss due to shrinkage, since clay brickwork is assumed to undergo expansion instead of shrinkage.

$$\begin{aligned}
 \text{Prestress loss due to thermal effect} &= \frac{(\text{thermal strain} \times \text{Elastic modulus of steel})}{\text{Working stress of steel}} \\
 &= \frac{680 \times 10^{-6} \times 165 \times 10^3}{627} \\
 &= \frac{112.2}{627} \\
 &= 17.89\%
 \end{aligned}$$

A.2 - Determination of working stress

$$\text{Working stress} = f_k / \gamma_m$$

where f_k = characteristic compressive strength of brickwork

$$\gamma_m = \text{partial factor of safety for material} = 2.3$$

From Fig. 1 Table 2 BS5628:Part 2: 1985, for mortar grade (ii) with Class B Engineering (clay), Class 4 (calcium silicate) and dense aggregate concrete blocks, the characteristic compressive strengths are 18.2, 7.9 and 10.6 MPa, respectively.

Thus the working stresses of the clay, calcium silicate and dense aggregate concrete masonry are 7.9, 3.4 and 4.6 MPa, respectively.

Appendix B

Measured Strains of Masonry at Various Positions

Table B1 - Clay Wall

(a) Diaphragm wall

Time in days	Average Overall Strain (10^{-6}) (Creep Wall)					Average Moisture Strain (10^{-6}) (Moisture Strain Wall)					
	*	A	B	C	D	Ave.	A	B	C	D	Ave.
0	0	0	0	0	0	0	0	0	0	0	0
20	134	161	175	157	157	157	46	41	48	44	45
40	206	239	245	214	226	226	78	79	81	76	78
60	266	294	294	257	278	278	108	112	121	90	108
80	317	337	325	286	317	317	131	136	138	108	128
100	355	366	351	304	344	344	150	148	149	115	140
120	376	387	368	320	363	363	156	158	153	120	147

(b) Fin wall

Time in days	Average Overall Strain (10^{-6}) (Creep Wall)							Average Moisture Strain (10^{-6}) (Moisture Strain Wall)							
	*	A	B	C	D	E	F	Ave.	A	B	C	D	E	F	Ave.
0	0	0	0	0	0	0	0	0	0	0	0	0	0	0	0
20	201	207	214	241	259	216	223	223	81	72	74	79	90	93	82
40	276	235	285	310	330	310	290	290	120	110	90	110	115	135	110
60	327	340	381	383	407	363	367	367	152	145	142	148	147	148	149
80	388	363	415	422	433	385	410	410	183	150	146	162	165	168	163
100	410	402	439	440	454	412	426	426	197	172	159	173	180	178	177
120	430	420	452	464	468	428	444	444	207	182	165	179	185	185	184

* Refer to Figs. 4.12 to 4.15

Measured Strains of Masonry at Various Positions

Table B.2 - Calcium Silicate Wall

(a) Diaphragm wall

Time in days	Average Overall Strain (10^{-6}) (Creep Wall)					Average Moisture Strain (10^{-6}) (Moisture Strain Wall)					
	*	A	B	C	D	Ave.	A	B	C	D	Ave.
0	0	0	0	0	0	0	0	0	0	0	0
20	191	191	192	197	193	77	70	79	73	75	
40	283	259	298	282	281	128	115	140	113	124	
60	359	330	383	365	360	178	170	197	170	179	
80	430	392	452	445	430	233	218	254	228	233	
100	484	421	507	516	482	272	235	297	277	270	
120	561	526	564	573	556	293	298	315	295	300	

(b) Fin wall

Time in days	Average Overall Strain (10^{-6}) (Creep Wall)							Average Moisture Strain (10^{-6}) (Moisture Strain Wall)							
	*	A	B	C	D	E	F	Ave.	A	B	C	D	E	F	Ave.
0	0	0	0	0	0	0	0	0	0	0	0	0	0	0	0
20	204	201	286	276	239	240	240	96	95	102	111	94	90	98	
40	292	294	391	379	351	345	345	148	144	177	176	143	153	157	
60	380	387	486	470	419	422	427	211	210	238	244	196	209	218	
80	464	480	552	551	491	488	504	275	260	298	276	246	254	268	
100	531	544	596	591	532	543	556	330	309	328	310	274	290	307	
120	546	583	611	629	538	593	583	349	328	345	341	288	311	327	

* Refer to Figs. 4.12 to 4.15

Measured Strains of Masonry at Various Positions

Table B.3 - Concrete Blockwork

(a) Diaphragm wall

Time in days	Average Overall Strain (10^{-6}) (Creep Wall)					Average Moisture Strain (10^{-6}) (Moisture Strain Wall)					
	*	A	B	C	D	Ave.	A	B	C	D	Ave.
0	0	0	0	0	0	0	0	0	0	0	0
20	197	207	187	207	200	59	69	68	78	68	
40	291	321	291	356	314	112	116	116	137	128	
60	343	413	338	423	378	142	164	139	177	160	
80	405	465	405	465	432	174	204	184	209	193	
100	425	505	465	495	473	185	234	234	226	220	
120	441	541	521	521	506	202	249	268	251	242	

(b) Fin wall

Time in days	Average Overall Strain (10^{-6}) (Creep Wall)							Average Moisture Strain (10^{-6}) (Moisture Strain Wall)							
	*	A	B	C	D	E	F	Ave.	A	B	C	D	E	F	Ave.
0	0	0	0	0	0	0	0	0	0	0	0	0	0	0	0
20	180	280	235	235	240	230	232	80	90	80	80	80	80	80	82
40	285	355	310	330	310	340	321	135	150	140	140	150	135	141	
60	368	463	408	440	400	480	426	170	195	185	190	200	180	186	
80	423	485	458	490	490	543	480	190	240	225	225	225	215	220	
100	480	535	502	540	530	607	530	220	270	255	250	250	250	250	
120	535	565	543	565	595	650	572	230	295	290	275	270	280	272	

* Refer to Figs. 4.12 to 4.15

Appendix C

Measured Strains of Mortar Prisms

Table C.1 - Mortar Prisms for Clay Walls

(a) Mortar Prisms for Diaphragm Walls

Time in days	Average Overall Strain (10^{-6}) (Average of 2 Readings on Creep Specimens)							Average Moisture Strain (10^{-6}) (Average of 2 Readings on Shrinkage Specimens)							
	Mort No.	1	2	3	4	5	6	Ave.	1	2	3	4	5	6	Ave.
0	0	0	0	0	0	0	0	0	0	0	0	0	0	0	0
20	1420	1370	1320	1280	1220	1220	1305	506	506	456	456	406	406	456	
40	2120	2100	1920	1910	1870	1870	1965	940	815	790	765	665	615	765	
60	2589	2489	2389	2289	2289	2289	2389	1138	1138	938	888	888	838	988	
80	2978	2673	2673	2573	2573	2478	2658	1200	1286	1200	1153	1103	1006	1158	
100	3072	2972	2872	2872	2772	2672	2872	1376	1441	1391	1191	1191	1186	1291	
120	3300	3100	3000	3000	2900	2700	3000	1422	1497	1557	1397	1247	1277	1397	

(b) Mortar Prisms for Fin Walls

Time in days	Average Overall Strain (10^{-6}) (Average of 2 Readings on Creep Specimens)							Average Moisture Strain (10^{-6}) (Average of 2 Readings on Shrinkage Specimens)						
	Mort No.	1	2	3	4	5	6	Ave.	1	2	3	4	5	6
0	0	0	0	0	0	0	0	0	0	0	0	0	0	0
20	2011	1906	1811	1606	1561	1556	1741	620	515	470	465	470	465	550
40	2733	2728	2613	2463	2433	2423	2563	1110	1105	1105	960	955	960	1033
60	3234	3119	2924	2829	2724	2629	2909	1300	1250	1250	1200	1150	1100	1208
80	3685	3780	3235	3130	3045	2920	3300	1700	1600	1500	1500	1400	1350	1508
100	3962	3882	3512	3292	3252	3152	3502	1815	1650	1585	1580	1450	1515	1600
120	3956	3851	3656	3451	3271	3256	3573	1860	1770	1650	1620	1500	1510	1650

Measured Strains of Mortar Prisms

Table C.2 - Mortar Prisms for Calcium Silicate Walls

(a) Mortar Prisms for Diaphragm Walls

Time in days	Average Overall Strain (10^{-6}) (Average of 2 Readings on Creep Specimens)							Average Moisture Strain (10^{-6}) (Average of 2 Readings on Shrinkage Specimens)							
	Mort No.	1	2	3	4	5	6	Ave.	1	2	3	4	5	6	Ave.
0	0	0	0	0	0	-	0	0	0	0	0	0	0	0	0
20	1155	1055	1180	980	1080	-	1090	409	529	529	559	579	499	517	
40	1789	1659	1779	1489	1634	-	1670	696	876	966	926	976	836	879	
60	2208	2058	2283	1783	1933	-	2053	952	1152	1252	1202	1272	1052	1147	
80	2430	2355	2655	1980	2180	-	2330	1165	1390	1390	1440	1400	1330	1353	
100	2632	2632	2907	2132	2407	-	2542	1302	1580	1605	1552	1602	1462	1517	
120	2800	2810	3185	2310	2560	-	2710	1440	1720	1810	1640	1750	1540	1650	

(b) Mortar Prisms for Fin Walls

Time in days	Average Overall Strain (10^{-6}) (Average of 2 Readings on Creep Specimens)							Average Moisture Strain (10^{-6}) (Average of 2 Readings on Shrinkage Specimens)						
	Mort No.	1	2	3	4	5	6	Ave.	1	2	3	4	5	6
0	0	0	0	0	0	0	0	0	0	0	0	0	0	0
20	1356	1266	1121	1456	1216	1391	1301	640	540	600	500	600	580	576
40	1662	1802	1752	2352	2052	1972	1912	1040	960	1040	900	1000	1060	1000
60	2528	2118	2128	2723	2423	2228	2357	1380	1340	1440	1200	1320	1480	1360
80	2595	2285	2685	3185	2880	2600	2704	1580	1670	1760	1680	1600	1660	1658
100	2652	2542	2952	3252	3047	2852	2882	1720	1740	1890	1800	1780	1900	1805
120	2769	2569	3069	3319	3269	2969	2994	1800	1880	1940	1840	1900	2000	1893

Measured Strains of Mortar Prisms

Table C.3 - Mortar Prisms for Concrete Block Walls

(a) Mortar Prisms for Diaphragm Walls

Time in days	Average Overall Strain (10^{-6}) (Average of 2 Readings on Creep Specimens)							Average Moisture Strain (10^{-6}) (Average of 2 Readings on Shrinkage Specimens)							
	Mort No.	1	2	3	4	5	6	Ave.	1	2	3	4	5	6	Ave.
0	0	0	0	0	0	0	0	0	0	0	0	0	0	0	0
20	1311	1166	1121	1056	1016	966	1106	550	500	500	490	480	500	500	
40	1847	1747	1672	1622	1597	1547	1672	827	872	852	782	732	752	802	
60	2268	2218	2168	2068	2018	1968	2118	1220	1170	1120	1120	1020	950	1100	
80	2593	2493	2393	2343	2343	2293	2410	1483	1383	1333	1333	1133	1133	1300	
100	2745	2645	2545	2545	2545	2445	2578	1575	1520	1450	1400	1250	1200	1400	
120	2874	2824	2724	2724	2624	2574	2724	1660	1630	1580	1479	1379	1279	1500	

(b) Mortar Prisms for Fin Walls

Time in days	Average Overall Strain (10^{-6}) (Average of 2 Readings on Creep Specimens)							Average Moisture Strain (10^{-6}) (Average of 2 Readings on Shrinkage Specimens)						
	Mort No.	1	2	3	4	5	6	Ave.	1	2	3	4	5	6
0	0	0	0	0	0	0	0	0	0	0	0	0	0	0
20	1675	1325	1195	1175	1175	1125	1275	685	635	610	555	535	535	593
40	2263	1863	1863	1763	1763	1663	1863	957	927	947	907	857	847	907
60	2704	2304	2294	2194	2154	1904	2259	1280	1225	1205	1105	1055	1055	1155
80	3055	2605	2555	2455	2365	2295	2555	1455	1405	1355	1355	1305	1255	1355
100	3271	2871	2771	2671	2571	2471	2771	1611	1581	1561	1511	1411	1401	1511
120	3494	3044	2994	2874	2774	2494	2944	1728	1708	1718	1618	1528	1528	1638

Appendix C

Measured Strains of Masonry Units

Table C.4 - Clay Units*

Time in days	Diaphragm						Fin					
	Average* Overall Strain (10 ⁻⁶)			Average** Moisture Strain (10 ⁻⁶)			Average* Overall Strain (10 ⁻⁶)			Average** Moisture Strain (10 ⁻⁶)		
Unit no.	1	2	Ave.	1	2	Ave.	1	2	Ave.	1	2	Ave.
0	0	0	0	0	0	0	0	0	0	0	0	0
20	20	40	30	-10	0	-8	20	55	42	-20	5	-5
40	25	40	33	-20	5	-8	25	60	43	-20	-5	-8
60	30	40	35	-20	0	-10	30	65	48	-20	-5	-10
80	30	40	35	-25	-10	-18	30	65	48	-10	-25	-18
100	40	40	40	-20	-10	-15	30	65	48	-15	-15	-15
120	45	40	43	-22	-18	-20	30	65	48	-23	-28	-26

* Average of 2 readings on creep specimens

** Average of 2 readings on moisture movement specimens.

Measured Strains of Masonry Units

Table C.5 - Calcium Silicate Units

Time in days	Diaphragm						Fin					
	Average Overall Strain (10^{-6})*			Average Moisture Strain (10^{-6} **)			Average Overall Strain (10^{-6})*			Average Moisture Strain (10^{-6} **)		
Unit no	1	2	Ave.	1	2	Ave.	1	2	Ave.	1	2	Ave.
0	0	0	0	0	0	0	0	0	0	0	0	0
20	135	145	140	60	40	50	140	210	175	45	55	50
40	195	205	200	100	50	75	200	300	250	95	105	100
60	287	232	260	165	75	120	305	315	310	140	140	140
80	347	272	310	200	100	150	355	365	360	180	190	185
100	400	320	360	240	140	190	380	410	395	205	225	215
120	445	335	390	270	150	210	420	440	430	230	230	230

* Average of 2 readings on creep specimens

** Average of 2 readings on moisture movement specimens.

Measured Strains of Masonry Units

Table C.6 - Concrete Block Units

Time in days	Diaphragm						Fin					
	Average Overall Strain (10^{-6})*			Average Moisture Strain (10^{-6})**			Average Overall Strain (10^{-6})*			Average Moisture Strain (10^{-6})**		
Unit no	1	2	Ave.	1	2	Ave.	1	2	Ave.	1	2	Ave.
0	0	0	0	0	0	0	0	0	0	0	0	0
20	180	190	185	90	80	85	195	145	220	75	85	80
40	270	210	240	120	100	110	300	300	300	140	100	120
60	290	290	290	130	150	140	295	425	360	165	155	160
80	290	350	320	120	180	150	365	435	400	185	195	190
100	325	405	365	150	220	185	400	470	435	210	220	215
120	350	465	410	175	245	210	430	510	470	226	246	236

* Average of 2 readings on creep specimens

** Average of 2 readings on moisture movement specimens.

APPENDIX D

Prediction of Elastic Modulus, Creep, Shrinkage and Prestress Loss using Composite Model (Brooks 1987a)

(a) Elastic modulus and creep (Clay diaphragm wall)

Using the following data;

where E_{by}^* = 29 GPa (Table 5.6);	E_m = 7.5 GPa (Table 5.5);
H = 1960 mm;	C = 26 courses;
$C + 1$ = 27;	b_y = 65 mm,
m_y = 10 mm;	A_w = 2.08×10^5 mm ² ;
A_b = 1.98×10^5 mm ² ;	A_m = 10×10^3 mm ²

* elastic modulus of clay unit between bed faces

Equation 3.8 becomes;

$$\frac{1}{E_{wy}} = \frac{0.862}{E_{by}} \left[\frac{1}{0.956 + 0.044 \frac{E_m}{E_{by}}} \right] + \frac{0.138}{E_m} \quad (D.1)$$

For effective modulus ($\frac{1}{E'_{wy}}$), Equation D.1 becomes

$$\frac{1}{E'_{wy}} = \frac{0.862}{E'_{by}} \left[\frac{1}{0.956 + 0.044 \frac{E'_m}{E'_{by}}} \right] + \frac{0.138}{E'_m} \quad (D.2)$$

Applying Equation 3.12 for the units and mortar, the effective modulus of the masonry units and mortar in Equation D.2 is determined as follows

$$C_{bs} = \frac{1}{E'_{by}} - \frac{1}{E_{by}} \quad (D.3)$$

$$\text{Thus } E'_{by} = \frac{1}{(C_{bs} + \frac{1}{E_{by}})} \quad \text{and} \quad E'_m = \frac{1}{(C_{ms} + \frac{1}{E_m})} \quad (D.4)$$

where C_{bs} = specific creep of unit between bed faces

C_{ms} = specific creep of mortar prisms

The predicted elastic moduli and creep are as tabulated below.

Time in days	C_{ms} ($10^{-6}/$ MPa)	E'_m (GPa)	C_{bs} ($10^{-6}/$ MPa)*	E'_{by} (GPa)	E'_{wy} (GPa)	C_{wy} ($10^{-6}/$ MPa)**	Stress x C_{wy} (10^{-6})
0	0	7.50	0	29.00	19.23	0	0
20	283	2.40	7.3	23.90	10.5	43.1	129
40	400	1.88	9.3	22.80	8.84	61.07	183
60	467	1.67	10	22.40	8.13	71.04	213
80	500	1.58	10.7	22.10	7.8	76.14	228
100	527	1.51	11	22.00	7.57	80.06	240
120	533	1.5	11.33	21.80	7.5	81.31	244

* C_{bs} = Specific creep between header faces x $\frac{\text{elastic modulus between header faces}}{\text{elastic modulus between bed faces}}$
= Specific creep between header faces x 1.66

** Specific creep

(b) Shrinkage (Clay diaphragm wall)

Using similar data for predicting creep, Eq. (3.13) becomes;

$$S_{wy} = 0.862 S_{by} + 0.138 S_m + \frac{0.862 (S_m - S_{by})}{1 + 21.5 \frac{E'_{by}}{E'_m}} \quad (D.5)$$

where S_{wy} = axial shrinkage of masonry;

S_{by} = axial shrinkage of brick or block;

E'_{by} = effective modulus of brick or block;

E'_m = effective modulus of mortar;

and S_m = shrinkage of mortar.

The predicted shrinkage at 20 day intervals is tabulated below.

Time in days	S_{by} (10^{-6})	S_m (10^{-6})	E'_m (GPa)	E'_{by} (GPa)	S_{wy} (10^{-6})
0	0	0	7.5	29.00	0
20	-3	456	2.4	23.90	62.1
40	-6	765	1.88	22.80	103
60	-10	988	1.67	22.40	131
80	-15	1158	1.58	22.10	150
100	-17	1291	1.51	22.00	167
120	-20	1397	1.5	21.80	179

(c) **Prediction of Prestress Loss of Diaphragm Clay Brickwork using Equation 6.3 (Dilger method)**

The following are the constants substituted into Eq. (6.3);

$$n_o = \frac{E_s}{E_{wy}} = \frac{175 \times 10^3}{20.36 \times 10^3} = 8.60$$

$$f_o = 3 \text{ N/mm}^2 \quad E_s = 175 \times 10^3 \text{ N/mm}^2$$

$$\rho = \frac{A_s}{A_{wk}} = \frac{491 \times 2}{2.08 \times 10^5} = 0.00472$$

$$y_1^2/r^2 = 0$$

$$f'r(t) = \alpha fr(t) \quad \alpha = 0.40 \text{ (from Fig.3.1)}$$

$$fr(t) = \text{relaxation of the steel (based on test value)}$$

The aging coefficient is determined from the following;

$$\chi(t, t_o) = \frac{3}{3 - f_t(t, t_o)} - \frac{1}{\phi(t, t_o)}$$

where $f_t(t, t_o)$ is a function of relaxation of brickwork. However to date no experimental data has been reported. The aging coefficient normally varies from 0.5 to 1.0. Tables D.3 and D.4 shows the effect of using the aging coefficient as 0.5 and 1, respectively in predicting prestress loss.

Eq. (6.3) becomes;

$$\delta f_s(t) = \frac{[25.8 (\frac{E_{wy}}{E'_{wy}(t, t_o)} - 1) + \epsilon_{sh}(t, t_o) 175 \times 10^3 + f'r(t)]}{(1 + 0.041 a)} \quad (D.6)$$

$$\text{where } a = (1 + \chi(t, t_o) [\frac{20.36}{E'_{wy}(t, t_o)} - 1]) \quad (D.7)$$

The predicted prestress loss at 20 day intervals, assuming $\chi = 1.0$, is tabulated in **Table D.3** below ;

Time in days	E'_{wy} (GPa)	C_{wy} (10^{-6})	a	ϵ_{sh} (10^{-6})	$f'r(t)$	δf_s	$(\delta f_s/629)$ 100
0	20.36	0	1	0	0	0	0
20	10.50	43.1	1.94	62	7.90	39.72	6.31
40	8.84	61.07	2.30	103	9.54	55.96	8.90
60	8.13	71.04	2.50	131	9.54	64.71	10.33
80	7.80	76.14	2.61	150	9.54	69.43	11.04
100	7.57	80.06	2.69	167	9.54	74.25	11.80
120	7.50	81.31	2.72	179	9.54	76.65	12.18

The predicted prestress loss at 20 day intervals, assuming $\chi = 0.5$, is tabulated in **Table D.4** below:

Time in days	E'_{wy} (GPa)	C_{wy} (10^{-6})	a	ϵ_{sh} (10^{-6})	$f'r(t)$	δf_s	$(\delta f_s/629)$ 100
0	20.36	0	1	0	0	0	0
20	10.50	43.1	1.47	62	7.90	40.47	6.60
40	8.84	61.07	1.65	103	9.54	57.35	9.12
60	8.13	71.04	1.75	131	9.54	66.55	11.59
80	7.80	76.14	1.81	150	9.54	72.04	11.43
100	7.57	80.06	1.84	167	9.54	76.64	12.18
120	7.50	81.31	1.86	179	9.54	79.13	12.58

(d) **Prediction of Prestress Loss of Diaphragm Clay Brickwork using Equation 3.17 (Abeles method)**

Prestress loss

Using the same constant as in Dilger method, the stress loss in Eq. (3.17) can be expressed as

$$\begin{aligned}
 PL &= K_n (PL_{cr} + PL_{sh}) + PL_r(t) \\
 &= 1 (25.8 \cdot [\frac{20.36}{E'_{wy}(t,t_0)} - 1] + \epsilon_{sh} 175 \times 10^3) + PL_r(t)
 \end{aligned}$$

The predicted prestress loss at 20 day intervals is as tabulated in **Table D.4** below.

time in days	E'_{wy} (GPa)	C_{wy} (10^{-6})	ϵ_{sh} (10^{-6})	$PL_r(t)$	δf_s	$(\delta f_s/629)$ 100
0	20.36	0	0	0	0	0
20	10.50	43.1	62	7.90	42.98	6.83
40	8.84	61.07	103	9.54	61.19	9.73
60	8.13	71.04	131	9.54	71.28	11.33
80	7.80	76.14	150	9.54	77.33	12.29
100	7.57	80.06	167	9.54	82.36	13.09
120	7.50	81.31	179	9.54	85.10	13.54

Appendix E

Re-prediction of Creep, Shrinkage and Prestress Loss using Composite Model

(a) Creep (clay diaphragm walls)

Shrinkage factor of mortar = 0.74 (Fig. 7.18)

Shrinkage factor of unit = 1.1 (Fig. 7.17)

Creep/shrinkage of mortar = 0.43/MPa (Fig. 7.21)

Creep/shrinkage of unit = 0.98/MPa (Fig. 7.23)

Mortar

Final specific creep of mortar = Creep/shrinkage of mortar x final shrinkage of mortar
where

final shrinkage of mortar = original shrinkage of mortar x Shrinkage factor of mortar
= $S_m \times 0.43$

Therefore the new specific creep of mortar = $0.43 \times S_m \times 0.74$

At 20 days after loading;

original shrinkage of mortar = 456×10^{-6}

Therefore the specific creep of mortar = $0.74 \times 456 \times 10^{-6} \times 0.43$
= 145×10^{-6} per MPa

Units

Since the shrinkage factor (1.1) and creep/shrinkage (0.98) ratio of the clay units are almost equal to unity, therefore there are no adjustments in the original creep and moisture movement of the units.

The new effective modulus of the mortar was determined by substituting the specific creep of mortar into Eq. D.4 (Appendix D). Similarly the creep of the walls was determined as in Appendix D (a).

The re-predicted creep of the clay diaphragm wall is tabulated in **Table E.1** below.

time in days	C_{ms} ($10^{-6}/$ MPa)	E'_m (GPa)	$*C_{bs}$ ($10^{-6}/$ MPa)	E'_{by} (GPa)	E'_{wy} (GPa)	C_{wy} ($10^{-6}/$ MPa)	Stress x C_w (10^{-6})
0	0	7.50	0	29.00	19.23	0	0
20	145	3.345	7.3	23.90	13.17	23.93	71.8
40	243	2.517	9.3	22.80	10.95	39.36	118
60	314	2.136	10	22.40	9.83	49.79	149
80	368	1.915	10.7	22.10	9.10	57.87	174
100	411	1.771	11	22.00	8.62	64.02	192
120	445	1.671	11.33	21.80	8.27	68.98	207

(b) Shrinkage (clay diaphragm wall)

Mortar

At 20 days after loading the original shrinkage of the mortar = 456×10^{-6}

By applying the shrinkage factor;

the final shrinkage of the mortar = $0.74 \times 456 \times 10^{-6} = 337 \times 10^{-6}$

Unit

Again, as in the creep, no adjustments on the original moisture expansion of the units was made.

The re-predicted shrinkage of the wall was determined by substituting the final shrinkage of mortar into Eq. D.5 (Appendix D).

The re-predicted shrinkage at 20 day intervals is tabulated in **Table E.2** below.

Time in days	S_{by} (10^{-6})	S_m (10^{-6})	Final S_m (10^{-6})	E'_m (GPa)	E'_{by} (GPa)	S_{wy} (10^{-6})
0	0	0	0	7.5	29.00	0
20	-3	456	337	3.59	23.91	52
40	-6	765	566	2.65	22.82	87
60	-10	988	731	2.23	22.48	113
80	-15	1158	867	1.99	22.15	135
100	-17	1291	95	1.84	21.99	151
120	-20	1397	1034	1.73	21.83	164

(c) Prestress loss (clay diaphragm wall)

Similar methods of predicting prestress loss as in Appendix D (Abeles and Dilger) were used in re-predicting the new prestress loss, i.e by substituting the re-predicted creep and shrinkage.

The re-predicted prestress loss (Abeles) at 20 day intervals is tabulated in **Table E.3** as follows:

time in days	C_{wy} (10^{-6})	ϵ_{sh} (10^{-6})	$PL_T(t)$	% Prestress Loss
0	0	0	0	0
20	72	52	7.90	6.25
40	118	87	9.54	8.39
60	149	113	9.54	9.91
80	174	135	9.54	11.13
100	192	151	9.54	12.02
120	207	164	9.54	12.77

Appendix F

Measured Strains of Mortar Prisms

Table F.1 - Creep and Shrinkage Mortar Prisms

(a) Mortar Prisms for Diaphragm Walls

Time in days	Mortar Prisms with Original Water/cement Ratio						Mortar Prisms with Reduced Water/cement Ratio					
	Average Overall Strain (10^{-6}) *			Average Moisture Strain (10^{-6})**			Average Overall Strain (10^{-6}) *			Average Moisture Strain (10^{-6})**		
	1	2	Ave.	1	2	Ave.	1	2	Ave.	1	2	Ave.
0	0	0	0	0	0	0	0	0	0	0	0	0
20	900	1000	950	500	500	500	700	500	600	450	400	425
40	1700	1500	1600	1000	900	950	1400	1200	1300	850	800	825
60	2300	2150	2250	1300	1250	1275	1700	1500	1600	1100	1000	1050
80	2800	2400	2600	1600	1500	1550	1900	1700	1800	1200	1100	1150
100	2900	2700	2800	1700	1600	1650	2000	1800	1900	1300	1100	1200
120	2900	2900	2900	1750	1650	1700	2000	1900	1950	1400	1100	1250

(b) Mortar Prisms for Fin Walls

Time in days	Mortar Prisms with Original Water/cement Ratio						Mortar Prisms with Reduced Water/cement Ratio					
	Average Overall Strain (10^{-6}) *			Average Moisture Strain (10^{-6})**			Average Overall Strain (10^{-6}) *			Average Moisture Strain (10^{-6})**		
	1	2	Ave.	1	2	Ave.	1	2	Ave.	1	2	Ave.
0	0	0	0	0	0	0	0	0	0	0	0	0
20	800	900	850	400	500	450	800	750	775	400	450	425
40	1700	1900	1800	1000	1000	1000	1300	1300	1300	800	850	825
60	2300	2400	2350	1350	1350	1350	1700	1650	1675	1100	1150	1125
80	2450	2600	2525	1500	1550	1525	1900	1850	1875	1200	1300	1250
100	3000	3000	3000	1800	1700	1750	2100	2050	2075	1300	1400	1350
120	3000	3200	3100	1800	1800	1800	2300	2200	2250	1350	1450	1400

* Average of 2 readings on creep specimens

** Average of 2 readings on shrinkage specimens